DEVELOPMENT OF OPTICALLY STIMULATED LUMINESCENCE DATING TECHNIQUES FOR APPLICATION TO TERRESTRIAL AND MARTIAN STUDIES

By

MICHAEL WAYNE BLAIR

Bachelor of Science
Western Kentucky University
Bowling Green, Kentucky
1999

Submitted to the Faculty of the
Graduate College of the
Oklahoma State University
in partial fulfillment of
the requirements for
the Degree of
DOCTOR OF PHILOSOPHY
December, 2005

DEVELOPMENT OF OPTICALLY STIMULATED

LUMINESCENCE DATING TECHNIQUES

FOR APPLICATION TO TERRESTRIAL

AND MARTIAN STUDIES

Dissertation Approved:

Dr. Stephen W. S. McKeever

Dissertation Adviser

Dr. Paul A. Westhaus

Dr. Robert J. Hauenstein

Dr. Elizabeth J. Catlos

Dr. A. Gordon Emslie

Dean of the Graduate College

ACKNOWLEDGEMENTS

Most importantly, I would like to thank my wife Melissa for supporting me throughout this long process. Without her support and reassurance, I may never have made it through.

I would like to thank Dr. Debabrata Banerjee for my initial instruction and training in the field of OSL dating. He gave me a firm foundation in the field and taught me things that would have taken much longer to learn on my own.

I appreciate the support of NASA and JPL through the Graduate Student Researcher's Program. Their fellowship and the support of Dr. Sam Kim have made this dissertation possible.

I have to thank all of my "labmates," including Dr. Von Whitley, Dr. Eduardo Yukihara, David Klein, and Gabriel Sawakuchi, for research-related discussions as well as all the coffee breaks. In particular, I would like to thank Dr. Regina Kalchgruber for her numerous discussions about the "Mars dating project" and her help in identifying martian minerals.

Finally, I owe many thanks to my advisor, Dr. Stephen W. S. McKeever. Despite his busy schedule as Vice President for Research and Technology Transfer, Dr. McKeever will always make time to discuss research issues with his students. Furthermore, his expertise and research philosophy has allowed me to study the OSL dating process from a physics perspective. This was my desire for a graduate education and could not have been fulfilled in any other laboratory.

TABLE OF CONTENTS

Chapter Page

1. INTRODUCTION 1

1.1. Introduction to Luminescence Dating....2
1.1.1. OSL Methods of Absorbed Dose Estimation....11
1.1.2. Anomalous Fading....21
1.2. Motivation for Using OSL Dating on Mars....24
1.2.1. Martian Fluvial Landforms....25
1.2.2. Martian Aeolian Landforms....31
1.3. Challenges to Developing OSL Dating for Mars....37
1.3.1. Mineral Composition....38
1.3.2. Polymineral Samples....42
1.3.3. Temperature Regime....43
1.3.4. Natural Dose Rates on Mars....44

2. DEVELOPMENT OF A SINGLE-ALIQUOT REGENERATIVE-DOSE POLYMINERAL OSL DATING PROCEDURE....48

2.1. Requisite Properties of a Single-Aliquot Regenerative-Dose Procedure....49
2.2. Experiments with Feldspars....51
2.2.1. Materials and Equipment....52
2.2.2. General TL/OSL Characterisitcs....54
2.2.3. Sensitivity Changes....58
2.2.4. Correcting for Sensitivity Change....64
2.2.5. OSL Dose Response....72
2.2.6. Dose Recovery Experiments....85
2.3. Experiments with Quartz....91
2.3.1. Materials and Equipment....92
2.3.2. Correcting for Sensitivity Change....92
2.3.3. OSL Dose Response....98
2.3.4. Dose Estimation and Dose Recovery Experiments....103
2.4. Experiments with Quartz and Feldpsars Mixtures....106
2.4.1. Materials and Equipment....107
2.4.2. Correcting for Sensitivity Change....107
2.4.3. OSL Dose Response....110
2.4.4. Dose Estimation and Dose Recovery Experiments....113
2.5. Concluding Remarks for Chapter 2....117

3. CHARACTERIZATION OF OSL PROPERTIES OF MARTIAN SIMULANTS AND MINERALS 122

3.1. Materials 124
3.2. Identification of Optically Active Traps 125
3.3. Correcting for Sensitivity Changes 129
3.4. Dose Response Curves 134
3.5. Dose Recovery Experiments 144
3.6. Concluding Remarks for Chapter 3 145

4. PROPERTIES OF MATERIALS IRRADIATED AND STIMULTED AT LOW TEMPERATURES 149

4.1. Potential Effects of Temperature on the Luminescence Process…. 149
4.2. A System to Irradiate and Measure OSL at Low Temperatures 155
4.3. OSL Properties of Materials Irradiated and Stimulated at Low Temperatures 158
4.3.1. Reproducibility 158
4.3.2. Luminescence Efficiency 158
4.3.3. Low Temperature TL 159
4.3.4. Effect of Measurement and Irradiation Temperature 162
4.4. Numerical Simulations 168
4.4.1. The Model and Parameters 168
4.4.2. Basic Luminescence Characteristics of the Model 176
4.4.3. Dose Recovery and Dose Estimation at Terrestrial Temperatures 187
4.4.4. Dose Recovery and Dose Estimation at Martian Temperatures 188
4.5. Further Numerical Simulations 196
4.5.1. Basic Luminescence Characteristics 198
4.5.2. Dose Recovery and Dose Estimation at Terrestrial Temperatures 206
4.5.3. Dose Recovery and Dose Estimation at Martian Temperatures 209
4.6. Dose Recovery for Irradiation at Low Temperatures 213
4.7. Concluding Remarks for Chapter 4 215

5. FUTURE DIRECTIONS 218

5.1. Martian Simulants and Dose Estimation Procedures 218
5.2. Temperature Considerations 219
5.3. Anomalous Fading 220
5.4. Bleaching Characterstics 222
5.5. Annual Dose Rate 224
5.6. Sample Sorting 225
5.7. Discussion 226

6. SUMMARY AND DISCUSSION 227

6.1. Summary 227
6.2. Discussion 230

REFERENCES 233

APPENDICES 246

APPENDIX A – RETROSPECTIVE DOSIMETRY USING BRICKS FROM THE SEMIPALATINSK REGION OF KAZAKHSTAN 246

APPENDIX B – PROGRESS TOWARDS DEVELOPING A MINIATURIZED OSL SYSTEM FOR IN-SITU MARTIAN STUDIES 272

APPENDIX C– ELECTRON PARAMAGNETIC MEASUREMENTS 281

LIST OF TABLES

Table Page

1.1. The standard SAR procedure as defined by Murray and Wintle (2000) 20

1.2. Mineral abundances of two mixtures (named OSU Mars-1 and OSU Mars-2) of Mars soil simulants 40

2.1. Comparison of maximum estimable dose for various feldspars using different stimulation procedures 84

2.2. Experimental procedures for dose recovery tests 86

2.3. Results of feldspar dose recovery experiments for blue-stimulated (20 aliquots), infrared-stimulated (5 aliquots), and post-IR blue-stimulated OSL (5 aliquots).....88

2.4. Results of feldspar dose recovery experiments where TL to 500^{o}C was measured after each T_i 89

2.5. The suggested modified SAR procedure (Murray and Wintle, 2000) for polymineral samples 120

3.1. The suggested modified SAR procedure (Murray and Wintle, 2000) for polymineral samples 123

3.2. Calculations of the maximum estimable doses and ages from fitting of the dose response curves (see text 143

3.3. Results of dose recovery experiments for the infrared-stimulated OSL signal from a post-IR blue stimulation sequence 147

3.4. Results of dose recovery experiments for the blue-stimulated OSL signal from a post-IR blue stimulation sequence 148

4.1. Parameters for the 4 traps and one recombination center used in the numerical simulations of low temperature traps and the OSL process.....171

4.2. Parameters for the 4 traps and one recombination center used in the numerical simulations of low temperature traps and the OSL process in Section 4.5 197

4.3. Procedural parameters and results for the dose recovery experiments conducted in the low temperature OSL system.....214

5.1. Spectral UV irradiance for Earth and Mars 223

6.1 Suggested polymineral dose estimation procedure.....229

A.1. Absorbed doses from the first slice (6-16 mm) of eight bricks 254

A.2. Absorbed doses from the depth-versus-dose profile of brick N1 263

A.3. Absorbed doses from the depth-versus-dose profile of brick N4 264

A.4. Absorbed doses from the first slice (6-16 mm) of the intercomparison samples.....265

LIST OF FIGURES

Figure Page

1.1. Band diagrams of the luminescence process 4

1.2. Simulation of a TL curve 7

1.3. Examples of (a) CW-OSL, (b) LM-OSL, and (c) POSL 9

1.4. Examples of a multiple-aliquot (a) additive-dose procedure and a (b) regenerative-dose procedure 13

1.5. Examples of dose recovery procedures....17

1.6. Mars Orbiter Camera (MOC) image of valley network in Newton Crater on Mars 26

1.7. An example of an outflow channel in the Zephryia region of Mars from MOC....27

1.8. Possible shoreline feature in Acidalia Planitia on Mars 28

1.9. MOC image of gullies on the side of a mesa in the south polar region 29

1.10. MOC image showing dunes in Chasma Boreale in the north polar region of Mars....32

1.11. MOC image of dunes in Noachis Terra 33

1.12. Intercrater dunes in Arabia Terra....34

1.13. Yardangs in the Aeolis region of Mars 35

1.14. Ternary diagram of feldspars showing both the plagioclase and alkali feldspars 41

1.15. The attenuation with depth of GCR and SPE in the martian regolith....47

2.1. Ternary diagram of feldspars showing the approximate positions of the samples 53

2.2. Mass normalized thermoluminescence (a), blue-stimulated OSL (b), and infrared stimulated OSL (termed IRSL) (c) 55

2.3. The effect of bleaching on TL 57

2.4. Sensitivity changes experienced by microcline 60

2.5. Examples of normalized OSL decay curves from the 7^{th} cycle of sensitivity change experiments 63

2.6. TL after repeated cycles of OSL measurement for albite 65

2.7. Tests of the sensitivity-correction procedure for microcline using two different preheating procedures 67

2.8. Same as Figure 2.7 except the results are for oligoclase 68

2.9. Same as Figures 2.7 and 2.8 except the results are for albite 69

2.10. Uncorrected (R_i only) dose-response curves for microcline 73

2.11. Same as Figure 2.10 except the results are for oligoclase 74

2.12. Same as Figures 2.10 and 2.11 except the results are for albite 75

2.13. Sensitivity-corrected (L_i) dose response curves for microcline, constructed using the modified SAR procedure 78

2.14. Same as Figure 2.13 except the results are for oligoclase 79

2.15. Same as Figures 2.13 and 2.14 except the results are for albite 80

2.16. Dose response curves using four different OSL signals for (a) microcline, (b) oligoclase, and (c) albite produced using SAR 83

2.17. Normalized OSL decay curves from the dose-recovery experiments with anorthoclase 90

2.18. Tests of sensitivity-correction procedure for quartz sample #495A 93

2.19. Same as Figure 2.18 except for sample #021714 94

2.20. Same as Figure 2.18 except for sample #022513 95

2.21. Same as Figure 2.18 except for sample #030218 96

2.22. Uncorrected (R_i only) dose response curves for quartz samples (a) 495A, (b) 021714, (c) 022513, and (d) 030218 99

2.23. Sensitivity-corrected (L_i) dose response curves for quartz samples (a) 495A, (b) 021714, (c) 022513, and (d) 030218 100

2.24. Sensitivity corrected dose response curves for a range of preheats for all of the quartz samples studied 101

2.25. Results of dose recovery experiments for the denoted quartz samples 104

2.26. Average D_e for the various quartz samples as noted 105

2.27. Tests of sensitivity-correction procedure for mixtures of quartz and feldspar as indicated 108

2.28. Same as Figure .2.27 except the OSL signal is the post-IR blue-stimulated signal 109

2.29. Uncorrected (R_i only) dose response curves for quartz and feldspar mixtures as noted 111

2.30. Sensitivity-corrected (L_i) dose response curves for quartz and feldspar mixtures as noted 112

2.31. Results of dose recovery experiments for the denoted quartz/feldspar mixtures 114

2.32. The average measured D_e from different samples containing quartz sample 495A 116

3.1. The effect of bleaching on TL for (a) JSC Mars-1, (b) OSU Mars-1, and (c) OSU Mars-2 127

3.2. The effect of bleaching on TL for martian meteorites as indicated 128

3.3. Tests of the sensitivity-correction procedure for (a) JSC Mars-1, (b) OSU Mars-1, and (c) OSU Mars-2 using the proposed SAR procedure 130

3.4. Tests of the sensitivity-correction procedure for martian meteorites using the proposed SAR procedure 131

3.5. Tests of the sensitivity-correction procedure for (a) JSC Mars-1, (b) OSU Mars-1, and (c) OSU Mars-2 using the proposed SAR procedure....132

3.6. Tests of the sensitivity-correction procedure for martian meteorites using the proposed SAR procedure....133

3.7. Uncorrected (R_i only) dose-response curves for (a) JSC Mars-1, (b) OSU Mars-1, and (c) OSU Mars-2....135

3.8. Uncorrected (R_i only) infrared-stimulated dose-response curves (from a post-IR stimulation method) for the studied martian meteorites 136

3.9. Uncorrected (R_i only) dose-response curves for (a) JSC Mars-1, (b) OSU Mars-1, and (c) OSU Mars-2....137

3.10. Uncorrected (R_i only) blue-stimulated dose-response curves (from a post-IR stimulation method) for the studied martian meteorites 138

3.11. Sensitivity-corrected dose-response curves for (a) JSC Mars-1, (b) OSU Mars-1, and (c) OSU Mars-2....139

3.12. Sensitivity-corrected infrared-stimulated dose-response curves (from a post-IR stimulation method) for the studied martian meteorites 140

3.13. Sensitivity-corrected dose-response curves for (a) JSC Mars-1, (b) OSU Mars-1, and (c) OSU Mars-2....141

3.14. Sensitivity-corrected blue-stimulated dose-response curves (from a post-IR stimulation method) for the studied martian meteorites 142

4.1. Mechanisms for thermal dependence of OSL decay 153

4.2. Diagram of the low temperature TL/OSL system....156

4.3. Normalized RL from albite and mixtures OSU Mars-1 and OSU Mars-2 as indicated....160

4.4. TL from three samples (as noted) that have been irradiated at –100°C (OSU Mars-1 and OSU Mars-2) and –125°C (albite) 161

4.5. OSL from samples (a) albite, (b) OSU Mars-1, and (c) OSU Mars-2 that have been irradiated at 25°C and stimulated at various temperatures 163

4.6. OSL from samples (a) OSU Mars-1 and (b) OSU Mars-2 that have been irradiated at various temperatures and stimulated at 25°C 165

4.7. OSL from samples (a) albite, (b) OSU Mars-1, and (c) OSU Mars-2 that have been irradiated and stimulated at the same temperature.....167

4.8. Band diagram representing the traps and recombination center for numerical modeling of low temperature traps and the OSL process.....170

4.9. TL from the model of Figure 4.8.....178

4.10. OSL dose response curves for the model of Figure 4.8.....180

4.11. RL results for the model of (a) Figure 4.8 and (b) albite, OSU Mars-1, and OSU Mars-2.....182

4.12. OSL from (a) the model for Figure 4.8 and (b) albite, (c) OSU Mars-1, and (d) OSU Mars-2 that have been irradiated at 25°C and stimulated at various temperatures.....183

4.13. OSL from (a) the model for Figure 4.8 and (b) OSU Mars-1, and (c) OSU Mars-2 that have been irradiated at various temperatures and stimulated at 25°C.....185

4.14. OSL from (a) the model for Figure 4.8 and (b) albite, (c) OSU Mars-1, and (d) OSU Mars-2 that have been irradiated at and stimulated at various temperatures.....186

4.15. Results of the dose recovery simulation for a known dose delivered at 0.1 Gy/s and 25^{o}C.....189

4.16. Results of the dose estimation simulation for a natural dose delivered at 2 mGy/yr and 25^{o}C.....190

4.17. Results of the dose recovery simulations for a known dose delivered at 0.1 Gy/s and -100^{o}C.....192

4.18. Results of the dose estimation simulations for a natural dose delivered at 2 mGy/yr and -100^{o}C.....194

4.19. TL from the original ((a) and (c)) and modified ((b) and (d)) models.....199

4.20. OSL dose response curves for the original ((a) and (c)) and modified models ((b) and (d)).....200

4.21. RL results for the model of (a) original model, (b) modified model, and (c) albite, OSU Mars-1, and OSU Mars-2.....201

4.22. OSL from (a) the original model, (b) the modified model, (c) albite, (d) OSU Mars-1, and (e) OSU Mars-2 that have been irradiated at 25°C and stimulated at various temperatures 203

4.23. OSL from (a) the original model, (b) the modified model, and (c) OSU Mars-1, and (d) OSU Mars-2 that have been irradiated at various temperatures and stimulated at 25°C 204

4.24. OSL from (a) the original model, (b) the modified model, (c) albite, and (d) OSU Mars-1, and (e) OSU Mars-2 that have been irradiated at and stimulated at various temperatures 205

4.25. Results of the dose recovery simulation with the modified model for a known dose delivered at 0.1 Gy/s and 25°C 207

4.26. Results of the dose estimation simulation with the modified model for a natural dose delivered at 2 mGy/yr and 25°C 208

4.27. Results of the dose recovery simulations with the modified model for a known dose delivered at 0.1 Gy/s and -100°C 210

4.28. Results of the dose estimation simulations with the modified model for a natural dose delivered at 2 mGy/yr and -100°C 211

A.1. Representation of the coring and slicing of the bricks from Semipalatinsk ... 249

A.2. Histograms for high sensitivity samples 255

A.3. Histograms for low sensitivity samples 256

A.4. Absorbed doses (natural doses not subtracted) as a function of median depth for brick N1 257

A.5. Histograms for brick N1 (up to 50 mm median depth) 258

A.6. Histograms for brick N1 (greater than 50 mm median depth) 259

A.7. Absorbed doses (natural doses not subtracted) as a function of median depth for brick N4 260

A.8. Histograms for brick N4 (up to 50 mm median depth) 261

A.9. Histograms for brick N4 (greater than 50 mm median depth) 262

A.10. Histogram for intercomparison sample 266

A.11. Depth-versus-dose profile for brick N1 with a background level of D_0 = 0.466 Gy subtracted 270

A.12. Depth-versus-dose profile for brick N4 with a background level subtracted 271

B.1. System block diagram for the OSL module as developed by Nomadics and OSU 273

B.2. Dose response for Kapton tape 275

B.3. Dose response for FEP tape 276

B.4. Drawing and photo of OSL chamber (supplied by Nomadics) 278

C.1. Examples of EPR spectra from feldspar minerals 285

C.2. EPR dose response curves for feldspar minerals 286

C.3. Examples of EPR spectra from quartz and feldspar mixtures 288

C.4. Dose response curves for quartz and feldspar mixtures 289

LIST OF SYMBOLS

λ	wavelength
τ	lifetime of electrons in trap

NOMENCLATURE

TL	Thermoluminescence
OSL	Optically stimulated luminescence
IRSL	Infrared stimulated luminescence
IR	Infrared
PIDDP	Planetary Instrument Definition and Development Program
JPL	Jet Propulsion Laboratory
CW-OSL	Continuous-wave optically stimulated luminescence
LM-OSL	Linearly modulated optically stimulated luminescence
POSL	Pulsed optically stimulated luminescence
UV	ultraviolet
PMT	Photomultiplier tube
D_e	Equivalent dose
Gy	Gray (J/kg)
SARA	Single aliquot/ regeneration and additive dose
SAR	Single-aliquot regenerative-dose
MOC	Mars Orbiter Camera
MGS	Mars Global Surveyor
U	Uranium
Th	Thorium
K	Potassium

GCR	Galactic cosmic ray
SPE	Solar particle events
JSC	Johnson Space Center
TES	Thermal Emission Spectrometer
THEMIS	Thermal Emission Imaging System
LET	Linear energy transfer
R_i	Regeneration dose OSL
T_i	Test dose OSL
L_i	Sensitivity-corrected OSL
LED	Light emitting diode
RR	Recycling ratio
Dc	Characteristic dose
ka	thousand years
C	Celsius
CH	Cutheat
PH	Preheat
RL	Radioluminescence
EPR	Electron paramagnetic resonance
NASA	National Aeronautics and Space Administration
GSRP	Graduate Student Researcher's Program
ESA	European Space Agency

CHAPTER ONE

INTRODUCTION

The surface of the Earth has been shaped by many geological processes, including aeolian and fluvial events. Establishing climatic chronologies and the temporal sequence of geomorphological patterns on the Earth's surface require information about the timing of these events. As such, much research has been devoted to developing absolute dating techniques for geologic events on Earth. Thermoluminescence (TL) (Aitken, 1985) and optically stimulated luminescence (OSL) (Aitken, 1998) dating have been particularly useful for dating aeolian and fluvial events as well as certain human activities (e.g., pottery manufacture) during the quaternary and holocene.

Recently, it has been suggested that OSL dating can be applied to extraterrestrial environments such as Mars (Lepper and McKeever, 2000). Although the surfaces of Mars and Earth look different, there is no reason to assume that the same type of geological processes have not been active, albeit at different times and scales. Mars has long been regarded as a cold, dead planet that has experienced little recent geological activity. However, data from recent remote sensing satellites such as Mars Odyssey and Mars Global Surveyor and landers/rovers such as Pathfinder, Spirit, and Opportunity have challenged that assumption. Data from these missions indicate that water has been active on the surface of Mars in the "recent" past (last one million years)

(Albee, 2003; Malin and Edgett, 2000) and that dune fields are still being created and modified (Pelkey *et al.,* 2003; Pelkey *et al.,* 2004). The potential of OSL dating to further the understanding of these phenomena has been recognized by several researchers (Doran *et al.,* 2004; Clifford *et al.,* 2000; Lepper and McKeever, 2000; McKeever *et al.,* 2003) as well as NASA as evidenced by recent funding of a NASA Planetary Instrument Definition and Development Program (PIDDP) project for OSL dating to the Jet Propulsion Laboratory (JPL) and OSU.

This work focuses on one aspect of the development of OSL dating for in-situ application on Mars, specifically, the development of a polymineralic OSL dating procedure. The need for this procedure will be expanded upon in the sections to follow. Also, the OSL properties of various minerals expected on Mars and of martian soil simulants and analogs will be discussed, including the properties of materials present in a simulated martian environment at low temperature. First, however, more in-depth introductions to TL and OSL dating, and martian geology will be given.

1.1. Introduction to Luminescence Dating

Luminescence dating is a specialized field of luminescence radiation dosimetry that is, in turn, part of the larger field of radiation dosimetry. Luminescence dating and radiation dosimetry exploit the fact that certain silicate materials store a record of the absorbed radiation dose in the material, and this information can be accessed by stimulating the sample either thermally or optically. Luminescence is emitted as a result of the stimulation, and the luminescence intensity is related to the absorbed dose. Luminescence dosimetry typically uses man-made materials such as aluminum-oxide doped with carbon (Al_2O_3:C) or lithium-fluoride doped with magnesium and titanium

(LiF:Mg,Ti), wheras luminescence dating takes advantage of naturally occurring dosimeters, such quartz and feldspars.

In either case, when these materials are exposed to radiation either in the environment or in the laboratory, atoms are ionized and the electrons and holes so liberated can subsequently become trapped at defects within the crystal structure (Figure 1.1 (b)). At some time after irradiation, the material can be stimulated either thermally (TL) or optically with appropriate wavelengths (OSL) and the trapped electrons are promoted to the conduction band (Figure 1.1 (c)). Some of the formerly trapped electrons then combine with trapped holes at recombination centers to produce luminescence, the wavelength of which is determined by the type of defect responsible for the recombination center (Figure 1.1 (d)). The emitted luminescence is then proportional to the trapped charge population and, therefore, the amount of radiation exposure.

The natural dosimeters used for TL and OSL dating are exposed to radiation in the natural environment in the form of alpha, beta, and gamma radiation from naturally occurring elements such as U, Th, and K as well as galactic cosmic rays. The absorbed radiation dose (absorbed energy/unit mass, measured in Gy=J/kg) accumulated as a result of this natural radiation can be determined in the laboratory through calibration, and the dose rate (Gy/year) can be measured in a variety of ways. Thus, the age of the sample can be determined by:

$$\text{Age(years)} = \frac{\text{Dose(Gy)}}{\text{Dose Rate(Gy/year)}} \tag{1.1}$$

assuming a constant dose rate over the age of the sample. It is important to note that the produced age is the time since the luminescence signal was last reset or zeroed. In the

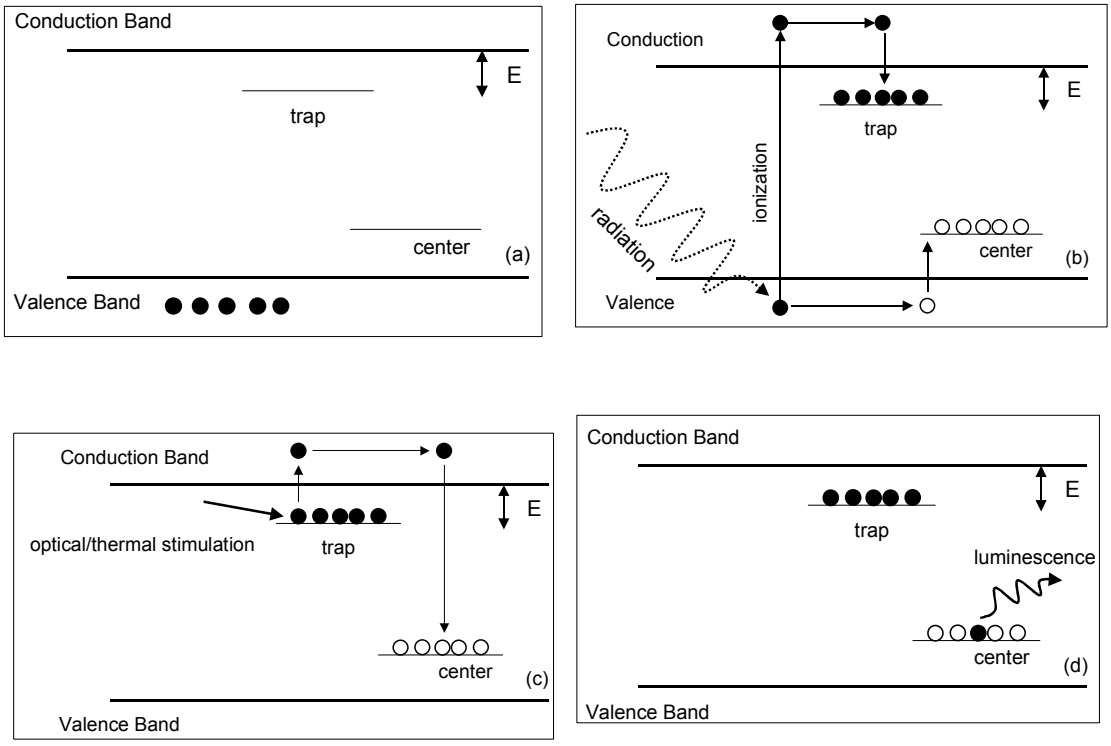

Figure 1.1 Band diagrams of the luminescence process: (a) crystal structure (b) irradiation and ionization of electrons and holes, (c) stimulation of electrons from traps, and (d) recombination of electrons with holes at a center to produce luminescence.

case of sediments, the resetting event is most often exposure to light during aeolian or fluvial transport, but the luminescence signal can also be reset by heating to a temperature sufficient to thermally empty the traps of interest, such as occurs in pottery manufacture.

Within this general concept of luminescence dating, there are several important aspects to be discussed. First, the electrons are not stored in the traps indefinitely. The probability per second of an electron escaping from a due to trap due to thermal stimulation can be described by λ (s^{-1})

$$\lambda = s * \exp(-\frac{E}{k_B * T}) \tag{1.2}$$

where s (s^{-1}) is the frequency factor which can be considered as the number of attempts to escape per second, E (eV) is the trap depth below the conduction band, k_B is Boltzmann's constant, and T (K) is the temperature. However, it is convenient to consider the average residence time of electrons in a trap or the lifetime τ (s)

$$\tau = \lambda^{-1} = s^{-1} * \exp(\frac{E}{k_B * T}). \tag{1.3}$$

The number of electrons remaining in a trap after some time t can then be given by the relationship

$$n = n_0 * \exp(\frac{-t}{\tau}) \tag{1.4}$$

where n is the number of electrons remaining and n_0 is the initial number of electrons (Aitken, 1985).

If we now consider that in natural samples the irradiation is continuous as opposed to laboratory experiments where the irradiation is more or less instantaneous, the fractional amount of charge lost during the age of the sample, t_s, is given by

$$\frac{n}{n_0} = \exp(\frac{1}{2} * \frac{-t_s}{\tau}), \tag{1.5}$$

and the lifetime of the trap needs to be about 10 times larger than the age of the sample for a 5 % loss of electrons. For natural materials, trap depths are usually 1-1.5 eV, and frequency factors are typically 10^9 to 10^{16} s^{-1} (Aitken 1985), leading to expected stable lifetimes of 3.5 x 10^5 to 1.4 x 10^{18} years at a storage temperature of 200 K (McKeever, 1985). This would correspond to possible maximum ages of thousands of years to millions of years.

The charge can be stimulated out of the traps in two ways. The first method exploits the previous relationship (Equation 4). As the temperature (T) is raised at a linear rate, the lifetime (τ) becomes smaller meaning that the electrons have a shorter residence time in the traps. The thermoluminescence (TL) signal is then proportional to the probability of escape multiplied by the number of traps remaining, or the number of traps remaining divided by the lifetime

$$\begin{aligned} TL &\propto n * \lambda = \frac{n}{\tau} \\ TL &\propto \frac{n_0 * \exp(\frac{-t}{\tau})}{\tau}. \end{aligned} \tag{1.6}$$

This leads to a TL glowcurve that rises rapidly with temperature to a characteristic or peak temperature and then decays with increasing temperature (assuming only one trap).

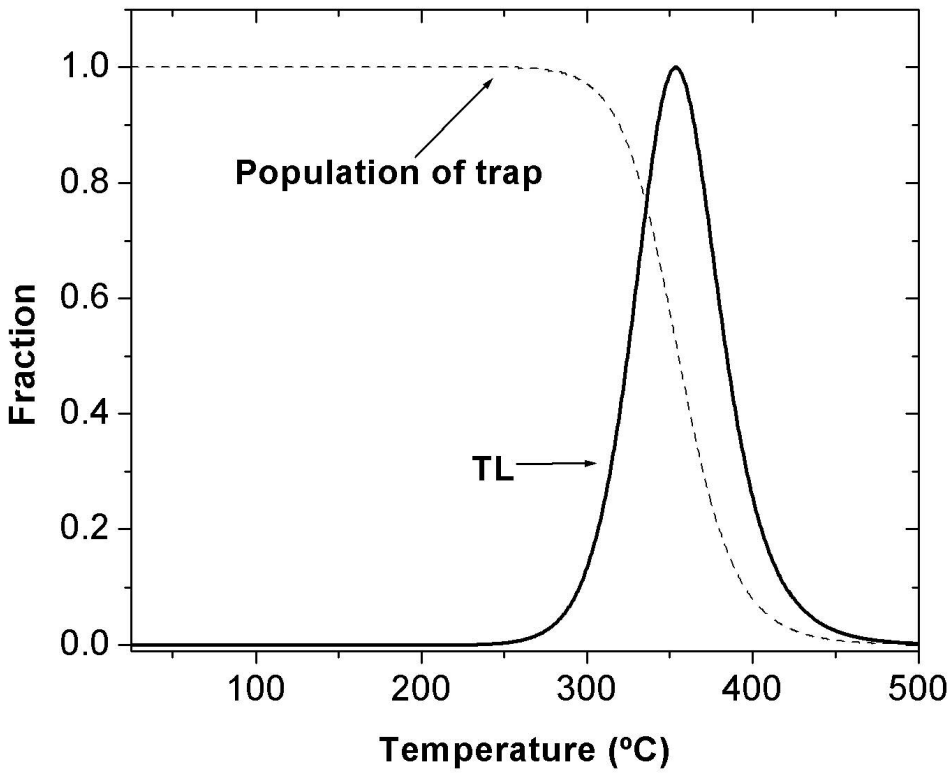

Figure 1.2 Simulation of a TL curve showing the TL curve (solid line) and the population of the trap (dashed line). The results have been normalized to the maximum values of each curve. The simulation was carried out using $s=10^{14}$ s^{-1} and E=1.7 eV as the parameters for the trap.

Figure 1.2 shows an example of a TL glowcurve along with the fraction of electrons remaining trapped.

The electrons can also be excited out of traps by optical stimulation if the light is of the appropriate wavelength. For electrons to be evicted from the traps by this method, the energy of the stimulation light must be equal to or greater than the trap depth. Thus, each trap has an associated photoionization cross-section $\sigma_0(\lambda)$ (m^2) and the optical excitation rate f (s^{-1}) is given by

$$f(\lambda) = \phi(\lambda) * \sigma_0(\lambda) \tag{1.7}$$

where $\varphi(\lambda)$ is the photon fluence (photons/m^2/s). The number of trapped electrons remaining (n) after time t is then given by

$$n = n_0 * \exp(-f * t) \tag{1.8}$$

where n_0 is the initial number of trapped electrons (Chen and McKeever, 1997). As the previous equation implies, the emitted luminescence decays exponentially for the simplest case of only one trap. However, there are several factors that can lead to non-exponential decay (at least not simple exponential decay) and even an initial rise in the OSL signal at the start of the stimulation. These circumstances will be explained as is necessary in the text. In general, the detection window for OSL must be chosen carefully so that the luminescence can be distinguished from the stimulation light.

Optical stimulation can also be carried out by a couple of different methods. In continuous-wave optically stimulated luminescence (CW-OSL), the sample is stimulated by light of a fixed wavelength (or a narrow range of wavelengths in the case of broadband sources) and power. This results in an exponential-like decay and is illustrated in Figure 1.3(a). CW-OSL was the first method of optical stimulation adopted

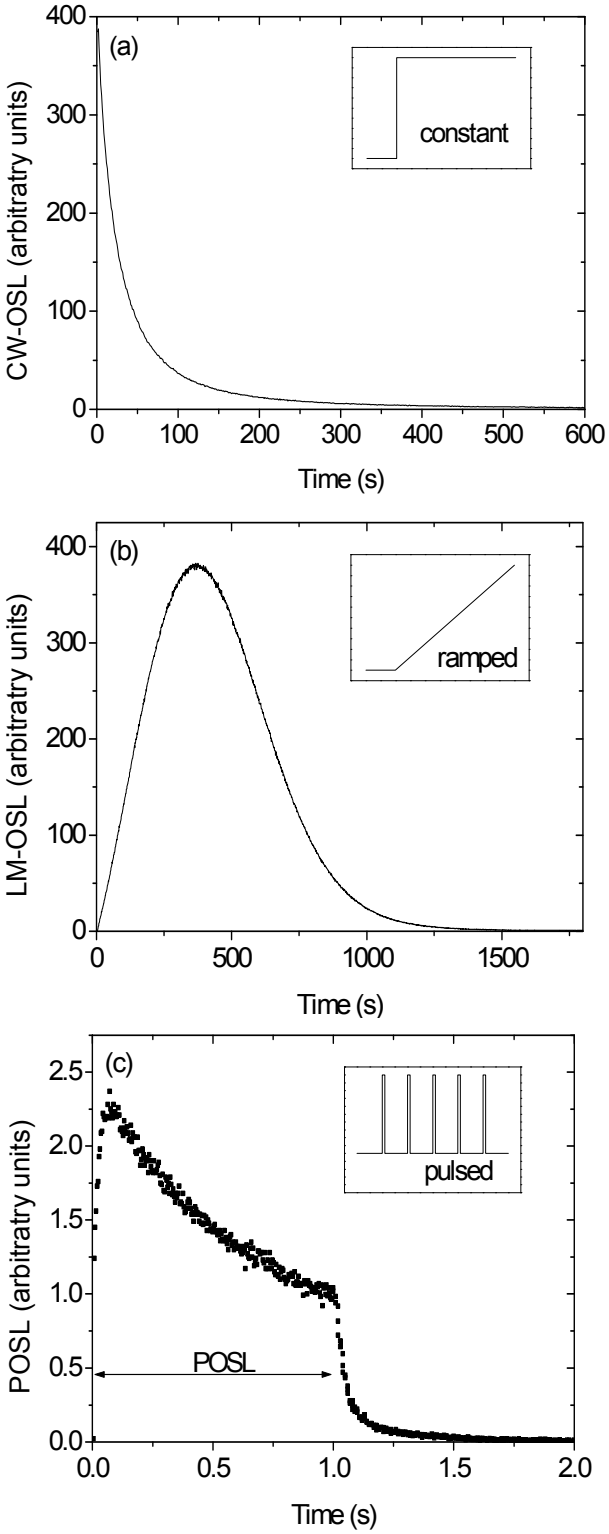

Figure 1.3 Examples of (a) CW-OSL, (b) LM-OSL, and (c) POSL. The insets show in what manner the stimulation was delivered. These results all are from Al_2O_3:C (graphs from Dr. Eduardo G. Yukihara, personal communication).

by Huntley *et al.* (1985) for dating sediments and continues to be the most popular choice for dating applications. Linearly modulated optically stimulated luminescence (LM-OSL) linearly ramps the optical power of the light resulting in a peak-shaped OSL curve where the peak is determined by the parameters of the trap (Bulur, 1996; Figure 1.3(b)). Later, it was shown that CW-OSL curves could mathematically be converted to LM-OSL curves (Bulur, 2000). Pulsed optically stimulated luminescence (POSL) uses pulses of laser light for stimulation and reads the luminescence signal between pulses eliminating the need for separate stimulation and detection windows (Figure 1.3(c)). This technique has produced very accurate results in personal radiation dosimetry as developed by OSU and Landauer, Inc (McKeever *et al.,* 1996; Akselrod and McKeever, 1999; Akselrod *et al.*, 2000). CW-OSL has been shown to be the most effective method of stimulation for OSL dating, and unless otherwise stated, all experiments in this work use the CW-OSL method.

When luminescence is emitted as in Figure 1.1 (c), the wavelength of the emitted luminescence is determined by type of defect responsible for the recombination center (e.g., blue/violet for silver impurities, or orange for manganese impurities) (Aiken, 1985). Thus, for a given material, a specific detection window is monitored. For natural materials used in dating applications, this is generally either a blue detection window using (for example) a BG-39 filter (transmits from 350-600 nm) or a UV detection window using a U-340 filter (transmits from 300-380 nm). For OSL experiments, separation of the stimulation and detection windows is a further consideration. Many OSL experiments use green or blue light stimulation, and the UV detection window is

therefore preferred. Some OSL dating techniques use infrared (IR) stimulation, and the blue window is then acceptable.

In general practice, luminescence dating uses automated systems to conduct experiments on a large number of samples. The experiments in this thesis, unless otherwise noted, use one of two Risø TL/OSL-DA-15 systems (Bøtter-Jensen *et. al.*, 2000). These systems can be programmed to perform TL and OSL measurements. The samples are placed on a 48-position carousel that delivers the samples to stations for the various processes. Both systems have $^{90}Sr/^{90}Y$ irradiation sources (delivering 0.112 Gy/s and 0.134 Gy/s respectively) for sample calibration. The samples can be thermally stimulated by linearly ramping the sample temperature, optically stimulated with blue LEDs (470nmΔ20nm), or with either an IR diode laser (830nmΔ10 nm) or an IR diode array (875 nm). Light collection is accomplished via a photomultiplier tube (PMT) with bialkali photocathode (Thorn-EMI 9235QA), and the appropriate filter pack can be placed in front of the PMT to limit the detection window. The entire system is controlled by the so-called "Minisys" which is a computer customized by Risø to run the TL/OSL reader. The Minisys is in turn connected to a desktop computer on which the various operations to be performed can be programmed.

1.1.1 OSL Methods of Absorbed Dose Estimation

Luminescence dating is concerned with finding two quantities, the equivalent dose D_e and the annual dose rate. Over the years, most research has focused on devising ways to measure D_e. The basic idea is to measure the natural luminescence signal from a sample, and then calibrate that sample's luminescence response to radiation to produce a dose response curve. Many methods have now been developed to determine D_e, and they

can be divided into two broad categories, namely multiple-aliquot methods and single-aliquot methods. An aliquot is simply a sub-sample, of typically 5-10 mg.

Multiple-aliquot methods

Multiple aliquot methods were first developed for TL dating and later adopted to OSL dating (Aitken 1985, 1998). Several aliquots (usually at least 20) are prepared from each sample and divided into 4 to 5 groups. The natural luminescence signal is measured from one group, and the average calculated to give the natural signal. The other groups can be treated in two different ways.

For the additive-dose method, the other groups of aliquots are given known radiation doses. The luminescence signal from the (natural + added) radiation dose is measured for each group, and the average for each group then calculated. The (natural + added) OSL signal is plotted against added dose and this results in a (natural + added) dose calibration curve. The curve is fitted, and extrapolation is used to find the dose-intercept which corresponds to the D_e as illustrated in Figure 1.4(a).

For the regenerative-dose method, all groups of aliquots (not including the natural group) first have their natural luminescence signals erased (either by heating or by bleaching), and known radiation doses are then given such that some doses are smaller than the natural dose and some doses are larger than the natural dose. The known radiation doses supposedly regenerate similar charge distributions as the natural irradiation and therefore similar luminescence signals. The regenerated luminescence signals can then be read and averaged for each group to produce a dose calibration curve. The calibration curve can be fitted and the natural dose interpolated rather than extrapolated as shown in Figure 1.4(b).

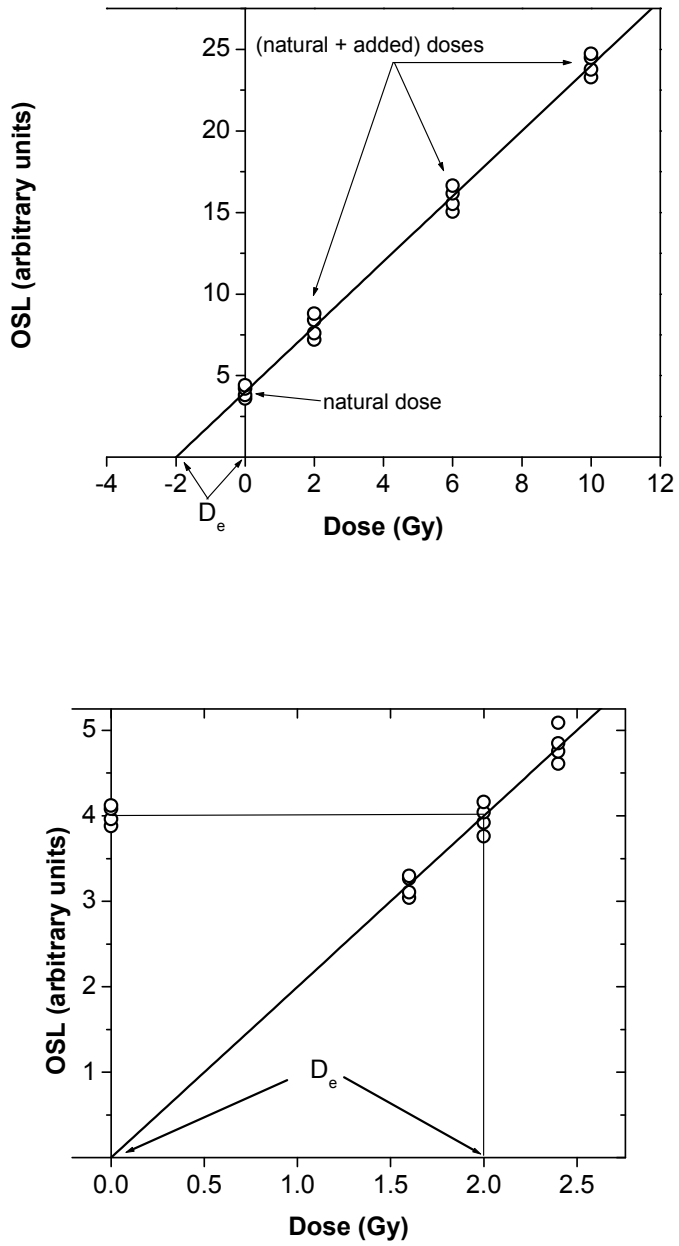

Figure 1.4 Examples of a multiple-aliquot (a) additive-dose procedure and a (b) regenerative-dose procedure. The graphs show the natural luminescence signal along with the signals from the calibration doses and indicate how the D_e is determined. The data has been simulated.

Each method has advantages and disadvantages. First, the methods require a large number of aliquots to produce one D_e; it is often difficult to produce multiple D_es. Before the advent of automated TL/OSL systems as described above, making multiple measurements on one aliquot involved intensive sample handling and long experiment times. Therefore, it was technically easier to use multiple-aliquot methods. Multiple-aliquot methods also require some sort of normalization between aliquots as the mass of each aliquot may vary as well as the number of luminescence grains per aliquot. Normalization can be accomplished by mass normalization (which can be tedious and does not account for a varying number of luminescent grains) or by using the initial decay of the natural OSL signal (the first 0.1 s) (Bøtter-Jensen *et al.*, 2003).

Multiple-aliquot methods include significant assumptions. All of the aliquots (and all of the grains on each aliquot) need to have been equally zeroed at deposition. In addition, each aliquot (or grain) needs to have been exposed to the same natural radiation dose, i.e., the dose rate was constant throughout the sample. If these conditions are not met, then multiple-aliquot methods produce some sort of an average D_e. Another implicit assumption is that all the aliquots (or grains) have the same luminescence sensitivity (luminescence produced per unit dose) and experience the same sensitivity changes. The sensitivity changes can be induced by either preheating or irradiation, and the sensitivity changes are usually specific to each aliquot or grain. Since each aliquot undergoes a limited number of irradiations and luminescence measurements, however (particularly in the additive-dose method), the chances of changing the luminescence sensitivity during the measurement procedure are reduced.

Single-aliquot methods

The advent of automated equipment and the increased use of OSL for luminescence dating made single-aliquot procedures both practical and advantageous. Single-aliquot procedures produce a D_e from each aliquot, reducing the amount of sample, sample preparation, and measurement time. In addition, since all the measurements are performed on the same aliquot, inter-aliquot normalization is not required further reducing both experimental time and uncertainty. Finally, single-aliquot procedures allow multiple D_e's to be easily produced, and the researcher can construct absorbed dose distributions for a particular sample. These absorbed dose distributions aid in identifying poorly bleached samples and/or aliquots and in the interpretation of the calculated ages.

The first single-aliquot work was performed on feldspars by Duller (1991). The work used both a regenerative-dose procedure and an additive-dose procedure. For the regenerative-dose procedure, the aliquot was first preheated to 220°C for 10 min to remove charge from unstable traps in the feldspar. (Preheating is often used in OSL dating procedures to remove any traps that are not stable over geologic time and will be discussed at length later.) The natural infrared-stimulated OSL signal was then read, and the aliquot was subjected to repeated cycles of laboratory irradiation, preheating, and OSL measurement as necessary to produce a calibration curve. Unfortunately, the samples tested exhibited large sensitivity changes (changes in luminescence per unit dose) due to the multiple irradiation, heating and stimulation cycles. The sensitivity changes were ascribed to "partial emptying of the trapped charge population," (Duller, 1991). As there was no known method at that time to correct for these sensitivity changes, the method was largely abandoned.

The additive dose procedure as developed by Duller (1991) involved using short (0.5 s) infrared-stimulated OSL measurements after each irradiation and a preheat to 220^{o}C for 10 min. Using a short infrared pulse enabled the total dose to be measured (natural dose plus added dose) without significant reduction of the trapped charge population. Although this method reduced sensitivity changes and improved the reproducibility of the measurements, a portion of the OSL signal is erased by each preheat to 220°C for 10 min. Consequently, a separate procedure had to be developed to correct for this loss of OSL.

A variation on this, called the single aliquot/regeneration and added dose (SARA) procedure, was proposed by Mejdahl and Bøtter-Jensen (1994). This procedure, as the name implies, combined the regenerative and additive dose methods. The method is not a true "single-aliquot" method since it actually requires four aliquots. Three aliquots are given radiation doses on top of the natural dose before reading the luminescence signal (a natural aliquot is not given a dose). A regeneration procedure is carried out to determine the natural dose plus added dose for each aliquot. The recovered dose is plotted against the added dose and extrapolation is used to determine D_e (Figure 1.5(a)). The method relies upon the assumption that all aliquots experience the same amount of sensitivity change, and that any sensitivity change is independent of dose. Initial tests indicated good agreement with independently dated materials.

Murray and Roberts (1998) developed a true single-aliquot procedure for quartz that also corrected for sensitivity changes. After preheating and measuring the natural OSL, the aliquot is subjected to several cycles of a regeneration dose (similar to the presumed D_e) and preheat. During each of these preheats, the TL is measured in order to

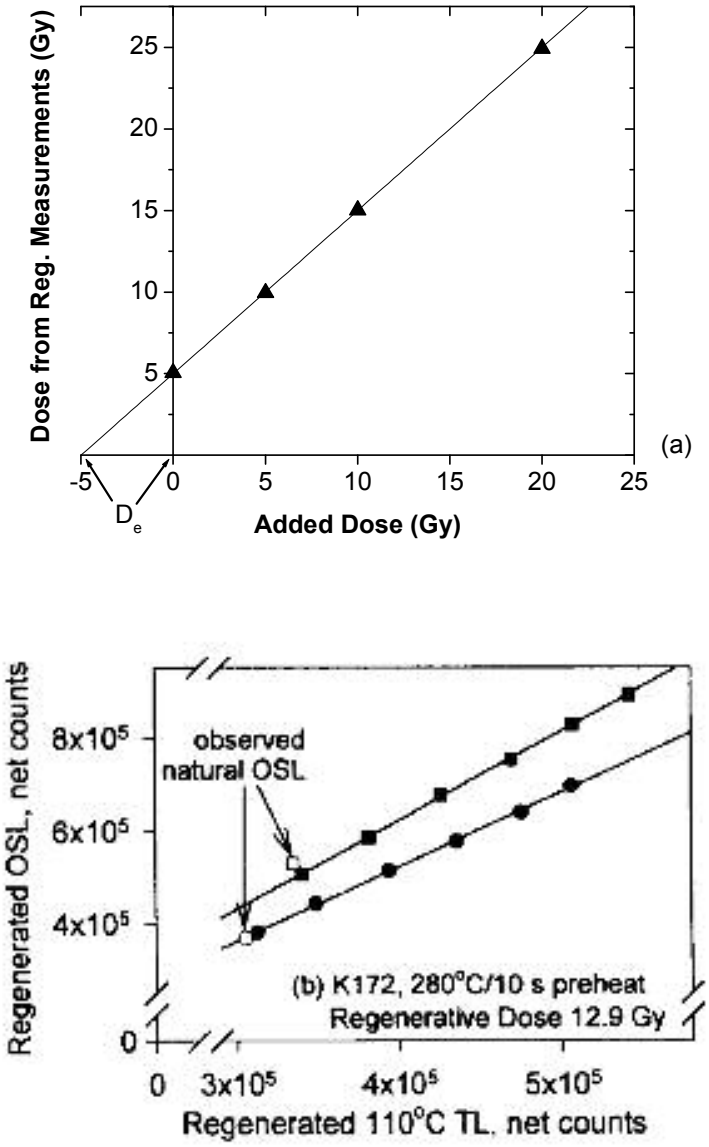

Figure 1.5 Examples of dose recovery procedures. (a) The SARA procedure where each point represents the recovered dose from a regeneration procedure from an aliquot with a (natural + added) dose. The graph of recovered dose vs. added dose can be extrapolated back to the x-axis to determine the D_e. The data is simulated. (b) An example of the single-aliquot procedure that uses the intensity of the 110°C TL peak in quartz to correct for sensitivity changes (from Murray and Roberts, 1998).

measure the intensity of the 110°C TL peak. The latter signal was shown in separate experiments to be proportional to the OSL sensitivity of quartz. The OSL signal is then plotted against the subsequent 110°C signal, and the data extrapolated back "to predict the natural OSL signal that would correspond to a dose" equal to the regeneration dose (Murray and Roberts, 1998). Since the natural OSL, regeneration dose, and equivalent natural OSL signal are known, the natural dose or D_e can be found by proportion (Figure 1.5(b)). Murray and Roberts (1998) also suggested that the aliquot can be given a small test dose after each regeneration OSL measurement, and the 110°C TL signal from this test dose can be used to correct for sensitivity changes. In this case, the regeneration OSL can be divided by the 110°C TL signal to produce a sensitivity-corrected calibration curve and natural signal, and the D_e can be extrapolated as in Figure 1.5 (b). Murray and Mejdahl (1999) used this latter sensitivity-correction procedure to show that D_es can be obtained that are in agreement with other procedures.

The above procedure is the basis for the single-aliquot regenerative-dose (SAR) procedure developed for quartz by Murray and Wintle (2000). The SAR procedure was later used to determine the accident dose in retrospective dosimetry (Banerjee *et al.*, 2000) and modified to be used with polymineral fine-grains (Banerjee *et al.*, 2001). The SAR procedure uses the OSL signal rather than the 110°C TL signal from a small test dose administered after the regeneration dose OSL measurement to monitor, and thereby correct for, any sensitivity changes that the sample experiences during the measurement. This sensitivity correction procedure was tested by repeatedly measuring the OSL signals from fixed regeneration and test doses, and plotting these signals against each other. If the correction is valid, the regeneration and test dose OSL signals should be proportional,

forming a straight line that passes through the origin. The SAR procedure again results in a sensitivity-corrected calibration curve, and the D_e can be interpolated from this curve. Table 1.1 lists the steps in the standard SAR procedure.

Note that two different heating procedures are used in the standard SAR procedure for the regeneration and test doses, i.e., the so-called "preheat" and "cutheat," respectively. The preheat consists of heating to a temperature T_P and holding at that temperature for a prescribed period t_P (= 10 s in Table 1.1). The cutheat merely consists of heating to a temperature T_C, and immediately cooling to room temperature. The cutheat temperature T_C is generally chosen so that only the optically active 110°C TL (the trap that produces a TL signal with a peak temperature of 110°C) trap is emptied, and hence the test dose OSL signal comes only from the 325°C TL trap which is the trap that gives rise to the natural OSL signal. Thus, it is assumed that the test dose irradiation and cutheat always give rise, "to the same trapped charge population," and any sensitivity changes are due to "changes in luminescence recombination probability," (Murray and Wintle, 2000). Although a cutheat temperature of 160°C is suggested, it was shown that recovered D_e had little dependence on T_C (Murray and Wintle, 2000).

Wallinga *et. al.* (2000a, 2000b) extended the SAR procedure to coarse-grain feldspars and attempted to recover known laboratory doses using the method. The heating regimen utilized a preheat of 290^{o}C for 10 s after the regeneration dose and a cutheat of 210^{o}C after the test dose. The authors found an underestimation of the known laboratory dose by 25 %. However, it is important to note that an independent test of the sensitivity correction procedure was not performed. Instead, a so-called "repeat point" (a fourth regeneration dose equal to the first regeneration dose) was added throughout the

1. Regeneration radiation dose (D_i)
2. Preheat at $T_P{}^oC^{\#}$ for 10 s
3. Measure OSL at 125^oC (R_i)
4. Fixed test radiation dose (TD_i)
5. Cutheat to $T_C{}^oC$ $^{\#}$
6. Measure OSL at 125^oC (T_i)
7. Repeat steps 1-6 for a range of regeneration doses including a repeat point and a 0 Gy Dose.
8. Find sensitivity-corrected OSL ($L_i=R_i/T_i$)

T_P and T_C determined from experiment

Table 1.1 The standard SAR procedure as defined by Murray and Wintle (2000). Note that different heating procedures are used after the regeneration dose (step 2) and test dose (step 5).

procedure and the recycling ratio (i.e., the ratio of the sensitivity-corrected values of the fourth and first regeneration doses) was monitored. Even though this ratio was near one (ideally, the ratio should equal 1), it still left open the possibility that the sensitivity correction yielded the same incorrect value both times. This discrepancy is important to note since the sensitivity-correction procedure was developed for quartz and not feldspathic materials.

On a separate set of samples, the same authors determined that the sensitivity changes were small and therefore they did not use a test dose normalization (i.e., no sensitivity correction). These samples yielded an underestimate of 27 +/- 11 %. The underestimations were explained by an increase in "the luminescence electron trapping probability" as a consequence of heating, despite the above-mentioned finding by these authors of small sensitivity changes. Also note that when sensitivity-correction was not used, the dose recovery errors were not significantly different than when correction procedures were used.

Further developments in single-aliquot regenerative-dose dating techniques, particularly with respect to feldspars, will be discussed in Section 2.

1.1.2 Anomalous fading

The discussion about the lifetime of charge in traps (bottom of page 5) while valid in many cases, does not apply to all materials. While attempting to use TL dating on feldspars from recent lava flows (5,000 to 50,000 years old), Wintle (1973) found that the TL curve after 3 days of storage was significantly less intense than the TL curve immediately after irradiation for traps that had theoretical lifetimes of the order of 10^5 years. This phenomenon was termed "anomalous fading." Wintle (1977) performed a

more detailed study of the fading from these materials and suggested several mechanisms, but no conclusion was reached as to the cause or remedy for anomalous fading.

Subsequent work on anomalous fading of feldspars has focused on two possible mechanisms to explain the phenomenon. The localized transition model involves closely spaced traps and recombination centers that share an excited state and hence a pathway exists for stable traps to be depleted of charge (Templer, 1986). Vicosekas (1985,1993) also proposed quantum tunneling as a possible mechanism to explain anomalous fading. This mechanism would require that a recombination center is in close enough spatial proximity to a trap that an electron has a finite probability of overcoming the energy barrier without any stimulation (either photons or phonons). Since the quantum tunneling model requires the close proximity of traps and recombination centers, a disordered lattice should show more fading. Experiments show this to be the case as high temperature feldpsars are more disordered and typically show higher rates of anomalous fading (Vicoseksas *et al.*, 1994).

The approaches to dealing with anomalous fading in luminescence dating can be grouped into three categories: removing anomalous fading, attempts to find stable signals, and correcting for anomalous fading. Assuming that anomalous fading was due to the localized transition model, Templer (1985) attempted to isolate stable signals from zircons. By storing the samples at an elevated temperature, electrons from any traps and recombination centers that share an excited energy level will recombine and leave only those trapped electrons that are stable. It was found that storage a 125°C for 2 days was sufficient to remove the unstable signal from these zircons while leaving the stable signal

unaffected. However, Spooner (1992) was not able to isolate a stable TL signal from feldspars after one month storage at 100°C and concluded that storage at elevated temperature could not be reliably used to eliminate anomalous fading in feldspars.

The first attempt to find a stable luminescence signal in feldspars used POSL techniques. Sanderson and Clark (1994) found that signals 40 ns – 8 μs after the laser pulse (470 nm) decayed the most, and signals that were either slower or faster did not show significant fading. Hence, by using POSL techniques, it should be possible to isolate a stable component. However, later work using IR stimulation (850 nm) was unable to distinguish a non-fading component (Clark *et al.,* 1997; Clark and Bailiff, 1998).

A second approach to isolating a stable luminescence signal in feldspars involves choosing a detection window that does not exhibit fading. Zink *et al.* (1995) found that while the typically-used blue window showed fading in the TL of many feldspars, the IR band (centered at 710 nm) does not show anomalous fading. Some effort was made to use the IR band for TL dating of feldspars (Vicosekas and Zink, 1999), but it was found that using the far-red (590nm to 750 nm) emission of feldspars to correct for fading in the blue (400nm to 590 nm) band was more effective (Vicosekas, 2000). The far-red luminescence signal has also been used to date feldspars and loess samples by infrared-stimulated OSL as this signal was found to not fade appreciatively (Lai *et al.*, 2002; Lai *et al.*, 2003; Fattahi and Stokes, 2003). Although these techniques appear to be very promising, it is technically somewhat challenging. Most PMTs that are sensitive in the far-red region require cooling to reduce the dark counts, and many optical stimulation

sources (particularly infrared sources) emit in the far-red region. Therefore, a careful choice of PMT type and filters for the stimulation source must be made.

Although Aitken (1995) cautioned against attempts to correct for anomalous fading, some progress has been made in this area recently. This approach to anomalous fading assumes that quantum tunneling is responsible for the loss of luminescence signal, and the signal therefore has a log (t) dependence. Huntley and Lamothe (2001) attempted to exploit the log (t) dependence of fading by measuring the amount of fading in K-feldspar aliquots after different storage periods using "short shines" (short OSL measurements). By plotting the fraction of OSL signal remaining versus log (t), they were able to calculate the fading rate and correct the measured D_es. However, the inaccuracies in the measurements made calculating slow fading rates difficult. Auclair *et al.* (2003) modified the SAR procedure in order to apply it to feldpsars (a further discussion of these modifications is in Section 2.2), and were able to very accurately measure fading rates. Using these fading rates, Auclair et al. (2003) were able to produce corrected ages that were in agreement with independent age controls. While this method of correction seems to be effective for young samples, it requires long storage times (up to a year) for the fading rates to be accurately measured.

1.2 Motivation for using OSL dating on Mars

Mars is often depicted as the most Earth-like planet in our solar system, yet it differs from Earth in several aspects. The atmosphere of Mars is very thin and does not contain much water. The current atmosphere of Mars contains the equivalent of 1 to 2 km^3 of ice, while Earth's atmosphere contains the equivalent of about 13,000 km^3 of ice (Zurek, 1992). The average ambient temperature on Mars is –63°C, with a large annual

variation of from –133 to 27 °C (Kieffer *et al.,* 1992). The weather patterns on Mars, while having some similarities to terrestrial weather patterns, are on a much more fierce scale. Wind on the planet creates huge dust clouds that often obscure the surface of the planet from observation (Albee, 2003). Yet, despite these and many other major differences between Mars and Earth, there are many aspects of martian geology that look familiar. The surface or Mars contains many depositional features that are good candidates for OSL dating.

1.2.1 Martian Fluvial Landforms

Although the current martian atmosphere does not support liquid water at the surface, there is evidence for a large amount of water on Mars. Most water currently on Mars is frozen in the polar caps, particularly the southern polar cap, in the form of "dirty water ice" or an ice and dust mixture (Titus, 2004). However, water on Mars was not always trapped in the polar regions. Evidence of fluvial features on Mars was first seen from the Mariner mission (Sagan *et al.*, 1973). More recent remote sensing and lander/rover missions to Mars have discovered an abundance of fluvial landforms.

Valley networks can be seen in many places on Mars (Figure 1.6). The valleys can range from long systems to small systems. The valleys were formed by fluvial action, but what type of fluvial action is unclear. The systems may have formed as a result of surface runoff, when runoff water concentrates and erodes the surface (Baker *et al.*, 1992). Alternatively, ground-water outflow may have undermined overlying rock and sediment to form the valleys (ground-water sapping) (Aharonson et al., 2002). In either case, most valley network systems are found in the Martian highlands and are thought to be 3.8 to 3.9 billion years old (Baker *et al.*, 1992).

Figure 1.6 Mars Orbiter Camera (MOC) image of valley network in Newton Crater on Mars. The valley may have been formed by liquid water, and the darker material may be sand that has since blown into the valley. The image was taken July 6, 2003 and is 2.3 km across (NASA/JPL/MSSS, MOC2-418).

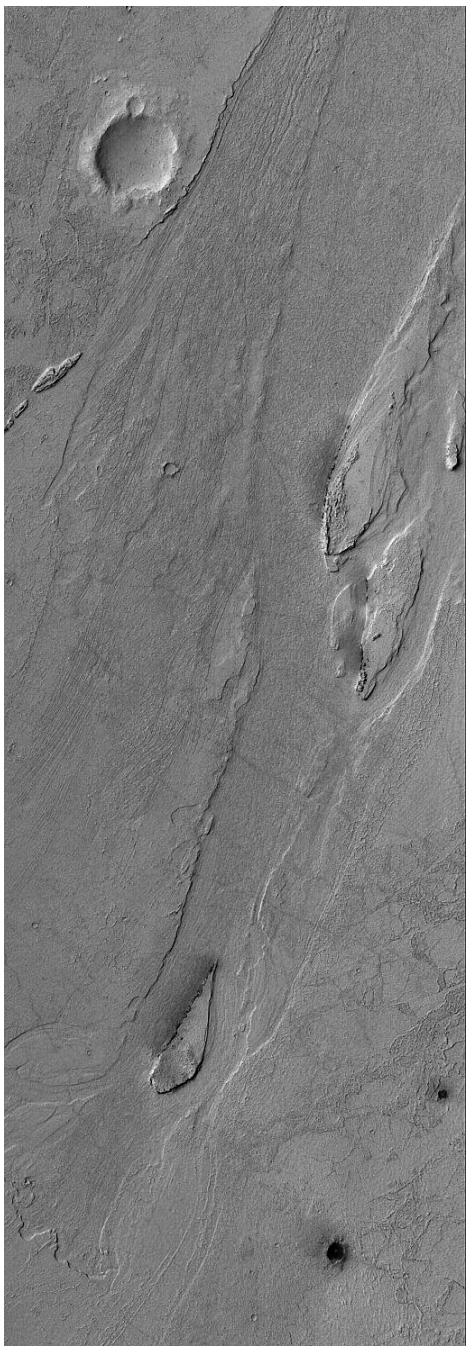

Figure 1.7 An example of an outflow channel in the Zephryia region of Mars from MOC. The picture covers an area about 3 km wide (NASA/JPL/MSSS, MOC2-941).

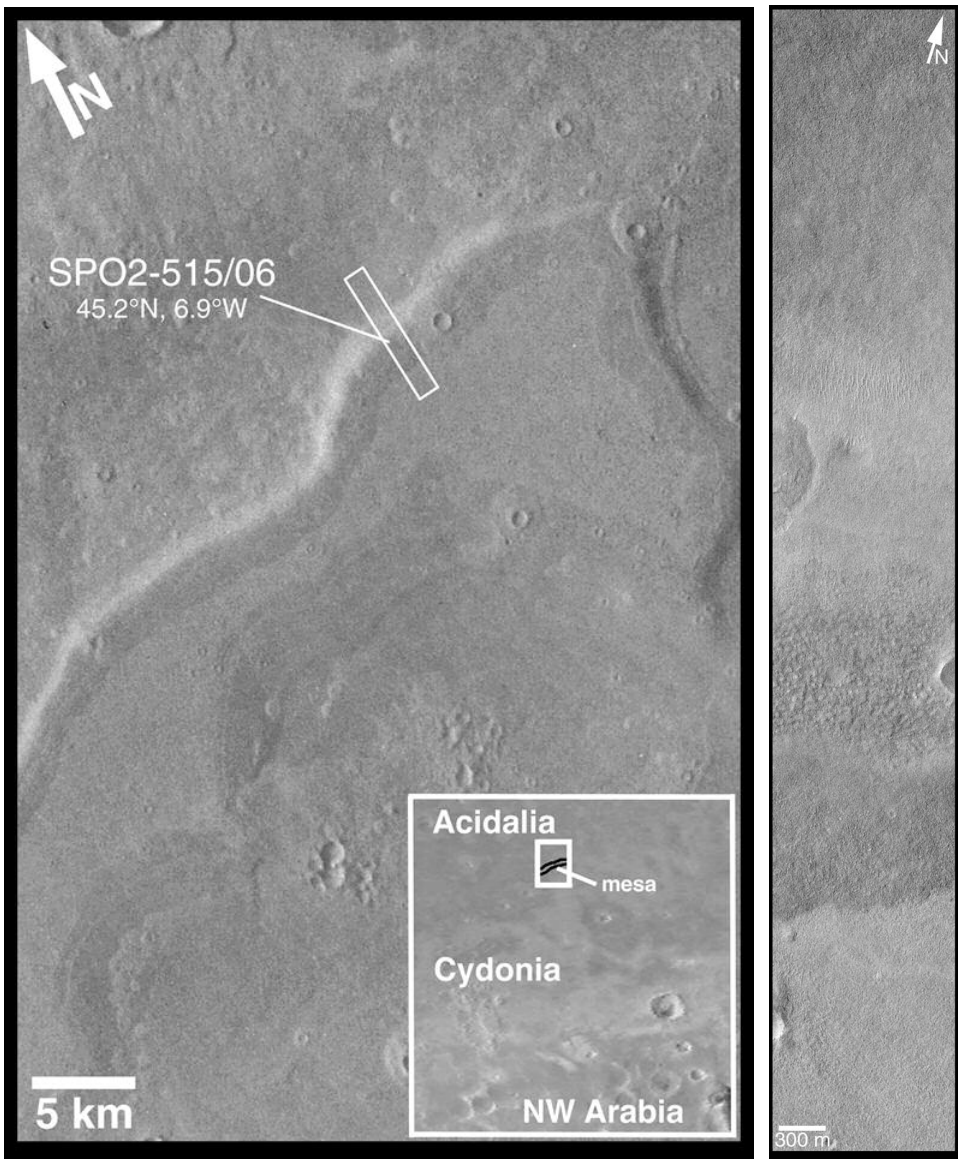

Figure 1.8 Possible shoreline feature in Acidalia Planitia on Mars (NASA/JPL/MSSS, MOC2-183). On the left is a wide angle view of the potential shoreline, and on the right is a narrow angle picture of the area in the white box.

Figure 1.9 MOC image of gullies on the side of a mesa in the south polar region. The dark material is probably wind-blown sand indicating that these gullies are relatively young (NASA/JPL/MSSS , MOC2-866).

Evidence for large amounts of flowing water can be seen in martian outflow channels (Figure 1.7). These channels are massive by terrestrial standards, and range up to 100 km wide and 2000 km long, with definite indicators of fluid flow such as bedforms (Baker *et al.*, 1992). Although numerous explanations have been offered for the formation of the outflow channels, including the flow of liquid hydrocarbons, lava, glaciers or ice streams, air (wind), and mud, only cataclysmic flooding accounts for all of the features of these channels (Baker *et al.*, 1992). Yet, the conditions under which these cataclysmic floods could have taken place is unclear, and it has been suggested that such floods could have occurred in the recent geological past or even under present martian conditions (Rodriguez et al., 2005). Due largely to the uncertainty of the formation mechanism, the ages of the outflow channels are uncertain and could range from 3.5 billion years ago to the present time (Doran *et al.*, 2004).

The possibility that lakes or oceans once existed on Mars was first suggested based upon Viking images (Parker *et al*. 1989, 1993). The same features that prompted this suggestion were later photographed by the Mars Orbiter Camera (MOC) aboard the Mars Global Surveyor (MGS) (Figure 1.8). A narrow angle image of this feature shows light and dark bands (the right image in Figure 1.8) that are most likely outcropping or layers of different rocks that have been exposed. The age of these fluvial features are important for ascertaining the possible habitability of Mars, and while the ages are unknown, any oceans on Mars are expected to date to the earliest history of the planet (Doran *et al.*, 2004).

Not all of the apparently fluvial landforms on Mars are assumed to be ancient. MOC images have revealed apparent gullies (Figure 1.9) on the walls of craters and

martian valleys in high latitude regions of Mars (Malin and Edgett, 2000). Although the origin of these gullies are unknown, the most likely explanations are overland flow, headward sapping, and debris flow- all of which involve water. These features are assumed to be recent features based upon appearance, are in areas with few or no craters, and are sometimes seen superimposed by dune fields (Doran *et al.*, 2004). While the fluvial origin of these features is fairly certain, it causes conflicts with the current understanding of the hydrological cycle on Mars and may require a refinement of some current notions.

1.2.2 Martian Aeolian Landforms

While the surface of Mars has been shaped by potentially recent fluvial events, the present landscape of Mars is known to have been largely defined by wind activity. Aeolian activity seems to have been the dominant geological force on Mars since shortly after its formation and the period of heavy cratering, and this activity is apparent in eroded craters, yardangs (bedrock that has been eroded by windblown sand), sand sheets, and sand dunes (Albee, 2003), as well as the global dust storms and dust devils for which Mars is well-known (Greeley *et al.*, 1992). These features represent potential OSL dating events.

Sand dunes are probably the most recognizable aeolian feature on Mars. These dunes are probably composed of 100 μm or smaller grains that are transported mainly by saltation. In saltation, grains are lifted (maybe 10 to 20 cm) by surface sheer stress from the wind and transported downwind (approximately 1 m) as they fall back to the ground. At this point, the grains can either bounce back into the air to be transported downwind again, or eject smaller dust-size grains into the wind that can then be carried along in

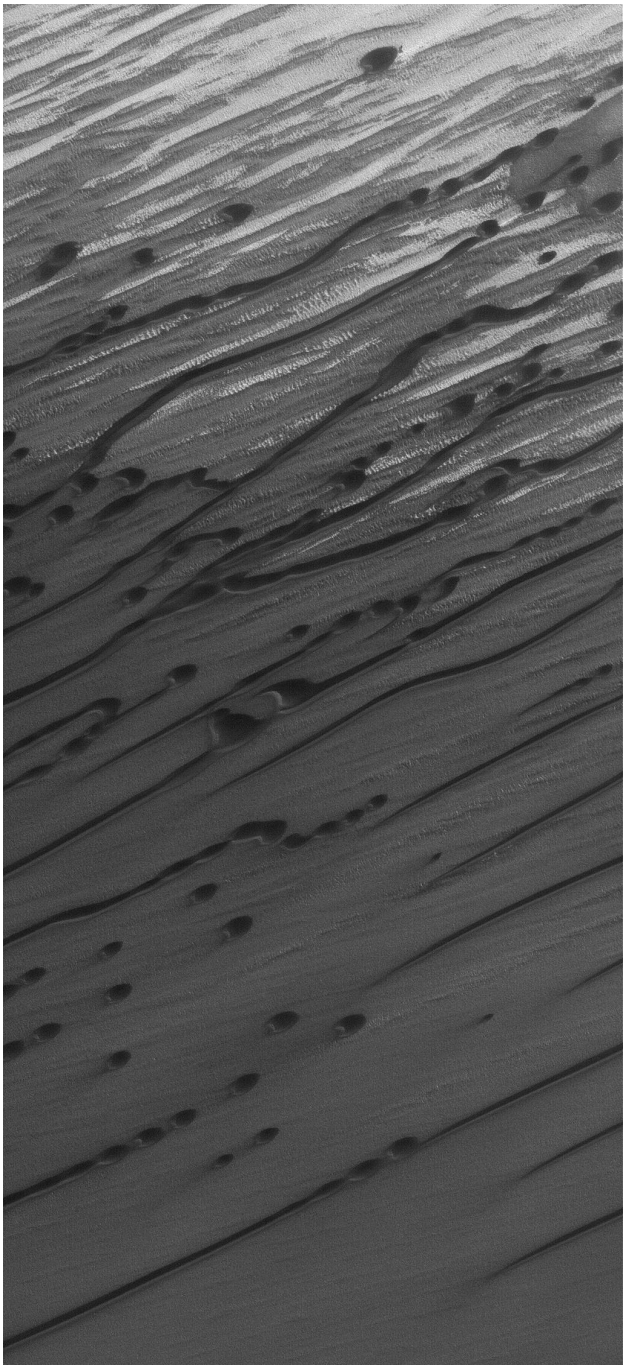

Figure 1.10 MOC image showing dunes in Chasma Boreale in the north polar region of Mars (NASA/JPL/MSSS, MOC2-1046).

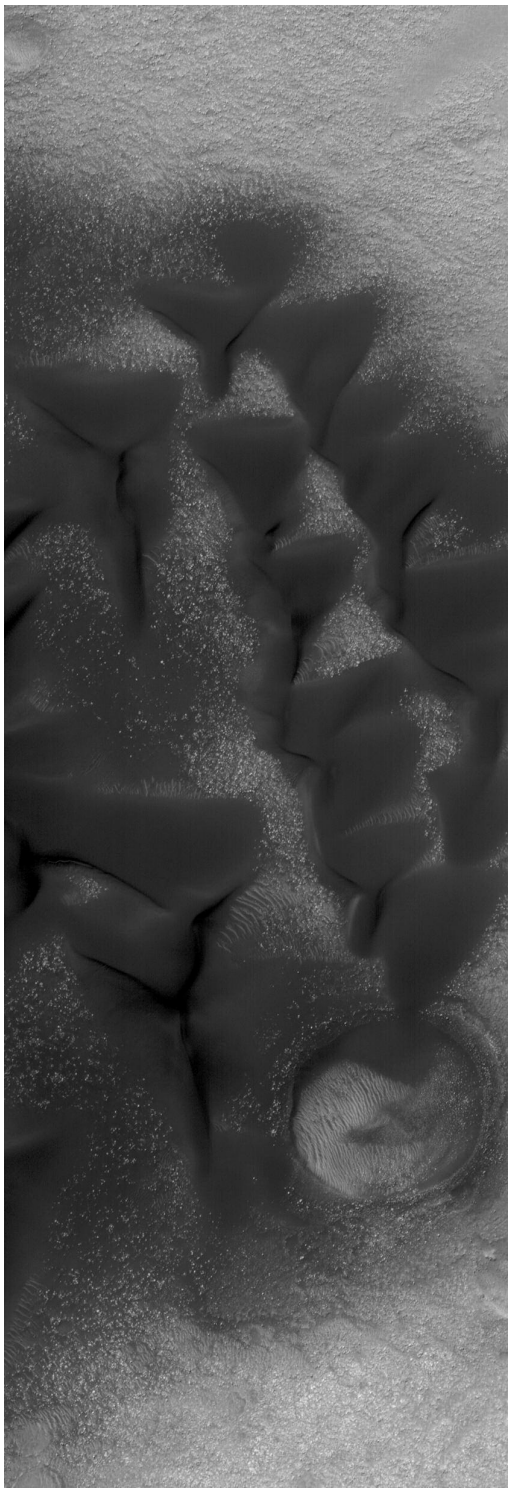

Figure 1.11 MOC image of dunes in Noachis Terra (NASA/JPL/MSSS, MOC2-998).

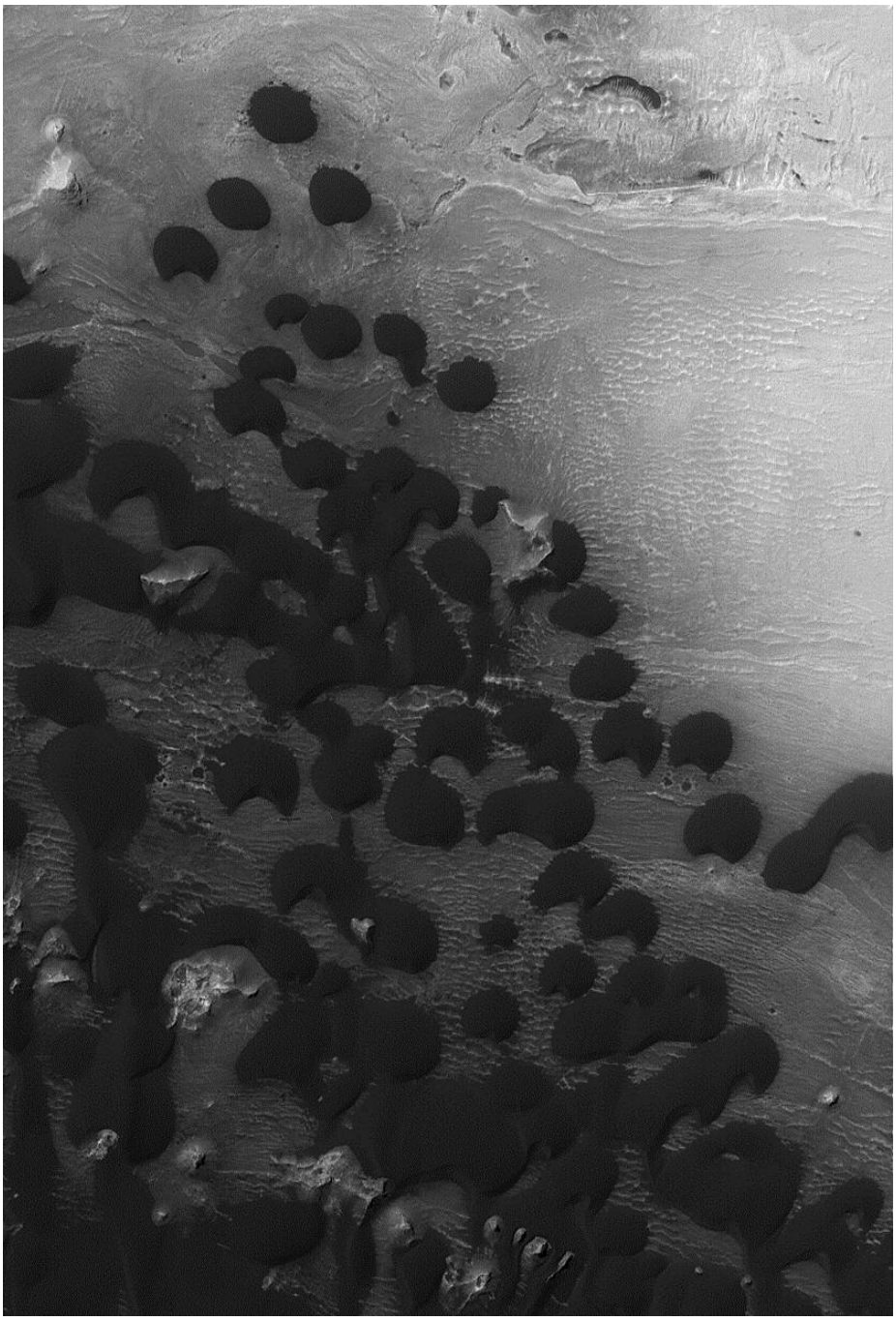

Figure 1.12 Intercrater dunes in Arabia Terra (NASA/JPL/MSSS, MOC2-984).

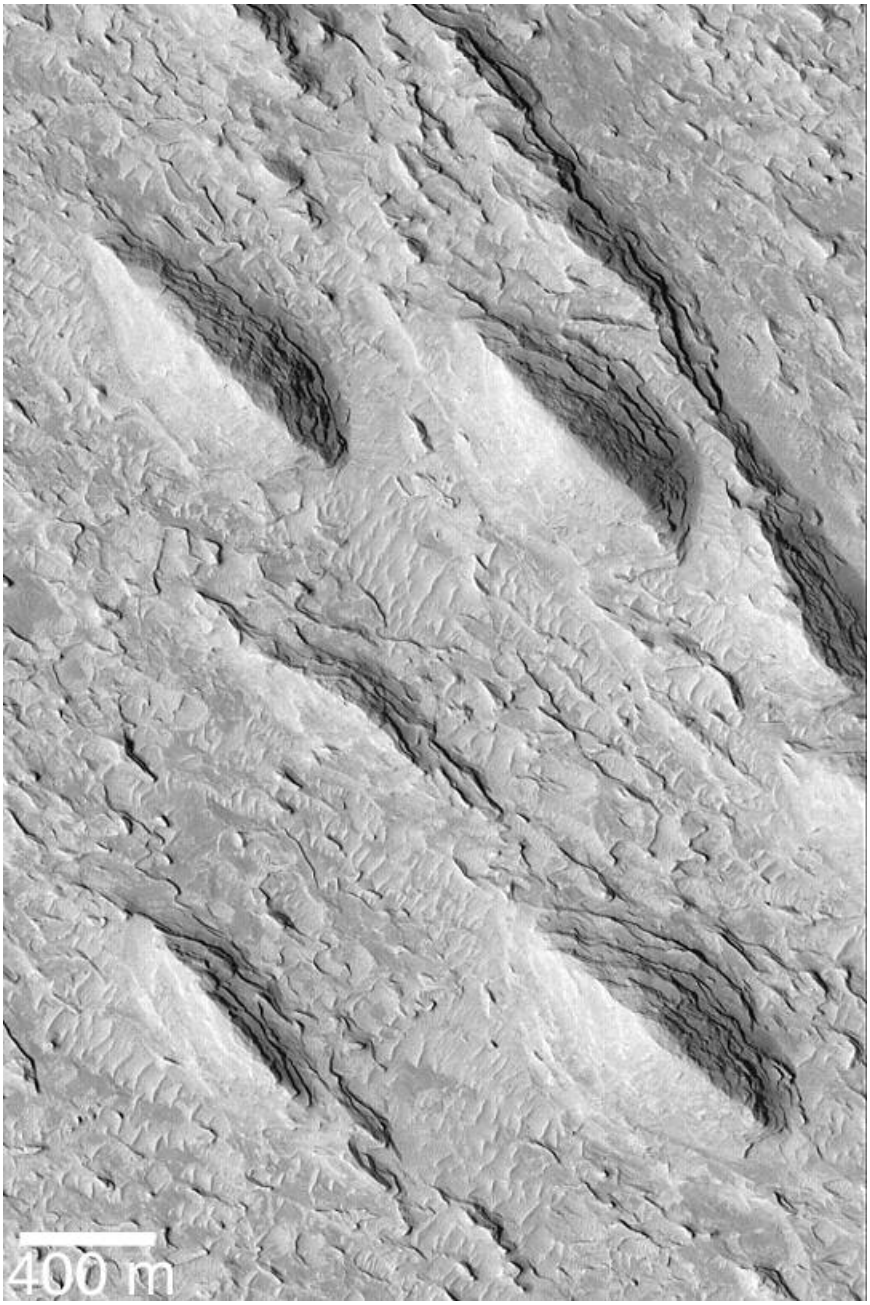

Figure 1.13 Yardangs in the Aeolis region of Mars (NASA/JPL/MSSS, MOC2-443).

suspension (Greeley, 1992). This mechanism has produced dunes in three main areas of Mars: a belt around the north polar ice cap (Figure 1.10), in the high latitudes of the southern hemisphere (Figure 1.11), and within craters in the southern hemisphere (intercrater dune fields, Figure 1.12). The dunes in the northern hemisphere indicate that the dominant wind direction is easterly north and westerly south, while the southern hemisphere dunes are more complex and are affected by local topography and complex wind patterns (Greeley *et al.*, 1992).

Complex wind patterns are also responsible for eroding many craters on the surface of Mars. This erosion often exposes outcropping of bedrock layers (Edgett and Malin, 2000; Pelkey *et al.*, 2004), deposits windblown material in specific areas of craters (Pelkey et al., 2003; Kuzmin *et al.*, 2001), and creates dunes and ripple like features (Pelkey et al., 2003; Zimbelman, 2003; Kuzmin *et al.*, 2001). At least some of the erosion and deposition appears to be occurring presently, and such crater deposits could represent an almost continuous record of the aeolian activity and atmospheric conditions on Mars.

Other examples on Mars of identifiable aeolian landforms include yardangs, which can be found in many areas of Mars including the Amazonis, Olympus Mons, Aeolis (Figure 1.13), Ares Valles, and Iapygia regions (Greeley *et al.*, 1992) and the north and south polar regions (Howard, 2000). Wind activity is also responsible for aeolian grooves and troughs in the equatorial and north and south polar regions (Greeley *et al.*, 1992; Howard, 2000; Bridges and Herkenhoff, 2002; Koutnik *et al.*, 2005), and wind streaks (areas where material has apparently been removed by wind) are often

associated with these features (Howard, 2000). All of these aeolian features can be chronologically dated via OSL dating.

1.3 Challenges to Developing OSL Dating for Mars

The previous sections have given a brief overview of the principles of OSL dating (Section 1.1) and geological features on Mars that are good candidates for in-situ OSL dating techniques, but many issues need to be addressed prior to OSL dating techniques being effectively applied to martian deposits. First, the soil on Mars contains different minerals than the soil on Earth with presumed little or no organic material. Many martian minerals may have the requisite properties for OSL dating, but they need to be tested and their properties characterized. Also, due to the constraints of space travel and exploration, chemical separation of minerals may not be possible with an in-situ instrument. As a result, OSL dating will need to be carried out on samples containing multiple minerals (polymineralic), and an OSL dating procedure has not currently been established for any mixture of minerals.

Second, the temperature regime of Mars is very different from that on Earth. The average temperature at the surface of Mars is –63 °C with a global range of –133°C - 27 °C (Kieffer *et al.,* 1992). This temperature regime could result in OSL properties very different from those normally encountered in terrestrial samples (see Chapter 4).

Finally, the radiation dose rate on Mars is much higher than on Earth and originates from different sources. On Earth, the natural radiation dose rate comes mainly from U, Th, and K within the soil with a much smaller component deriving from Galactic Cosmic Rays (GCR). However, on Mars, the GCR rate is much higher due to a thinner atmosphere and lower magnetic field, while the dose rate due to radioactive minerals is

thought to be lower based upon studies of martian meteorites. The method of determining the radiation dose rate on Mars and appropriate radiation calibration techniques have not been identified at this time. Each of these challenges will be discussed in more detail in the following sections.

1.3.1 Mineral Composition

In terrestrial applications, OSL dating requires separation of specific minerals from sedimentary deposits. Quartz (SiO_2) is usually preferred, since the mineral does not exhibit anomalous fading (Section 1.12), but feldspar minerals ($(K,Na,Ca)AlSi_3O_8$) and zircons ($ZrSiO_4$) are often used (Aitken, 1985, 1998). However, the Thermal Emission Spectrometer (TES) (Christiansen *et al.*, 1992, 2001) aboard the Mars Global Surveyor (MGS) generally has not detected any quartz in the martian soil (Bandfield, 2002). Furthermore, while feldspars are abundant in the regolith of Mars, the type of feldspars are not the type that are generally employed for terrestrial OSL dating.

Several materials have been suggested for martian soil analogs and simulants. Small pieces of the martian crust have been found on Earth in the form of meteorites (Kerr, 1987). While these martian meteorites are the only martian regolith on Earth and some OSL characterization studies have been conducted on them (see Chapter 3), the meteorites are typically cumulates and do not match well with the spectral characterization of the martian surface (Bandfield, 2002). Based upon reflectance spectra, soil from the Pu'u Nene volcano on Mauna Kea, Hawaii has been selected as a martian soil simulant and named JSC Mars-1 (Allen *et al.*, 1998). JSC Mars-1 is composed of altered volcanic ash and very closely matches the reflectance spectra of the bright regions of Mars with the exception of absorption bands for OH and H_2O. The soil simulant

consists of magnetic and non-magnetic fractions, both of which are made up of feldspar, magnetite, pyroxene, olivine, and volcanic glass. The magnetic fraction has a larger proportion of magnetite (Allen *et al.*, 1998). The simulant is available for scientific research, and the OSL properties of the material are described in Chapter 3. Although JSC Mars-1 closely matches the reflectance spectra of martian regolith, it was chosen based upon limited data.

More recent data from the TES instrument aboard MGS has suggested slightly different mixtures of minerals for analogs of martian soil. Spectra from these instruments distinguish two different types of regolith on Mars, namely Type I (basaltic mineralogy) and Type II (andesitic mineralogy). Both types of regolith, according to TES results, are composed of plagioclase feldspars, pyroxenes (primarily augite and diopside), and hematite, and the Type II material contains an abundance of obsidian or volcanic glass (Bandfield *et al*., 2000; Bandfield, 2002). Based upon these results, two mixtures of martian soil simulants have been created in the OSL dating laboratory at OSU by Dr. Regina Kalchgruber (personal communication). The compositions of these mixtures is given in Table 1.2.

More detailed descriptions of the mineral composition of the martian regolith can be obtained by studying the TES spectra along with results from the Thermal Emission Imaging System (THEMIS) on Mars Odyssey (Christensen *et al.*, 2004), and the Miniature Thermal Emission Spectrometers (Mini-TES) on the Mars Exploration Rovers (Christensen *et al.*, 2003). The above TES studies identified only the broad categories of plagioclase feldspars and pyroxenes, and several specific minerals can fall into these categories. The term plagioclase feldspars refers to a group of feldspar minerals that fall

Group/Mineral	OSU Mars-1 (%)	OSU Mars-2 (%)
Quartz		
K-feldspar		
Plagioclase Bytownite Andesine Labradorite	65	45
Pyroxene Augite Diopside	30	10
Obsidian		40
Hematite	5	5

Table 1.2 Mineral abundances of two mixtures (named OSU Mars-1 and OSU Mars-2) of Mars soil simulants. The table lists mineral groups that may be present on Mars and the percentage of each mineral group in each type of mixture. The plagioclase feldspars were equal parts bytownite, andesine, and labradorite, and the pyroxenes were equal parts augite and diopside. These mixtures were created in the OSL dating laboratory at OSU by Dr. Regina Kalchgruber and are based upon the results in Bandfiled *et al.* (2000), Bandfield (2002), and Milam (2004).

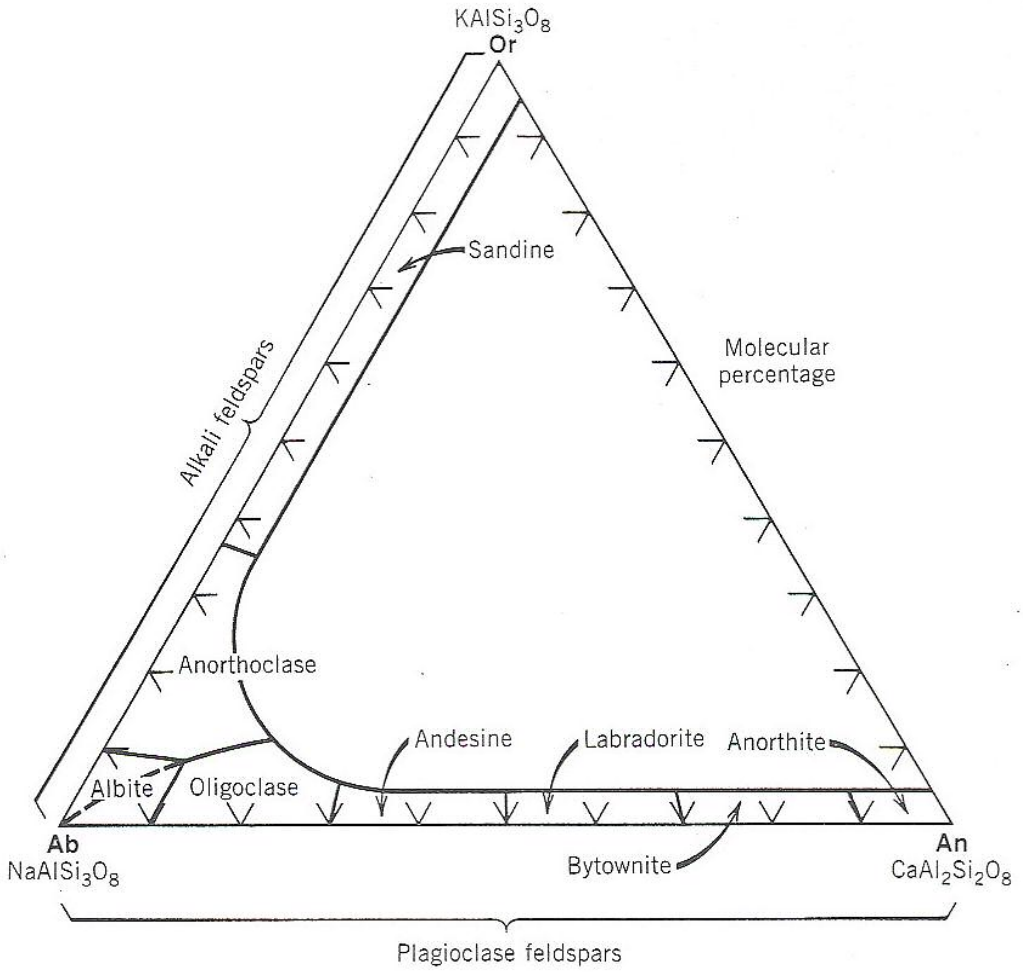

Figure 1.14 Ternary diagram of feldspars showing both the plagioclase and alkali feldspars. Terrestrial OSL dating typically uses alkali feldspars or plagioclase feldspars that are more sodic. However, feldspars on Mars are more calcic. (Reproduced from Klein and Hurlbut, Jr., 1993).

between $CaAl_2Si_2O_8$ (anorthite) and $NaAlSi_3O_8$ (albite) on the ternary diagram of feldspars as opposed to the alkali feldspars that fall between $NaAlSi_3O_8$ and $KAlSi_3O_8$ (orthoclase) (Figure 1.14; Klein and Hurlbut, Jr., 1993). By studying the spectra produced by all three of the previously mentioned instruments, Milam *et al.* (2004) were able to determine that the plagioclase feldspars on Mars are mostly of calcic composition, and as a result the feldspars used in the above mentioned "martian mixtures" are equal parts bytownite, andesine, and labradorite, each obtained from Ward's Natural Science Establishment, Inc., USA. This particular composition is important from an OSL dating standpoint as most terrestrial OSL dating applications that use feldspar minerals use alkali feldspars that are dominated by K-feldspars. As such, the OSL properties of more calcic plagioclase feldspars are poorly understood and require further study (see Sections 2.2, 3.3, and 3.4).

1.3.2 Polymineral samples

As previously mentioned, terrestrial OSL dating is usually carried out on mineral separates. Working with only one mineral type (i.e., quartz, k-feldspar) is technically simpler as the measurement procedures can be tailored to the particular mineral type and the associated errors are reduced. Unfortunately, due to the restrictions of remote spacecraft operation, chemical mineral separation will probably not be possible on an in-situ OSL dating instrument on Mars. As a consequence, procedures must be developed to estimate the natural dose from polymineral samples.

No OSL dating procedures have been developed for dating polymineral samples, especially polymineral samples composed of undetermined minerals. However, some research has been conducted on isolating a quartz-dominated signal in the presence of

feldspar minerals. Banerjee *et al.* (2001) modified the SAR procedure for polymineral fine-grains, where chemical separation is not possible, by first stimulating with infrared light then stimulating with blue light (the so-called post-IR blue stimulation sequence). The IR stimulation reduces the influence of the feldspar grains while leaving the quartz grains unaffected, and the blue stimulation then produces an OSL signal that is quartz dominated. This same procedure was used successfully by Roberts and Wintle (2003) for polymineral fine-grains, and by Wallinga *et al.* (2002) to extract a quartz-dominated OSL signal in the presence of feldspar contamination for coarse-grain samples. The effects of a post-IR measurements procedure as well as other modifications to the SAR procedure to adapt it to polymineral samples will be further explored in Chapter 2.

1.3.3 Temperature Regime

On Earth, most minerals that are dated by OSL dating are assumed to have been near room temperature (20°C) for the entirety of their storage period. However, on Mars the average ambient temperature is much lower (-63°C) with a large annual variation (-133°C to 27°C) (Kieffer *et al.*, 1992). For OSL dating purposes, a lower storage temperature such as on Mars can have profound implications for the procedures used to recover the natural radiation dose.

In the previously outlined OSL dating procedures (Section 1.1.1), a preheat is employed to isolate traps that are stable over the geologic time period of interest. These traps typically have a peak at ~300°C if the TL of the mineral is measured. However, at lower ambient temperatures, the normal dosimetric traps and other typically unstable traps could be geologically stable, and low temperature traps (with peak temperatures below 20°C) may become important in the charge trafficking process. Also, the

measurement temperature is often chosen so that it is higher than the peak temperature of optically-sensitive traps that do not contribute to the natural signal and have been emptied by the preheating procedure. In this case, charge liberated by optical stimulation cannot be retrapped by these unstable traps. Therefore, if minerals that have been stored at lower temperatures on Mars are to be used for OSL dating purposes, preheating procedures and temperatures and OSL measurement temperatures may have to be adjusted.

In addition, the optical stimulation process is temperature dependant. While optical stimulation is the primary way that charge is evicted from traps in OSL dating, the process can be thermally assisted (McKeever *et al.*, 1997b). If OSL is measured at a higher temperature the charge will be evicted more rapidly from the traps resulting in a faster OSL decay. On the other hand, if the optical stimulation or bleaching is carried out a lower temperature (e.g., -60°C on Mars), the process is less efficient. This could have an impact on both the dose recovery experiment and the time necessary to bleach the samples in nature.

The recombination process can also be temperature dependant. Many recombination centers are subject to thermal quenching whereby an increasing measurement temperature increases the probability of non-luminescent recombination (Bøtter-Jensen *et al.*, 2003). So, measuring OSL at a lower temperature could produce more luminescence per electron evicted from the traps. All these phenomena must be considered when devising a dose recovery procedure, and experiments to determine these parameters will be discussed in Chapter 4.

1.3.4 Natural Dose Rates on Mars

The focus of this dissertation is to develop a dose recovery procedure that can be used for OSL dating of martian sediments. However, this procedure only determines the numerator of the OSL dating equation (Equation 1). To use the OSL dating equation, the natural radiation dose rate (in mGy/yr) needs to be determined. On Earth, the contribution from radioactive elements within the soil can be determined by neutron activation analysis, high resolution gamma spectrometry, or use of Thermoluminescence Dosimeters (TLDS) (Aitken, 1998), and the contribution from Galactic Cosmic Rays (GCR) can be calculated based upon the geographical location and depth of the sediments (Prescott and Hutton, 1998). On Mars, however, the natural radioactivity from the soil cannot be directly measured (at least not by the same means that are used on Earth), and the GCR contribution to the natural radiation dose rate is not completely defined.

Some estimates of the dose rate on Mars do exist however. Martian meteorites have been studied to give an estimate of the natural radiation dose rate on Mars due to radioactive elements within the soil of 0.4 mGy/yr (Milekowsky *et al.*, 2000). While martian meteorites may not be wholly representative of martian soil (Bandfield, 2002), it is doubtful that this estimate is in gross error. Therefore, it is thought that the radiation dose rate on Mars due to radioactive elements is much lower than the corresponding rate on Earth (~2 mGy/yr).

However, the radiation dose rate due to GCR and Solar Particle Events (SPE) shows the opposite trend. Modelling of the martian atmosphere using the Mars Global Reference Atmospheric Model (Mars-GRAM 2001) and particle transport using a version of the HZETRN code (High Z (atomic number) and energy transport; Wilson *et al.*, 1995) indicates that the global average radiation dose rate at the surface of Mars is 51 mGy/yr

from GCR and 2.7 mGy/yr from SPE (McKeever *et al.*, 2003). This dose rate is to be contrasted with the dose rate due to cosmic rays on Earth of approximately 1 mGy/yr. Although the radiation dose rate due to cosmic rays does attenuate with depth in the regolith as shown in Figure 1.15, at a depth of 2 m the dose rate is only diminished by a factor of 2. Therefore, down to a depth of 2m, the natural radiation dose rate on Mars is dominated by the cosmic dose and ranges from 54 mGy/yr (at the surface) to approximately 27 mGy/yr at a depth of 2m. These estimates represent a global average and can be refined for the particular location of interest. In addition, the calculations will be improved through the data currently being produced by the martian radiation environment experiment (MARIE, http://marsprogram.jpl.nasa.gov/odyssey/technology/marie.html) on board Mars Odyssey and future such experiments that measure the cosmic ray dose at Mars.

The high flux of GCR and SPE on Mars presents another potential problem. Any OSL dating technique requires a radiation source for calibration purposes. Obviously, the radiation produced by this source covers a very small range of energy and is essentially a low linear energy transfer (LET) source. While the GCR and SPE spectrum does have a large LET range, 95% of the absorbed dose comes from particles with an LET less than ~10 keV/μm (Benton and Benton, 2001), and it is these low LET particles that give rise to the OSL signal. Therefore, using a single, low LET source such as an x-ray system is justifiable (McKeever *et al.*, 2003).

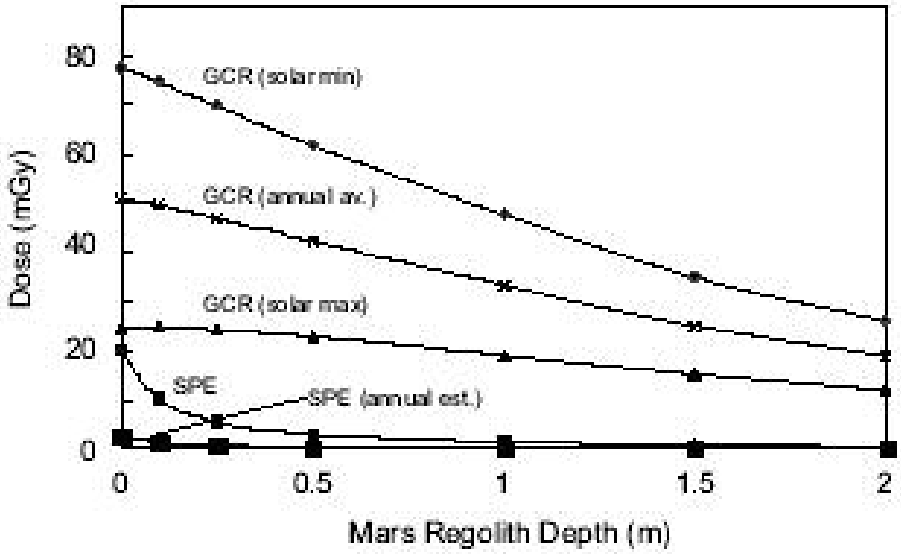

Figure 1.15 The attenuation with depth of GCR and SPE in the martian regolith. Note that even at a depth of 2 m the dose rate is reduced by a fact of ~2. (Reproduced from McKeever *et al.*, 2003).

CHAPTER TWO

DEVELOPMENT OF A SINGLE-ALIQUOT REGENERATIVE-DOSE POLYMINERAL OSL DATING PROCEDURE

As discussed in Chapter 1, a single-aliquot regenerative-dose procedure has already been developed for OSL dating of quartz (the SAR procedure; Murray and Wintle, 2000), and extended to polymineral fine-grain samples by Banerjee *et al.* (2001). However, on Mars, any OSL dating techniques will need to be able to measure the absorbed dose in polymineralic samples of varying grain size. Furthermore, most luminescent minerals on Mars may be feldspathic in origin, and attempts to use the SAR procedure with feldspars have been largely unsuccessful (Wallinga *et al.*, 2000a, 2000b). Therefore, a suitable single-aliquot regenerative dose procedure still needs to be developed for coarse-grain (larger than 10 μm) feldspars and polymineral samples.

Some work has already been attempted at developing such a procedure. Lamothe et al. (2001) suggested slight changes for the SAR procedure when determining equivalent doses for feldspars. The changes consist of making the cutheat equal to the preheat (both temperature and time) and bleaching with a solar simulator after each OSL measurement (Huot and Lamothe, 2003). The modified procedure has been used to study the fading rates of individual feldspars (Auclair *et al.*, 2003) and to study the luminescence of fractured feldspar grains (Huot and Lamothe, 2003). Although this modified SAR procedure has allowed the recovery of known laboratory

doses, the underlying assumptions of the sensitivity-correction procedure need to be tested, and the procedure applied to a suite of minerals (including polymineralic samples) if it is to be accepted as a suitable dose recovery technique for OSL dating on Mars.

2.1. Requisite Properties of a Single-Aliquot Regenerative-Dose Procedure

The basic elements and methods for the SAR procedure have been discussed in Section 1.1.1. The most important innovation of the SAR procedure is the built-in correction for sensitivity changes during the procedure. The major underlying assumption for the sensitivity-correction procedure is that the change in the OSL signal (or TL signal in earlier versions) measured after the test dose is an accurate measure of the sensitivity change exhibited by the OSL signal due to the regeneration dose. This assumption can be easily tested by performing repeated cycles of the SAR procedure with a fixed regeneration dose. If the test dose OSL signal (T_i) correctly measures the sensitivity changes of the regeneration dose OSL signal (R_i), the two signals will be directly proportional, i.e., plotting the regeneration dose OSL versus the test dose OSL will form a straight line that passes through the origin within uncertainty limits.

Once a test dose signal has been found that satisfactorily meets the above assumption, a few further assumptions of the SAR procedure can be tested. One goal of the SAR procedure is to build-up a sensitivity-corrected dose response curve. If the sensitivity-correction procedure is working correctly, the sensitivity-corrected OSL from any given dose can be measured at any point in the procedure. This leads to incorporating a "repeat point" in the SAR procedure (such as discussed in Section 1.1.1) where a small regeneration dose can be repeated at different points in the procedure. When the SAR procedure is used to recover the D_e from the linear portion of the dose

response curve, this repeat point is generally chosen to be equal to the first regeneration dose. For a full dose response curve, a repeat point within the linear region is generally chosen and repeated throughout the procedure. In either case, dividing the sensitivity-corrected OSL signal from the repeat point by the sensitivity-corrected OSL signal from the initial dose should yield a value near 1.0.

Dose response curves also highlight another advantage of the SAR procedure, although it is not necessarily a requisite property. Supralinearity has been observed in the dose response curves of many materials (Chen and McKeever, 1997) where a linear section of a dose response curve is followed by a section that has a greater-than-linear response (supralinearity) which is in turn followed by a section that exhibits less than linear response (sublinearity) until eventual saturation. Rather than interpreting supralinearity as an over response at high doses, it should be interpreted as an under response at low doses. At lower doses, competing traps that cannot be optically stimulated have not been completely filled and therefore trap some charge that would otherwise be trapped by the optically-active trap (or traps). At higher doses, the competing traps are saturated (or nearly saturated) and the optically-active traps become more effective at trapping charge. The subsequent OSL signals are more intense, producing the supralinear behavior (Kristianpoller *et al.*, 1974). However, Banerjee (2001) found that the sensitivity-correction within the SAR procedure removed the supralinearity from quartz dose response curves and produced linear to saturation (sublinear) curves. Such a dose response curve makes analysis and mathematical description much easier and improves the ability determine an absorbed dose.

Before a SAR-type procedure can be used to determine the radiation dose absorbed from the natural environment, the procedure needs to be tested by recovering a known laboratory dose. For this procedure, the aliquots to be tested are first bleached to remove any natural or residual signal. Then, a known dose is given to the aliquots in the laboratory, and this dose is treated in the same way as the natural radiation dose. Using a known dose delivered at a known dose rate eliminates many uncertainties involved in the dose recovery process of OSL dating such as uncertainties and/or fluctuations in the natural radiation dose rate, variability in atmospheric conditions, and incomplete bleaching at deposition. The SAR-type dose recovery process is then carried out to determine the laboratory ("natural") absorbed dose, and the recovered dose can be divided by the known dose to produce a dose recovery ratio. In general practice, the dose recovery ratio should be between 0.95 and 1.05 (in other words, a 5 % error) for the known dose to be successfully recovered.

The final test of any dose recovery procedure used in luminescence dating is recovering a natural dose. In the best scenario, the dose recovery procedure can be tested on samples that have independent age controls, i.e., the sediments or sediments from the same layer have been dated by another chronological dating method such as radiocarbon dating. If this final test is passed, the dose recovery procedure can be used for routine OSL or TL dating procedures.

2.2 Experiments with feldspars

As a first step to developing a polymineral dose recovery procedure, experiments were undertaken with various coarse-grain feldspars. The samples were first studied to determine under what conditions sensitivity change was or was not produced. Based

upon these results, several variations of the SAR sensitivity-correction procedure were tested, and dose response curves were constructed using these various methods. Finally, known doses were recovered using some of the variations of the SAR procedure.

2.2.1 Materials and Equipment

Five feldspar specimens were studied, namely: microcline, oligoclase, anorthoclase, albite, and andesine (obtained from Ward's Natural Science Establishment, Inc., USA). Figure 2.1 shows the positions of the samples on the feldspar ternary diagram. (Bytownite was also chosen, but initial experiments showed low luminescence sensitivity. Bytownite was therefore not investigated further.) Test chips of the samples were crushed using a mortar and pestle, and the grains were sieved to separate the 90-125 μm grain fraction. For luminescence measurements, the grains were deposited on stainless steel discs using silicone spray.

The experiments were carried out on the two Risø TL/OSL-DA-15 systems (Bøtter-Jensen *et. al.*, 2000) described earlier in Section 1.1. Although experiments were conducted using both systems, all reported data except infrared-stimulated dose response curves were obtained with the system utilizing an IR diode laser (830nmΔ10 nm, ~400 mW/cm^2). Luminescence detection was made through Hoya U-340 filters of 7.5 mm total thickness, which transmit mainly between 270-390 nm. The detection window was chosen since an eventual goal of the study is to apply the developed techniques to quartz and polymineral samples. The heating rate for all experiments was $5^oC/s$. Blue-stimulated OSL measurements were carried out at 125^oC (again, this temperature was chosen as future plans are to use the methods with quartz and mixtures of quartz and other materials); infrared-stimulated OSL measurements were performed at 60^oC. The

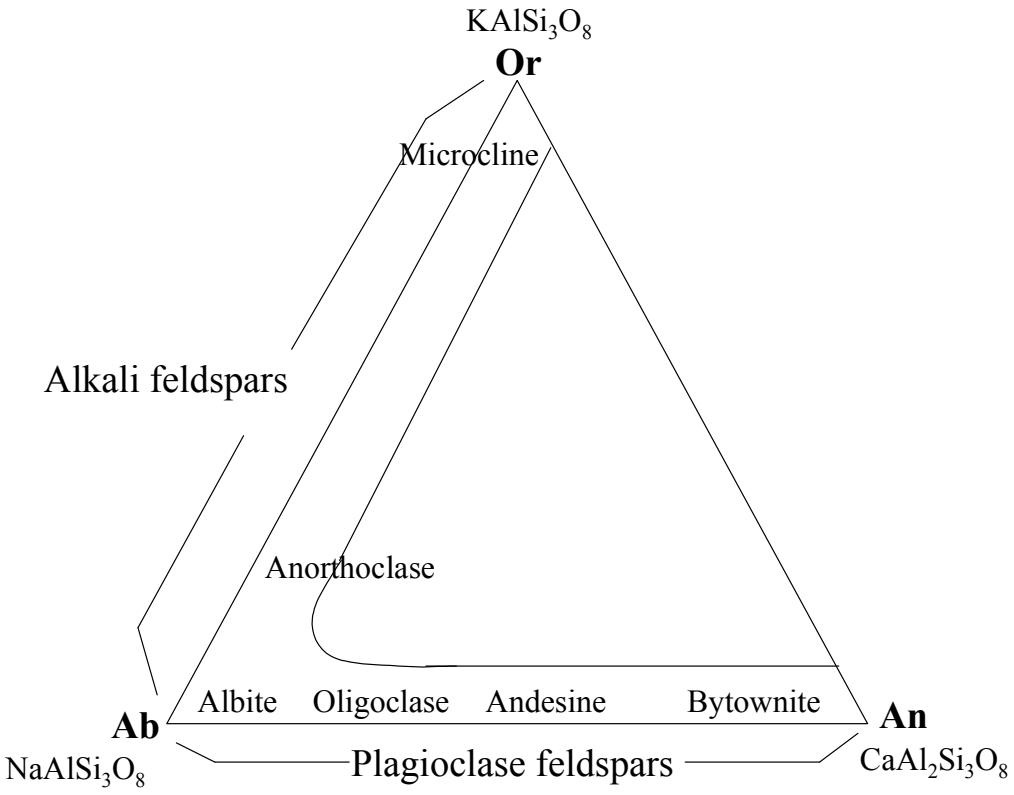

Figure 2.1 Ternary diagram of feldspars showing the approximate positions of the samples. The exact chemical composition of the samples is not known and was not determined for these studies. Although bytownite was initially selected in order to incorporate as much of the diagram as possible, initial investigations revealed low luminescence levels and bytownite was not investigated further.

PMT integration time for TL and OSL was 0.2 s. The OSL signal was defined as the integrated counts from the first 1 s of stimulation (either 100 s or 300 s total stimulation time) minus the average counts per second from the last 5 s of stimulation (taken as the definition of the "background").

2.2.2 General TL/OSL Characteristics

Figure 2.2 shows the mass normalized TL, blue-stimulated OSL, and infrared-stimulated OSL signals after heating to 500^{o}C (to empty all traps of their charge), an irradiation of 5 Gy, and a preheat of 220^{o}C for 10 s for all samples. In general, the feldspars exhibit a broad TL peak from 200-400^{o}C. Previous work has identified two TL peaks centered at 250-280^{o}C and 330^{o}C (Duller, 1997), but no attempt was made here to resolve the overall glow curves into peaks as development of TL dating methods is not the eventual goal of this project. From the blue-stimulated OSL (Figure 2.2(b)) and infrared-stimulated OSL (Figure 2.2 (c)) graphs, we can see that all samples have a significant background (tail of the decay curve) for the blue-stimulated data while the background is small for the infrared-stimulated data. By comparing the blue-stimulated and infrared-stimulated data, we can also see that oligoclase, albite, and microcline produce large infrared-stimulated OSL signals and strong quickly decaying ("fast") components in the blue-stimulated OSL decay curves. On the other hand, anorthoclase and andesine produce weak infrared-stimulated OSL signals and do not show a strong fast component in the blue-stimulated OSL, indicating that infrared-stimulated OSL and the fast component of blue-stimulated OSL are connected. The use of the terms "slow" and "fast" component do not necessarily imply physically distinct traps or components

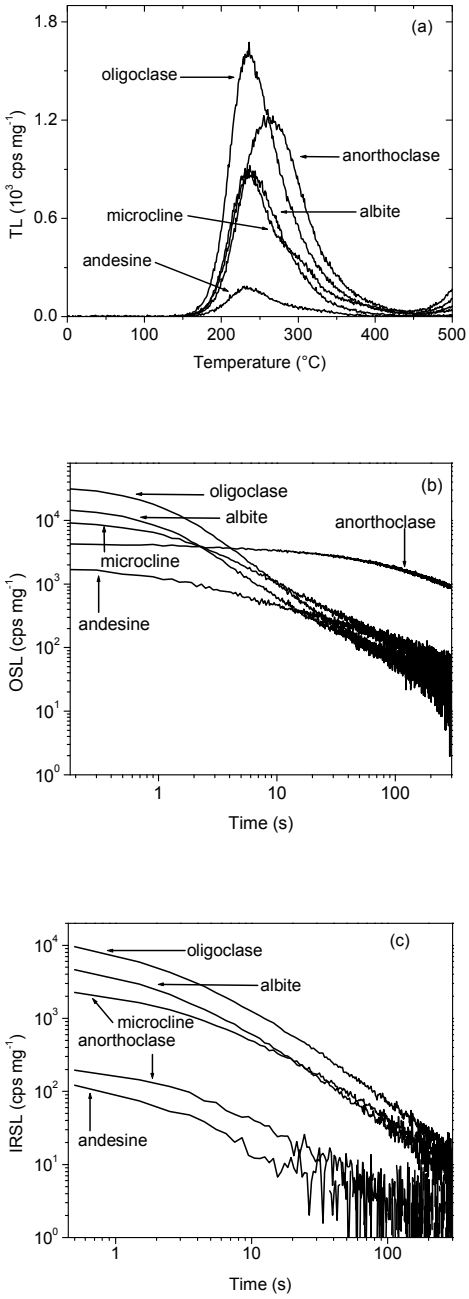

Figure 2.2 Mass normalized thermoluminescence (a), blue-stimulated OSL (b), and infrared-stimulated OSL (termed IRSL) (c), after irradiation of 5 Gy and a preheat to 220^{o}C for 10s.

that can be mathematically described, but are used here merely to refer to the rapidly and slowly decaying parts of the OSL decay curves.

The general effect of OSL stimulation on the TL curves was also studied. Figure 2.3 shows TL glow curves after irradiation and after blue-stimulated, infrared-stimulated, or post-IR blue-stimulated (infrared stimulation followed by blue stimulation) OSL measurements. It is important to note that any OSL stimulation reduces the entire TL curve implying that OSL and TL access either a common recombination center or the same electron traps (Bøtter-Jensen et al., 1991; Duller and Bøtter-Jensen, 1993). Infrared stimulation always reduces the TL curve less than either blue-stimulated or post-IR blue-stimulated OSL, and the latter two stimulation methods reduce the TL curve to the same level.

It has been suggested that these phenomena can be explained by an OSL signal consisting of two types of traps, one stimulated only by blue-green light and one stimulated both by blue-green and infrared light (Duller and Bøtter-Jensen, 1993). The data presented here suggests that the infrared-sensitive traps give rise to a majority of the fast component in blue-stimulated OSL from feldspars while the slow component comes from the traps stimulated only by blue light. Similar results led other authors to use post-IR blue-stimulated OSL within a polymineral fine-grains SAR dating procedure (Banerjee *et al.*, 2001; Roberts and Wintle, 2003) to reduce the influence of feldspar and enhance the quartz contribution to the blue-stimulated OSL. Using the post-IR blue-stimulated OSL signal has also been suggested for obtaining a pure quartz signal from coarse-grained quartz samples that are contaminated with feldspar grains or inclusions (Wallinga *et al.*, 2002).

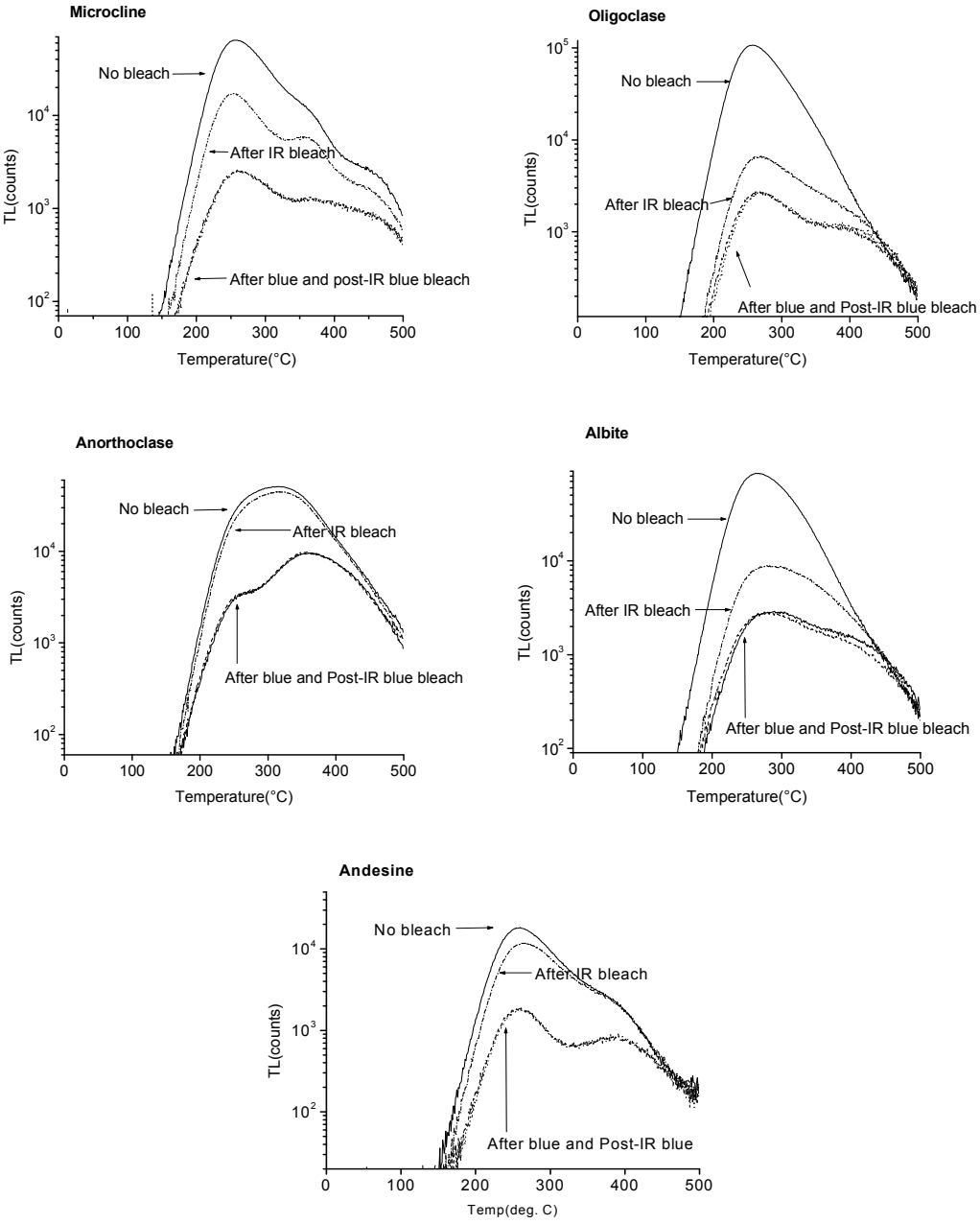

Figure 2.3 The effect of bleaching on TL. The samples were given a 5 Gy dose, preheated to 220°C for 10s, bleached with indicated stimulation sources for 300s, and TL was then measured to 500°C.

2.2.3 Sensitivity changes

One obstacle to developing a single-aliquot dating procedure for coarse grain feldspars has been the presence of sensitivity changes induced by repeated irradiations, preheating, and luminescence measurements (Duller, 1991, 1995). Sensitivity changes in feldspars have been explained as being due to a build-up of charge within the traps (Duller, 1991) and an "increase in electron trapping probability as a consequence of heating" (Wallinga *et. al.*, 2000b). In either case, this obstacle could be overcome by either eliminating sensitivity changes or developing procedures to correct for the changes such as is done in the SAR procedure for quartz (Murray and Wintle, 2000; Banerjee *et. al.*, 2001).

Before attempts were made to correct for sensitivity changes, experiments were undertaken to determine under which conditions sensitivity changes occur in these samples. For these experiments, sensitivity was defined as luminescence per unit test dose. Sensitivity changes were then determined to be changes in the detected luminescence when a sample was subjected to 7 cycles of a fixed dose (5 Gy), fixed preheat (220 ^{o}C for 10 s, to remove unstable signals), and measurement procedure (either TL or OSL). At the beginning of each of these cycles of measurement, the aliquots were heated to 450 ^{o}C to empty charge from all traps.

TL

When TL curves (measured to 450^{o}C) from the above experiment are plotted on the same graph, the curves overlie each other for all samples. Specifically, by integrating from 250^{o}C to 450^{o}C to define the TL signal, there is less than a 3% difference. Thus,

there is no evidence of sensitivity changes with repeated cycles of irradiation, preheat, and TL measurement to 450°C.

OSL

Sensitivity change experiments were also performed using blue-stimulated OSL, infrared-stimulated OSL, and post-IR blue-stimulated OSL (100 s measurements in each case). For blue-stimulated OSL and infrared-stimulated OSL, all samples showed an increase of more than 15% (nearly 50% in some cases) in the OSL signal over 7 cycles. The results are exemplified by microcline in Figure 2.4, and are consistent with earlier findings (Duller, 1991; Richardson, 1994; McKeever et al., 1997a). The post-IR blue-stimulated OSL (both the infrared-stimulated signal and blue-stimulated signal) results were similar, but the sensitivity changes were smaller (13%-49% for infrared-stimulated OSL and 5%-40%for blue-stimulated OSL). It is important to note that the absolute increase of the OSL signal is much greater than that of the background OSL, so the sensitivity changes are real and not the result of subtracting a changing background from a constant signal. However, the background OSL grows at a faster rate than the OSL signal in each type of measurement.

As expected from the results of Figure 2.2, the background levels from repeated cycles of blue-stimulated and post-IR blue-stimulated OSL are nearly identical in all cases. However, the OSL signals, which are mainly the "fast components" of the OSL decay curves, are much smaller for post-IR blue-stimulated OSL. Subsequently, the remaining fast components appear to demonstrate a smaller sensitivity change. If, as has been suggested by Duller and Bøtter-Jensen (1993), there are two types of traps in feldspathic materials, one set accessible only to blue light stimulation and one set

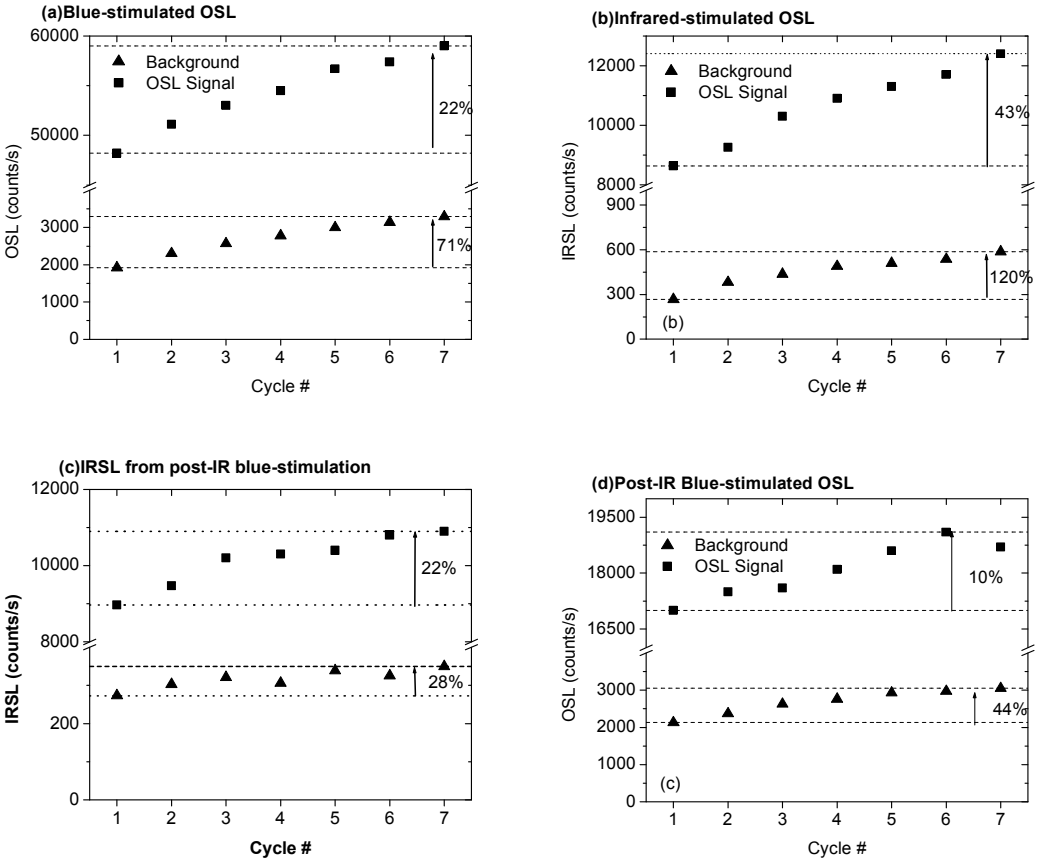

Figure 2.4 Sensitivity changes experienced by microcline during 7 repeated cycles of 5 Gy dose, preheat to 220°C, and OSL measurement for 100 s. The values of the background (triangles) and signal (squares) and the % change are plotted for three different OSL signals: (a) blue-stimulated (b) infrared-stimulated (c) infrared-stimulated OSL (IRSL) from post-IR blue-stimulation, and (d) post-IR blue-stimulated. Note that in each case, the absolute increase is larger for the signal than the background, but the % change is greater for the background.

accessible to both blue and infrared light stimulation, we can remove a proportion of the sensitivity change caused by the infrared-stimulated traps (mainly the "fast" OSL signal) by using post-infrared blue-stimulated OSL.

In addition, the sensitivity changes displayed by the infrared-stimulated OSL from a post-IR blue-stimulation sequence are significantly smaller than those of the (only) infrared-stimulated OSL. The phenomenon can again be explained by a set of traps sensitive to only blue stimulation and a set of traps sensitive to both infrared and blue stimulation. When only infrared-stimulation is used, those traps not sensitive to infrared stimulation are not emptied during OSL measurements and are less effective at capturing charge during subsequent irradiations. Therefore, the infrared sensitive traps become more and more effective at capturing charge during irradiation and experience larger sensitivity changes. In the other case, when the samples are stimulated by blue light after infrared stimulation, competition effects during irradiation are more equal from cycle to cycle and the resulting sensitivity changes are smaller.

OSL Followed by TL

Since repeated measurement cycles using TL showed little sensitivity change, it was speculated that measurement cycles using OSL followed by a TL measurement would also produce little sensitivity change. To test this idea, the above measurement procedure was performed using blue-stimulated OSL, infrared-stimulated OSL, and post-IR blue-stimulated OSL to measure the luminescence (100 s measurements in each case), and each OSL measurement was immediately followed by a TL measurement to 450^{o}C.

For all cases, the degree of sensitivity change over 7 repeated cycles decreased substantially as compared with the previous results. The maximum sensitivity changes

were 3% for blue-stimulated OSL, 13% for infrared-stimulated OSL (some samples had low infrared-OSL levels and hence a lot of scatter in the data which was seen as apparent sensitivity changes), and 5% for post-infrared blue-stimulated OSL. In addition, most samples did not show a clear trend (i.e., a continual increase or decrease) but rather the sensitivity changes appeared to be random fluctuations in the data. It is important to note that the background levels, i.e., the tail of the OSL decay curves, are proportionally smaller when a TL measurement is performed after each cycle (Figure 2.5). Richardson (1994) and McKeever et al. (1997a) saw similar effects when TL was used to zero sedimentary feldspar samples after each OSL measurement. These latter studies saw a large decrease in sensitivity after the first cycle, due to charge that had accumulated during the geological history of the samples, but no more sensitivity change was observed in subsequent cycles.

Accumulation of charge in the TL traps

The preceding experiments indicate that sensitivity changes occur in these feldspar specimens during repeated cycles of irradiation, preheating, and OSL measurement. Duller (1991) explained sensitivity changes in feldspars by "a progressive build-up of trapped charge" which altered the rate of trap filling during subsequent irradiations. Annealing the samples to 450^{o}C after each OSL measurement empties this charge and ensures the same level of competition for charge capture during each irradiation and thereby reduces the amount of sensitivity change observed. However, it is not clear in what traps or centers the charge builds up during repeated cycles when the sample is only bleached.

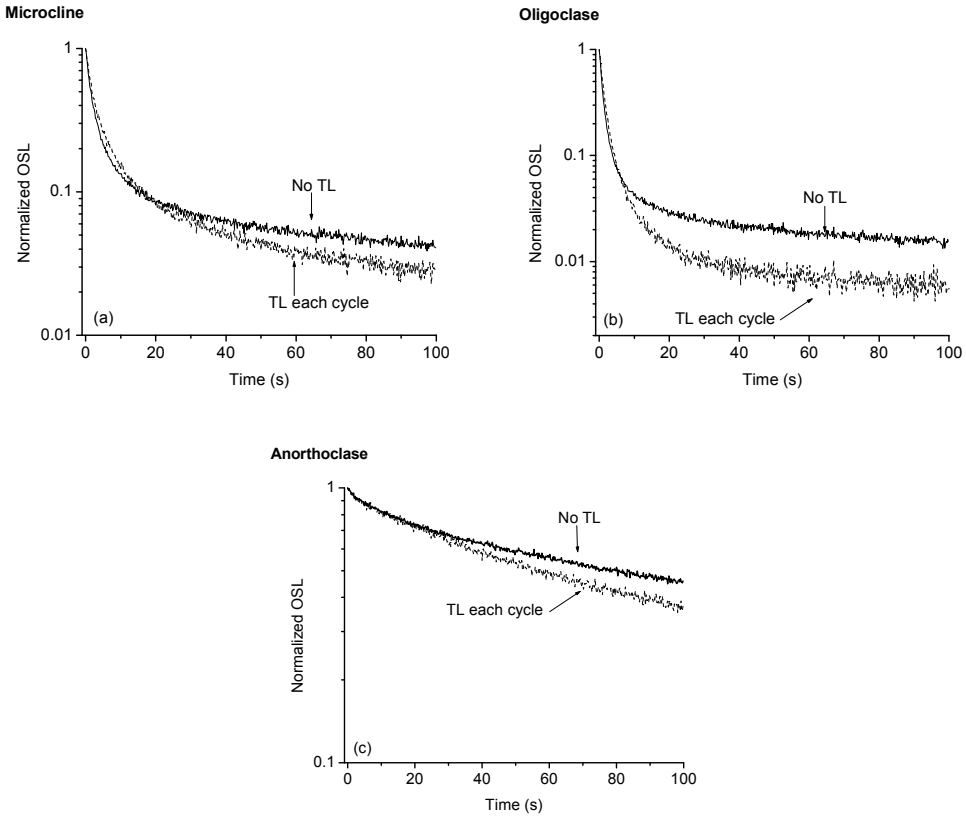

Figure 2.5 Examples of normalized OSL decay curves from the 7th cycle of sensitivity change experiments. The two different curves represent the first experiment (No TL) where no TL measurements were made and the second experiment (TL each cycle) where a TL measurement to 450^{o}C was made after each OSL measurement.

Experiments were carried out on all samples to determine the extent of trapped charge build-up after repeated cycles of irradiation, preheating, and OSL stimulation. The experiments used cycles of OSL stimulation consisting of: (1) 20 Gy dose, (2) Preheat at 220^{o}C for 10 s, and (3) OSL measurement for 300 s. The sequence begins by measuring TL (to 500^{o}C) after a 20 Gy dose and a 220^{o}C for 10 s preheat. Then, TL (to 500^{o}C) was measured immediately after 1 cycle of OSL stimulation, 2 cycles of OSL stimulation, and so on up to 7 cycles of OSL stimulation. The experiments were carried out with both blue-stimulated and infrared-stimulated OSL.

Figure 2.6 shows representative glow curves from albite. Preheating and blue-stimulated OSL (Figure 2.6 (a)) removes charge from the low temperature TL traps (<~250^{o}C), but charge begins to build-up in the high temperature region (>300^{o}C) with repeated cycles. Even though IR stimulation appears to preferentially empty low temperature TL traps as seen by Duller (1995), after 7 cycles of OSL stimulation with IR the entire TL curves are more intense than the initial glow curves (Figure 2.6 (b)). This effect is more pronounced in anorthoclase, for which IR stimulation affects the TL curve little (Figure 2.3). The build-up of charge in TL traps with repeated cycles of OSL stimulation is important since previous experiments (Figure 2.3) showed all TL traps contribute to the OSL signals, and therefore a build-up of charge will result in increasing OSL signals with repeated cycles (i.e., sensitivity change).

2.2.4 Correcting for Sensitivity Change

Even though it has been shown that sensitivity changes can be largely eliminated from feldspars by heating the material to ~450^{o}C after OSL measurement, a sedimentary material is unlikely to have had its traps emptied in nature by heating to ~450^{o}C. Rather,

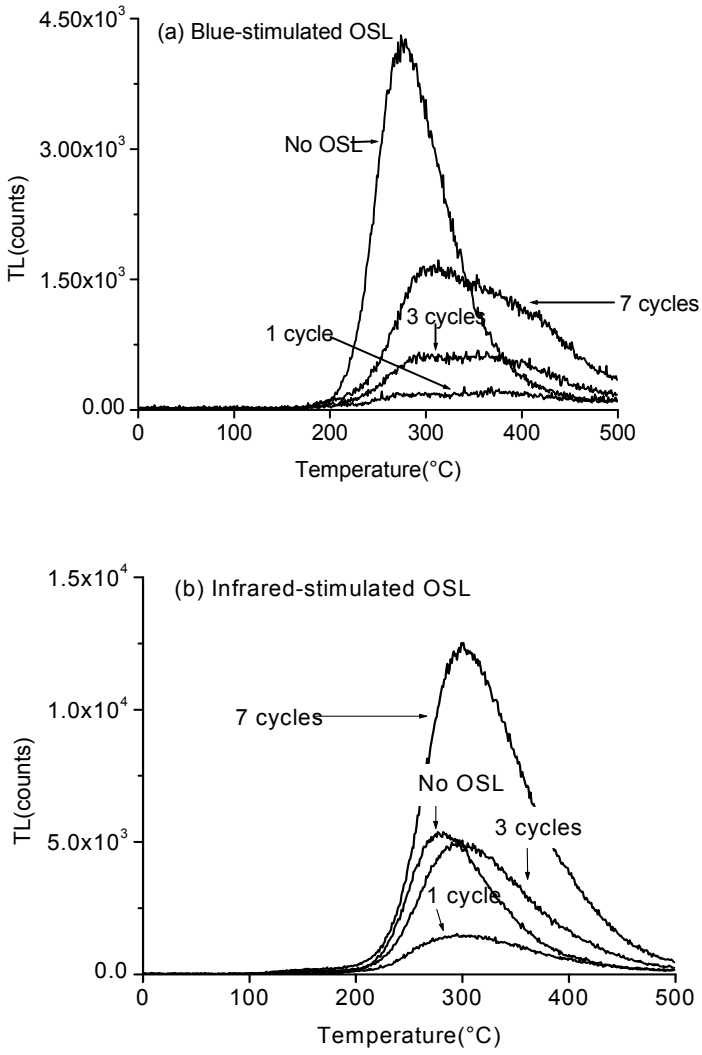

Figure 2.6 TL after repeated cycles of OSL measurement for albite. A cycle of OSL measurement is irradiation (20.04 Gy), preheat at 220^{o}C for 10 s, and OSL measurement for 300s. (a) blue-stimulated OSL and (b) infrared-stimulated OSL.

the "zeroing event" for sedimentary feldspars is typically exposure to light during transport. As a result, a method must be devised to correct for any laboratory-induced sensitivity changes as well as the natural sensitivity changes materials may have experienced. At this point, only those sensitivity changes induced in the lab will be discussed.

As a test of the sensitivity-correction procedure, an aliquot was subjected to repeated cycles of the SAR procedure with a fixed regeneration dose. As discussed in Section 2.1, if the sensitivity-correction procedure is working properly, a plot of regeneration dose OSL (R_i) vs. test dose OSL (T_i) will result in a straight line that is consistent with the origin indicating that the two signals are proportional to each other (Murray and Wintle, 2000).

Cutheat vs. Preheat

The above procedure was used to check the validity of a test dose correction method using two different heating procedures. All OSL measurements were for 100s. A regeneration dose of 6 Gy and a test dose of 1.44 Gy were used for blue-stimulated OSL, whereas infrared- and post-IR blue-stimulated OSL experiments used a 36 Gy regeneration dose and a 9 Gy test dose. In one case, the preheat (10 s duration) was varied from 160°C to 300°C and the cutheat was fixed at 160°C (but not held at this temperature). In the other case, the preheat was varied in the same manner, but the cutheat was chosen to be equal to the preheat (in both temperature and duration).

Representative results for microcline, oligoclase, and albite are shown for three stimulation methods (blue, infrared, and post-IR blue) and four OSL signals (blue-stimulated, infrared-stimulated, infrared-stimulated from post-IR blue stimulation

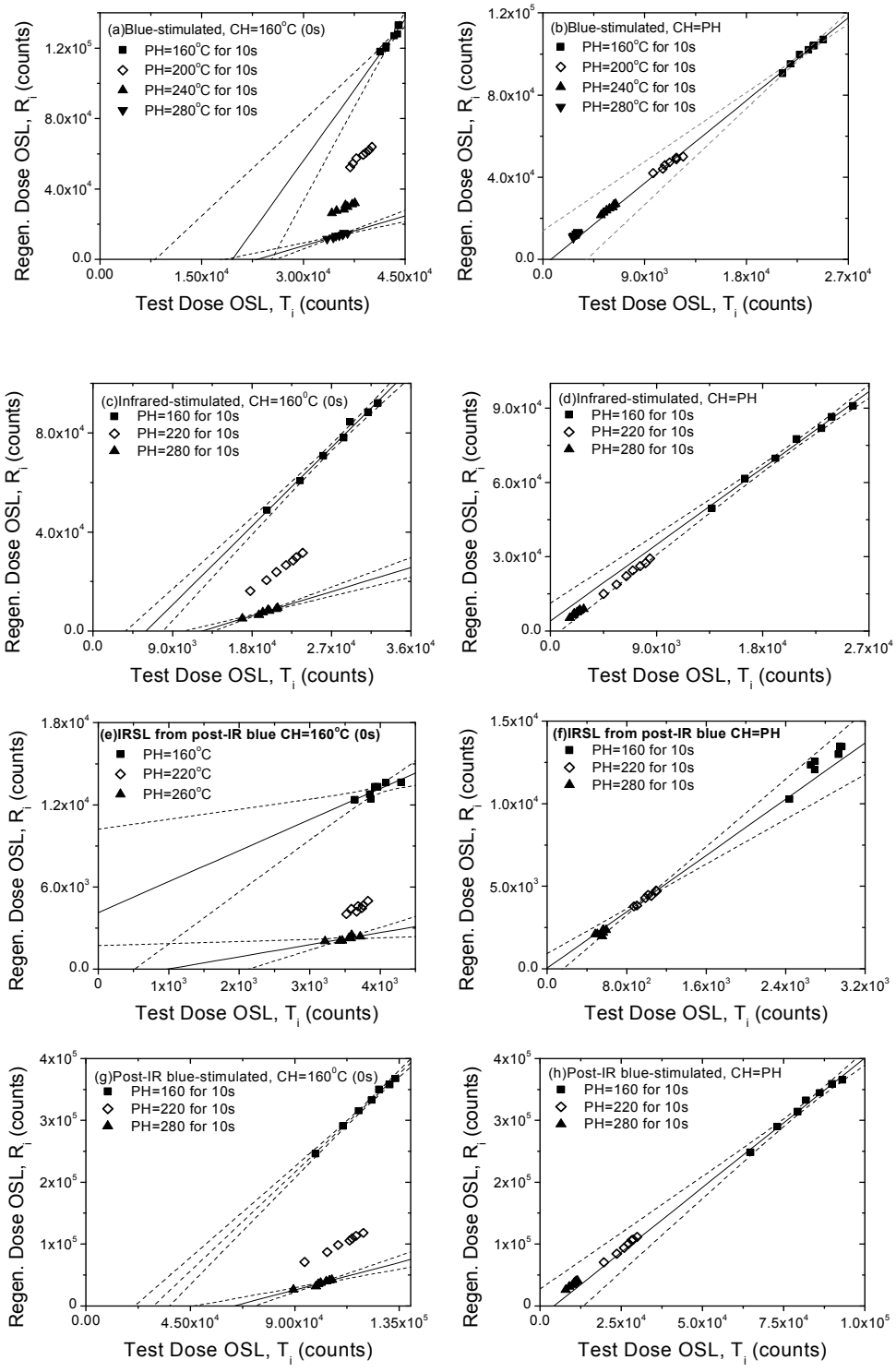

Figure 2.7 Tests of the sensitivity-correction procedure for microcline using two different preheating procedures. The figures use the indicated stimulation method. In (a), (c), and (e), the cutheat was fixed at 160°C. In (b), (d), and (f), the cutheat was equal to the preheat (time and duration). The dashed lines represent the 95% confidence level of a linear fit.

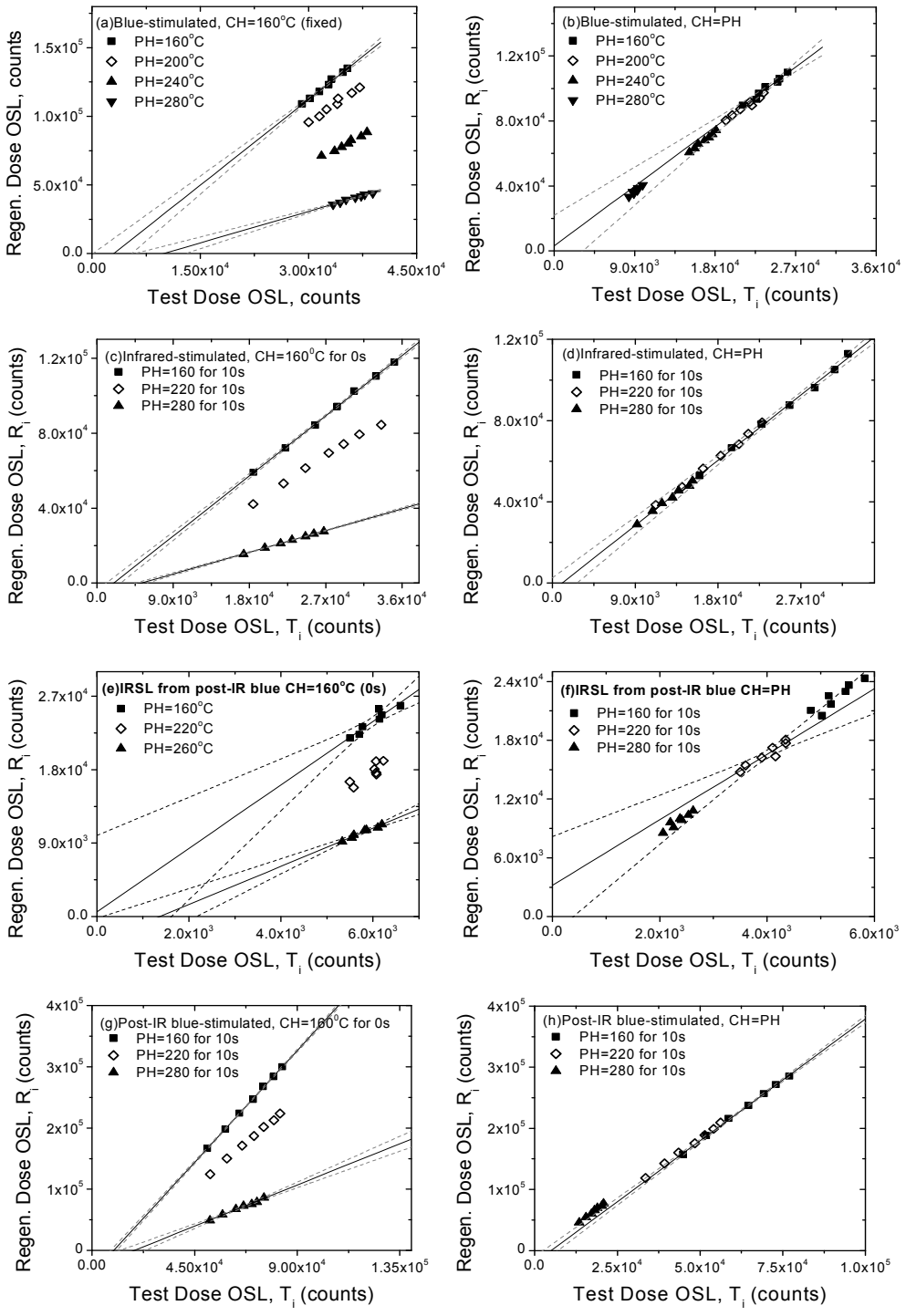

Figure 2.8 Same as Figure 2.7 except the results are for oligoclase.

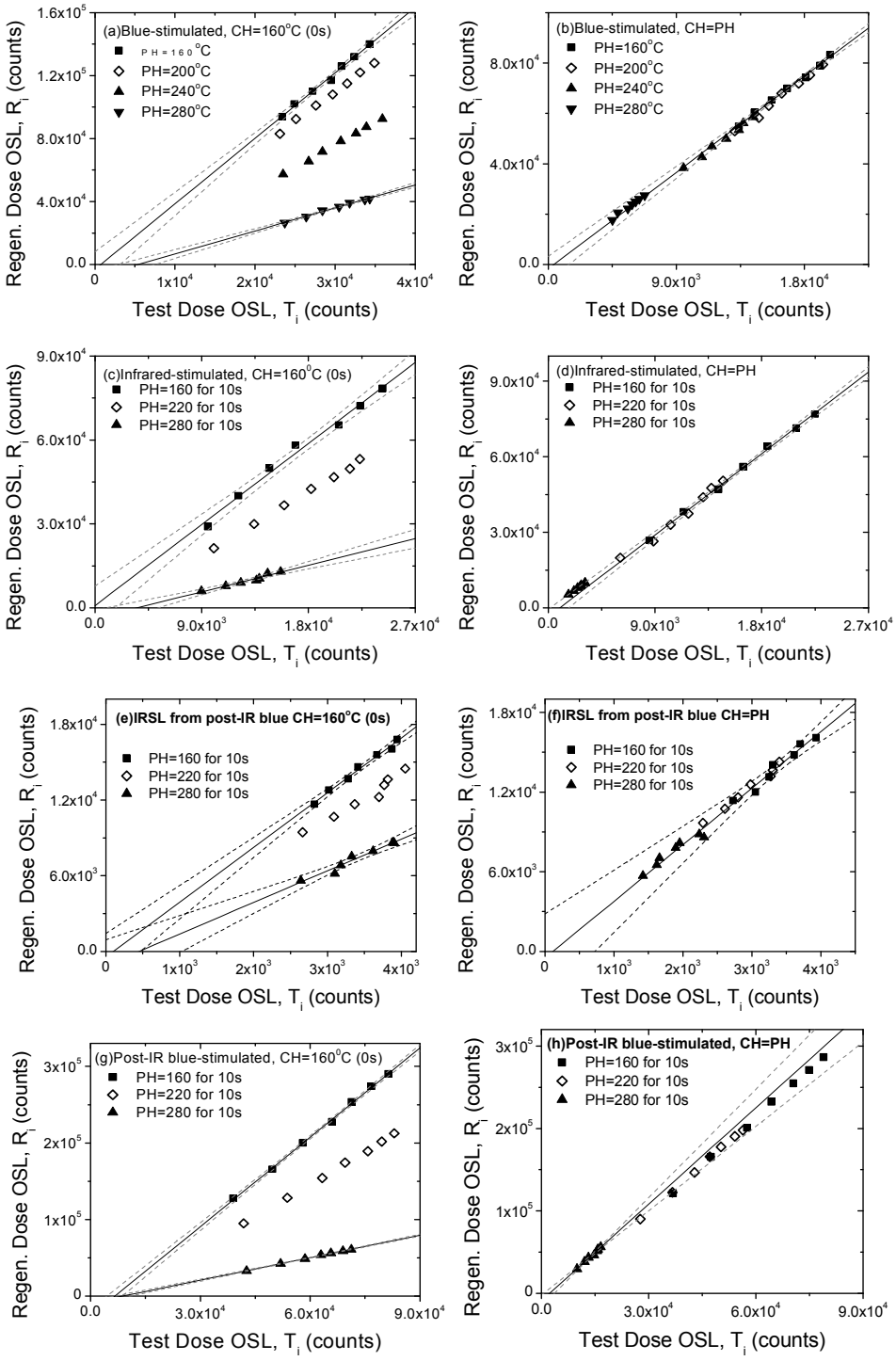

Figure 2.9 Same as Figures 2.7 and 2.8 except the results are for albite.

sequence, post-IR blue-stimulated) in Figures 2.7, 2.8, and 2.9 respectively. From the experiments where the cutheat and preheat are equal in both time and duration (on the right), it can be seen that the linear relationship is consistent with the origin (i.e., the signals correlate). In addition, the ratio (slope) between R_i and T_i remains constant for preheats in the range between 160°C and 280°C.

In the experiment where the cutheat was fixed at 160°C (on the left, Figures 2.7, 2.8, and 2.9), it can be seen that R_i and T_i are not correlated for microcline when the cutheat and preheat are not equal in both temperature and duration. This is not strictly true for all samples (e.g., oligoclase and albite, Figures 2.9 and 2.10 respectively) as it was found that a best-fit line was consistent with the origin for a low temperature preheat (i.e., 160°C for 10 s). Yet, for all cases, as the difference between the cutheat and preheat temperatures increases, the intercept increases and the slope decreases. An increasing intercept (T_i intercept in this case) can be interpreted as T_i and R_i exhibiting different sensitivity changes.

Although Preusser (2003) showed that using a cuheat (200°C) lower than the preheat (290°C) produced reliable dose estimations for particular samples, finding a cutheat/preheat combination that gives the correct dose does not test the underlying assumptions of the SAR procedure. The current experiments have shown that for feldspars the test dose heating should generally be equal to the regeneration dose heating in both temperature and duration (i.e., cutheat = preheat). Considering the implications of Figure 2.3, this should not be a surprising result. OSL, whether infrared- or blue-stimulated, reduces the entire TL curve. Although this does not necessarily mean that the charge in the TL traps is being directly stimulated (Duller and Bøtter-Jensen, 1993), the

two signals are in some way linked (possibly via a common recombination center or centers). Thus, if the samples are preheated differently following the regeneration and test doses, different trap distributions and OSL signals will be measured.

Based upon these results, all future experiments that used a sensitivity-correction procedure employed a cutheat that was equal to the preheat.

Dependence on size of test dose

The previous experiments were conducted for a test dose that is ~25% of the regeneration dose. However, this does not guarantee that all regeneration dose/test dose combinations will produce the same results. To test this, the sensitivity-correction procedure was repeated for 7 cycles with a fixed preheat (=cutheat) of 220^{o}C for 10 s and three different regeneration dose/test dose combinations. In the first case, the test dose (1.2 Gy) was ~10% of the regeneration dose (12 Gy), in the second case the test dose was ~1% of the regeneration dose (120 Gy, and in the final case the test dose was ~0.5% of the regeneration dose (240 Gy).

For blue-stimulated OSL, the best-fit straight line in a regeneration OSL vs. test dose OSL plot passes through the origin (95 % confidence level) for all regeneration dose/test dose combinations that were tested. However, as the regeneration dose increased and approached the non-linear part of the dose-response curve (typically ~100 Gy), the fitting errors increased. This may represent greater uncertainties in sensitivity-corrected signals in the non-linear portion of the dose-response curves or may represent the inability of small test doses to correct for sensitivity changes induced by relatively large radiation doses.

Using TL in the sensitivity-correction procedure

Previous results have shown that sensitivity changes induced in the lab can be largely eliminated by including a TL measurement after an OSL measurement. Experiments were then conducted to determine if a TL measurement could be used with the sensitivity-correction procedure. Repeated cycles of the sensitivity-correction procedure (with a fixed preheat of 220°C) were performed for all feldspar samples, but an extra step of a TL measurement to 450°C after each T_i was added.

The results were as expected based upon previous experiments. R_i and T_i measurements showed little change from cycle to cycle. The resulting R_i vs. T_i plot showed a cluster of points, and the sensitivity-corrected OSL remained constant.

2.2.5 OSL Dose Response

The SAR sensitivity-correction procedure was used to construct OSL (blue-stimulated, infrared-stimulated, and post-IR blue-stimulated) dose response curves both with and without a TL measurement (to 500°C) after each T_i. For these experiments, all preheats (and cutheats) were 220°C for 10 s and all OSL measurements were for 300 s. The samples were given 11 regeneration doses (i=1-11) in the range from 5–2000 Gy while the test dose remained fixed at 10 Gy. After the 2000 Gy regeneration dose, a dose of 10 Gy was given (i=12; equal to the second dose; $D_{12}=D_2$), and the sensitivity-corrected OSL value was compared to L_2 to obtain the recycling ratio ($RR=L_{12}/L_2$). Finally, a 0 Gy dose (i=13) was given to determine if measurable recuperation was present. Recuperation is a measure of the charge from optically inactive traps that can be transferred to the traps responsible for OSL during preheating.

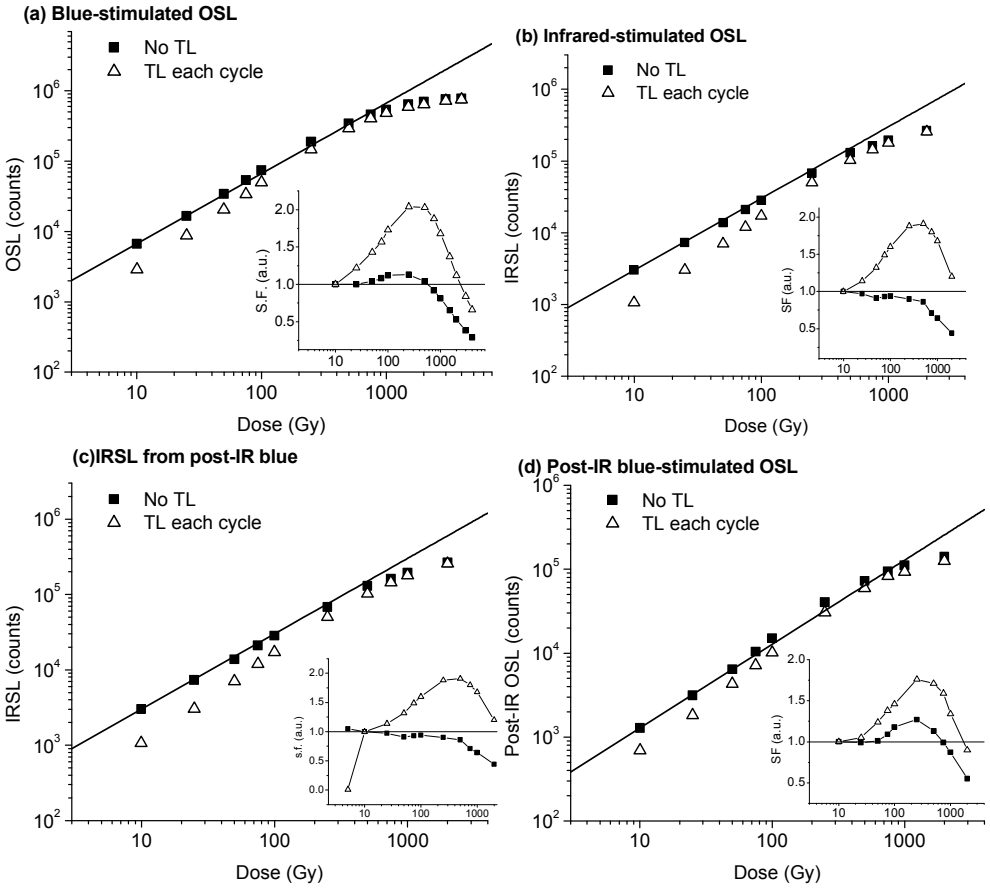

Figure 2.10 Uncorrected (R_i only) dose-response curves for microcline. Three different OSL signals were used: (a) blue-stimulated OSL, (b) infrared-stimulated OSL (used 875 nm IR diode array), and (c) post-IR blue-stimulated OSL. All preheats were 220°C for 10s and all OSL measurements were for 300s. The dose-response was performed in two different ways: without any TL measurement (No TL, filled squares) and with a TL measurement to 500°C after each test dose OSL measurement (TL each cycle, open triangles). The supralinearity factor, as defined by Chen and McKeever (1997), is shown in the inset of each graph. Note the log-log scale.

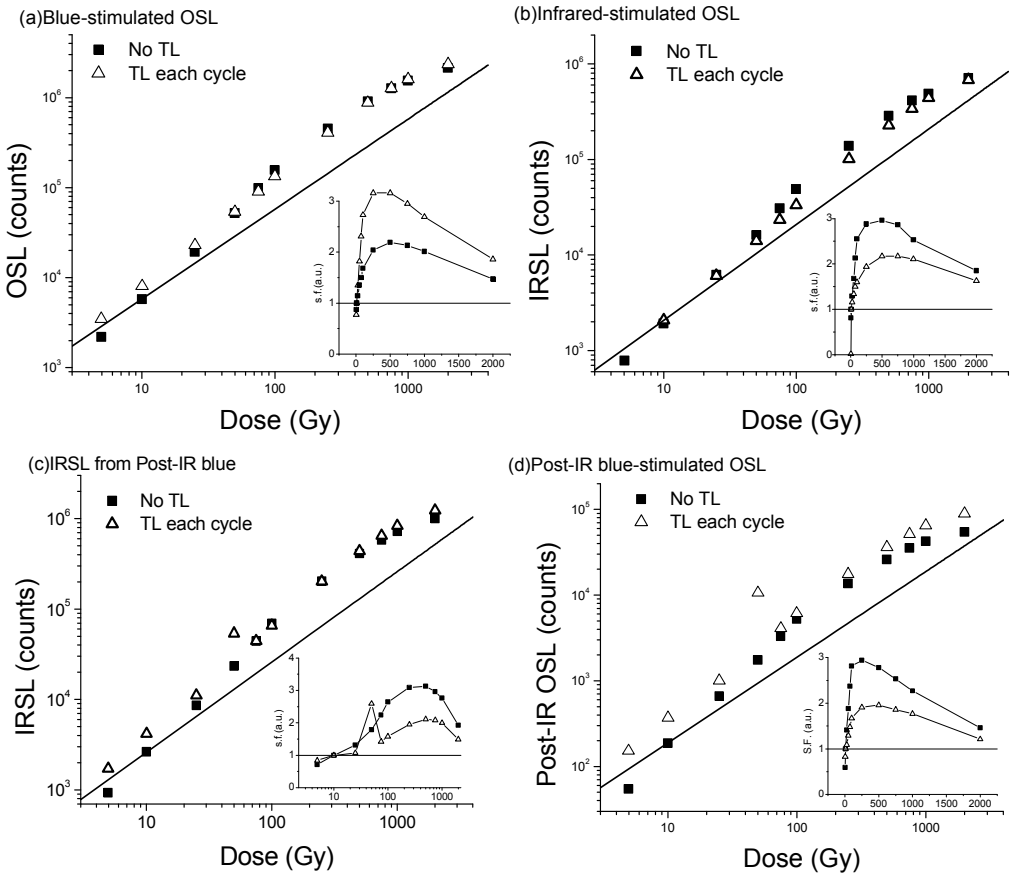

Figure 2.11 Same as Figure 2.10 except the results are for oligoclase.

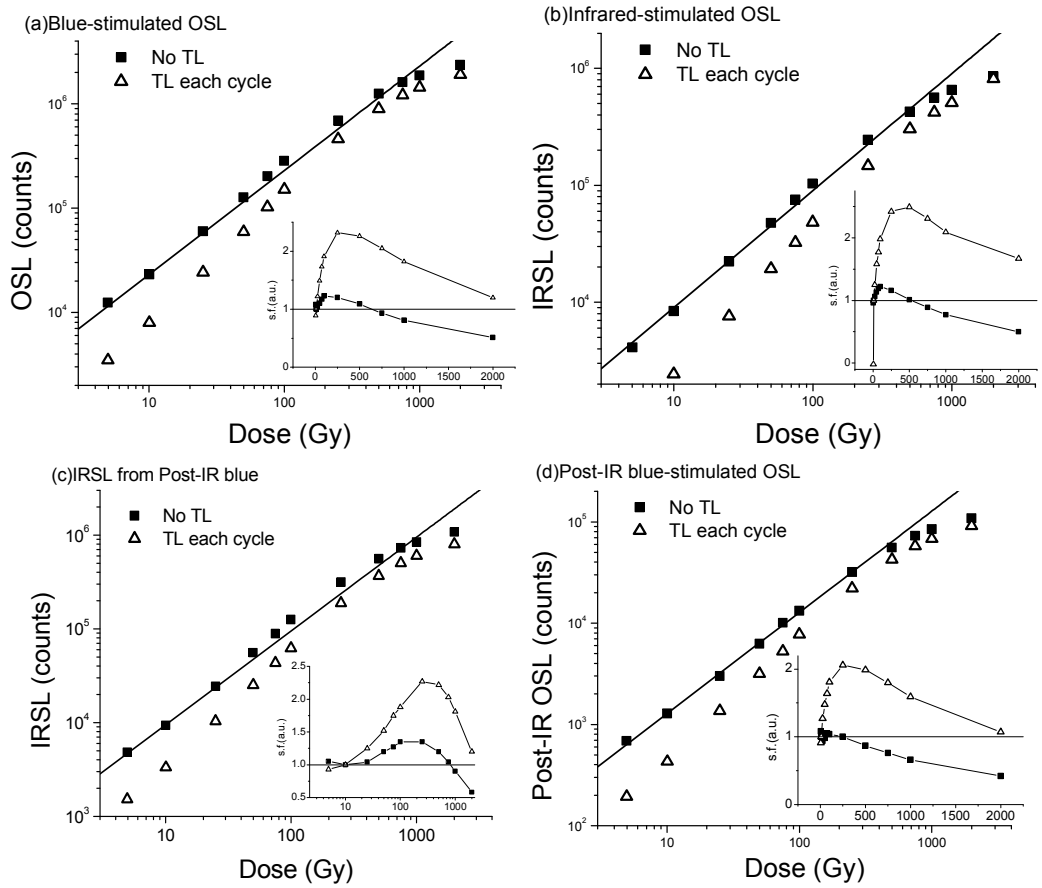

Figure 2.12 Same as Figures 2.10 and 2.11 except the results are for albite.

Examples of the uncorrected (R_i only) dose-response curves for microcline, oligoclase, and albite (both with and without a TL measurement to 500°C after each cycle) are shown in Figures 2.10, 2.11, and 2.12 respectively. The insets of these graphs also show the supralinearity factors as defined by Chen and McKeever (1997)

$$f(D) = \frac{S(D)/D}{S(D_1)/D_1} \tag{2.1}$$

where D_1 is the normalization dose in the linear region of the growth curve and $S(D_1)$ is the corresponding luminescence signal. The supralinearity factor is then defined in terms of OSL per regeneration dose, with f(D)>1 indicating supralinearity that may or may not indicate sensitivity change. Other samples (anorthoclase, andesine) show similar results, indicating that heating reduces the sensitivity of the samples as seen previously by Wallinga et al. (2000a) (for oligoclase, the background was reduced more than the initial intensity, hence there was an apparent increase in OSL signal when the integral signal is used). The linear-supralinear-saturation behavior is consistent with a competing trap model (Chen and McKeever, 1997; Kristianpoller et al., 1974) in which a large pre-dose (the geological/natural dose in the present case) effectively fills the competitors and the dosimetric trap(s) become more effective at producing luminescence. When the sample is heated, however, the competitors as well as the dosimetric trap(s) are emptied. On subsequent irradiation, the dosimetric trap(s) are then less effectively filled (because of competition) and the result is a supralinear OSL-versus-dose response curve.

The supralinearity of the dose response when a TL measurement is used in each cycle points to another aspect of the observed sensitivity changes. The experiments have shown that using a TL measurement after each cycle eliminates sensitivity changes caused by an accumulation of charge in competitors due to incomplete zeroing of the

sample. However, the uncorrected dose response curves suggest that sensitivity changes still do occur when a TL measurement is used each cycle (i.e., supralinearity is present). Since supralinearity should correctly be interpreted as an under-response at low doses (rather than an over-response at high doses) when the competitors are more effective at trapping charge, then, not only are sensitivity changes cycle dependent as Duller (1991) found, but they are also dose dependent as suggested by Richardson (1994).

For the largest dose given (2000 Gy), the cycle with a TL measurement yielded OSL signals that were 5-20 % lower than the cycle without a TL measurement. However, this difference will probably depend upon the natural dose, the geologic dose, and the degree of bleaching in nature, i.e., the degree to which competing traps have been filled or emptied in nature. In addition, the dose-response curves including a TL measurement showed much larger supralinearity. Such behavior is common to materials that exhibit sensitivity change due to competition effects at high doses (Chen and McKeever, 1997).

The sensitivity-corrected dose-response curves and recycling ratios (RR) for microcline, oligoclase, and albite are shown in Figures 2.13, 2.14, and 2.15 respectively. For both measurement processes, the curves show a linear-to-sublinear (saturation) response (no supralinearity). The same behavior has been seen when using the SAR procedure for quartz (Banerjee, 2001).

For the sensitivity-corrected dose-response curves, the recycling ratios were typically close to 1.0. When a TL measurement was included in the procedure, the recycling ratios generally ranged from 1.0 to 1.10, but when a TL measurement was not used in the procedure, the recycling ratio was usually greater than 1.10.

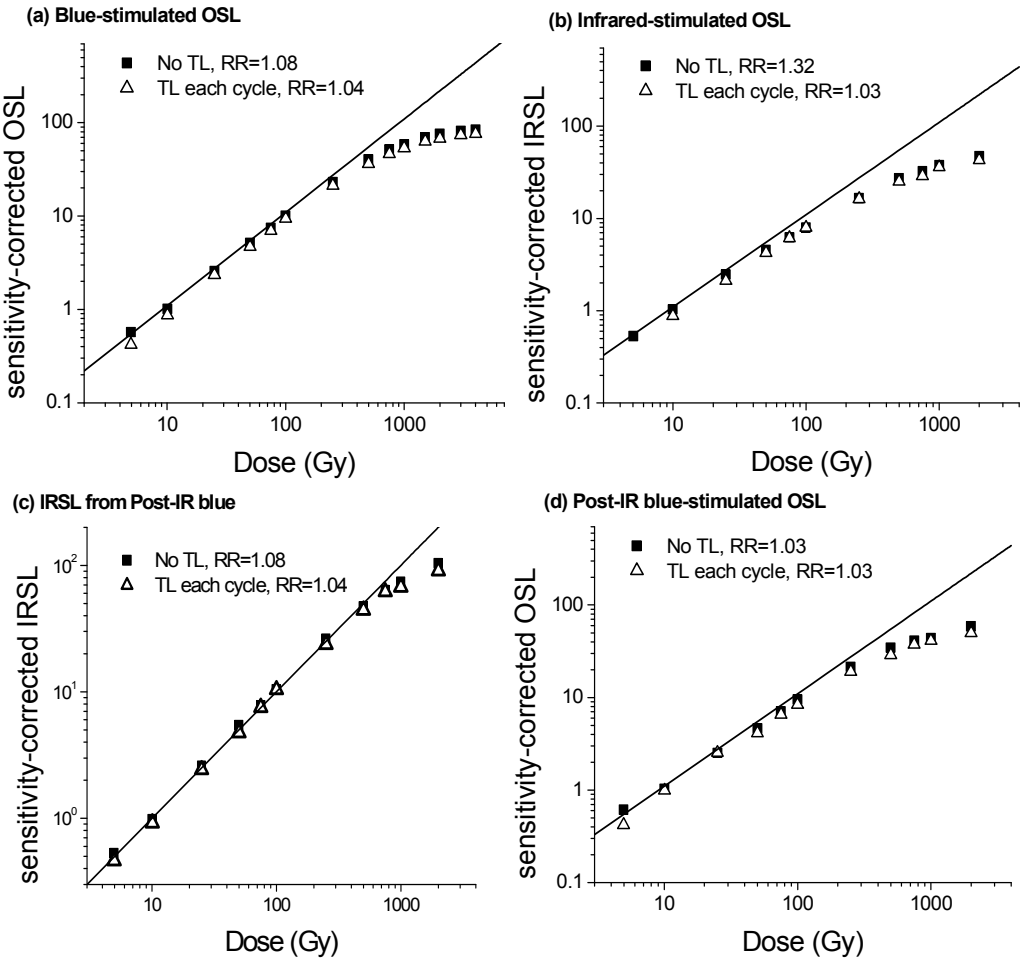

Figure 2.13 Sensitivity-corrected (L_i) dose response curves for microcline, constructed using the modified SAR procedure. Results from three OSL signals are again shown: (a) blue-stimulated (b) infrared-stimulated (used 875 nm IR diode array), and (c) post-IR blue-stimulated. Again, the experiment was conducted without TL measurements (No TL, filled squares) and with a TL measurement to 500°C (TL each cycle, open triangles) after each T_i, and the recycling ratios are given (RR). A line denoting linearity has also been added to the graph. Note the log-log scale.

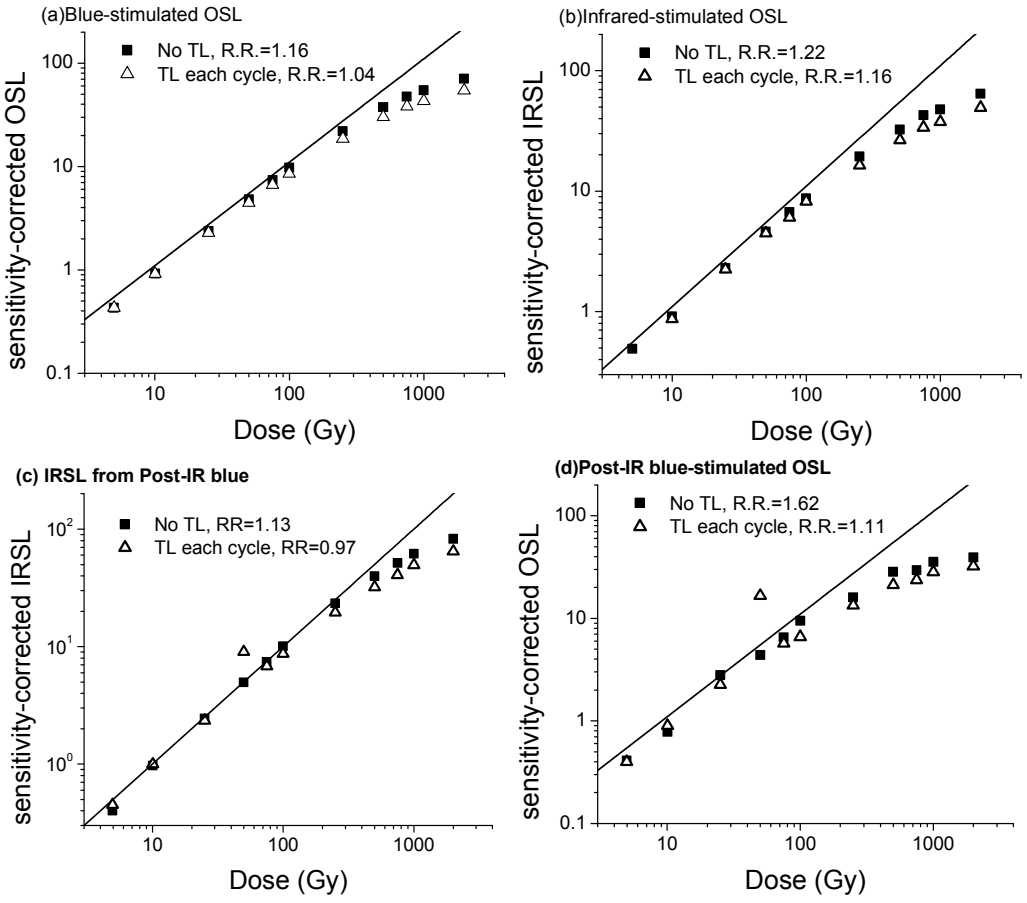

Figure 2.14 Same as Figure 2.13 except the results are for oligoclase.

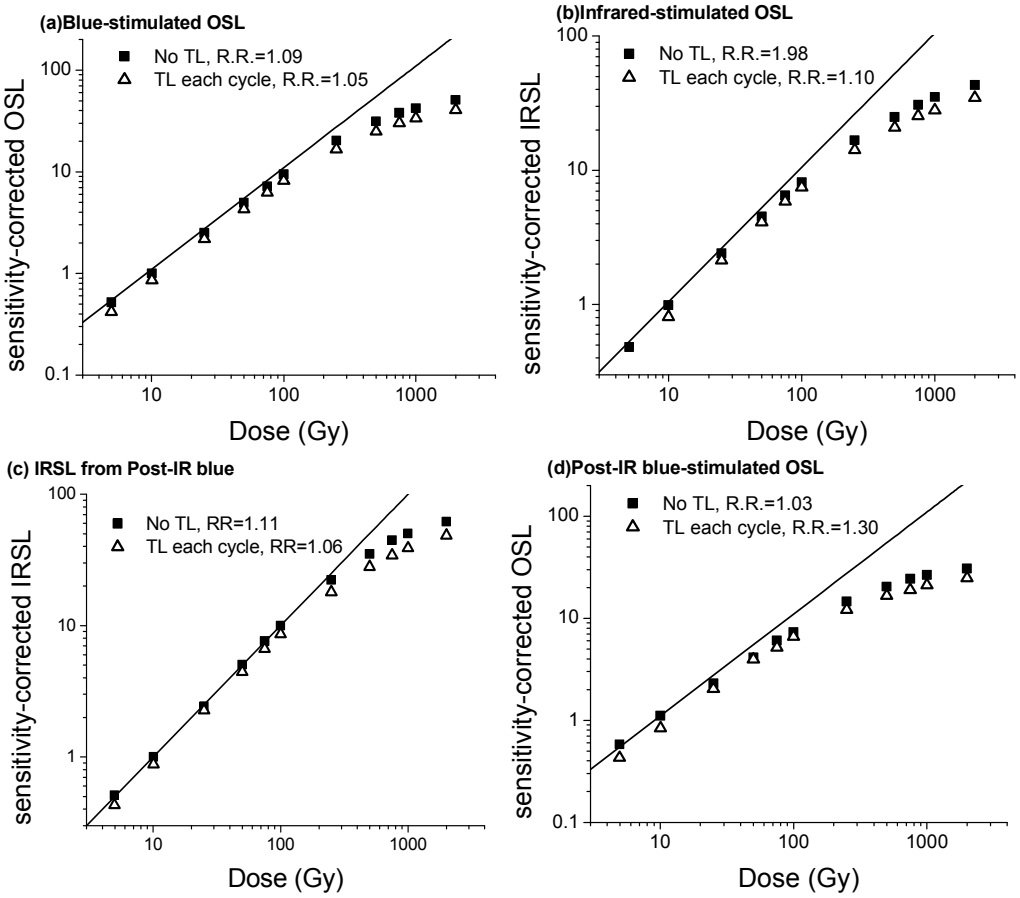

Figure 2.15 Same as Figures 2.13 and 2.14 except the results are for albite.

Recycling ratios greater than 1.10 can be explained by studying the slow component of the OSL decay curves. In the procedure where TL was not measured after each test dose OSL, the OSL decay curves for the test dose after the 2000 Gy dose, the repeat regeneration dose, and subsequent test dose (all 10 Gy doses), have decreasing backgrounds or slow components. This implies that the background or slow component is not constant during the measurement (i.e., a significant slow component has "built-up" and is being slowly bleached). If the background is decreasing during OSL measurement, then the OSL signal (as defined in this paper) will consist of the fast component plus the initial slow component minus the tail of the slow component. The repeat R_i signal in this case contains a larger proportion of the initial slow component than the T_i, resulting in a recycling ratio greater than 1.10.

Optical Stimulation Method for Feldspars

Results have been presented for three different stimulation methods (infrared stimulation, blue stimulation, and blue stimulation after infrared stimulation) and four different OSL signals that result from these stimulation methods. The post-IR blue-stimulation methods was first suggested by Banerjee *et al.* (2001) and later utilized by Wallinga *et al.* (2002) and Roberts and Wintle (2003) to isolate a quartz signal from either polymineral fine-grains samples or quartz samples with feldspar contamination. The infrared stimulation largely eliminates the "fast component" of feldspar OSL, and subsequent stimulation by blue produces an OSL signal where the fast component arises from quartz grains. Yet, analyzing dose response curves from feldspars illustrates another potential advantage of the post-IR blue-stimulation sequence.

The dose response curves of microcline, oligoclase, and albite for all of the studied OSL signals are plotted in Figure 2.16. The dose response curves for all of the samples were fitted with a single saturating exponential of the form:

$$y = a(1 - e^{\frac{-D}{Dc}}) \tag{2.1}$$

where y is the sensitivity-corrected luminescence, a is the asymptotic value of the sensitivity-corrected luminescence, D is the dose, and Dc is the characteristic dose. Following Banerjee et al. (2002), the maximum estimable dose can be found from D=3.5*Dc. Table 2.1 compares these maximum estimable doses for the IR-stimulated OSL, and the IR-stimulated OSL from a post-IR blue stimulation sequence. The calculations show that using the IR-stimulated signal from a post-IR blue-stimulation sequence generally significantly increases the maximum estimable dose (although not in all cases, e.g., albite and andesine), compared to blue-, IR-, and post-IR blue-stimulation. The increase in maximum estimable dose (as compared to the infrared-stimulated signal) ranges over 340-2630 Gy (considering errors) or 170-1310 ka (based upon a dose rate of 2 Gy*ka^{-1}). However, it needs to be pointed out that these are only estimates based upon laboratory procedures and at this point it remains to be seen how effective the various procedures are at measuring an equivalent dose or depositional age.

Using this post-IR blue-stimulation method may extend the potential age range for feldspars (the presented results are only for laboratory dose response curves), but the procedure may also more closely approximate natural conditions. Numerous researchers have shown that IR stimulation only removes a portion of the trapped charge in feldpsars (Duller, 1997). By emptying only IR sensitive traps, charge builds-up in the competitors

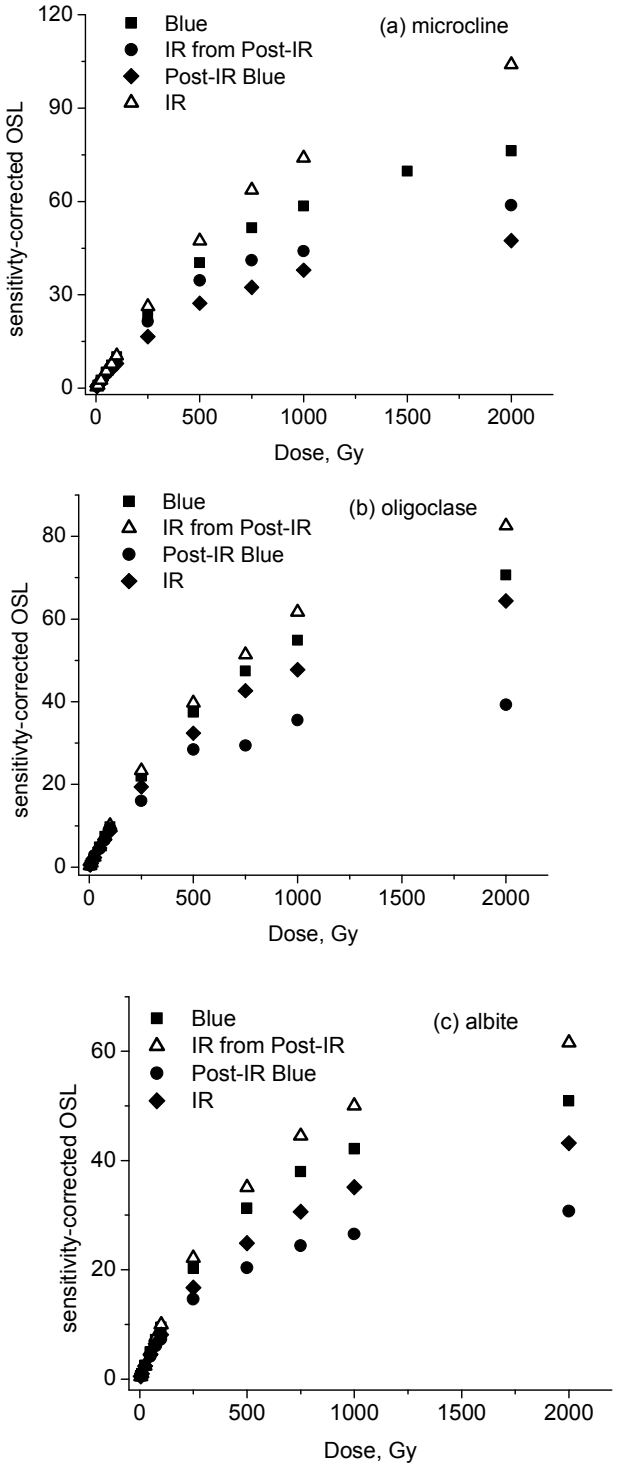

Figure 2.16 Dose response curves using four different OSL signals for (a) microcline, (b) oligoclase, and (c) albite produced using SAR. The stimulation wavelength is indicated in the caption.

Mineral	Stimulation	Max. Est. Dose (10^2 Gy)
microcline	IR	22.0 ± 0.14
	IR from Post-IR	36.0 ± 0.13
oligoclase	IR	28.0± 0.11
	IR from Post-IR	31.0 ± 0.10
anorthoclase	IR	12.0 ± 0.12
	IR from Post-IR	35.0± 0.20
albite	IR	20.0 ± 0.10
	IR from Post-IR	21.0 ± 0.08
andesine	IR	30.0± 0.30
	IR from Post-IR	32.0± 0.19

Table 2.1 Comparison of maximum estimable dose for various feldspars using different stimulation procedures. See text for details of fitting equation used.

and reduces competition during subsequent irradiation. Therefore, the IR-sensitive traps become more effective at trapping charge and saturate at a smaller dose. When IR stimulation is followed by blue stimulation, a greater amount of trapped charge is released (Duller, 1997) and competition effects are more pronounced during subsequent irradiation. This means that a higher dose would be required to saturate the IR-sensitive traps. Huot and Lamothe (2003) used a solar simulator to bleach feldspar samples after each test dose OSL measurement. The latter situation may more closely approximate natural conditions since in nature sediments are bleached by the entire solar spectrum (or at least more than just IR wavelengths) which empties the IR-sensitive traps as well as the competitors.

2.2.6 Dose Recovery Experiments

Dose recovery experiments, such as are described in Section 2.1, were carried out using blue- (20 aliquots), infrared- (5 aliquots), and post-IR blue-stimulation (5 aliquots). For blue-stimulated OSL, the samples were annealed and both a geologic dose (either 750 Gy or 100Gy) and geologic bleaching (1300 s of bleaching with the blue diodes) were simulated. For infrared- and post-IR blue-stimulated OSL, the "as received" samples were first preheated and bleached. The remainder of the experimental conditions are given in Table 2.2. Since no conclusion had as yet been made as to whether or not heating (i.e., TL) should be included in the sensitivity-correction procedure, two different forms of dose recovery experiments were conducted. In one set of experiments, no TL measurements were made, while in the other set, a TL measurement to 500^{o}C was performed after each T_i.

Blue stimulation

1. OSL for 300 s
2. TL to 500oC
3. 1000 Gy (microcline) or 750 Gy (others) simulated geologic dose
4. OSL for 1300 s
5. Known dose given (~9 Gy)
6. Dose recovery: TDi =2 Gy, Di = 8,10,12,8, and 0 Gy

Infrared and post-IR stimulation

1. Preheat at 220oC for 10 s
2. OSL for 300 s
3. Known dose given (18 Gy)
4. Dose recovery: TDi = 5 Gy, Di = 16,20,24,16, and 0 Gy

Table 2.2 Experimental procedures for dose recovery tests.

Table 2.3 gives the dose recovery ratio (recovered dose/given dose), the recycling ratio (L4/L1, regeneration doses 1 and 4 were equal to each other), and the recuperation (L5, regeneration dose 5 was 0 Gy) along with the standard deviation of the mean for each sample from the experiments conducted without making any TL measurements. With the exception of the post-IR data for anorthoclase, all the known doses could be recovered to within a 5% error. In addition, the recycling ratios were generally close to 1.0 indicating that the procedure corrected for laboratory-induced changes, and very little recuperation was seen. However, anorthoclase when stimulated with blue light did produce a low recycling ratio (0.94 ± 0.04) and produced an average negative recuperation value. The anorthoclase data presents a problem and will be discussed further.

Table 2.4 presents the same data as Table 2.2 for the case when TL was measured after each T_i. For blue- and infrared-stimulated OSL, the known dose could generally be recovered to within 5% (again, anorthoclase presented serious problems as will be discussed). However, for the post-IR data, the dose recovery ratios (except for oligoclase) were greater than 1.11 while the recycling ratios ranged from 0.94-1.01 and recuperation values ranged from 0.006-0.02.

Annealing (measuring TL) after each T_i may improve precision in the laboratory procedure, but depending upon the signal used, could lead to larger errors in equivalent dose estimation. Figure 2.17 partly explains why. The graphs show the normalized OSL decay curves from anorthoclase for the "natural dose" and the second regeneration dose for both procedures (with and without a TL measurement). For infrared-stimulated OSL (Figure 2.17 (b)), all three decay curves have the same general shape, and errors from the

Sample	Signal	Dose Rec. Ratio	Recycl. Ratio	Recuperation
Microcline	Blue-OSL	0.997 ± 0.006	0.999 ± 0.004	0.006 ± 0.001
	IRSL	1.03 ± 0.01	0.99 ± 0.01	0.056 ± 0.001
	IRSL before blue	1.03 ± 0.01	1.00±0.01	0.010±0.001
	Post-IR OSL	1.06 ± 0.02	0.98 ± 0.01	-0.04 ± 0.01
Oligoclase	Blue-OSL	0.988 ± 0.003	1.002 ± 0.002	0.0109 ± 0.0004
	IRSL	0.99 ± 0.01	1.02 ± 0.01	0.025 ± 0.001
	IRSL before blue	1.01±0.01	1.03±0.01	0.009±0.001
	Post-IR OSL	1.03 ± 0.06	1.01 ± 0.05	-0.020 ± 0.005
Anorthoclase	Blue-OSL	0.93 ± 0.04	0.94 ± 0.04	-0.68 ± 0.06
	IRSL	1.06 ± 0.02	0.99 ± 0.04	0.09 ± 0.01
	IRSL before blue	0.98±0.03	0.98±0.04	0.01±0.02
	Post-IR OSL	1.07 ±0.01	0.99 ± 0.01	-0.01 ± 0.03
Albite	Blue-OSL	0.984 ± 0.001	0.999 ± 0.002	0.0196 ± 0.0005
	IRSL	0.997 ± 0.004	1.00 ± 0.01	0.045 ± 0.001
	IRSL before blue	1.04±0.02	0.96±0.02	0.01±0.01
	Post-IR OSL	1.03 ± 0.01	0.99 ± 0.01	-0.02 ± 0.01
Andesine	Blue-OSL	1.004 ± 0.007	0.996 ± 0.005	-0.033 ± 0.003
	IRSL	1.00 ± 0.06	0.96 ± 0.04	0.02 ± 0.01
	IRSL before blue	1.05±0.02	0.95±0.02	0.00±0.01
	Post-IR OSL	1.057 ± 0.008	0.98 ± 0.01	0.000 ± 0.003

Table 2.3 Results of dose recovery experiments for blue-stimulated (20 aliquots), infrared-stimulated (5 aliquots), and post-IR blue-stimulated OSL (5 aliquots). The "Dose Rec. Ratio" is the ratio of the recovered dose to the known dose, the "Recycling Ratio" is L_4/L_1 (the first and fourth regeneration doses are equal), and "Recuperation" is L_5 resulting from a 0 Gy regeneration dose. All reported errors are the standard deviation of the mean.

Sample	Signal	Dose Rec. Ratio	Recycl. Ratio	Recuperation
Microcline	Blue-OSL	1.045 ± 0.004	0.995 ± 0.005	-0.0011 ± 0.0003
	IRSL	1.09 ± 0.01	0.98 ± 0.03	0.000 ± 0.002
	IRSL before blue	1.096±0.004	1.02±0.02	0.001±0.001
	Post-IR OSL	1.14 ± 0.01	0.94 ± 0.02	0.006 ± 0.002
Oligoclase	Blue-OSL	1.008 ± 0.003	1.000 ± 0.004	0.008 ± 0.001
	IRSL	1.02 ± 0.01	1.00 ± 0.01	-0.001 ± 0.001
	IRSL before blue	1.00±0.02	0.99±0.02	0.001±0.002
	Post-IR OSL	0.96 ± 0.03	1.01 ± 0.04	0.01 ± 0.01
Anorthoclase	Blue-OSL*			
	IRSL	1.02 ± 0.02	0.96 ± 0.02	0.00 ± 0.02
	IRSL before blue	1.05±0.04	0.99±0.04	-0.01±0.03
	Post-IR OSL	1.18 ± 0.02	0.99 ± 0.01	0.002 ± 0.001
Albite	Blue-OSL	1.017 ± 0.002	1.001 ± 0.002	0.0009 ± 0.0003
	IRSL	1.06 ± 0.01	1.01 ± 0.01	0.002 ± 0.002
	IRSL before blue	1.14±0.02	1.00±0.01	0.000±0.001
	Post-IR OSL	1.12 ± 0.01	0.99 ± 0.02	0.02 ± 0.01
Andesine	Blue-OSL	1.051 ± 0.009	1.00 ± 0.01	0.013 ± 0.003
	IRSL	1.04 ± 0.02	1.01 ± 0.08	-0.03 ± 0.04
	IRSL before blue	1.2±0.1	0.9±0.1	0.5±0.4
	Post-IR OSL	1.13 ± 0.01	1.00 ± 0.02	0.009 ± 0.004

*Data could not be analyzed. See text for reason.

Table 2.4 Results of dose recovery experiments where TL to 500°C was measured after each T_i. All calculations and experimental procedures are the same as Table 2.3.

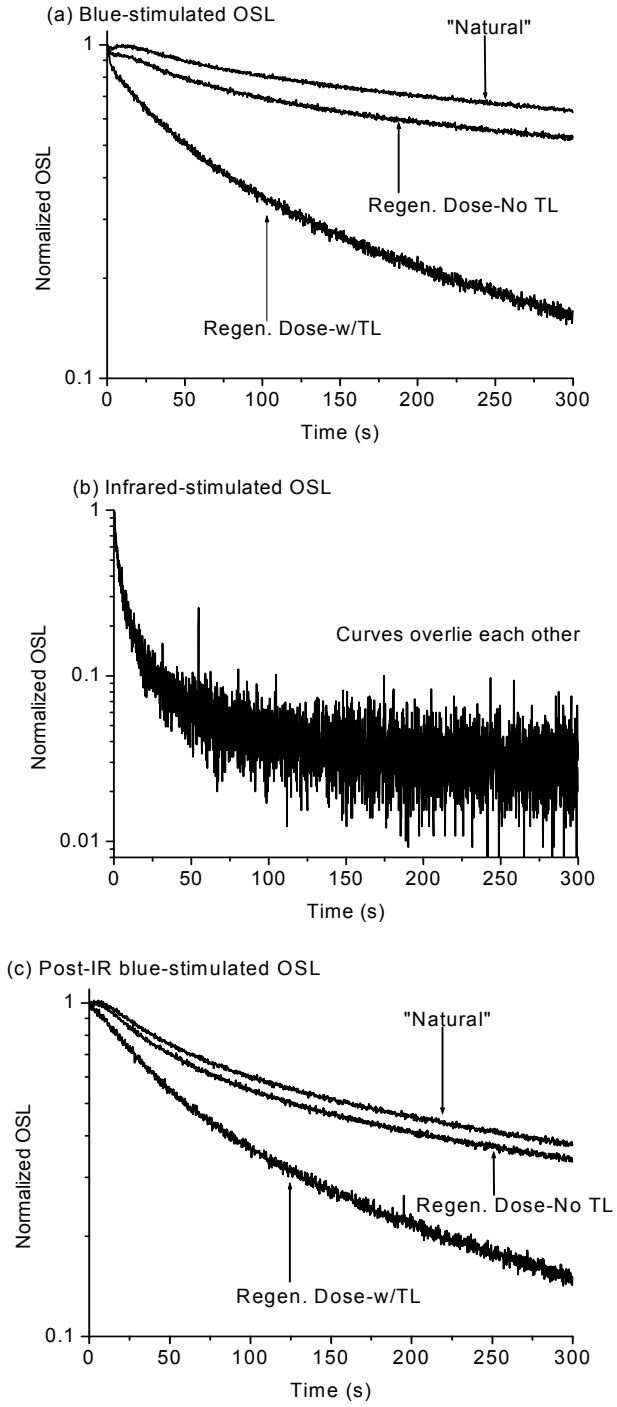

Figure 2.17 Normalized OSL decay curves from the dose-recovery experiments with anorthoclase. Each graph shows the known ("Natural") OSL and the second R_i with (Regen. Dose-No TL) and without a TL measurement (Regen. Dose-w/TL) after each T_i. Results are shown for each method of OSL stimulation: (a) blue, (b) infrared: and (c) post-IR blue.

dose recovery experiments were similar. However, for blue-stimulated and post-IR blue-stimulated OSL, the curve from the experiments including TL to 500°C after each T_i shows a much smaller relative background level than either of the two decay curves that have not been annealed to 500°C. In these cases, when the samples are annealed to 500°C during the dose recovery process, different charge populations are measured from the natural dose and regeneration doses. Therefore, we cannot expect the regeneration dose signals to accurately estimate the natural dose.

As noted, anorthoclase presented serious problems for the blue-stimulated OSL dose recovery experiments. Figure 2.17 (a) shows that the "natural" OSL decay curve had an initial increase, and several subsequent regeneration and test dose OSL decay curves showed the same phenomenon when TL was not incorporated in the measurement procedure. For the 0 Gy dose, the effect often led to a negative value as the initial part of the OSL decay curve was less intense than the tail of the decay curve, and hence the average recuperation value is negative. Also, when TL was measured to 500°C after each T_i, the slow component of the OSL was greatly reduced which led to a proportionally larger OSL signal. These phenomena often led to sensitivity-corrected "natural" signals much smaller than comparable regeneration signals, and hence very low recovered doses (even negative recovered doses in extreme cases where TL was measured after each T_i). Therefore, the results have not been shown.

2.3 Experiments with Quartz

The previous section showed that the SAR procedure could be adapted to coarse-grain feldspars if the same preheating procedure is used after the regeneration and test doses (i.e., cutheat = preheat). While most luminescent materials on Mars will be of

feldspathic composition as discussed in Section 1.3.1, for the outlined procedure to be a true polymineral procedure, the sensitivity-correction procedure must be shown to be valid for all types of minerals including quartz. This section investigates using a preheat in place of a conventional cutheat for coarse-grain quartz samples.

2.3.1 Materials and Equipment

Four different quartz samples were used for these experiments. One of the quartz samples used (495A, from the OSU lab) was a sedimentary sample from Texas of grain size 90-125 μm. The other three quartz samples (021714, 022513, 030218) were in the 180-220 μm grain range fraction and were supplied by Dr. Andrew Murray of Risø National Labs. For luminescence measurements, the grains were deposited on stainless steel discs using silicone spray, and the previously described Risø TL/OSL-DA-15 system was used.

2.3.2 Correcting for Sensitivity Change

Experiments were undertaken to test the SAR sensitivity-correction procedure following laboratory radiation doses delivered to the four quartz samples to determine if the regeneration and test dose signals are directly proportional. The samples were first preheated (220 ºC for 10 s) and bleached with blue LEDs for 500 s at 125 ºC. Seven cycles of the SAR procedure with a fixed regeneration dose of 6 Gy, a test dose of 1.44 Gy, and OSL stimulations at 125 ºC for 100 s were then performed. This sequence was carried out for preheats ranging from 160-300 ºC for 10 s in 20º increments, and two different test dose heating procedures were tested. In one case, the cutheat was fixed at 160 ºC for 0 s, while in the other case the cutheat was replaced by a preheat equal to the preheat used after the regeneration dose.

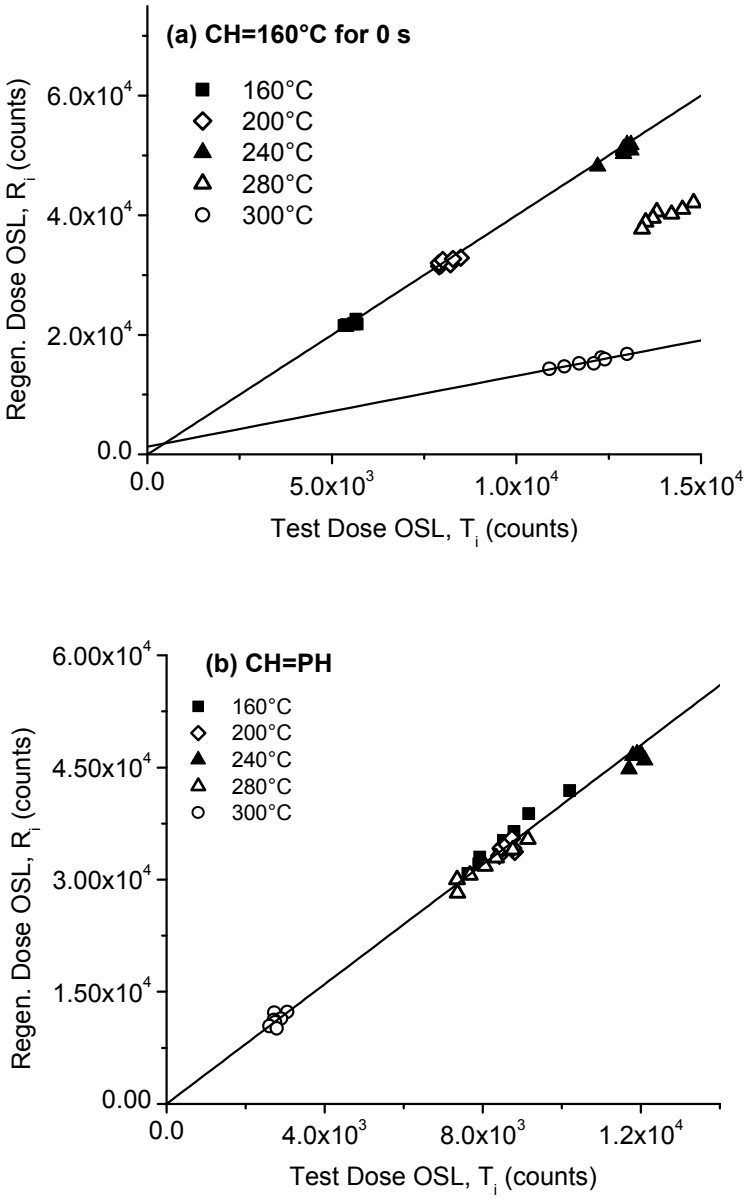

Figure 2.18 Tests of sensitivity-correction procedure for quartz sample #495A. The preheats used are indicated in the figure. (a) used a fixed cutheat of 160°C while (b) used a cutheat equal to the previous preheat in both temperature and duration. Note: The 200 °C data in (b) is overlain by the 160 °C and 280 °C data.

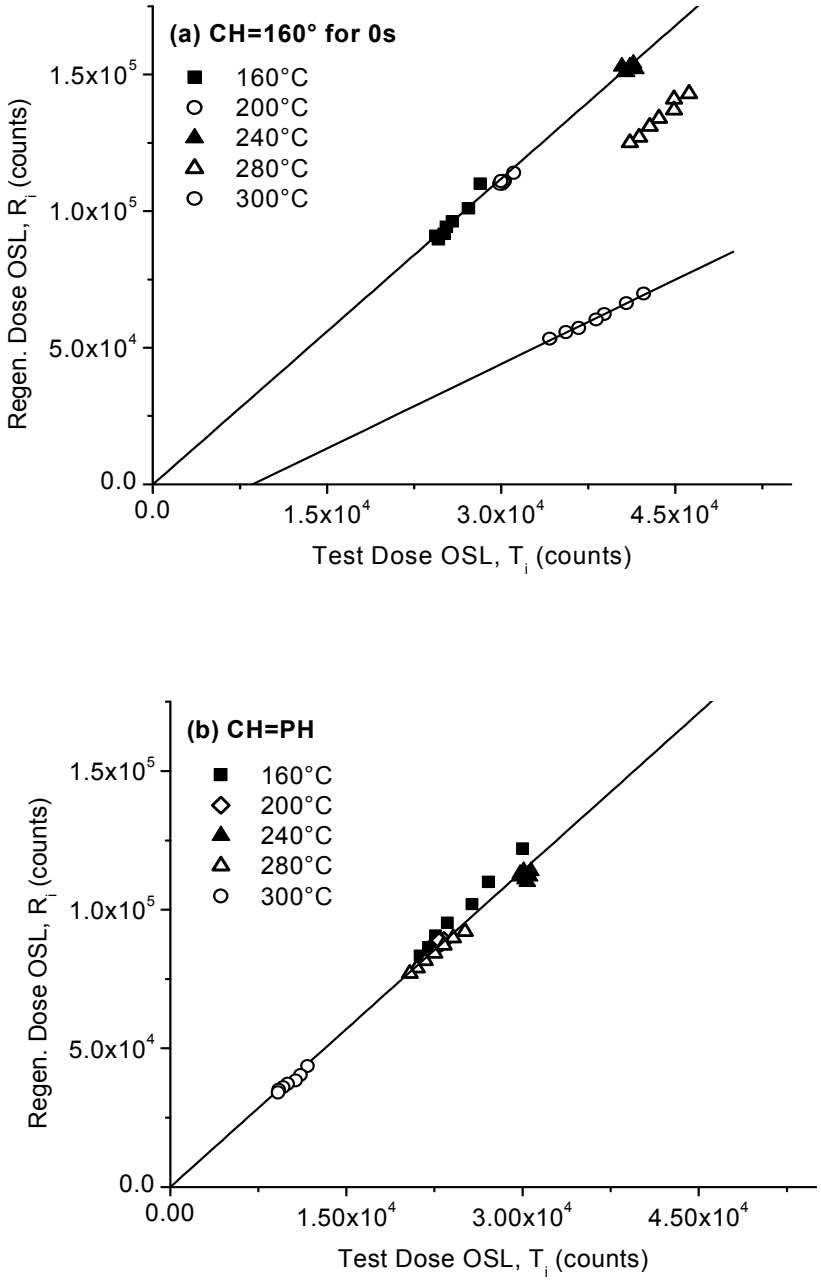

Figure 2.19 Same as Figure 2.18 except for sample #021714.

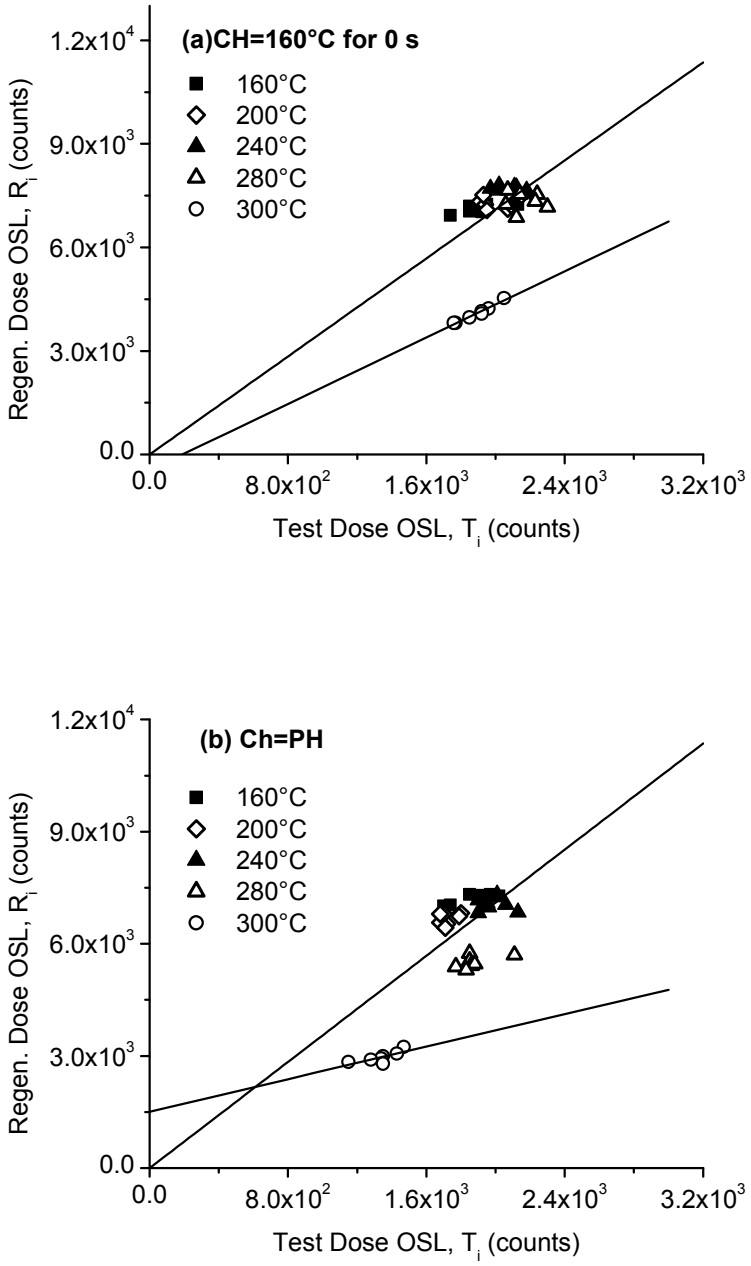

Figure 2.20 Same as Figure 2.18 except for sample #022513.

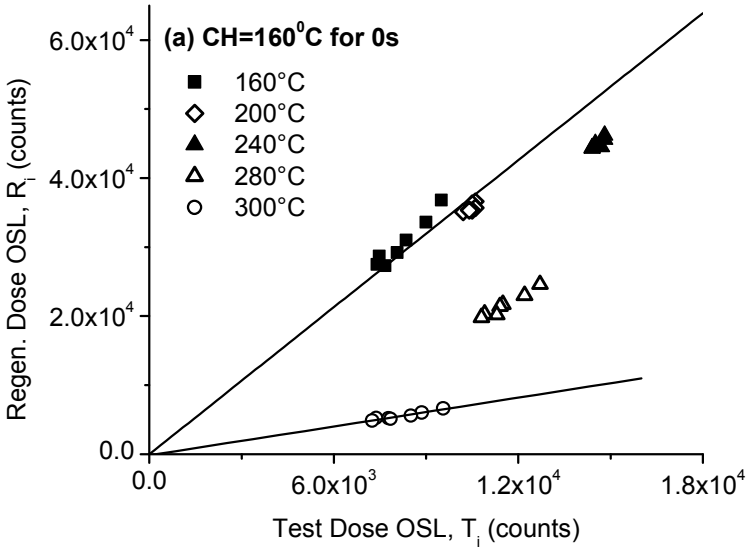

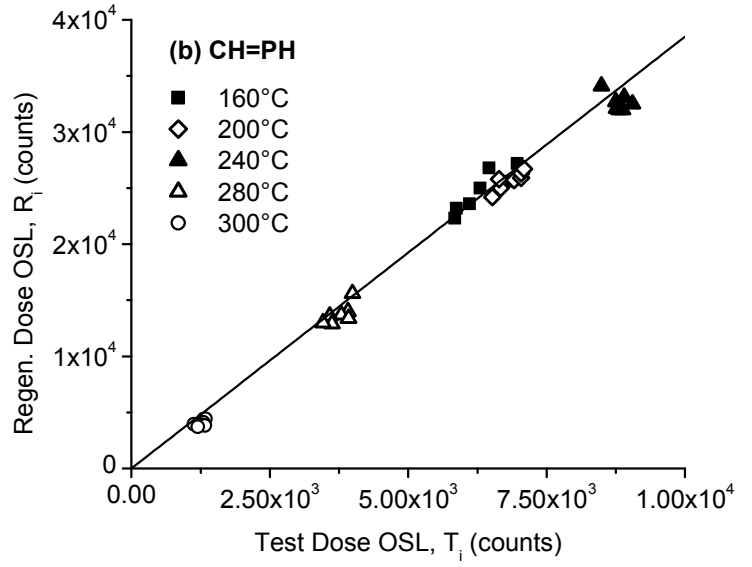

Figure 2.21 Same as Figure 2.18 except for sample #030218.

Results for the above experiment are shown in Figures 2.18-2.21. The graphs show regeneration dose OSL versus test dose OSL for the two different cases. For a fixed cutheat of 160 ºC (graph (a) in the four figures), the procedure appears to be effective for preheats 160-260 ºC, but experiments that use higher preheats typically show a significant intercept. When the cutheat is equal to the preheat (graph (b) in the four figures), there appears to be a small intercept for a preheat of 160-180 ºC, but the sensitivity-correction appears to be valid for preheats 200-300 ºC. These results agree with previous work on the SAR procedure for quartz (Murray and Wintle, 2000) in that a low temperature cutheat can be effective, and potentially extend previous findings in that the cutheat can not only vary in temperature but also in duration (e.g., the cutheat can be replaced by a preheat under certain conditions).

Based upon the presented data, it is difficult to determine if using a preheat in place of a cutheat changes the sensitivity of the sample (the sensitivity appears to be reduced, but this may be due to the same aliquots being used repeatedly). However, even if using a preheat after the test dose does change the sensitivity of the sample, the regeneration and test dose OSL measurements are directly proportional. Therefore, the cutheat within the SAR procedure may be replaced by a preheat (equal to the regeneration preheat) over certain preheat temperature ranges. While Murray and Wintle (2000) found little dependence of the recovered equivalent dose (D_e) on cutheat temperature, the study did not specifically test the use of a preheat in place of the cutheat. In order to develop a true polymineral procedure, this procedure needed to be tested directly as it has previously been shown (Auclair *et al.*, 2003; Huot and Lamothe, 2003; Section 2.2) that the cutheat must be equal to regeneration dose preheat for feldspar

samples. Note however, that the present data are only for laboratory irradiations, and the effectiveness of the proposed modifications for recovering D_e from sedimentary samples cannot be evaluated at this point.

2.3.3 OSL Dose Response

The dose response of the four quartz samples was measured using both a conventional cutheat (e.g., 160°C for 0 s) and a preheat after the test dose equal to the preheat after the regeneration dose. Both of these methods were used to produce dose response curves for preheats from 160°C to 300°C (each for 10 s) in 20° increments. Even though replacing the cutheat with a preheat has been shown to be effective for sensitivity-correction, experiments with a conventional cutheat were still performed so that dose response curves produced using the modified procedure could be compared to a "standard".

Uncorrected dose response curves produced from only the regeneration dose signals (R_i) are shown in Figure 2.22. Very little difference can be seen between the two methods, and neither method produces any supralinearity in these samples. However, using a preheat in place of a cutheat does seem to produce slightly less OSL from the largest doses (250 Gy and 500 Gy), and the lower OSL intensity can probably be attributed to competition during irradiation. When using a conventional cutheat, some traps are not emptied during the test dose measurement that are emptied when using a preheat. Then, during subsequent irradiation, those traps that are full do not compete for charge and the dosimetric trap becomes more effective at trapping charge resulting in a larger OSL. Still, this effect is small in most samples.

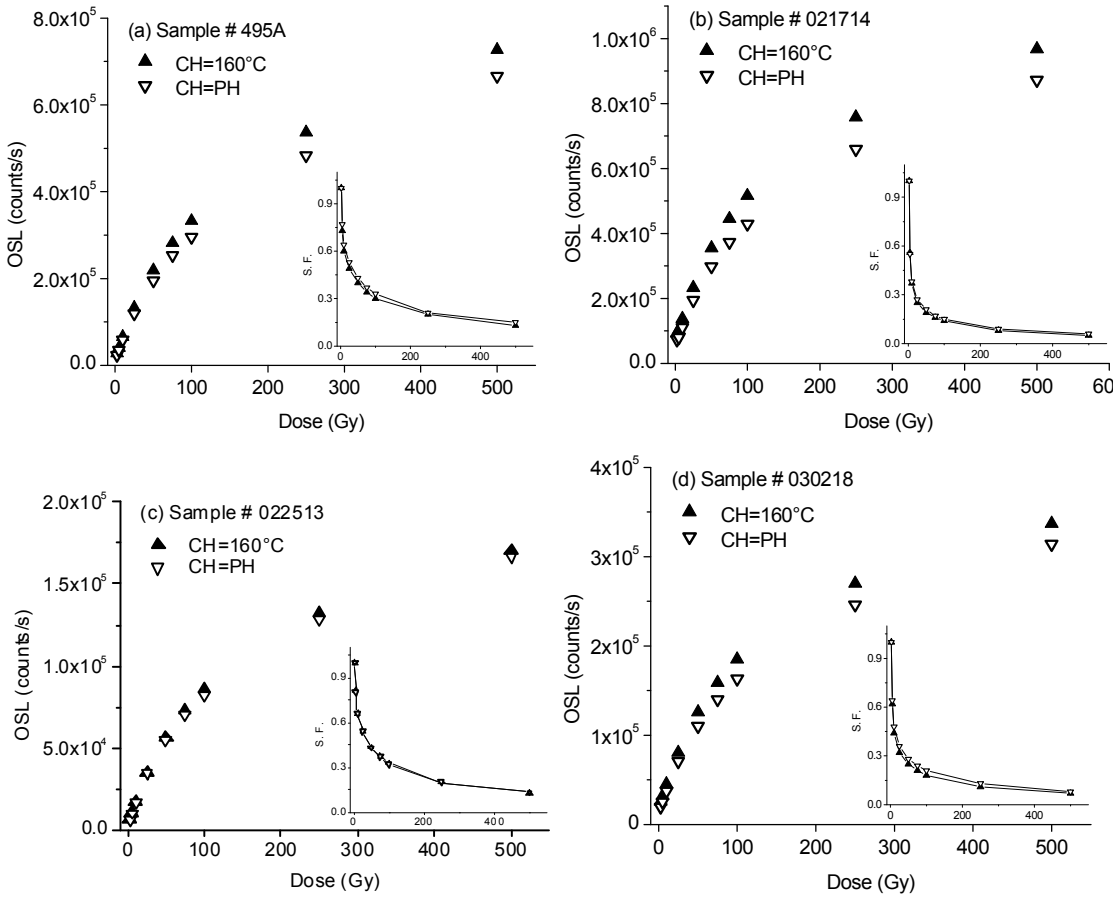

Figure 2.22 Uncorrected (R_i only) dose response curves for quartz samples (a) 495A, (b) 021714, (c) 022513, and (d) 030218. Blue-stimulated OSL was used for all experiments.. All preheats were 260°C for 10s and all OSL measurements were for 300s. The supralinearity factor, as defined by Chen and McKeever (1997), is shown in the inset of each graph.

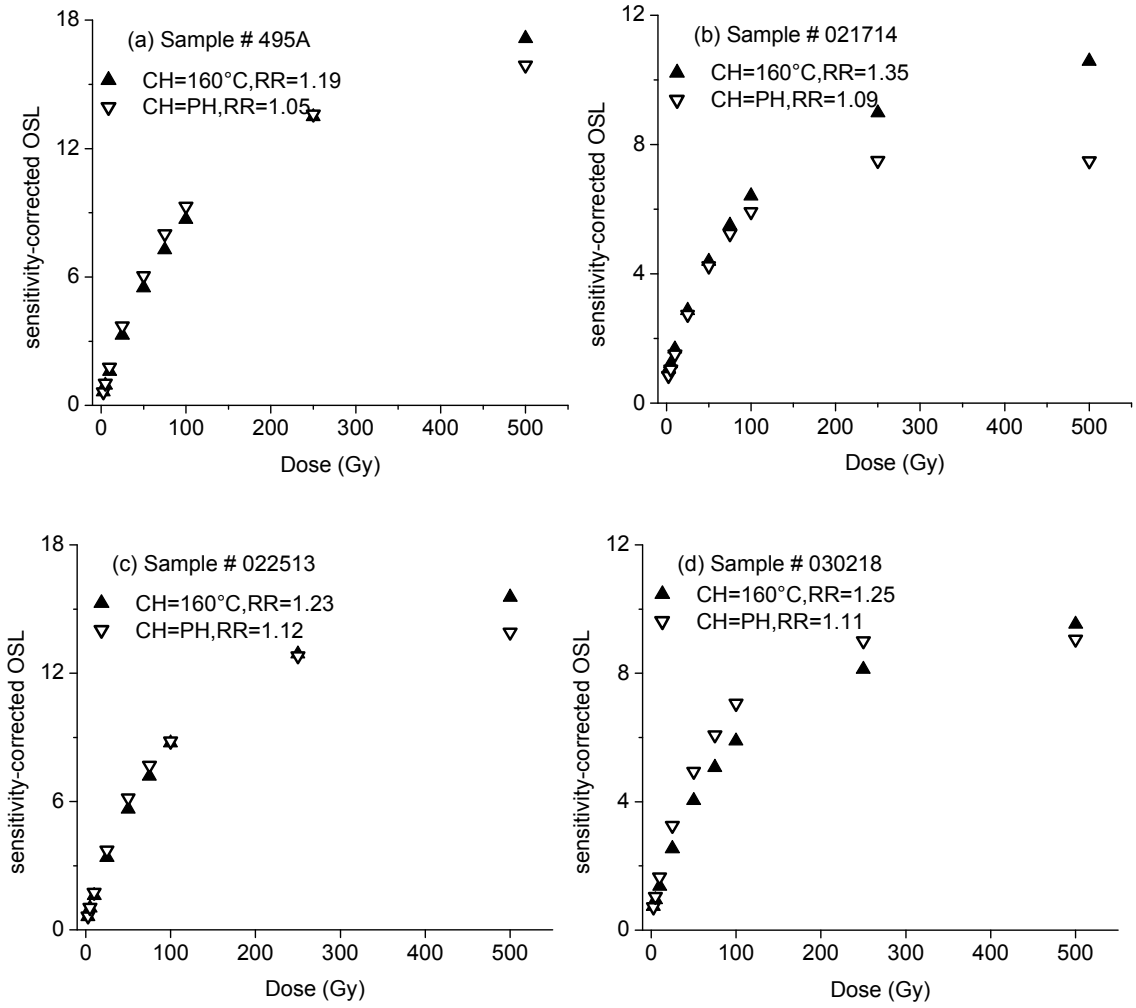

Figure 2.23 Sensitivity-corrected (L_i) dose response curves for quartz samples (a) 495A, (b) 021714, (c) 022513, and (d) 030218, constructed using both the modified SAR procedure and the traditional approach (e.g., CH =160°C for 0 s). All of the experiments used blue-stimulated OSL, and the recycling ratios are given (RR).

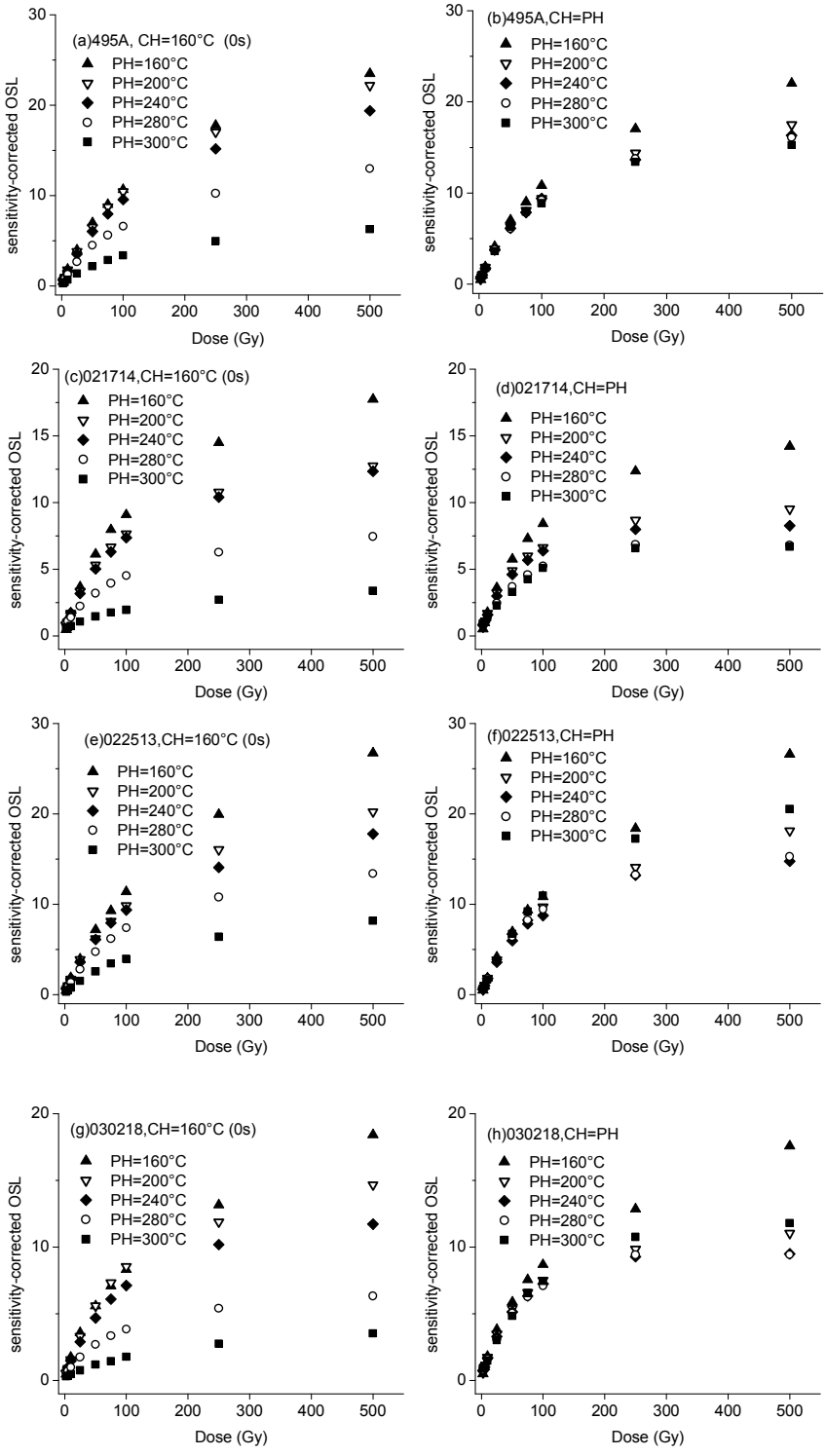

Figure 2.24 Sensitivity corrected dose response curves for a range of preheats for all of the quartz samples studied (sample numbers as noted in graphs). In the left column (graphs (a), (c), (e), and (g)), a traditional cutheat of 160°C for 0 s was used. In the right column (graphs (b), (d), (f), and (h)), a preheat equal to the preheat after the regeneration dose was used in place of a cutheat.

Sensitivity-corrected dose response curves are shown in Figure 2.23. Again, not much difference can be seen between the two methods (at least for this preheat temperature), although using a preheat in place of a cutheat does result in a smaller L_i signal probably attributable to the competition effects discussed previously. However, when dose response curves from a range of preheats are plotted on the same graph (Figure 2.24), a difference in the two methods does become apparent. In the left hand column of Figure 2.24 when a conventional cutheat of 160°C for 0 s is used in the sensitivity-correction procedure, the sensitivity-corrected values (L_i) for high temperature preheats (greater than or equal to 280°C) are significantly lower than when using lower temperature preheats. While this effect is more pronounced in the sublinear region of the curves, it is even apparent in the linear portion. On the other hand, when the conventional cutheat is replace by a preheat equal to the preheat after the regeneration dose (the right column in Figure 2.24), the L_i values are much more consistent when using different preheats, particularly for preheats with a temperature greater than 160°C. This effect can be explained by the proportionality of the two signals as discussed in Section 2.3.2.

When using high temperature preheats (greater than or equal to 280°C), a portion of the main dosimetric trap (for OSL, the main dosimetric trap has a peak temperature of 325°C in quartz) is eroded with each preheat. Therefore, the subsequent OSL signal arises from only a portion of the trap. Yet, when a conventional cutheat is used after the test dose, the OSL signal arises from the entire dosimetric trap. Therefore, the OSL signal from the test dose is proportionally larger than the OSL signal from the regeneration dose, and the two signals are not proportional as previously seen in Section

2.3.2. Consequently, using a conventional cutheat in combination with a preheat greater than 280°C could yield incorrect sensitivity-corrected values. When the cutheat is replaced by a preheat, the test dose OSL signal arises from the same proportion of the dosimetric trap as the regeneration dose OSL signal for high temperature preheats. For low temperature preheats (less than 180°C), however, replacing the cutheat with a preheat may not be valid since the sensitivity changes in this case may not be dominated by competition effects during irradiation and optical stimulation (Murray and Wintle, 2000).

2.3.4 Dose Estimation and Dose Recovery Experiments

As a final test of applying the proposed procedure to quartz, dose estimation and dose recovery experiments were undertaken. Since the quartz samples were natural samples that still contained a natural dose, D_es could be estimated from all the samples using both a conventional cutheat and a preheat in place of the cutheat. As a further test of the validity of the procedure, dose recovery experiments were conducted for known doses in both the linear and sublinear portions of the dose response curves.

The D_e estimation was performed using both a traditional cutheat and a preheat in place of the cutheat. The results of these estimates are given in Figure 2.26, along with an independent estimate of the D_e for sample 495A provided by Dr. Regina Kalchgruber (personal communication). These estimates do not show any significant difference in the precision of the sensitivity-correction methods, and the results from sample 495A imply that replacing the cutheat by a preheat is accurate as well.

Dose recovery experiments were performed by first preheating the samples at 260°C for 10 s, bleaching the samples with blue light for 100 s, giving the samples a

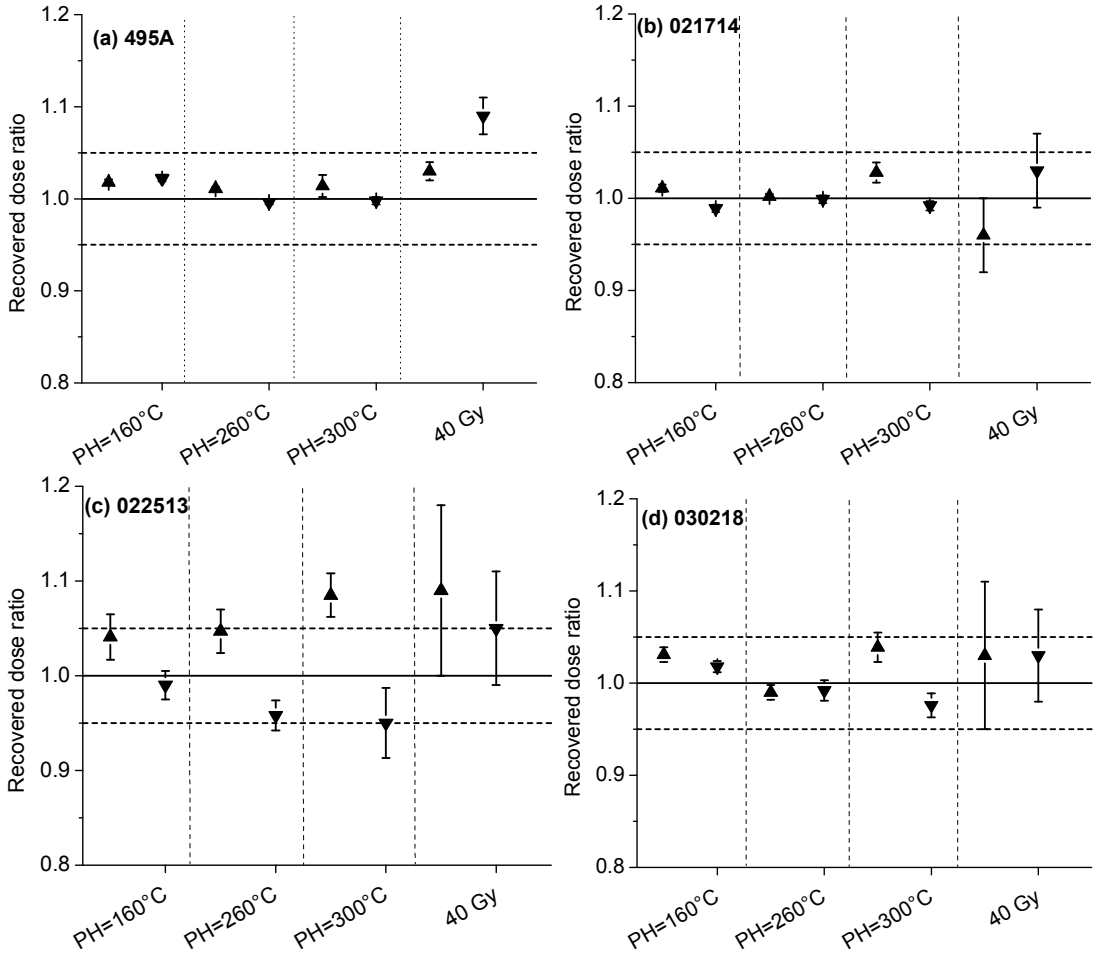

Figure 2.25 Results of dose recovery experiments for the denoted quartz samples. For each preheat, the dose was recovered using a conventional cutheat of 160°C for 0 s (upward pointing triangle) and using a preheat in place of a cutheat (downward pointing triangle). The 40 Gy dose was recovered using a 260°C for 10 s preheat and was chosen as it is in the sublinear region of the dose response curve. The horizontal dashed lines represent ± 5% error.

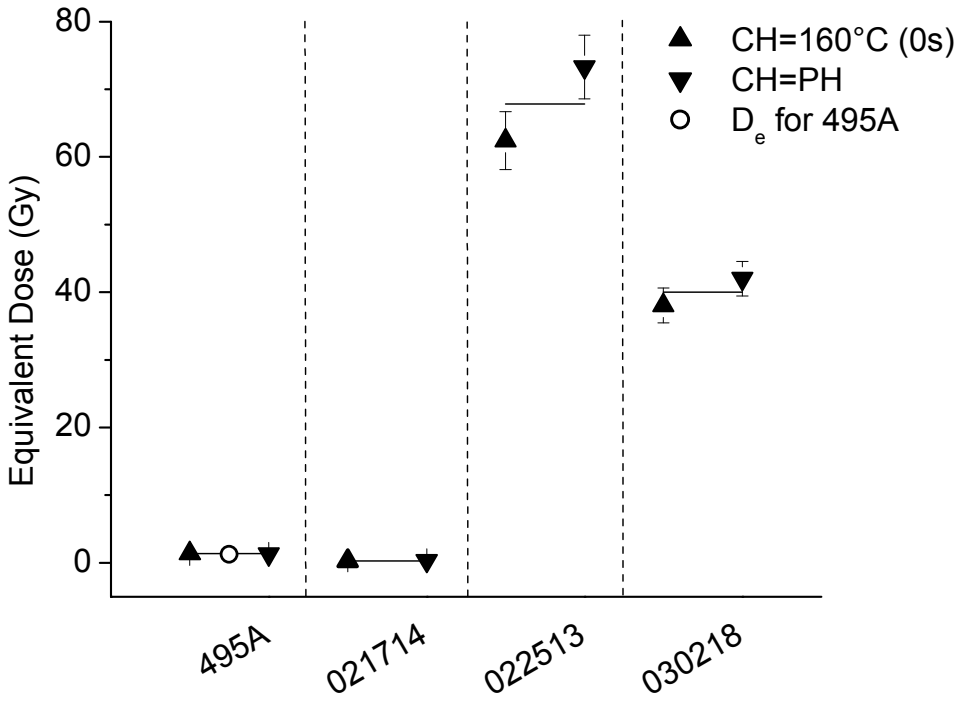

Figure 2.26 Average D_e for the various quartz samples as noted. For each sample, the D_e was estimated using a conventional cutheat (upward pointing triangles) and by replacing the cutheat with a preheat (downward pointing triangles). The horizontal line in each case represents the average or the two D_e estimates. In addition, an independent estimation of the D_e for sample 495A was provided by Dr. Regina Kalchgruber (personal communication) as indicated in the graph by an open circle.

known radiation dose, then recovering that dose using the SAR procedure. The known dose was recovered using both a conventional cutheat (160° for 0 s) and by replacing the cutheat with a preheat. In addition, the dose recovery experiment was performed using a 4 Gy known dose and preheats of 160°C, 260°C, and 300°C (each for 10 s), and a 40 Gy known dose (chosen as this was in the sublinear region of the dose response curve) with a 260°C for 10 s preheat. The experiments with a 4 Gy known dose was performed for 24 samples, while the experiments with a known dose of 40 Gy used 12 samples. The average dose recovery ratios (recovered dose/given dose) from all these variations of the dose recovery experiment are given in Figure 2.25.

The graphs in Figure 2.25 show that in almost all cases the known dose can be recovered with less than a 5 % error when the standard deviations of the data are considered. In the two cases where the errors were greater than 5 %, the error was 7 % for one case (sample 495A, 40 Gy known dose with the cutheat replaced by a preheat) and 6% for the other case (sample 022513, 4 Gy known dose with a conventional cutheat and a preheat of 300°C for 10 s). Although it is important that a known dose can be recovered under all these different circumstances, it is more important that no clear difference can be discerned between the two methods.

2.4 Experiments with Quartz and Feldspar Mixtures

The two previous sections have investigated modifications to the SAR procedure with the goal of developing a polymineral procedure that can estimate the D_e from a variety of minerals. Section 2.2 studied coarse-grain feldspar samples and concluded that the SAR procedure could be used with these materials if the conventional cutheat was replaced by a preheat equal to the preheat after the regeneration dose and if a post-IR

blue-stimulation OSL sequence was used. Then, in Section 2.3, it was shown that the conventional cutheat could be replaced by a preheat (under certain conditions) for coarse-grain quartz samples. In this section, different mixtures of coarse-grain quartz and feldspar samples will be studied in an attempt to test the proposed modifications to the SAR procedure.

2.4.1 Materials and Equipment

Three different mixtures of sediments were prepared from materials already studied. The mixtures contain the quartz sample 495A and the feldspar albite. One mixture (Mixture #1) was 75 % quartz and 25 % feldspar, another mixture (Mixture #2) was 50 % quartz and 50 % feldspar, and the third mixture (Mixture #3) was 25 % quartz and 75% feldspar. All the percentages are weight percentages of the total mixture, and all the experiments were performed on the previously described Risø TL/OSL dating apparatus.

2.4.2 Correcting for Sensitivity Change

Although sensitivity change experiments were performed for all these mixtures, the results are not given here, as they are largely the same as previous sections. However, the effectiveness of two different sensitivity-correction procedures is still discussed here, one using a conventional cutheat of 160°C for 0 s and one replacing the cutheat with a preheat. The results are reported only for the two OSL signals from the post-IR blue-stimulation sequence.

Results from the sensitivity-correction procedure tests are given in Figures 2.27 (infrared-stimulated OSL (IRSL) from post-IR blue-stimulation sequence) and 2.28 (post-IR blue-stimulated OSL). It is important to point out that only feldspars can be optically

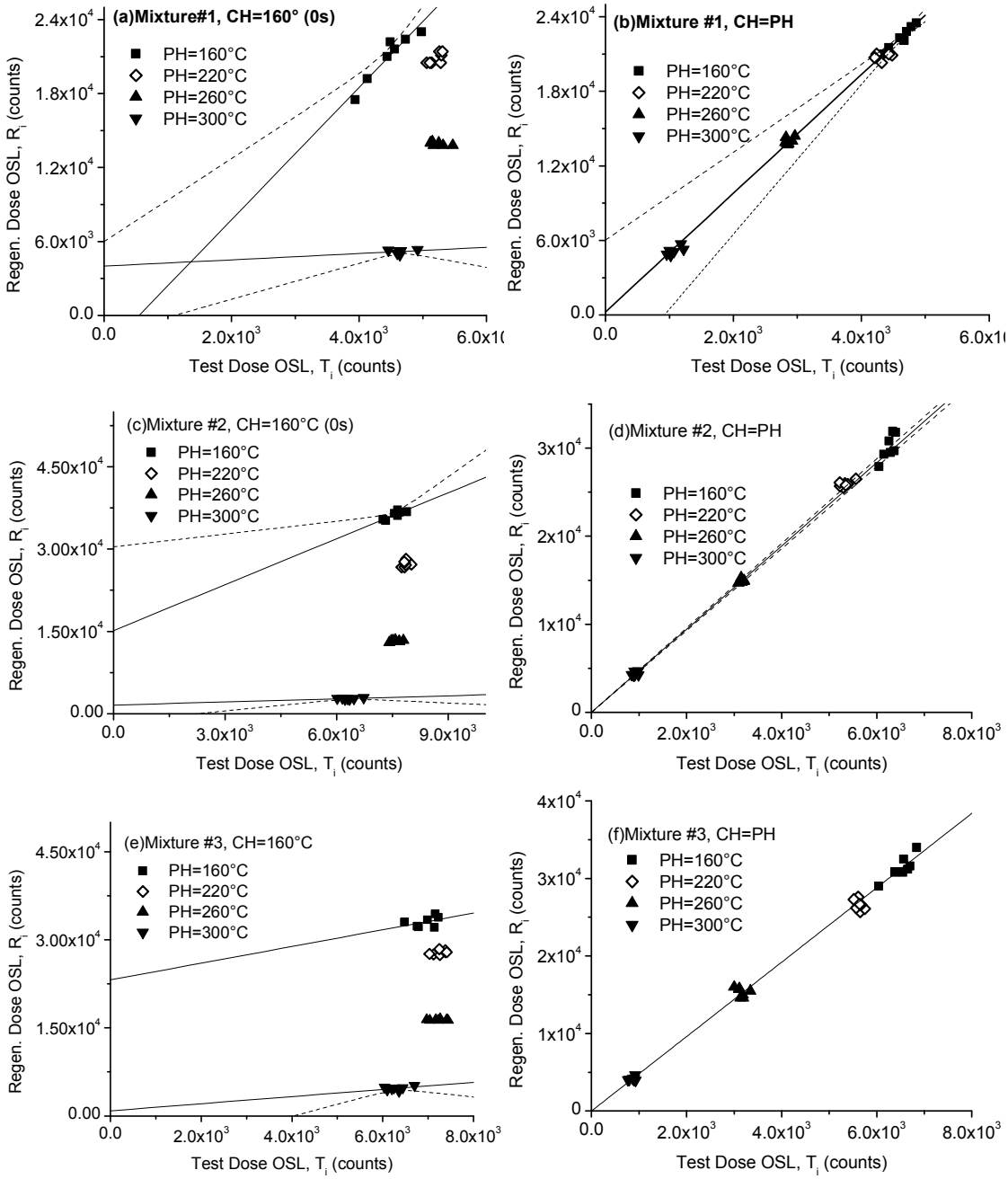

Figure 2.27 Tests of sensitivity-correction procedure for mixtures of quartz and feldspar as indicated. The OSL signal is the IR-stimulated signal from a post-IR blue-stimulation sequence. The preheats used are indicated in the graphs. The graphs on the left used a fixed cutheat of 160°C while the graphs on the right used a cutheat equal to the previous preheat in both temperature and duration.

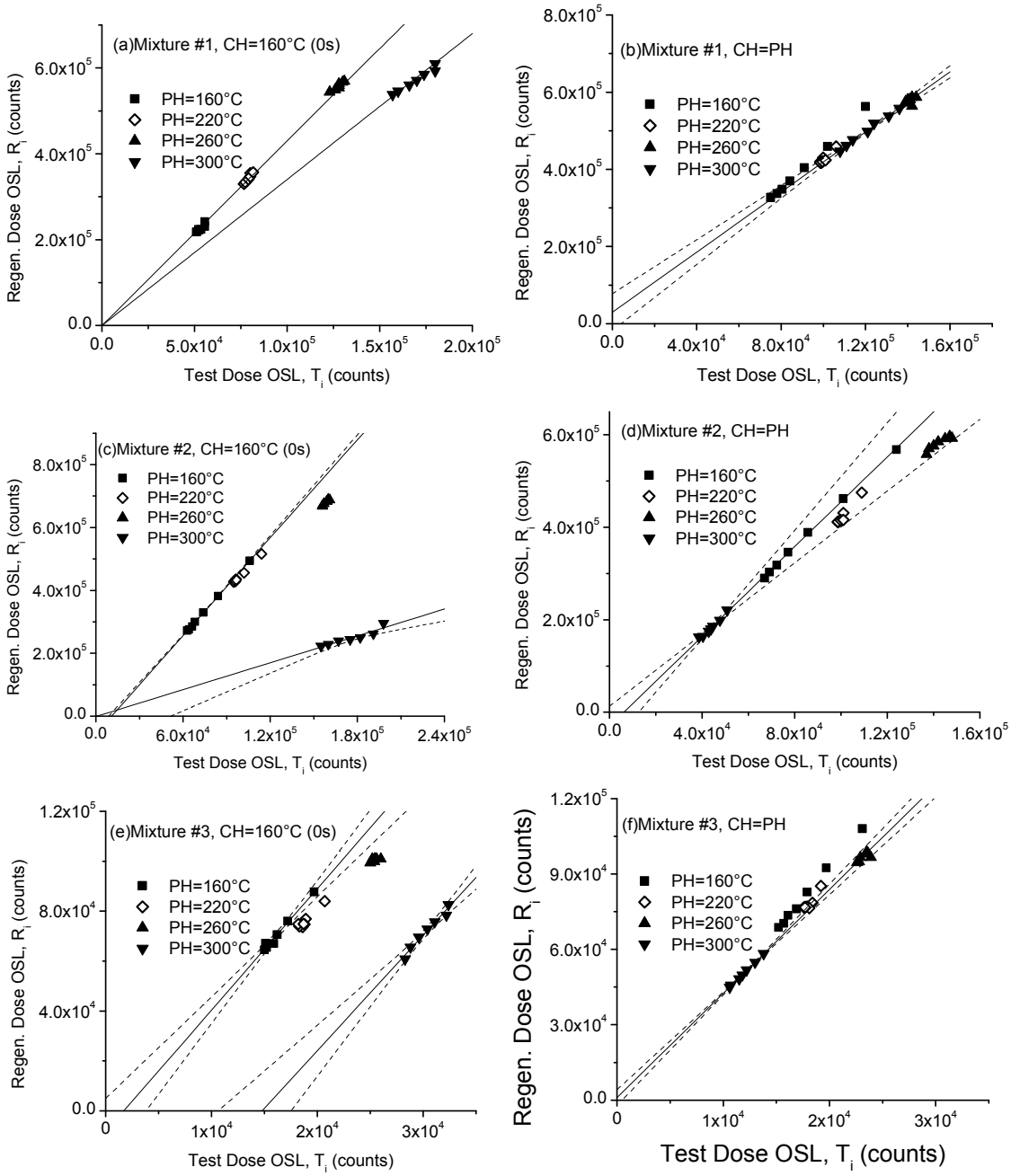

Figure 2.28 Same as Figure .2.27 except the OSL signal is the post-IR blue-stimulated signal.

stimulated by IR light, and these figures show that. Figure 2.27 shows the IR stimulated results, and these results are very similar to the results for feldspar separates (Section 2.2.4, Figures 2.7-2.9) in that the cutheat should be replaced by a preheat for the most effective sensitivity-correction procedure. However, for the post-IR blue-stimulated OSL (a quartz-dominated signal in this case) data (Figure 2.28), it can be seen that either method is effective up to a preheat of 300°C for 10 s. At this temperature, the conventional cutheat becomes less effective when using quartz as previously seen by others (Murray and Wintle, 2000). Considering both figures we see that replacing the conventional cutheat by a preheat seems to be effective in the most situations (i. e, both signals over the largest preheat range).

2.4.3 OSL Dose Response

OSL dose response curves for all the mixtures were produced by using a preheat in place of a cutheat and using a post-IR blue-stimulation sequence. The uncorrected (R_i only) dose response curves along with the supralinearity factors are shown in Figure 2.29 for all three mixtures. The infrared-stimulated OSL (IRSL, graphs (a), (c), and (e)) results are very similar to previous results from albite (Figure 2.12 (c)), and the blue-stimulated OSL results (graphs (b), (d), and (f)) are very similar to the results for quartz sample 495A (Figure 2.22 (a)). The corresponding sensitivity-corrected OSL results in Figure 2.30 also show similar results to previous experiments for the corresponding materials. The apparent separation of a feldspar-dominated signal (IRSL from a post-IR blue-stimulation sequence) and a quartz-dominated signal (post-IR blue-stimulated OSL) agrees with and supports earlier findings of other authors (Banerjee *et al.*, 2001; Wallinga *et al.*, 2002; Roberts and Wintle, 2003).

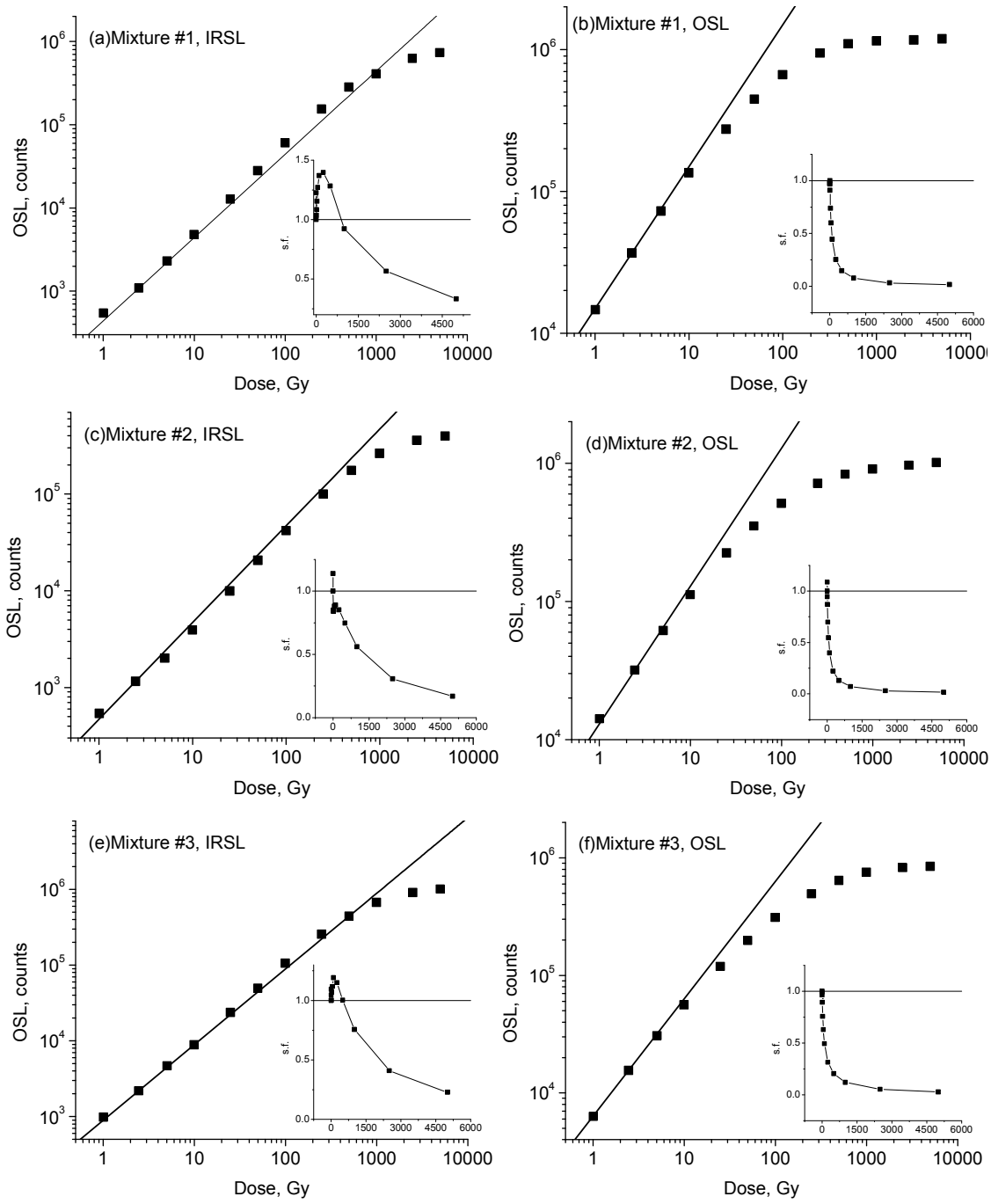

Figure 2.29 Uncorrected (R_i only) dose response curves for quartz and feldspar mixtures as noted. The graphs in the left column (graphs (a), (c), and (e)) are for the infrared-stimulated OSL (IRSL) from a post-IR blue-stimulation sequence, and the graphs in the right column (graphs (b), (d), and (f)) are the post-IR blue-stimulated OSL. All preheats were 260°C for 10s, all OSL measurements were for 300s, and the cutheat was replaced by a preheat in all cases. The supralinearity factor, as defined by Chen and McKeever (1997), is shown in the inset of each graph. Note the log-log scale.

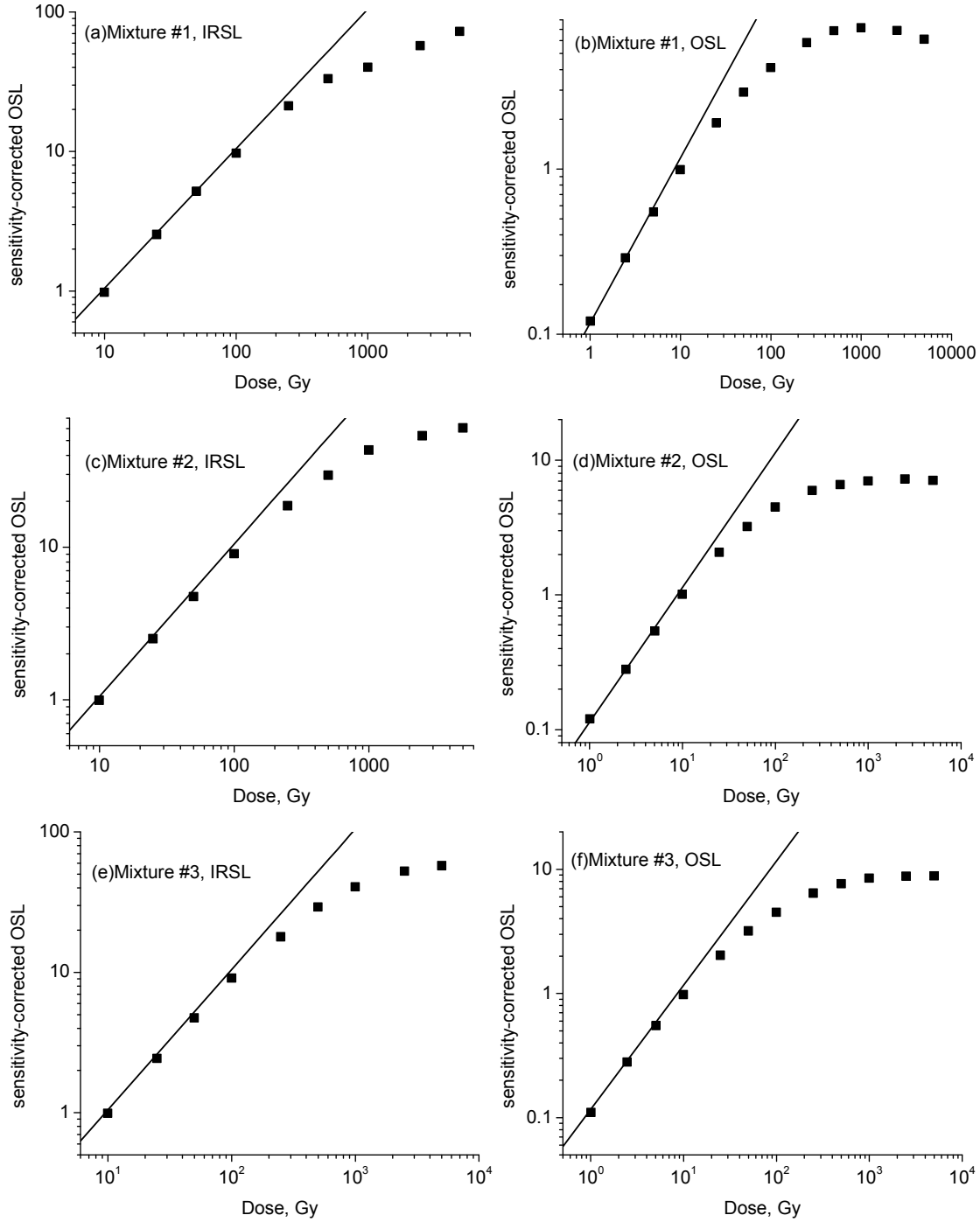

Figure 2.30 Sensitivity-corrected (L_i) dose response curves for quartz and feldspar mixtures as noted. The graphs in the left column (graphs (a), (c), and (e)) are for the infrared-stimulated OSL (IRSL) from a post-IR blue-stimulation sequence, and the graphs in the right column (graphs (b), (d), and (f)) are the post-IR blue-stimulated OSL. All preheats were 260°C for 10s, all OSL measurements were for 300s, and the cutheat was replaced by a preheat in all cases. Note the log-log scale.

2.4.4 Dose Estimation and Dose Recovery Experiments

The final set of experiments for testing the proposed polymineral procedure was to estimate the D_e and recover a known dose from the quartz and feldspar mixtures in various ways. The D_e estimation experiments were possible as the mixtures were created with unbleached samples of 495A which still contained the natural signal. The dose recovery experiments were conducted using a conventional cutheat and a preheat in place of the cutheat for an unknown dose in the linear portion of the dose response curve and a variety of preheats. In addition, dose recovery experiments were also conducted for unknown doses in the sublinear portion of the dose response curve, but only when using a preheat in place of a cutheat.

The results from the dose recovery experiments are summarized in Figure 2.31. This figure shows results from all 3 mixtures for both the infrared-stimulated and blue-stimulated OSL from a post-IR blue-stimulation sequence. For each mixture and signal, the average dose recovery ratio (24 samples in each case, the samples were given a 4 Gy known dose) and standard deviation of the mean is given for three different preheats (160°C, 260°C, and 300°C each for 10 s) while using a conventional cutheat of 160°C for 0 s and while using a preheat in place of a cutheat. In addition, an average dose recovery ratio (from 12 samples) was calculated for each mixture when a 40 Gy known dose was given (chosen as it is in the sublinear potion of the dose response curve) and a 260°C for 10 s preheat was used in combination with a preheat in place of a cutheat. The figure indicates that a small known dose (4 Gy) can be recovered with less than a 5 % error from all of the mixtures using either method and any preheat, although using a traditional cutheat generally results in a larger error.

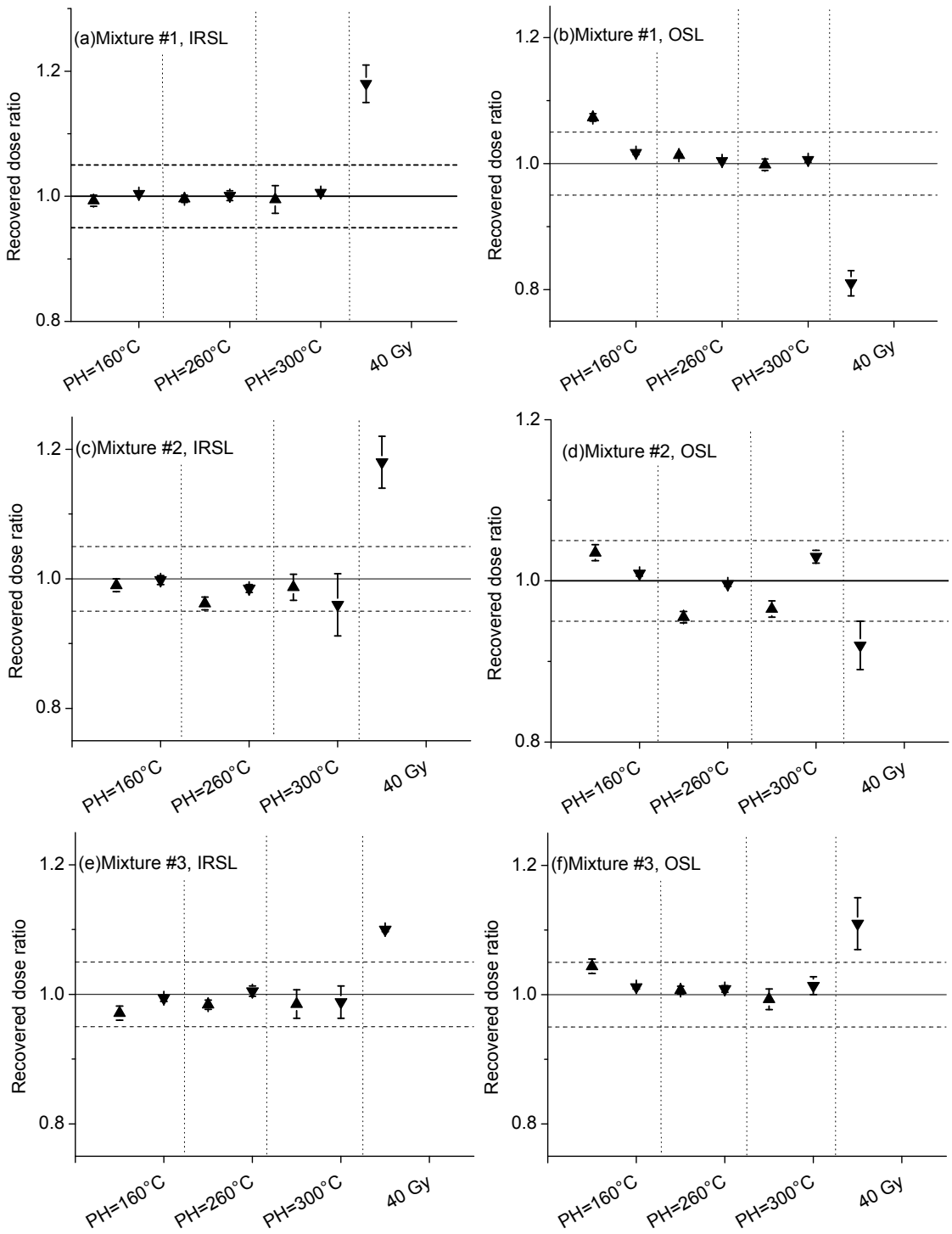

Figure 2.31 Results of dose recovery experiments for the denoted quartz/feldspar mixtures. For each preheat, the dose was recovered using a conventional cutheat of 160°C for 0 s (upward pointing triangle) and using a preheat in place of a cutheat (downward pointing triangle). The 40 Gy dose was recovered using a 260°C for 10 s preheat and was chosen as it is in the sublinear region of the dose response curve. The horizontal dashed lines represent ± 5% error.

While the sublinear known dose (40 Gy) could generally be recovered with less than a 10 % error, the errors were sometimes much larger (e.g., Mixture #1). To recover these sublinear doses, a complete dose response curve for each sample is measured after measuring the known dose, and the dose response curve was then fitted with a saturating exponential function of the form of Equation 2.1. The sensitivity-corrected value of the known dose was then used to estimate the known dose and derive the dose recovery ratio. However, this fitting function may not be appropriate, and tests indicated that using a linear approximation with OSL signals from doses near the known dose (local slope approximation) might be more effective. This discrepancy and potential source of error was not investigated further.

The results of D_e estimation are summarized in Figure 2.32. The figure shows an independent estimate of D_e from Dr. Regina Kalchgruber (personal communication), the previous D_e estimates (Figure 2.26) from the pure quartz sample 495A, and D_e estimates from both Mixture #2 (50 % quartz/50 % feldspar) and Mixture #1 (75 % quartz, 25 % feldspar) for preheats of 160°C, 260°C, and 300°C (each for 10 s) where the conventional cutheat was replaced by a preheat. For the two mixtures of quartz and feldspar, the D_e was estimated from the post-IR blue-stimulated OSL signal, as this signal is quartz-dominated. An attempt was also made to estimate the D_e from Mixture #3 (25 % quartz/75 % feldspar), but the results were erroneous as the feldspar luminescence could not be sufficiently bleached by IR stimulation in order to produce a quartz-dominated post-IR blue-stimulated OSL signal. However, the figure does show that the independent estimate and the two estimates from the pure quartz sample are consistent with each other and that mixtures are consistent under certain conditions (e.g., Mixture #2 using a 300°C

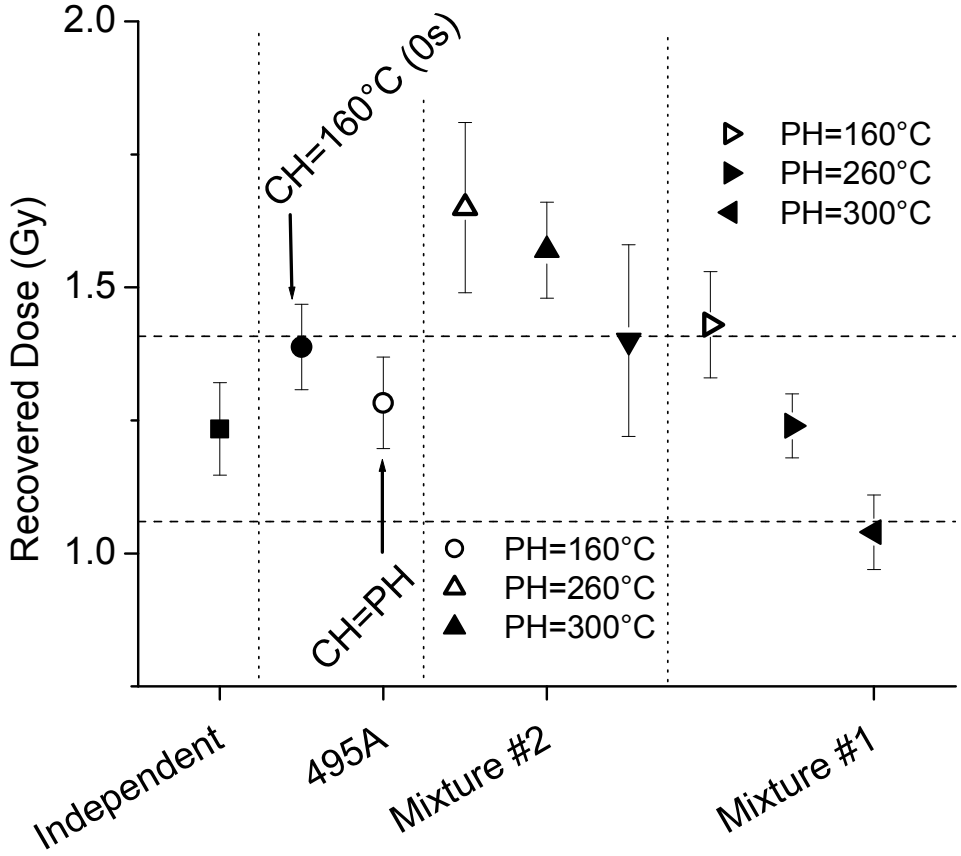

Figure 2.32 The average measured D_e from different samples containing quartz sample 495A. The error bars represent the 1-sigma (standard deviation of the mean) error. The "Independent" value is from Dr. Regina Kalchgruber (personal communication), "495A" represents the pure quartz sample measured for this dissertation, "Mixture #2" is the 50 % quartz/50 % feldspar mixture, and "Mixture #1" is the 75 % quartz/25 % feldspar mixture. The dashed lines represent the 2-sigma error for the "independent" estimate of D_e.

for 10 s preheat). Although these results do not prove that the proposed procedure can accurately date polymineral samples, the presented data do imply that signals from different minerals can be separated by the choice of stimulation method and can produce reliable results with the appropriate choice of preheat temperature and sensitivity-correction procedure.

2.5 Concluding Remarks for Chapter 2

This chapter has been concerned with developing a single-aliquot regenerative-dose OSL dating procedure for estimation of the D_e from polymineral samples. The overriding motivation for developing this procedure is that it will be necessary if OSL dating is to employed on an in-situ instrument on Mars, but the procedure could be useful for terrestrial applications as well.

In the field, geologists often have the desire for rough ages of sediments but do not have a reliable method of determining the ages. A field instrument for OSL dating would be useful in such a situation, and a procedure that does not require mineral separation would make the instrument more practical. Alternatively, if samples are collected to be dated by OSL in the laboratory, the geologist (or potentially archaeologist) may not require the accuracy or precision provided by dates derived from mineral separates. Instead, dates from polymineral samples, which are probably less accurate and certainly less precise, may be suitable to the situation. These dates would be less labor-intensive and time-consuming as mineral separation is not required, and could potentially be less expensive than the OSL dating methods currently available. Such a situation could lead to different prices for different methods of OSL dating that can be chosen based upon the needs and budget of the field geologist.

A suggestion for a polymineral procedure was investigated and tested in this chapter. The procedure is based upon the SAR procedure (Table 1.1) developed for dating coarse-grain quartz (Murray and Wintle, 2000) and later extended to polymineral fine-grain samples (Banerjee *et al.*, 2001). However, this procedure (as developed) has not been generally able to recover known doses from coarse-grain feldspar samples (Wallinga *et al.*, 2000a, 2000b) except in certain circumstances (Preusser, 2003). Section 2.2 showed that by replacing the conventional cutheat in the SAR procedure with a preheat equal in temperature and duration to the preheat after the regeneration dose, the SAR procedure could recover known doses given to coarse-grain feldspar samples. In addition, by using the infrared-stimulated OSL signal from a post-IR blue-stimulation sequence, it is possible to slightly extend the range of doses that can be estimated and more closely approximate the natural bleaching of the samples. Other researchers have seen similar results (Lamothe *et al.*, 2001; Huot and Lamothe, 2003; Auclair *et al.*, 2003), although a solar simulator was used to bleach the samples after IR stimulation in those cases.

The experiments in Section 2.2 also found that sensitivity changes in feldspars can be largely eliminated by annealing the samples to 500°C after each test dose OSL measurement. This method was later abandoned for D_e estimation, as it does not simulate the conditions that most minerals experience in nature. However, this phenomenon could be the basis for a different type of procedure. Duller (1992) noticed the same phenomena and suggested a single-aliquot procedure for coarse-grain feldspars where the samples were annealed after each OSL measurement. This procedure could be used to cross-calibrate radiation sources on different instruments. Although apparently

effective, it did not contain any method of sensitivity-correction, and it was shown that sensitivity changes can be seen even when the samples are annealed (Section 2.2, p. 17; Figures 2.10-2.12). Therefore, incorporating a sensitivity-correction method as suggested here with Duller's suggested procedure could provide a very accurate method for cross-calibration.

The suggested changes to the SAR procedure were further tested on other samples. In Section 2.3 it was shown that replacing the traditional cutheat with a preheat can be effective for correcting sensitivity changes experienced by coarse-grain quartz samples. Although this result does not directly contradict earlier findings (Murray and Wintle, 2000), it is important for development and acceptance of the procedure to directly test it. Furthermore, when using a preheat instead of a cutheat, the D_e can be effectively estimated and known doses (even those in the sublinear portion of the growth curve) can be recovered using the procedure.

Finally, the full procedure (Table 2.5) was tested on three different mixtures of quartz and feldspars in Section 2.4. The procedure can correct for sensitivity changes for these mixtures (Figures 2.27 and 2.28) and correct for any supralinearity in the samples (Figures 2.29 and 2.30). More importantly, the D_e could be precisely estimated in most cases (Figure 2.32), with the notable exception of Mixture #3 (25 % quartz/75 % feldspar), and known doses from the linear portion of the dose response curve could be recovered to within a 5 % error (Figure 2.31). Unfortunately, doses from the sublinear portion of the dose response curve could not always be accurately recovered, but this may be due to the fitting function that was chosen as discussed previously. While these results may not be relevant for martian sediments as quartz is not expected in large abundances

1. Regeneration radiation dose (D_i)
2. Preheat at $T_P{}^oC^{\#}$ for 10 s
3. Measure IRSL @ 60°C (IR_i)
4. Measure OSL at 125^oC (R_i)
5. Fixed test radiation dose (TD_i)
6. Preheat at $T_P{}^oC^{\#}$ for 10 s
7. Measure IRSL @ 60°C (IT_i)
8. Measure OSL at 125^oC (T_i)
9. Repeat steps 1-8 for a range of regeneration doses including a repeat point and a 0 Gy Dose.
10. Find sensitivity-corrected IRSL ($IL_i=IR_i/IT_i$)
11. Find sensitivity-corrected OSL ($L_i=R_i/T_i$)

T_P determined from experiment

Table 2.5 The suggested modified SAR procedure (Murray and Wintle, 2000) for polymineral samples. Note the same heating procedures are used after the regeneration dose (step 2) and test dose (step 5), and that a post-IR blue-stimulation sequence is used.

on Mars (Bandfield, 2002), the ability to measure mineral specific signals from a polymineral sample is important for potential terrestrial applications.

The modified SAR procedure meets the basic requirements of a single-aliquot procedure for several different specific minerals and some mixtures of those minerals. However, the procedure cannot be confidently adopted for either terrestrial or martian applications at this point. For martian applications, the procedure needs to be tested for minerals expected in the martian regolith and martian soil simulants. In addition, the procedure needs to be used to estimate D_es from terrestrial polymineral samples with independent age controls.

CHAPTER THREE

CHARACTERIZATION OF OSL PROPERTIES OF MARTIAN SIMULANTS AND MINERALS

The preceding chapter developed an OSL dating procedure for potential use with polymineral samples either in a terrestrial setting (e.g., a geological field instrument) or an a robotic instrument to perform *in situ* dating of martian soils. The developed procedure was based upon the SAR procedure (Murray and Wintle, 2000) for coarse grain quartz and contains some small but significant changes. First, in order to correct for sensitivity changes in feldspars, the traditional cutheat used after the test dose must be replaced by a preheat equal in temperature and duration to the preheat used after the regeneration dose (Section 2.2.4). This replacement was also shown to be valid for pure quartz samples as well as quartz and feldspar mixtures (Sections 2.3.2 and 2.4.2). Second, the OSL stimulation procedure should consist of both infrared and blue stimulation (Sections 2.2.5 and 2.4.5). Using this stimulation procedure more closely mimics natural bleaching of the sediments (as compared with infrared only stimulation), reduces sensitivity changes in feldspars, extends the potential age-range of feldspars, and allows the separation of feldspar-dominated (infrared stimulated OSL) and quartz-dominated (blue stimulated OSL) signals. The proposed procedure is outlined in Table 3.1 (same as Table 2.5).

1. Regeneration radiation dose (D_i)
2. Preheat at $T_P{}^oC^{\#}$ for 10 s
3. Measure IRSL @ 60°C (IR_i)
4. Measure OSL at 125^oC (R_i)
5. Fixed test radiation dose (TD_i)
6. Preheat at $T_P{}^oC^{\#}$ for 10 s
7. Measure IRSL @ 60°C (IT_i)
8. Measure OSL at 125^oC (T_i)
9. Repeat steps 1-8 for a range of regeneration doses including a repeat point and a 0 Gy Dose.
10. Find sensitivity-corrected IRSL ($IL_i=IR_i/IT_i$)
11. Find sensitivity-corrected OSL ($L_i=R_i/T_i$)

T_P determined from experiment

Table 3.1 The suggested modified SAR procedure (Murray and Wintle, 2000) for polymineral samples. Note the same heating procedures are used after the regeneration dose (step 2) and test dose (step 5), and that a post-IR blue-stimulation sequence is used.

The current chapter tests the underlying assumptions of the proposed procedure for various martian simulants (JSC Mars-1, OSU Mars-1, and OSU Mars-2) and minerals (i.e., martian meteorites) while characterizing the basic luminescence properties of these minerals. All of the samples were fixed by silicone spray on stainless steel disks, and the experiments were conducted in one of the previously described Risø TL/OSL DA-15 systems (using the IR laser diode). First, the effect of bleaching on the TL curves was measured to determine what traps are optically sensitive. The OSL sensitivity changes of the minerals were studied and the proposed procedure was tested to see if it can correct for the observed sensitivity changes. The modified SAR procedure was then used to determine the dose response curves for the minerals to determine the linear and sublinear portions of the curves along with the theoretical maximum absorbed doses that can be estimated from these minerals. Finally, dose recovery tests, in both the linear and non-linear portions of the dose response curve, were also conducted.

3.1 Materials

The martian simulant JSC Mars-1 has previously been described in Section 1.3.1. The simulant is derived from the Pu'u Nene volcano on Mauna Kea, Hawaii and was chosen by JSC based upon reflectance spectra. The luminescence properties of the coarse grain (Lepper and McKeever, 2000) and fine grain (Banerjee *et al.*, 2002) fractions of JSC Mars-1 have previously been studied in detail, so an in-depth study of this material will not be undertaken here.

The martian simulants OSU Mars-1 and OSU Mars-2 have previously been described in Section 1.3.1. The simulants were created by Dr. Regina Kalchgruber based upon recent data from Mars Global Surveyor (Bandfield *et al.*, 2000; Bandfield 2000).

The simulants consist of plagioclase feldspars, pyroxenes, hematite, and obsidian (Table 1.2). A more detailed study of the luminescence characteristics of both martian simulants developed by OSU is given in Kalchgruber *et al.* (in press), but the relevant tests for the proposed procedure are given here.

Most martian meteorites do not match well with the spectral characteristics of the martian surface and therefore may not be representative of martian soils[1] (Bandfield, 2002). However, they are the only martian samples currently available and are therefore worthy of study. As such, the basic luminescence characteristics of four martian meteorites have been studied (provided by Dr. Derek Sears of the University of Arkansas). The meteorites are designated as ALH 77005,74, Shergotty (SH 400), Zagami, and EET 79001,74. Some of the basic luminescence properties have been previously studied (Banerjee *et al.*, 2002), and the TL results were found to be consistent with meteorites that contain feldspar in the low temperature ordered state. In this section, various tests using the proposed procedure are carried out on these martian meteorites.

3.2 Identification of Optically Active Traps

The optically active traps (i.e., those traps that bleach when exposed to light) for all of the materials were identified in the same way. A TL measurement to 500°C was first made to empty any charge in the TL traps. The samples were then given a 300 Gy (5000 Gy for JSC Mars-1) dose, stored for 600 s, and the TL to 500°C was measured again. The TL signal was then measured a third time after 300 Gy doses and bleaching

[1] The martian meteorites are generally composites of bedrock material and therefore should not be expected to have the same spectral characteristics of the martian surface. The meteorites have the same mineralogy as the martian surface but differ in the specific composition as the meteorites generally show a greater variety (Bandfield, 2002).

by infrared, blue, and a post-IR blue stimulation sequence. (Appropriate pauses were added so that the TL was always measured 600 s after irradiation.)

The effect of bleaching by different wavelengths on the TL of JSC Mars-1, OSU Mars-1, and OSU Mars-2 is shown in Figure 3.1. For JSC Mars-1, OSU Mars-1, and OSU Mars-2, infrared stimulation appears to affect mainly lower temperature traps below 250°C with little change in the TL curve above this temperature. Blue and post-IR blue stimulation both reduce the TL curve up to about 400°C, although in each case the TL curve is unaffected for temperatures above 400°C. It is important to note, however, that a significant TL signal remains above 100°C for infrared stimulation and above 250°C for blue stimulation after 300 s of stimulation. Yukihara *et al.* (2002) found that a significant luminescence signal remains even after 1800 s of bleaching. This unbleached charge could cause important competition effects during the OSL dating process.

The effect of bleaching by different wavelengths on the TL of the studied martian meteorites is shown in Figure 3.2. Three of the meteorites (ALH 77005,74, Shergotty, and EET 79001,170) show a large TL peak near 100°C while Zagami does not exhibit a clear TL peak at any temperature. All of the meteorites, though, appear to have an almost continuous distribution of TL traps that is typical of feldspathic materials. Unlike the previous simulants studied, infrared, blue, and post-IR blue stimulation seem to affect mostly the same traps although blue and post-IR blue stimulation more effectively bleach the traps. Also, there is a significant residual TL signal after applying any of the bleaching methods.

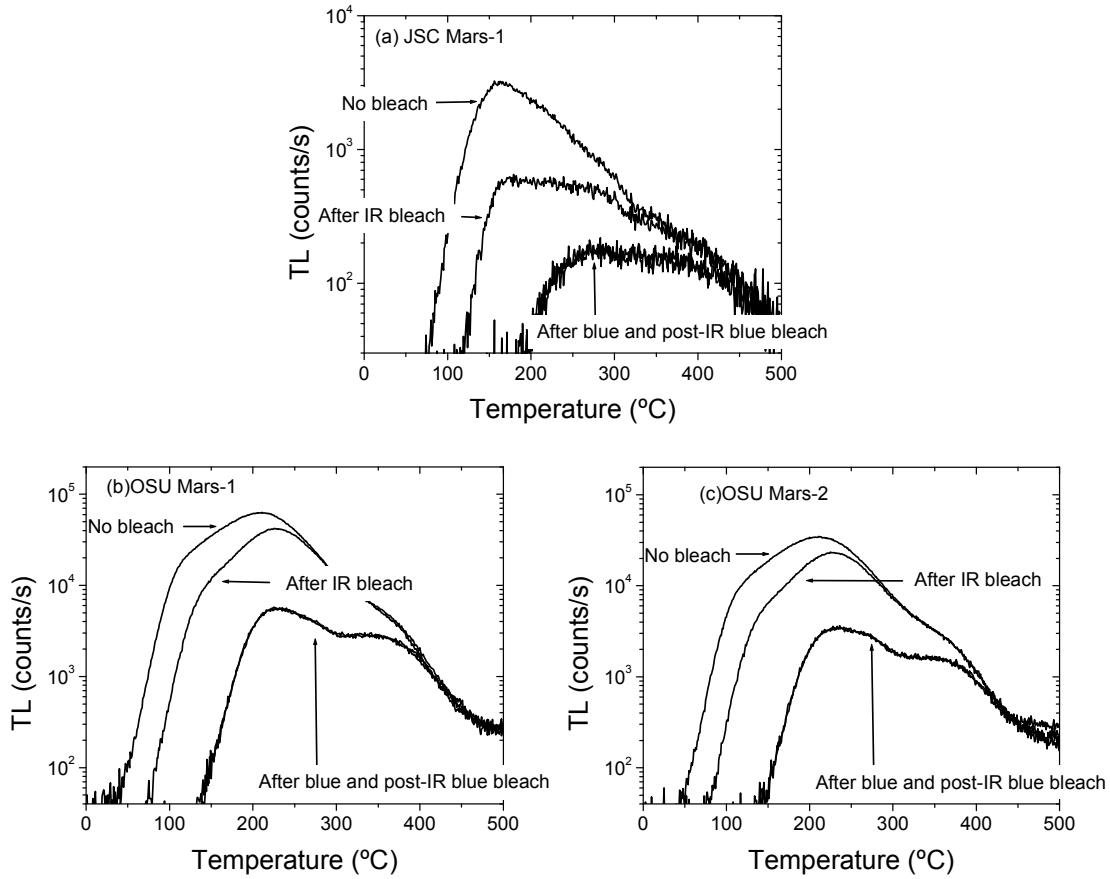

Figure 3.1 The effect of bleaching on TL for (a) JSC Mars-1, (b) OSU Mars-1, and (c) OSU Mars-2. The samples were given either a 5000 Gy (JSC Mars-1) or a 300 Gy (OSU Mars-1 and Mars-2) dose, bleached with the indicated stimulation sources for 300s, and TL was then measured to 500°C.

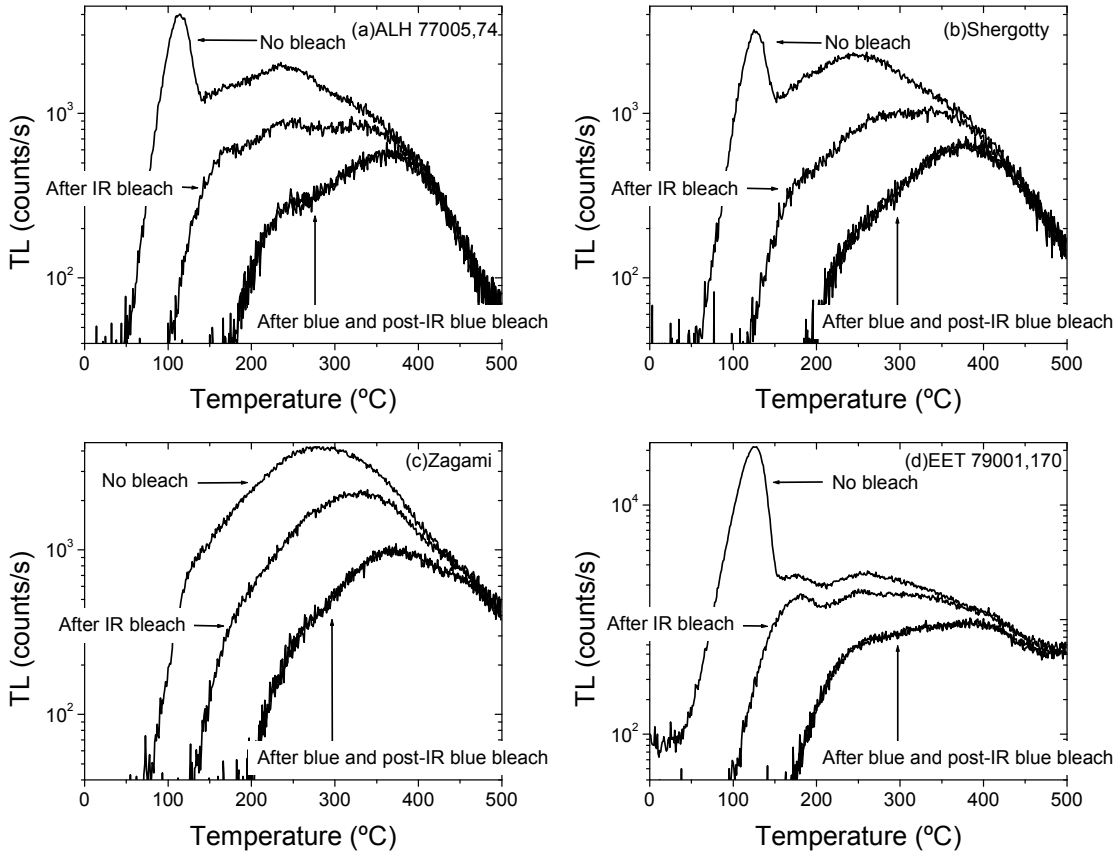

Figure 3.2 The effect of bleaching on TL for martian meteorites as indicated. The sample was given a 300 Gy dose, bleached with indicated stimulation sources for 300s, and TL was then measured to 500°C.

3.3 Correcting for Sensitivity Changes

The same procedure used in Chapter 2 to test the sensitivity-correction procedure was used for these samples. The results for infrared-stimulated OSL are shown in Figures 3.3 (JSC Mars-1, OSU Mars-1, and OSU Mars-2) and 3.4 (martian meteorites), and the results for blue-stimulated OSL are shown in Figures 3.5 (JSC Mars-1, OSU Mars-1, and OSU Mars-2) and 3.6 (martian meteorites). For each preheat temperature the martian simulants showed little sensitivity change for either stimulation wavelength used. As a result, the OSL intensities tend to cluster around one point. In this case, sensitivity correction is not necessary, but the SAR procedure and sensitivity correction method can be used. However, it should be noted that OSU Mars-1 and OSU Mars-2 did show some small OSL sensitivity change when using low temperature preheats (160°C and 200°C) and infrared stimulation. Furthermore, the regeneration OSL signals and the test dose OSL signals were not proportional. These trends were not as apparent in the blue-stimulated OSL data. Based upon these observations, it is concluded that the proposed procedure can be used for sensitivity-correction with the martian simulants, but low temperature preheats (below 200°C) should not be used.

The results of the sensitivity-correction test for the martian meteorites when using the infrared-stimulated OSL signal are shown in Figure 3.4 and the results when using the blue-stimulated signal are show in Figure 3.6. The graphs of Figure 3.4 show a lot of scatter, but the data for all of the samples and both OSL signals tends to cluster around a line of best fit (but the slope of the line is unique for each sample and signal). Thus, dose estimation using materials similar to the studied martian meteorites may yield large

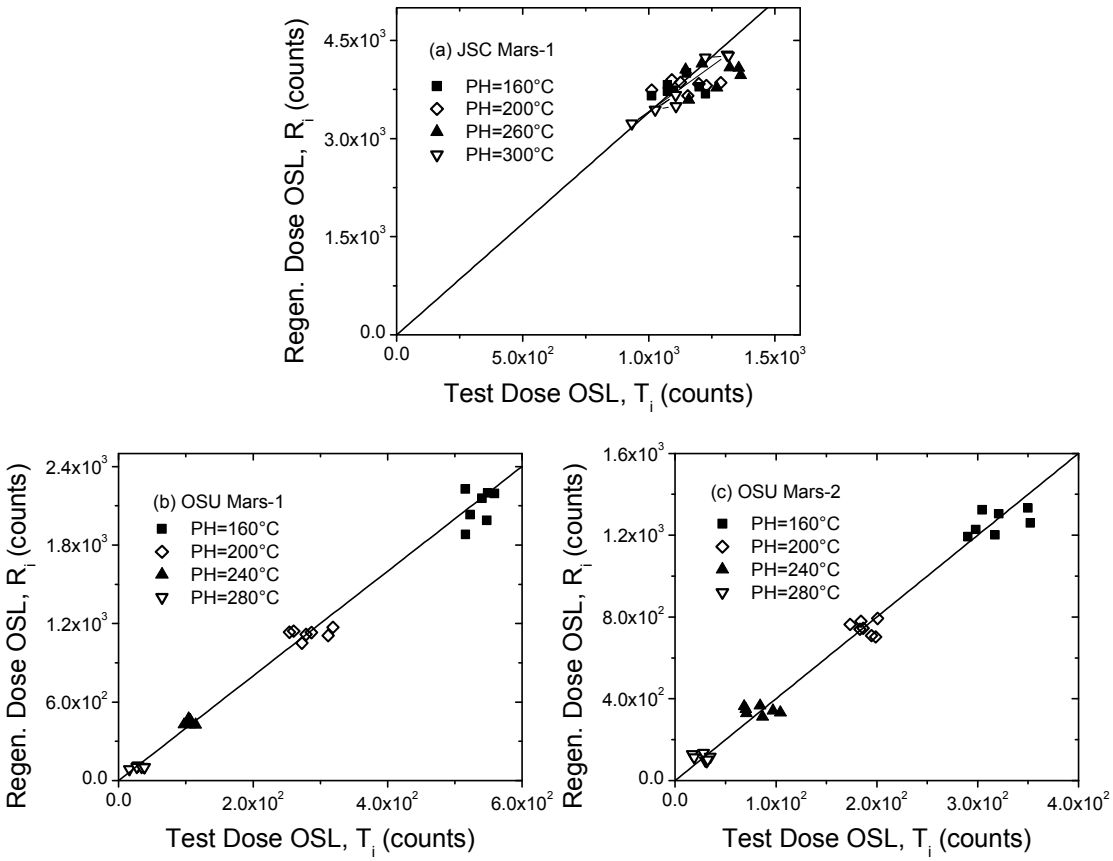

Figure 3.3 Tests of the sensitivity-correction procedure for (a) JSC Mars-1, (b) OSU Mars-1, and (c) OSU Mars-2 using the proposed SAR procedure. The figures use infrared-stimulated OSL (as part of a post-IR blue stimulation sequence). The straight lines represent a visual best fit of the data.

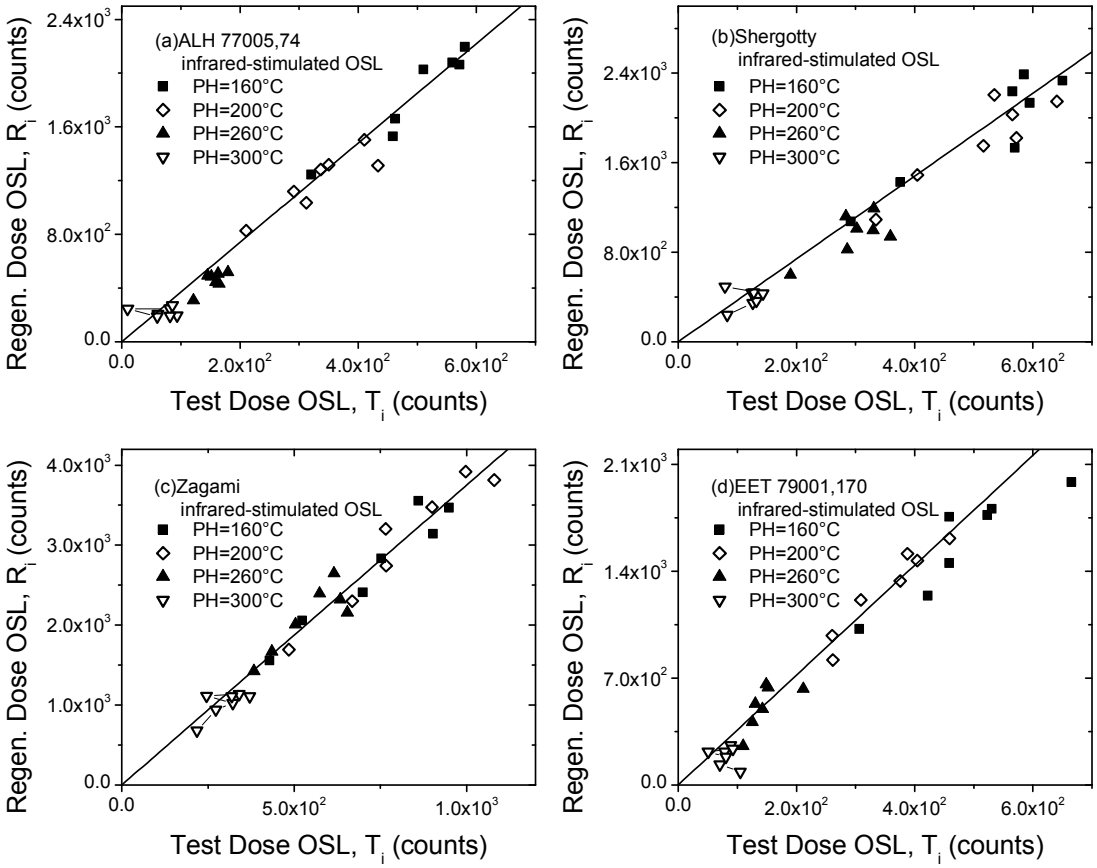

Figure 3.4 Tests of the sensitivity-correction procedure for martian meteorites using the proposed SAR procedure. The figures use the infrared-stimulated OSL from a post-IR blue stimulation sequence. The straight lines represent a visual best fit of the data.

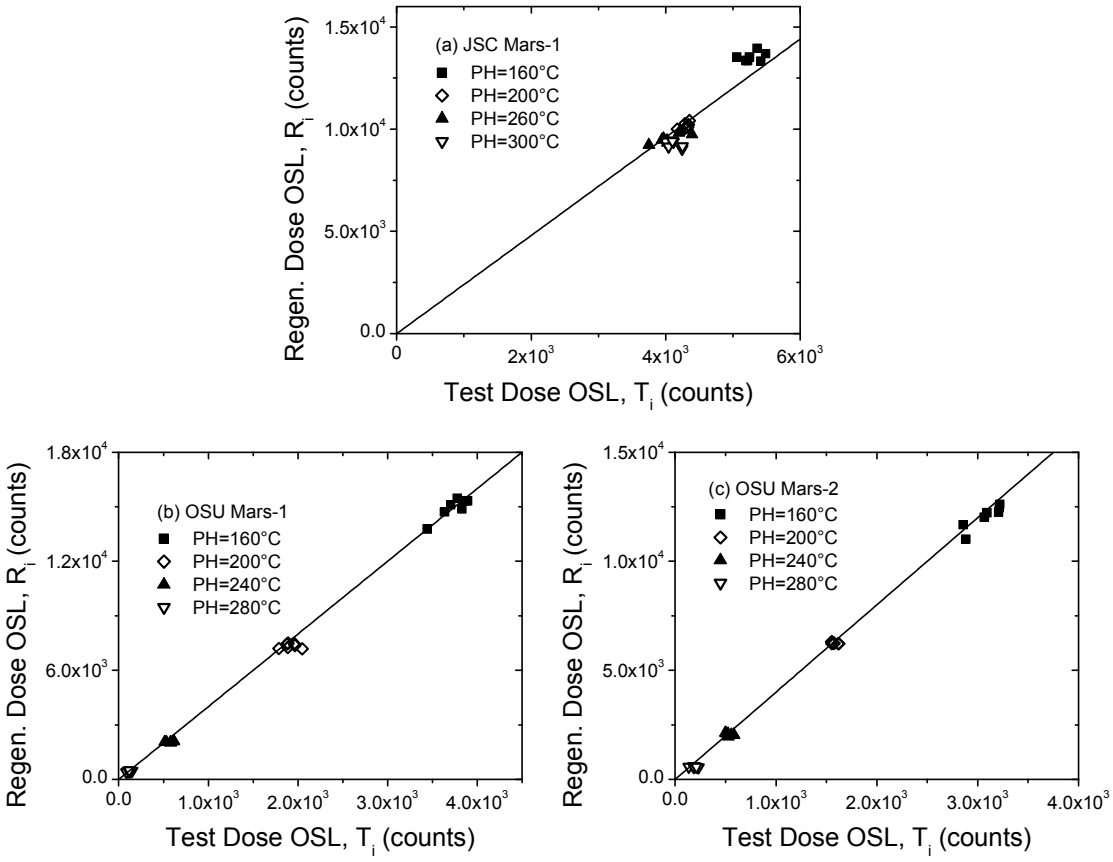

Figure 3.5 Tests of the sensitivity-correction procedure for (a) JSC Mars-1, (b) OSU Mars-1, and (c) OSU Mars-2 using the proposed SAR procedure. The figures use blue-stimulated OSL (as part of a post-IR blue stimulation sequence). The straight lines represent a visual best fit of the data.

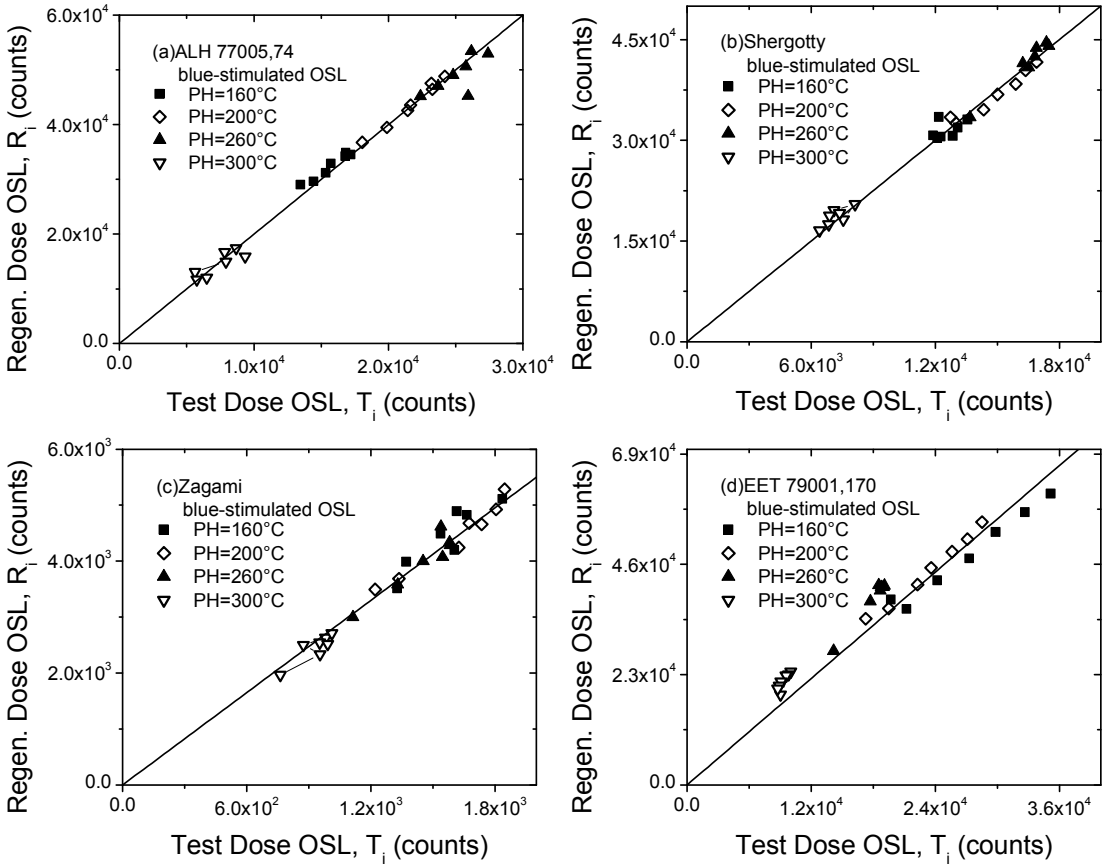

Figure 3.6 Tests of the sensitivity-correction procedure for martian meteorites using the proposed SAR procedure. The figures use the blue-stimulated OSL from a post-IR blue stimulation sequence. The straight lines represent a visual best fit of the data.

uncertainties (due to counting statistics and fitting errors). Nevertheless, the proposed sensitivity-correction procedure is shown to be valid for these materials.

3.4 Dose Response Curves

Examples of uncorrected (regeneration dose OSL or R_i only) dose response curves along with the supralinearity factors as defined by Chen and McKeever (1997)

$$f(D) = \frac{S(D)/D}{S(D_1)/D_1} \tag{3.1}$$

are shown in Figures 3.7 (infrared-stimulated OSL for martian simulants), 3.8 (infrared-stimulated OSL for martian meteorites), 3.9 (blue-stimulated OSL for martian simulants), and 3.10 (blue-stimulated OSL for martian meteorites). For JSC Mars-1, the infrared-stimulated OSL exhibit a large linear range but low luminescence intensities while the blue-stimulated OSL did not show any linearity but larger luminescence intensities. For OSU Mars-1, both the infrared-stimulated OSL and blue-stimulated OSL have slight supralinearity at dose of several hundred Gy before the signals begin to saturate at around 1000 Gy. OSU Mars-2, on the other hand, does not show any supralinearity in the infrared-stimulated OSL signal, and the supralinearity is only about 20% at the maximum for the blue-stimulated OSL signal. The martian meteorites (Figures 3.8 and 3.10) do not show any supralineraity if the 5 Gy dose is ignored (this signal was typically near the detection limit and hence was not reliable). The lack of large supralinearity factors indicates that there are few optically inactive competing traps in these simulants (see discussion of supralinearity in Section 2.1).

The sensitivity-corrected ($L_i=R_i/T_i$) dose response curves are shown in Figures 3.11 (infrared-stimulated OSL for martian simulants), 3.12 (infrared-stimulated OSL for martian meteorites), 3.13 (blue-stimulated OSL for martian simulants), and 3.14 (blue-

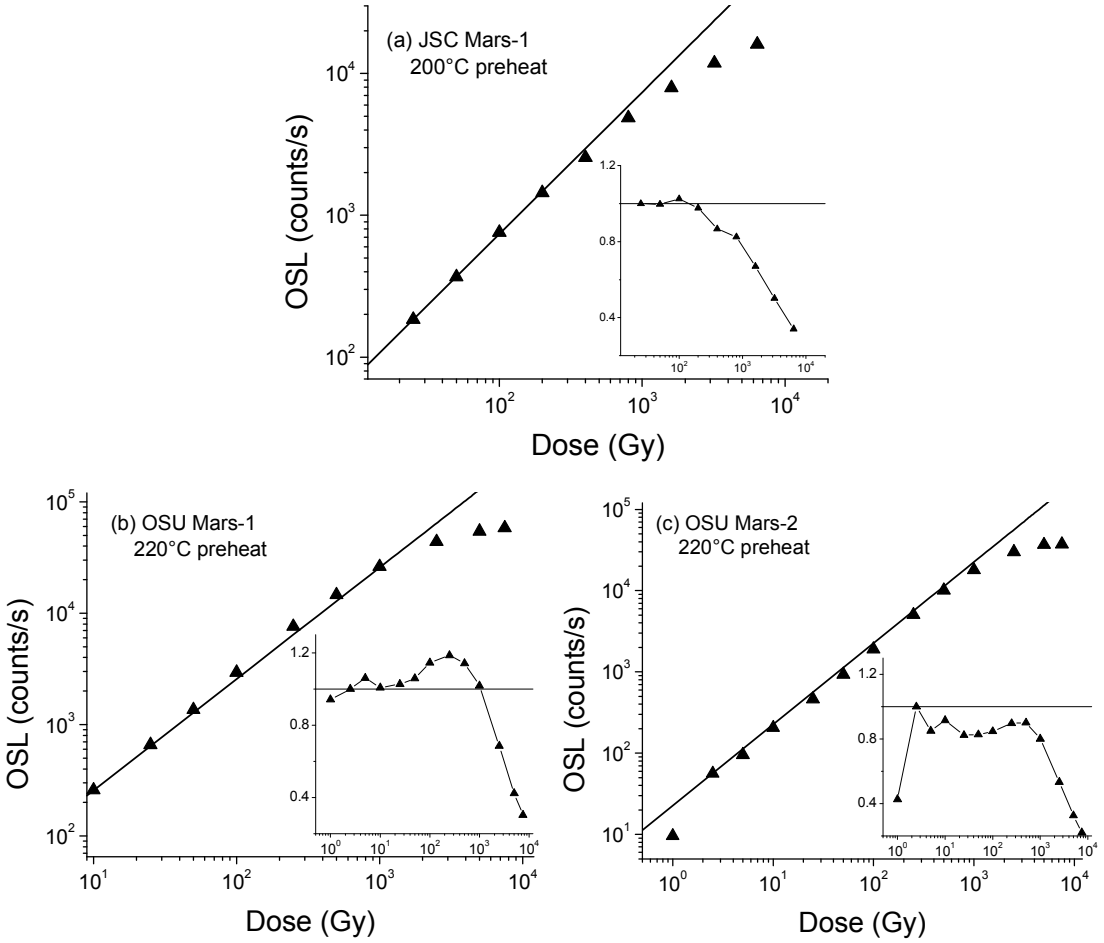

Figure 3.7 Uncorrected (R_i only) dose-response curves for (a) JSC Mars-1, (b) OSU Mars-1, and (c) OSU Mars-2. The figures use infrared-stimulated OSL (as part of a post-IR blue stimulation sequence). The supralinearity factor, as defined by Chen and McKeever (1997), is shown in the inset of each graph. Note the log-log scale.

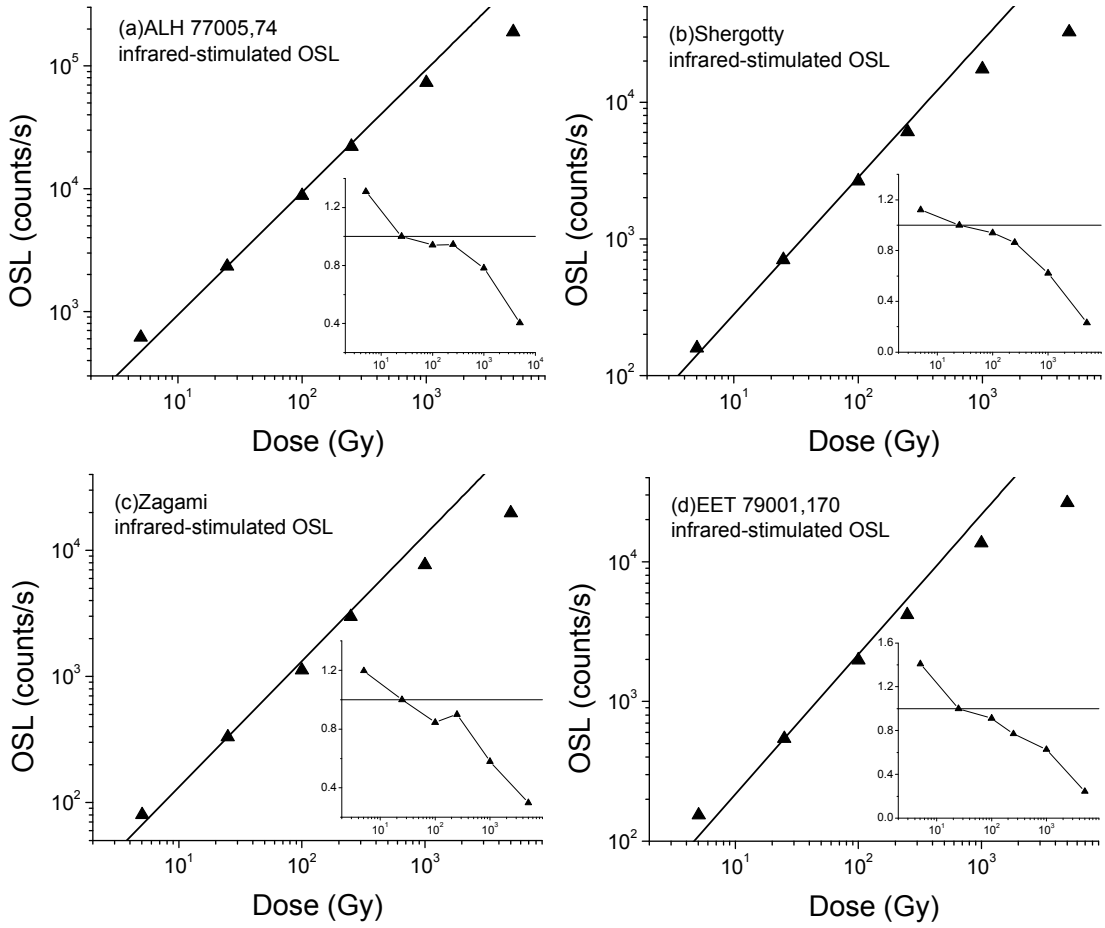

Figure 3.8 Uncorrected (R_i only) infrared-stimulated dose-response curves (from a post-IR stimulation method) for the studied martian meteorites. The supralinearity factor, as defined by Chen and McKeever (1997), is shown in the inset of each graph. A 200°C preheat was used. Note the log-log scale.

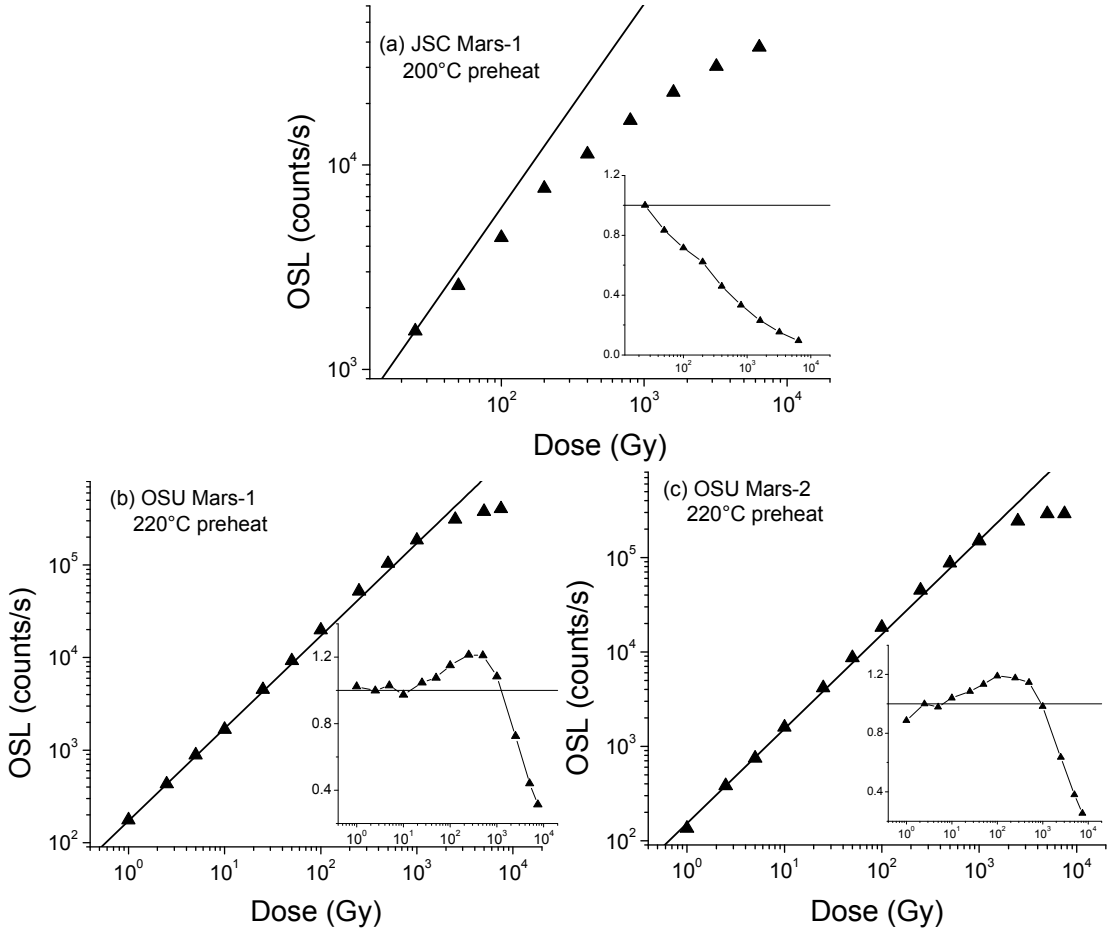

Figure 3.9 Uncorrected (R_i only) dose-response curves for (a) JSC Mars-1, (b) OSU Mars-1, and (c) OSU Mars-2. The figures use blue-stimulated OSL (as part of a post-IR blue stimulation sequence). The supralinearity factor, as defined by Chen and McKeever (1997), is shown in the inset of each graph. Note the log-log scale.

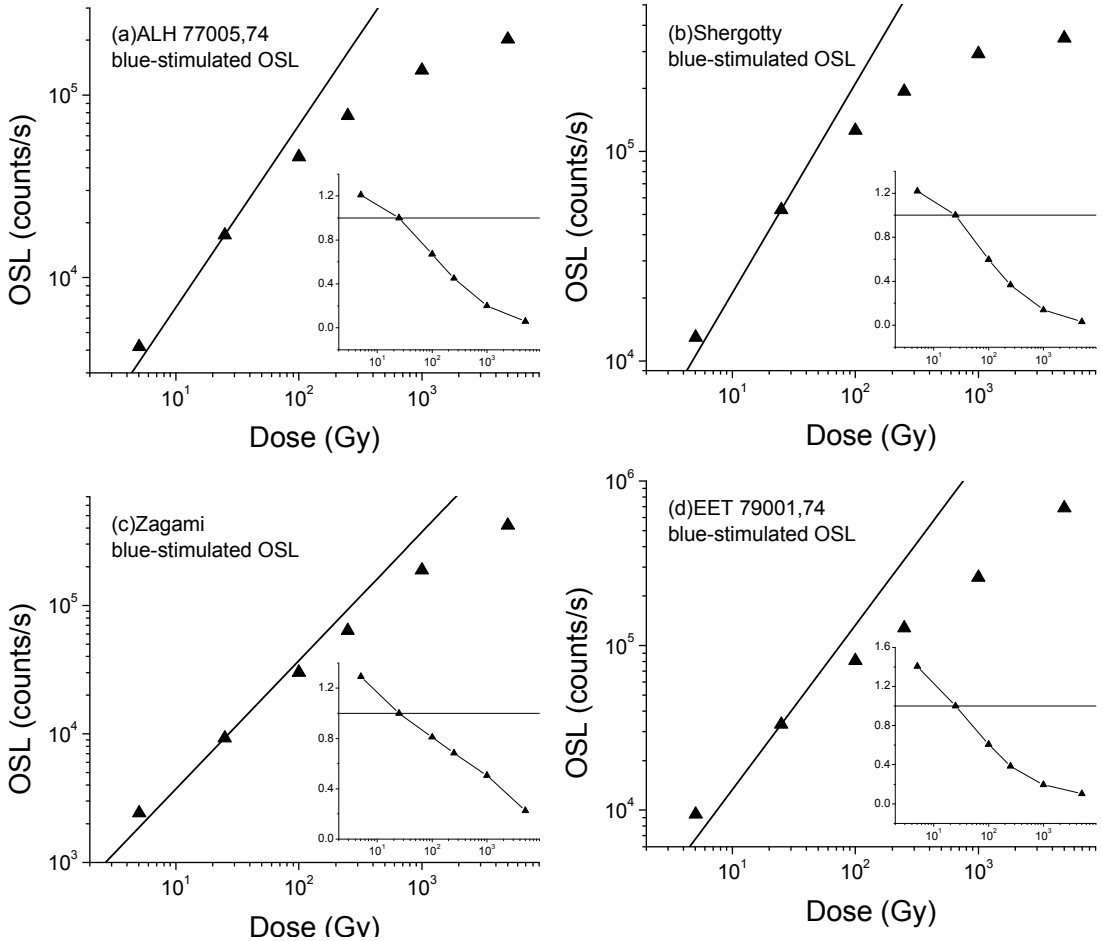

Figure 3.10 Uncorrected (R_i only) blue-stimulated dose-response curves (from a post-IR stimulation method) for the studied martian meteorites. The supralinearity factor, as defined by Chen and McKeever (1997), is shown in the inset of each graph. A 200°C preheat was used. Note the log-log scale.

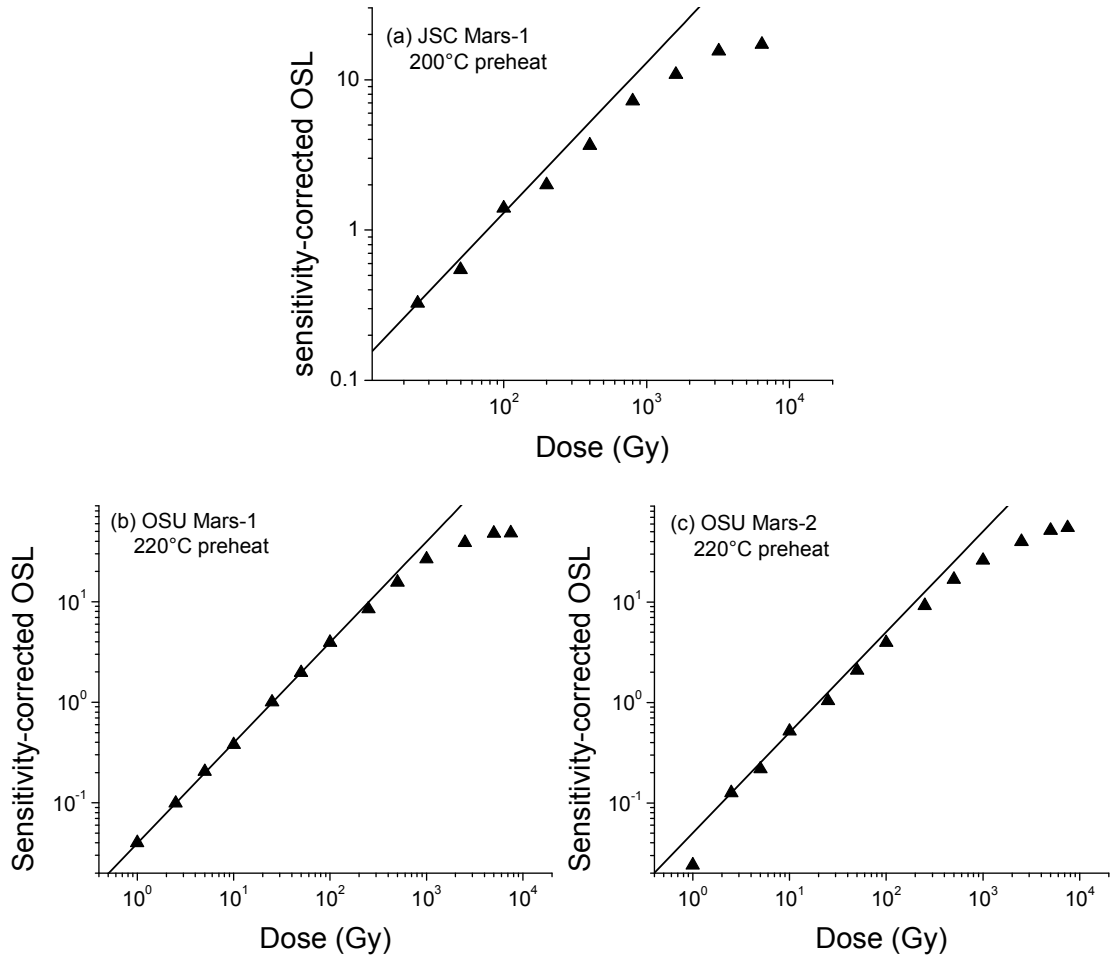

Figure 3.11 Sensitivity-corrected dose-response curves for (a) JSC Mars-1, (b) OSU Mars-1, and (c) OSU Mars-2. The figures use infrared-stimulated OSL (as part of a post-IR blue stimulation sequence). Note the log-log scale.

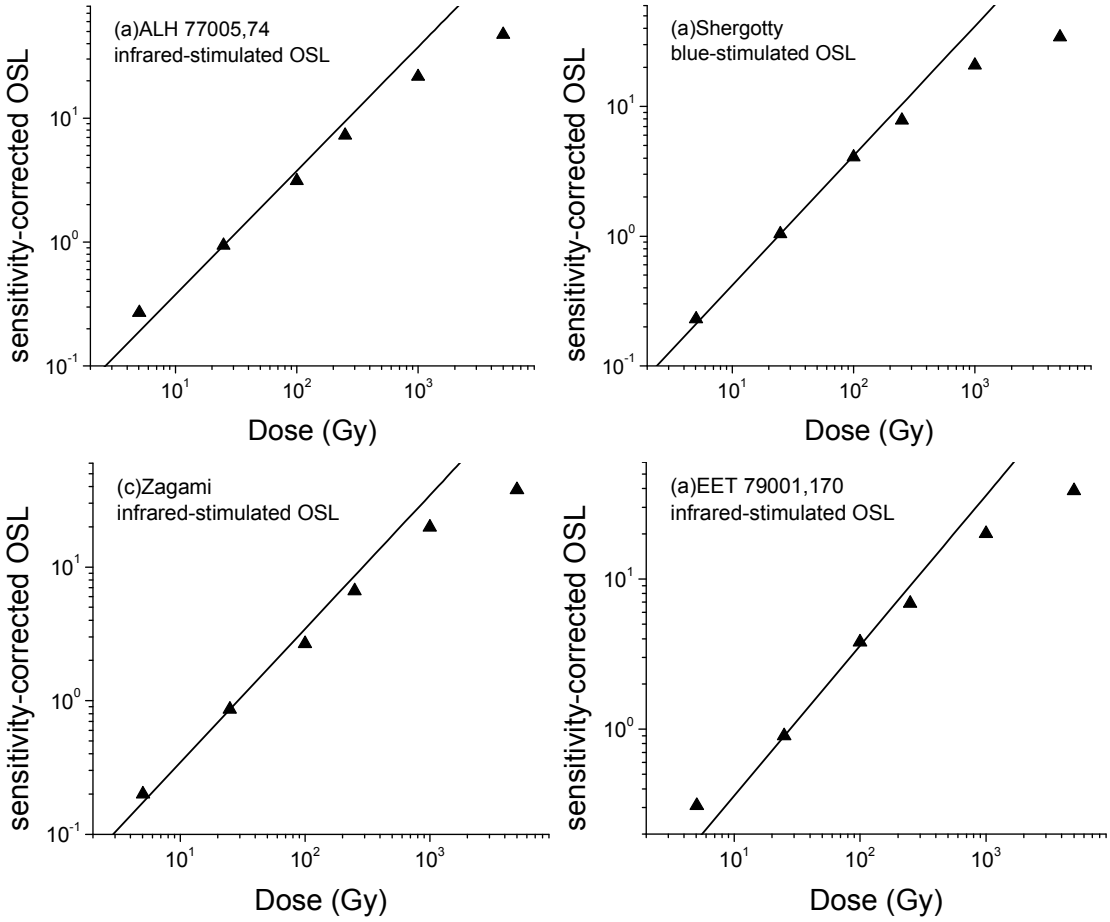

Figure 3.12 Sensitivity-corrected infrared-stimulated dose-response curves (from a post-IR stimulation method) for the studied martian meteorites. A 200°C preheat was used. Note the log-log scale.

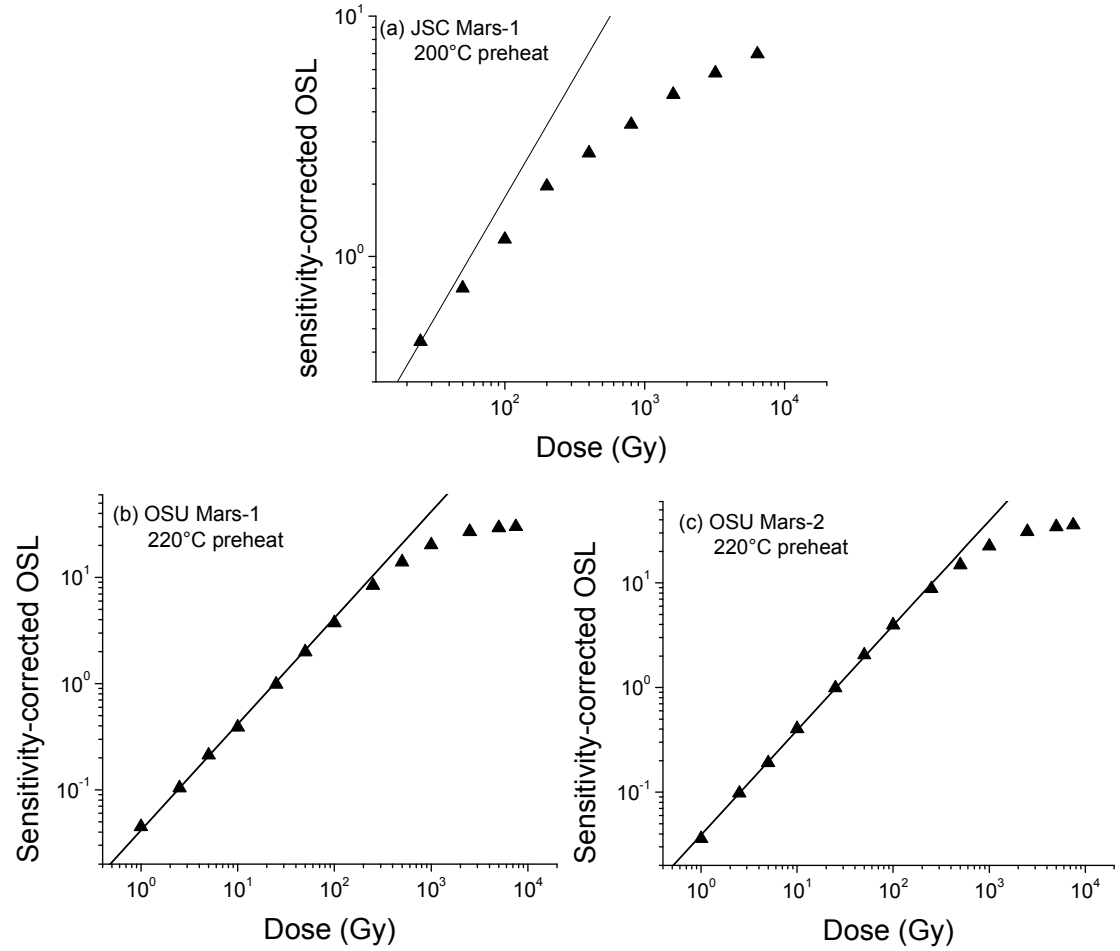

Figure 3.13 Sensitivity-corrected dose-response curves for (a) JSC Mars-1, (b) OSU Mars-1, and (c) OSU Mars-2. The figures use blue-stimulated OSL (as part of a post-IR blue stimulation sequence). Note the log-log scale.

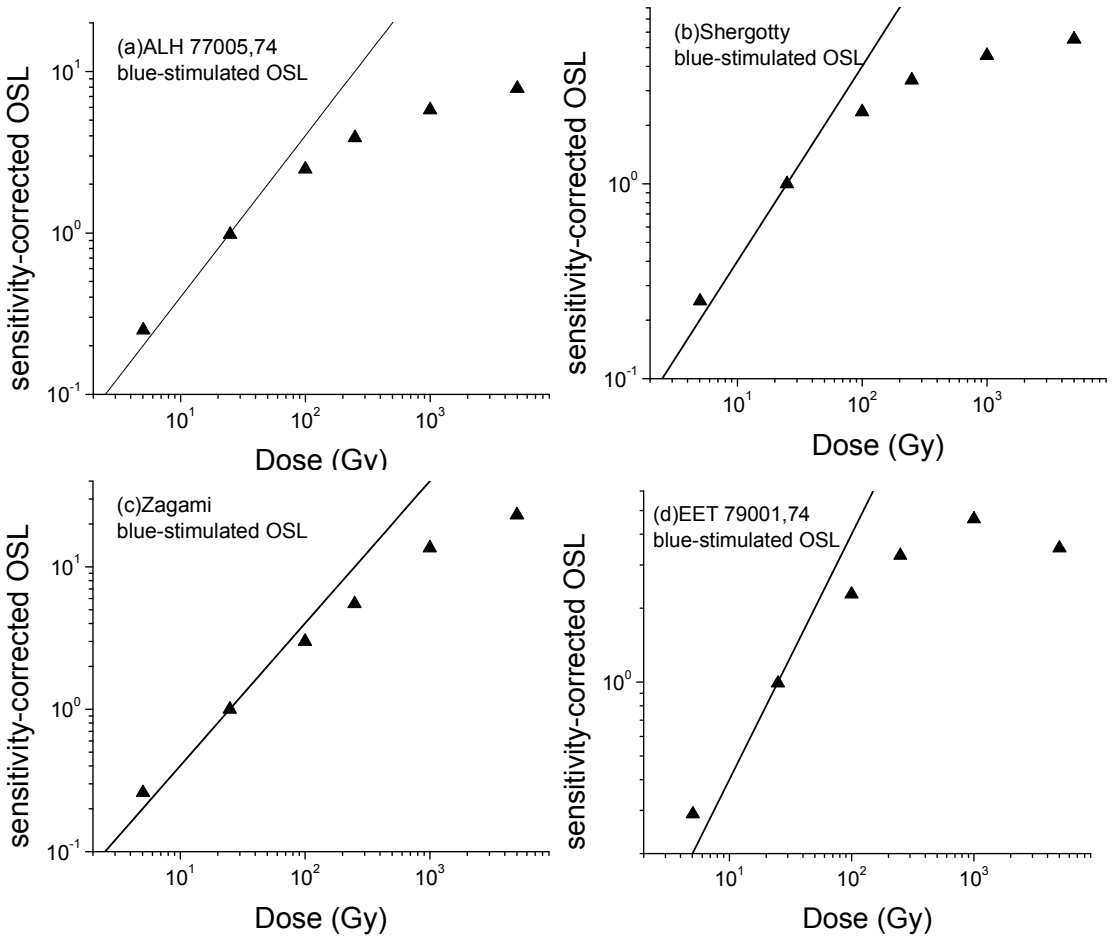

Figure 3.14 Sensitivity-corrected blue-stimulated dose-response curves (from a post-IR stimulation method) for the studied martian meteorites. A 200°C preheat was used. Note the log-log scale.

Sample	Infrared-stimulated OSL		Blue-stimulated OSL	
	Max dose (Gy)	Max age (ka)	Max dose (Gy)	Max age (ka)
JSC Mars-1	5500	111	2100	41
OSU Mars-1	4400	88	2700	53
OSU Mars-2	4900	98	3100	62
ALH 77005,74	5700	115	230	16
Shergotty	3300	67	520	11
Zagami	4700	95	3200	64
EET 79001,170	4500	89	350	7

Table 3.2 Calculations of the maximum estimable doses and ages from fitting of the dose response curves (see text). The calculations for both OSL signals from a post-IR blue stimulation sequence are presented. The maximum estimable age is based upon an average dose rate of 50 mGy/yr.

stimulated OSL for martian meteorites). Any supralinearity present in the uncorrected dose response curves is eliminated by the sensitivity correction. Most samples (JSC Mars-1 and the martian meteorites) show a very small (if any) linear range, but OSU Mars-1 and OSU Mars-2 both display a long linear range followed by a quickly saturating portion of the sensitivity-corrected dose response curve.

The method of Section 2.2.5 was used to calculate the maximum estimable dose (and therefore maximum estimable age, based upon a dose rate of 50 mGy/yr) for each material. The results of these calculations are given in Table 3.2 and show a wide range of maximum depositional ages that could be obtained with these materials. Generally, the maximum age that could be estimated from the infrared-stimulated OSL signal is larger than the maximum age that could be estimated from the blue-stimulated OSL signal for any given mineral mixture. For the infrared-stimulated OSL signal, the maximum estimable age ranges from 67 ka (Shergotty meteorite) to 115 ka (ALH 77005,74 meteorite). For the blue-stimulated OSL signal, the maximum estimable age ranges from 7 ka (EET 79001,170 meteorite) to 64 ka (Zagami meteorite). The time span of the geological framework that could be constructed using OSL dating on Mars will then be highly dependent upon the minerals that are present in the martian regolith.

3.5 Dose Recovery Experiments

Dose recovery experiments were undertaken for all of the martian simulants and meteorites using known doses in both the linear and non-linear regions of the respective dose response curves and the same preheats used to construct the respective dose response curves. The dose recovery ratios, average recycling ratios, and average recuperation values for all of the dose recovery experiments (see Chapter 2 for

definitions), along with the dose recovered for each experiment, are given in Tables 3.3 and 3.4. The reported errors are the standard deviation of the mean for the martian simulants (JSC Mars-1, OSU Mars-1, and OSU Mars-2), and the standard deviation for the martian meteorites unless otherwise noted.

For the martian simulants, doses from both the linear and non-linear portions of the dose response curves could be recovered with less than a 5% error with either IR or blue stimulation (from a post-IR blue stimulation sequence). In addition, the recycling ratios were generally close to 1.0 and the recuperation was negligible. Dose recovery experiments with the martian meteorites could only be carried out on two aliquots due to the small amount of each meteorite available. Still, the known doses could generally be recovered with an acceptable error with large uncertainties.

3.6 Concluding Remarks for Chapter 3

Chapter 3 focused on characterizing the basic luminescence properties of various martian simulants and meteorites. In particular, various tests were performed to determine the suitability of the proposed procedure (Table 3.1) for dating polymineral samples. All of the samples showed bleaching characteristics typical of feldspathic samples in that either infrared or blue stimulation reduced the entire TL curve (i.e., no individual TL peak seems to give rise to the OSL signal). Even though the simulants and meteorites showed little or no sensitivity changes under repeated cycles of dose, preheating, and OSL measurement, the sensitivity correction of the proposed procedure is valid for both the simulants and meteorites. The sensitivity correction method also produced dose response curves without any supralinearity, and statistical analysis of the sensitivity-corrected dose response curves indicate that ages as old as 115 ka could be

produced from minerals similar to the tested materials. Finally, known doses from both the linear and non-linear portions of the respective dose response curves could be accurately recovered using the proposed procedure, although the uncertainties for the martian meteorites were generally large.

Sample	Infrared-stimulated OSL		
	Dose Rec. Ratio	Recycling Ratio	Recuperation
JSC- Mars-1			
100 Gy (9)	1.01±0.04	1.01±0.10	0.11±0.06
300 Gy(10)#	1.02±0.03	1.03±0.08	0.06±0.01
OSU Mars-1			
15 Gy (10)	0.99±0.04	1.07±0.04	-0.01±0.01
1000.048 Gy (5)	0.94±0.13	1.02±0.04	0.04±0.03
OSU Mars-2			
15 Gy (10)	1.01±0.04	1.04±0.05	0.00±0.01
1000.048 Gy (5)	0.93±0.14	0.99±0.03	0.03±0.01
ALH 77005,74			
100 Gy (2)	0.98±0.1	0.95±0.01	0.08±0.09
249.984 Gy (2)	1.02±0.04	1.05±0.01	0.19±0.17
Shergotty			
100 Gy (2)	0.95±0.54	0.95±0.01	-0.04±0.09
249.984 Gy (2)	0.99±0.06	0.88±0.02	0.06±0.01
Zagami			
100 Gy (2)	0.85±0.17	1.03±0.03	0.07±0.04
249.984 Gy (2)	1.07±0.25	0.85±0.30	0.10±0.13
EET 79001,170			
100 Gy (2)	0.93±0.32	0.97±0.15	0.06±0.01
249.984 Gy (1)*	1.07±0.08	1.24	0.05

used local slope approximation rather than fitting dose response curve

* errors are based upon fitting errors.

Table 3.3 Results of dose recovery experiments for both the infrared-stimulated OSL signal from a post-IR blue stimulation sequence. For each sample, doses were recovered in the linear (first entry) and non-linear (second entry) portions of the dose response curve.

Sample	Blue-stimulated OSL		
	Dose Rec. Ratio	Recycling Ratio	Recuperation
JSC- Mars-1			
100 Gy (9)	0.97±0.04	1.05±0.03	0.06±0.02
300 Gy(10)#	1.00±0.02	1.01±0.03	0.09±0.01
OSU Mars-1			
15 Gy (10)	1.00±0.02	1.04±0.01	0.03±0.02
1000.048 Gy (5)	0.92±0.03	1.16±0.02	0.07±0.01
OSU Mars-2			
15 Gy (10)	0.97±0.02	1.02±0.02	0.01±0.01
1000.048 Gy (5)	0.93±0.02	1.11±0.02	0.05±0.01
ALH 77005,74			
100 Gy (2)	1.17±0.49	0.99±0.01	0.01±0.01
249.984 Gy (2)	1.01±0.10	1.07±0.01	0.08±0.01
Shergotty			
100 Gy (2)	1.09±0.56	1.03±0.03	0.02±0.02
249.984 Gy (2)	0.89±0.15	1.06±0.33	0.06±0.01
Zagami			
100 Gy (2)	1.01±0.51	1.01±0.01	0.02±0.01
249.984 Gy (2)	0.86±0.25	1.10±0.09	0.10±0.02
EET 79001,170			
100 Gy (2)	1.23±0.15	0.97±0.01	0.02±0.01
249.984 Gy (1)*	0.89±0.06	1.00	0.10

used local slope approximation rather than fitting dose response curve

* errors are based upon fitting errors.

Table 3.4 Results of dose recovery experiments for both the blue-stimulated OSL signal from a post-IR blue stimulation sequence. For each sample, doses were recovered in the linear (first entry) and non-linear (second entry) portions of the dose response curve.

CHAPTER FOUR

PROPERTIES OF MATERIALS IRRADIATED AND STIMULATED AT LOW TEMPERATURES

As previously mentioned (Section 1.3.3), due to the lower average ambient temperature on Mars, sedimentary deposits on the planet may have been naturally bleached (luminescence signal zeroed) and irradiated at much lower temperatures for a significant portion of their storage time. As the luminescence process is known to be temperature dependent in numerous ways (Aitken, 1985, 1998), it is important to study expected martian minerals when they have been irradiated and stimulated at lower temperatures. A system to perform these experiments has been designed and built at OSU, and this chapter discusses some of the initial experiments with that system and their implications for applying OSL dating to Mars.

4.1 Potential Effects of Temperature on the Luminescence Process

As discussed briefly in Section 1.3.3, the luminescence process is temperature dependent in several ways and at different points in the process. Potentially the most important effect of storage temperature is that it determines which traps are geologically stable and unstable. By the argument in Section 1.1, the average residence time of electrons in the traps or lifetime τ(s) is given by

$$\tau = \lambda^{-1} = s^{-1} * \exp(\frac{E}{k_B * T}) \quad (1.3)$$

where first-order kinetics are assumed. T is the ambient storage temperature, and the highest storage temperature determines the geological stability of the trap. Furthermore, this lifetime needs to be at least 10 times larger than the age of the sample for an insignificant amount of charge to have been lost from the trap during the storage period t_s

i.e., $$\frac{n}{n_0} = \exp(\frac{1}{2} * \frac{-t_s}{\tau}), \quad (1.5)$$

where n and n_0 are the final and initial populations of the trap respectively. Clearly then, the lower the ambient storage temperature of the sediments, the longer the lifetime of charge in the traps and the number of geologically stable traps increases. This phenomenon has several potential effects on the dose recovery procedure.

During natural irradiation, the dose rate is several orders of magnitude lower than typical irradiation dose rates used in the laboratory. For example, the terrestrial natural dose rate is on the order of 2 mGy/yr, while the Risø systems generally have dose rates of 100 mGy/sec or approximately 3 x 10^9 mGy/yr. If the leakage rate from a trap at temperature T is comparable to the filling rate (for a given dose rate) then that trap will not be populated. Thus, due to the difference in dose rates, some traps that contribute to TL or OSL in the laboratory will not contribute to the natural signal. As an example, consider the 110°C TL peak in quartz. This peak can clearly be seen in TL after laboratory irradiation, allowing the sensitivity of the 110°C peak to be used to correct for sensitivity changes in quartz (see Section 1.1.1). The trap causing the 110°C TL peak can also contribute to OSL and this led to the use of a cutheat in the SAR procedure. However, the 110°C peak cannot be seen in the natural TL (or OSL) from sedimentary

quartz samples since the trapped charge is stable in the peak for only about 30 minutes at terrestrial ambient temperatures. As a result, the 110°C trap remains more or less empty during natural irradiation udnder terrestrial conditions. However, if the ambient temperature is considerably lower such as on Mars, geologically unstable peaks such as these in quartz, may contribute to the natural OSL signal although they may still not be geologically stable. In this way such traps can affect the charge trafficking process in nature. Thus, experiments need to be conducted to identify low temperature peaks in the martian simulants that may be stable under martian conditions and to determine if these traps are important in competition processes during irradiation and optical stimulation.

Thus a lower ambient temperature could result in additional traps contributing to the natural OSL signal, and may also increase the number of traps that are geologically stable. For terrestrial dating applications, a preheat of at least 200°C for 10 s is generally used to isolate geologically stable traps. Since a lower ambient temperature, such as on Mars, could result in traps below 200^{o}C being geologically stable, the necessary preheat could be at a considerably lower temperature. This in turn has some advantages as far as in-situ instrumentation on a spacecraft. If the preheat temperature for martian samples can be lower than that typically used in the laboratory on Earth, both time and power can be conserved.

The above discussion concerns the effects of low temperature on the luminescence process during irradiation of the minerals, but the stimulation process can be temperature dependent as well. Many dosimetric materials display an increase of around 1% per degree Celsius in the initial part of the OSL decay curve with increasing stimulation temperature above room temperature (Aitken, 1998; McKeever *et al.*, 1997b;

Murray and Wintle, 1998), and this is generally attributed to thermal assistance that can be a result of multiple mechanisms as summarized in Figure 4.1 (Bøtter-Jensen *et al.*, 2003).

The simplest explanation for a temperature dependence of OSL decay is that charge evicted by optical stimulation can be retrapped by lower temperature traps and either restimulated or lost to the OSL process if the trap is not optically active (Figure 4.1 (a)). Raising the stimulation temperature prevents retrapping and results in a faster OSL decay with a larger intensity (McKeever *et al.*, 1997b; Markey *et al.*, 1997). Similar reasoning led to using a stimulation temperature of 125°C for quartz so that the 110°C TL peak could be kept empty during optical stimulation. A lower ambient temperature could alter the needed value of the stimulation temperature in order to prevent this effect.

The other mechanisms to explain thermal dependence of OSL decay curves all involve direct "thermal assistance". Hütt *et al.* (1988) proposed that optical stimulation can promote electrons into an excited state, and thermal energy then excites the electron to the conduction band (Figure 4.1(b)). The mechanism was proposed to explain infrared stimulation of feldspars where the energy of the stimulating light is much smaller than the measured energy depth of the trap. Poolton et al. (1995a, 1995b) noted, however, that the required thermal energy for feldspars was dependent upon the optical stimulation energy in opposition to the previous model. A model based upon optical stimulation to an excited "donor" state and subsequent thermal stimulation or hopping to an excited "acceptor" state that produces the luminescence was then proposed (Figure 4.1(c)). This explanation was later modified slightly and involved band tail states, but the recombination was still through a hopping process (Poolton *et al.*, 2002a, 2002b). These

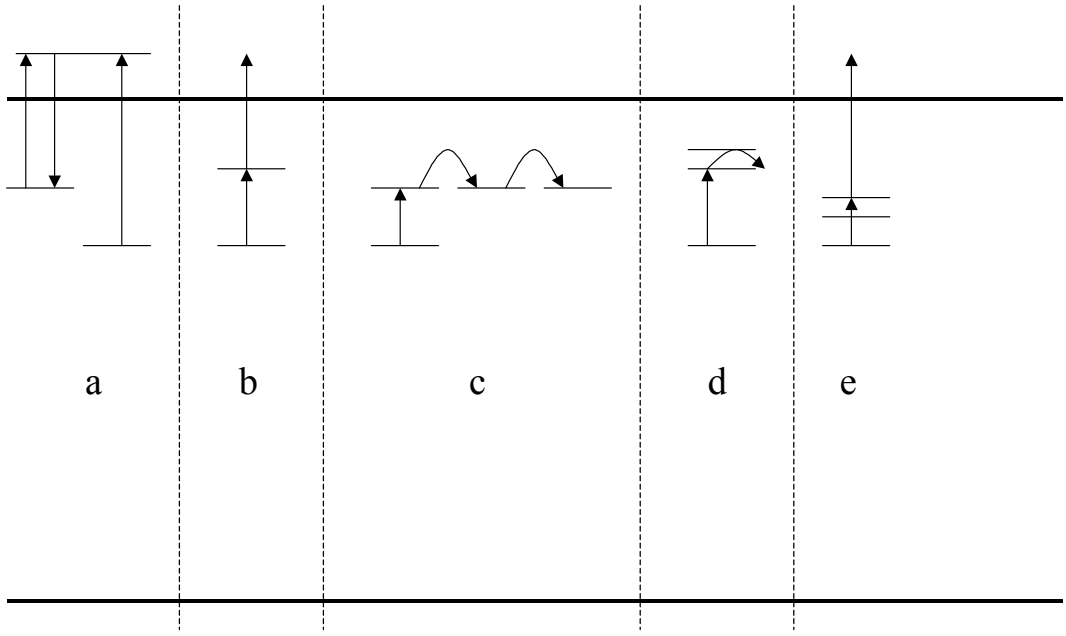

Figure 4.1 Mechanisms for thermal dependence of OSL decay (adapted from Bøtter-Jensen, 2003). The effects explained in the text are: (a) shallow traps, (b) thermal eviction from an excited state, (c) donor-accepting hopping, (d) band tail states hopping, and (e) multiple ground states.

mechanisms are the most likely mechanisms to be active in martian minerals as the luminescent minerals are expected to be feldspathic.

A different mechanism has been suggested to explain the thermal dependence of OSL decay curves in quartz. In quartz, the thermal activation energy is seen to increase smoothly with increasing temperature, as opposed to the Hütt model where the increase is either independent of optical excitation energy or varies discreetly with it. Spooner (1994) introduced a model where electrons can be thermally stimulated to one of several vibrational states and then be optically stimulated to the conduction band (Figure 4.1(e). This model has been very effective to explain the thermal dependence of quartz OSL decay curves and has therefore been very useful on Earth, but since quartz is not present on Mars in large quantities this mechanism is unlikely to be active in most martian samples.

Although the amount of charge liberated increases with increasing OSL measurement temperature, the OSL signal itself does not always increase due to the thermal dependence of the recombination process. Many materials exhibit a phenomenon called thermal quenching or "the loss of luminescence efficiency with increasing temperature" (Bøtter-Jensen et al., 2003). The effect involves the recombination center dissipating the energy from recombination in a way other than producing luminescence, more than likely as heat (Aitken, 1985). In one of the early studies of thermal quenching in quartz, Wintle (1975) used the following expression to describe the luminescence efficiency

$$\eta = \frac{1}{1 + C * \exp(\frac{-W}{k_B * T})} \tag{4.1}$$

where C is a constant, W is the thermal activation energy (eV), k_B is Boltzmann's constant ($eV*K^{-1}$), and T is the temperature (K). The thermal activation energy varies by material, and the effect of thermal quenching is usually not significant for temperatures near room temperature. However, since experiments to measure the thermal activation are typically carried out at or above room temperature, the efficiency at room temperature is chosen to be near 1.0. Measurements at a lower temperature could reveal new aspects of thermal quenching for many materials.

Considering the ways in which the luminescence process can be affected by the ambient temperature as well as the temperature at which experiments are carried out, research into the properties of minerals irradiated and stimulated at low temperatures is necessary. The possibility of additional traps contributing to the natural OSL and altering competition effects during irradiation as well as additional geologically stable traps means that preheating temperatures (and potentially procedures) may need to be changed. In addition, both the stimulation efficiency (thermal dependence of OSL decay) and luminescence efficiency (thermal quenching) are affected by the OSL measurement temperature, in potentially opposite ways. Therefore, the optimal OSL stimulation temperature needs to be found for materials that have been stored and irradiated at a low temperature. The next section will describe a system that has been built to address these issues, and later sections will discuss some initial experiments conducted to answer these questions.

4.2 A System to Irradiate and Measure OSL at Low Temperatures

A diagram of the low temperature OSL system developed at Oklahoma State University by the author and Dr. Eduardo G. Yukihara is shown in Figure 4.2. The entire

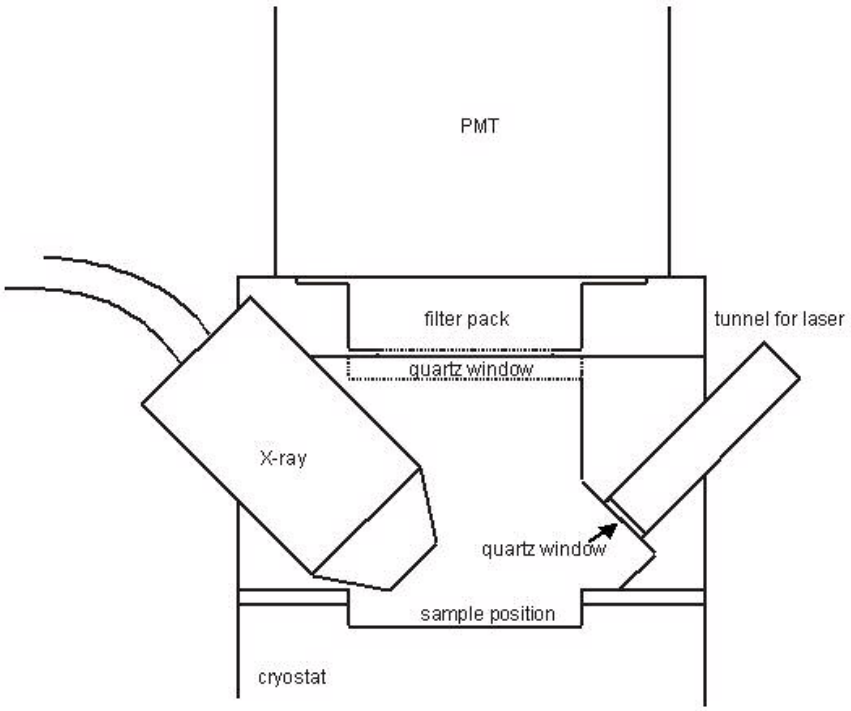

Figure 4.2 Diagram of the low temperature TL/OSL system.

system is controlled by a LabView program written by Dr. Yukihara. The system consists of a cryostat, an irradiation/stimulation unit, and a detection unit. The cryostat is able to cool the sample to –150ºC using liquid nitrogen pumped through the system by a manual pump, or to heat to 200ºC using two 50 W pencil heaters from Watlow. Due to the low temperatures reached during the experiments, the cryostat is maintained at a vacuum level of approximately 5 x 10^{-4} Torr by a turbomolecular pump. The nitrogen flow and the heaters are controlled by an Omega CN3251 temperature/process controller and custom control box. The irradiation/stimulation unit is fitted with an X-ray tube on one side, and a quartz window for optical stimulation on the other side. The detection is accomplished by a photomultiplier tube (PMT) operating in photon-counting mode using a Standford Research SR400 photon counter. A filter pack containing UV transmitting Hoya U-340 filters (transmission between 290 nm and 390 nm) was used to prevent the stimulation light from reaching the PMT.

Irradiations were performed using a 40 kV Moxtek X-ray tube, transmission anode type, operating at 35 kV and 100 μA. The tube has a beryllium window with dimensions 0.25 mm of thickness by 2 mm of diameter. This particular X-ray tube was chosen for its small size and low power consumption (4 W), and is a candidate for the miniaturized OSL instrument for Mars. The dose rate was sometimes changed between sets of experimental measurements when the tube position was changed, and the dose rate at the time of the experiment is noted in later sections.

Optical stimulation was performed using a 100 mW Diode Pump Solid State (DPSS) green laser (532 nm) from Extreme Lasers Inc. (USA) operating in continuous-wave mode. An optical fiber bundle was initially used to direct the laser light through the

tunnel (see Figure 1) and diffuse the light over the sample. The fiber bundle was later replaced by a liquid light guide. The power of the diffused laser light at the sample position, measured with a Newport 1830-C power meter and an 818-ST Newport detector, was approximately 10 mW/cm^2. An electronic shutter was used to control the stimulation.

4.3 OSL Properties of Materials Irradiated and Stimulated at Low Temperatures

Using the above system, the general OSL properties of several different minerals and mixtures of minerals irradiated and stimulated at low temperatures have been studied. The system was first tested by Dr. Yukihara using a standard quartz sample from Riso National Labs (180-220 μm grain size). Results of experiments performed on albite (the same albite as previously discussed in Chapter 2) and mixtures OSU Mars-1 and OSU Mars-2 (described in Section 1.3.1 and Table 1.2) are described below.

4.3.1 Reproducibility

The first experiment for each material was to test if both the system and the material yielded reproducible results. The samples were first bleached with blue light (600 s for albite, 300 s for the Mars mixtures). Then, the samples were subjected to 5 cycles of irradiation (2 Gy for albite, 5 Gy for the Mars mixtures) and OSL stimulation (600 s for feldspars, 300 s for Mars mixtures) while maintained at a temperature of 25°C. The resulting OSL curves overlap each other, and the OSL intensity (total area under the curve minus a background signal) varied by only 3 % for albite, 4 % for OSU Mars-1, and 5 % for OSU Mars-2. The system can then be used to reliably measure OSL from these samples.

4.3.2 Luminescence Efficiency

The luminescence efficiency was studied by monitoring the radioluminescence (RL) under constant irradiation as the sample is cooled from room temperature to -125ºC for albite and –100°C for the Mars mixtures. RL is produced during irradiation when electrons in the conduction band recombine with holes at recombination centers (Bøtter-Jensen *et al.*, 2003). RL is therefore a measure of the efficiency with which the recombination centers produce luminescence. The normalized results are presented in Figure 4.3, and all samples show an increase in RL with decreasing temperature. However, the increase for the Mars mixtures is considerably less than for albite.

The observed increase in luminescence efficiency is most easily explained by thermal quenching. Significant thermal quenching has been reported in the literature for feldspar samples (Duller 1997; White *et al.*, 1986; Vicosekas *et al.*, 1994; Barnett and Bailiff, 1997), but most of those experiments were conducted on orthoclase specimens and used detection windows with wavelengths greater than 400 nm. In addition, more than one recombination center (wavelength) could be monitored with the detection window used in the current experiments. Therefore, the increase in luminescence efficiency could be due to multiple recombination centers that do not contribute to luminescence at room temperature (or above) due to thermal instability or quenching. The system has now been fitted with a monochromator in order to help answer this question, but experiments have not been conducted as part of this work.

4.3.3 Low Temperature TL

In order to identify low temperature traps, the samples were irradiated at –125 ºC with 50 Gy for albite and at –100°C with 10 Gy for the Mars mixtures and heated to room temperature at a heating rate of approximately 0.3 ºC/s. The dashed lines in Figure

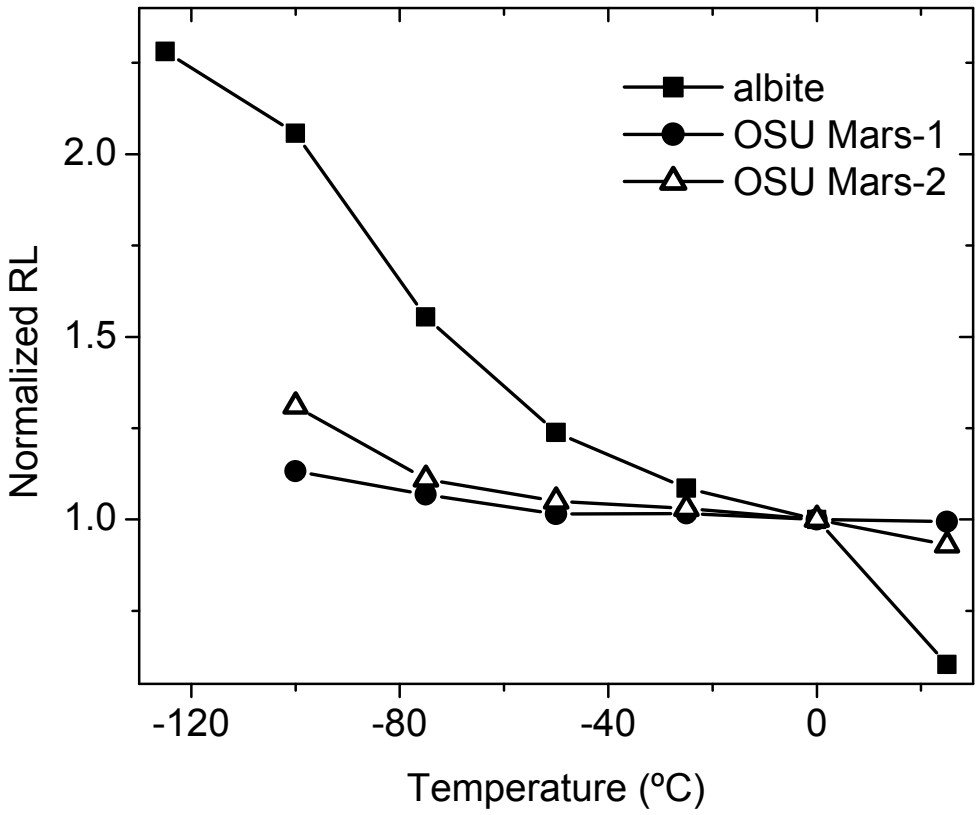

Figure 4.3 Normalized RL from albite and mixtures OSU Mars-1 and OSU Mars-2 as indicated. The RL was normalized to the value at 0°C.

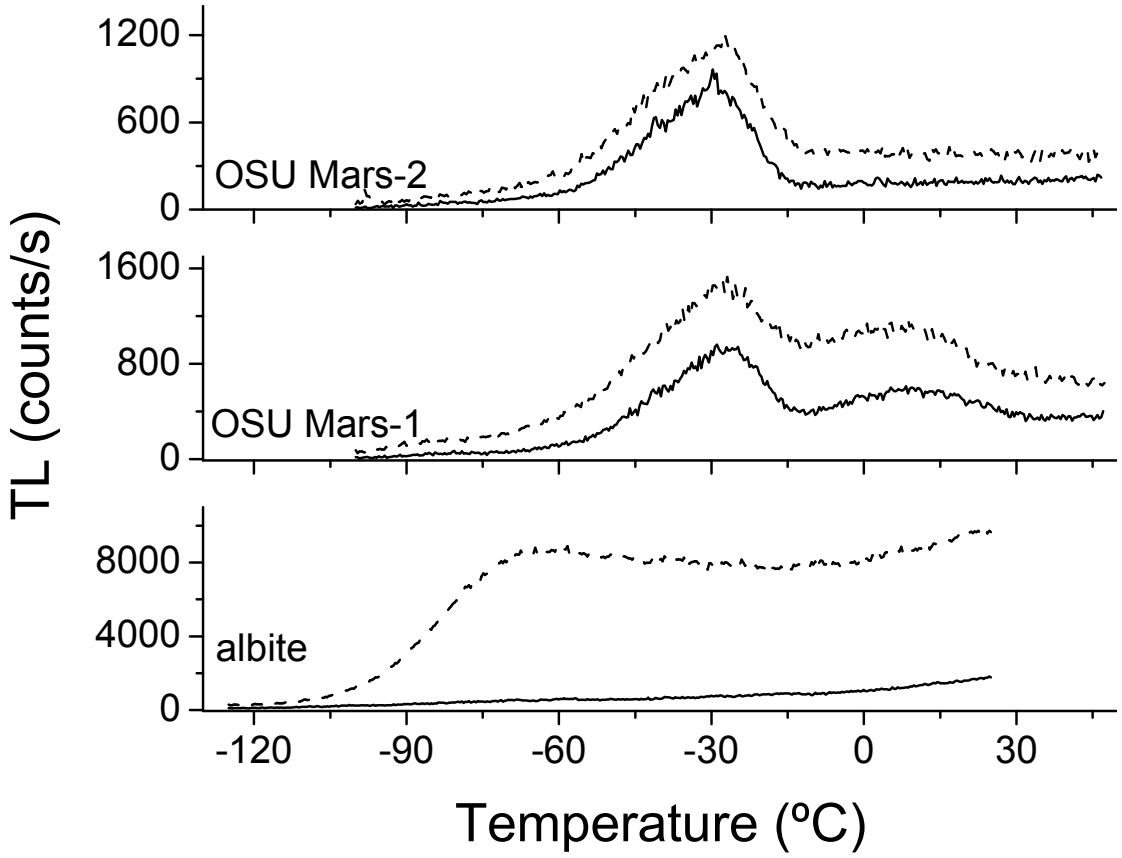

Figure 4.4 TL from three samples (as noted) that have been irradiated at –100°C (OSU Mars-1 and OSU Mars-2) and –125°C (albite). The dashed line represents the TL measured immediately after irradiation, and the solid line represents the TL measured after irradiation and bleaching.

4.4 show the TL from these experiments. Albite produces a TL signal between –100°C and room temperature with a clear broad peak around –50 ºC. Both of the Mars mixtures show TL peaks near –30°C, and OSU Mars-1 shows an additional TL peak near room temperature. Although it is difficult to determine the number of components of these TL curves, these low temperature peaks indicate the presence of trapping states that are relatively stable at temperatures below –20 ºC and unstable at temperatures higher than that.

To examine the optical sensitivity of these trapping centers, the same procedure was repeated but a laser bleach for 300 s for the Mars mixtures and 600 s for albite at –125 ºC was introduced after irradiation. Comparing the TL curve after bleaching (solid lines, Figure 4.4) with the original TL curve (dashed lines), it can be seen that these trapping levels are optically sensitive. The low temperature traps for albite are almost completely emptied indicating that these traps can be an important part of the OSL process. However, the low temperature traps for the Mars mixtures were only partially emptied by bleaching and these traps may not be as important in the OSL process.

4.3.4 Effect of Measurement and Irradiation Temperature

The effect of temperature on the OSL measurements was investigated by irradiating the samples at room temperature with 5 Gy for the Mars mixtures and 2 Gy for albite, and performing the OSL readout at different temperatures between room temperature and –100 ºC. Some of the OSL curves obtained are plotted in Figure 4.5, and the insets show the integral OSL intensities as a function of temperature.

For albite, the OSL initially decreases as the OSL measurement temperature is lowered, reaching a minimum at –25 ºC, and below these temperatures the signal

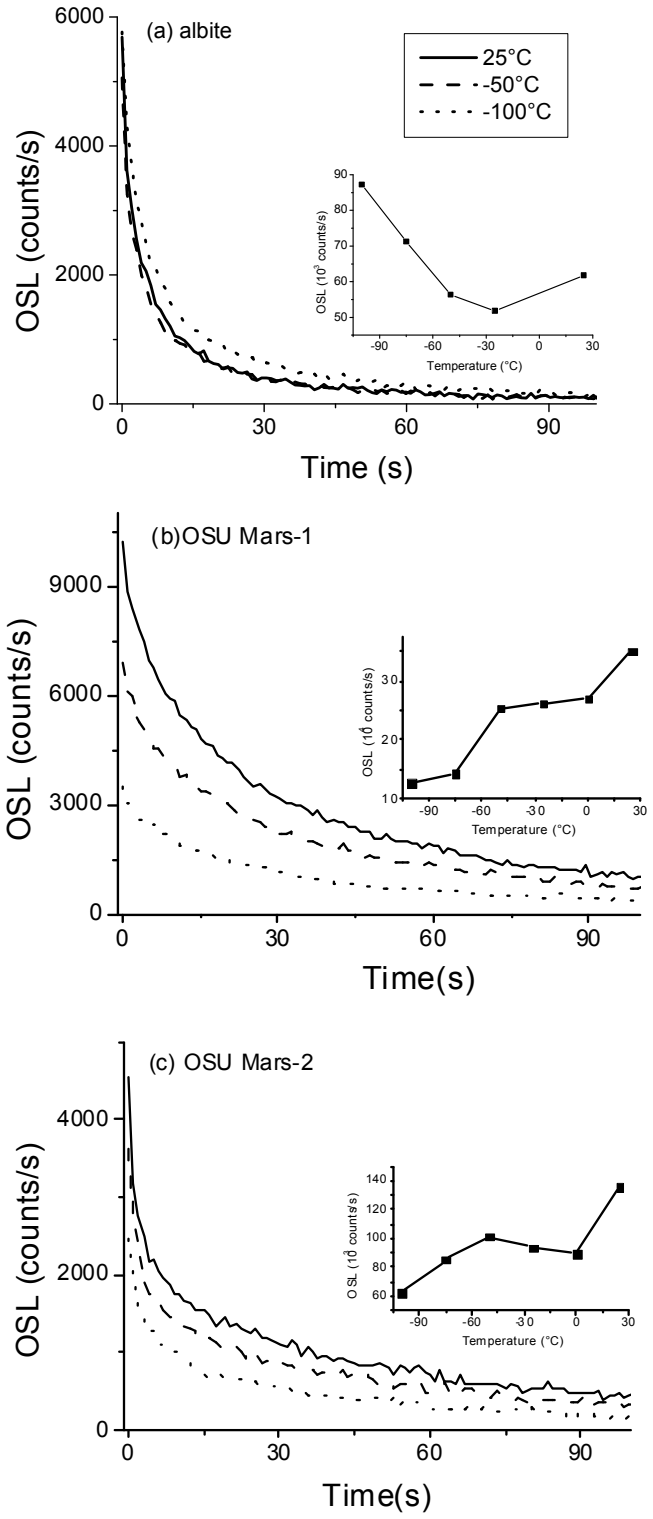

Figure 4.5 OSL from samples (a) albite, (b) OSU Mars-1, and (c) OSU Mars-2 that have been irradiated at 25°C and stimulated at various temperatures as described in the text. OSL decay curves for various temperatures are shown, and the insets show the total OSL signal at each temperature.

increases again. The data can be explained by the combination of two processes: retrapping at the low temperature trapping states and the temperature dependence of the luminescence efficiency. Since the irradiation is performed at room temperature, the same traps are filled every time. However, as the temperature is lowered, trapping states that were thermally unstable start to become stable, which means that they become a competitor during the recombination process. As a result, the OSL signal decreases. However, as the temperature is lowered even more for the OSL measurements, the luminescence efficiency starts to increase (Figure 4.3) resulting in an increased OSL intensity.

For the Mars mixtures, however, we see an almost continual decrease in OSL intensity. For these mixtures, there was very little increase in luminescence efficiency with decreasing temperature (Figure 4.3). Consequently, competition during the recombination process, as discussed above, is dominant.

The effect of irradiation temperature on OSL production was studied for the Mars mixtures by irradiating the samples at various temperatures from –100°C to 25°C and measuring OSL at 25 °C. As in Figure 4.5, the resulting OSL curves and integral OSL signals are shown in Figure 4.6. Neither sample showed a substantial change in the integrated OSL signal (20 % decrease for OSU Mars-1, 22% increase for OSU Mars-2), and an initial decrease is followed by a slight increase in integrated OSL as the irradiation temperature is lowered. The initial decrease is probably a result of traps near room temperature becoming more effective at trapping charge as the irradiation temperature is lowered. The subsequent increase may be a result of charge from the low temperature

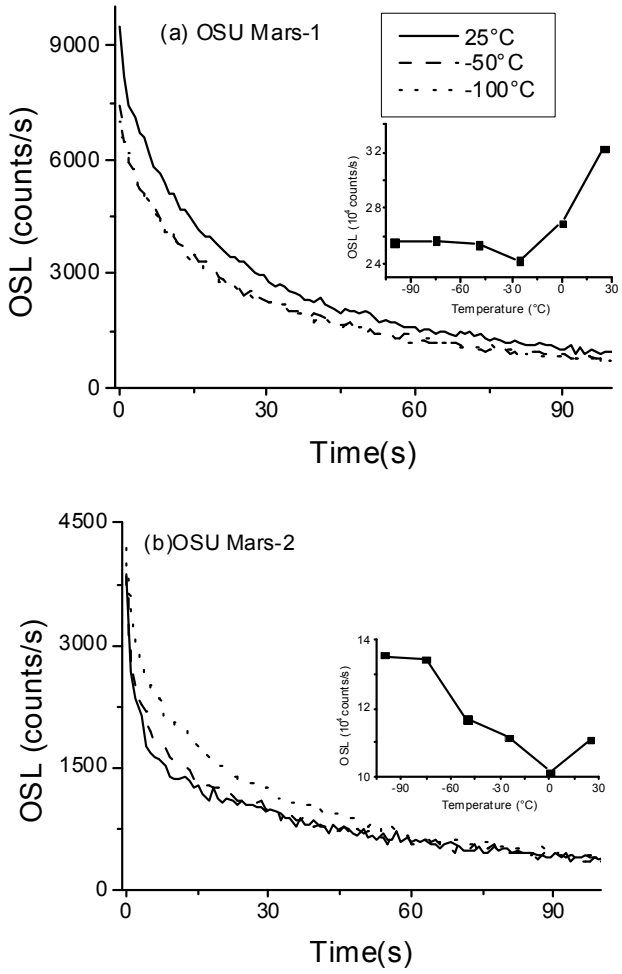

Figure 4.6 OSL from samples (a) OSU Mars-1 and (b) OSU Mars-2 that have been irradiated at various temperatures and stimulated at 25°C as described in the text. OSL decay curves for various temperatures are shown, and the insets show the total OSL signal at each temperature.

traps that are filled at lower irradiation temperatures being thermally released during heating and then retrapped in more stable traps.

We also performed the irradiations and OSL measurements at the same temperature. For this, the samples were cooled to the specified temperature and bleached for 300 s for the Mars mixtures and 600 s for albite. This was followed by irradiation with 5 Gy for the Mars mixtures and 2 Gy for albite, and OSL measurement, with the sample being kept at the same temperature. The result of this investigation is presented in Figure 4.7. The OSL output increases significantly for albite as the temperature is lowered, and a moderate increase is seen for the Mars mixtures. The lower the sample temperature, the higher the number of stable trapping states which are able to capture the free charge carriers created by the irradiation. Coupled with that, the luminescence efficiency increases at low temperatures. The net result is an increased OSL output, but the low temperature traps for the Mars mixtures have been shown to be much less important in the OSL process.

The presence of trapping states with high optical sensitivity below room temperature (Figure 4.4) is significant for dating applications. These states are probably not stable over geologic time scales (even in colder environments) and therefore may not contribute to the natural signal. However, if laboratory irradiations were performed at low temperatures, these states would be populated and therefore would contribute to subsequent calibration OSL measurements. Either the irradiations need to be performed at higher temperatures to keep the traps empty, or preheating procedures need to be developed to minimize the influence of the low temperature traps. This situation is

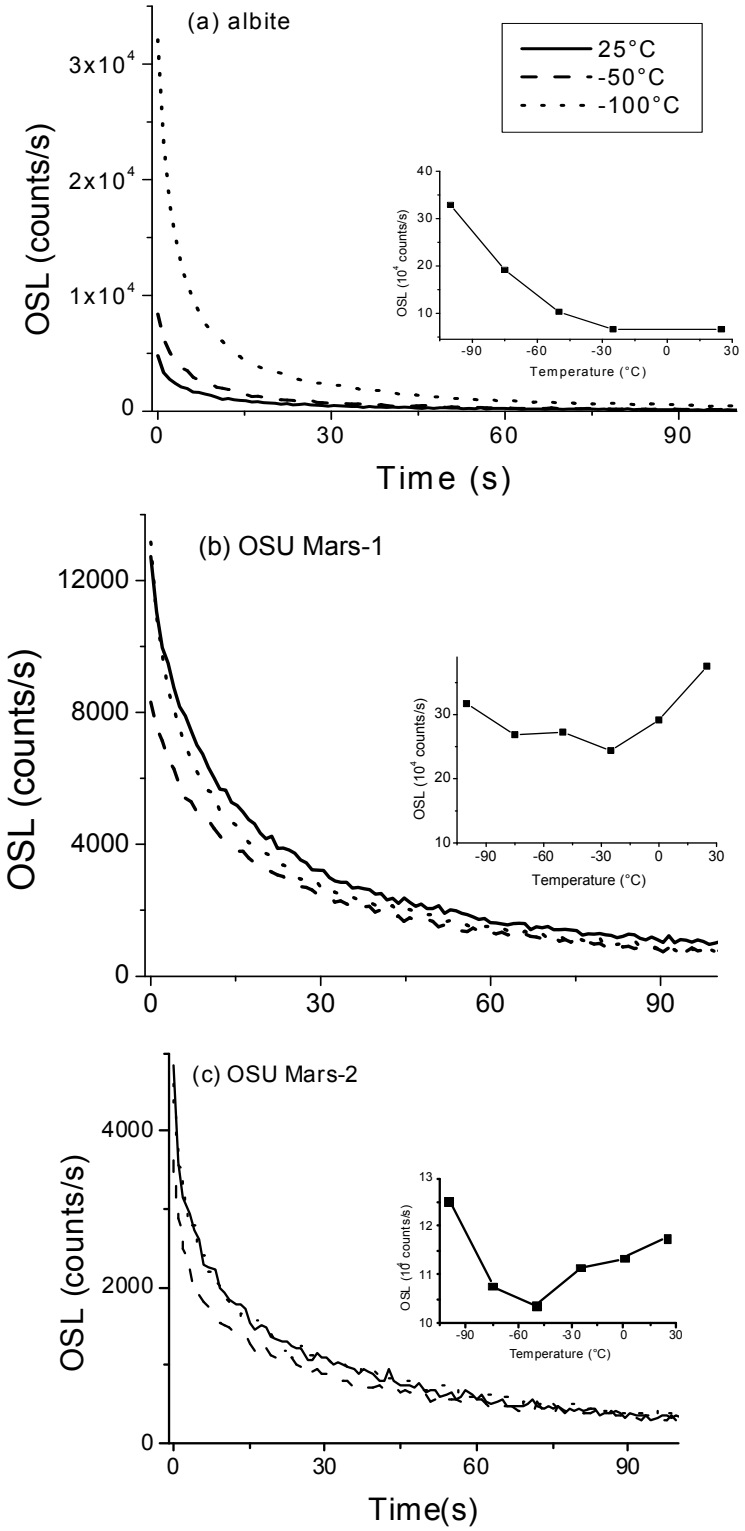

Figure 4.7 OSL from samples (a) albite, (b) OSU Mars-1, and (c) OSU Mars-2 that have been irradiated and stimulated at the same temperature as described in the text. OSL decay curves for various temperatures are shown, and the insets show the total OSL signal at each temperature.

analogous to the influence of the trap causing the 110 ºC TL peak in quartz, and other low temperature traps, in conventional terrestrial OSL dating.

Figures 4.3 and 4.5 show that all OSL measurements must be performed at the same temperature to avoid varying luminescence efficiencies. However, measuring OSL at the lowest temperature and highest efficiency may not be advisable. As discussed previously, any low temperature traps will need to be emptied during a dating procedure. This leads to the possibility of optically stimulated charge being retrapped in the low temperature traps if the OSL is measured at these temperatures, as seen in Figure 4.5. Therefore, appropriate irradiation temperatures, OSL measurement temperatures, and preheating procedures still need to be determined.

4.4 Numerical Simulations

In order to guide further experiments, numerical simulations of an idealized crystal were carried out. Such simulations have been carried out by numerous researchers in the past in order to better understand the luminescence process, explain observed phenomena, and suggest future experimental procedures. In the present case, numerical simulations are being conducted to aid in the understanding of the charge trafficking process when low temperature traps are present and to limit the number of experiments that need to be conducted while determining the optimum irradiation and OSL measurement temperatures. The following sections give the model equations and parameters used and the basic luminescence properties of the model.

4.4.1 The Model and Parameters

The current model is based upon previous work by other researchers (Bøtter-Jensen *et al.*, 1995; McKeever *et al.*, 1997a, 1997b; McKeever and Chen, 1997; Chen and

McKeever, 1997; Bailey, 2001). All of these models simulate luminescence from a crystal by considering a valence band, a conduction band, trapping states within the band gap, and recombination centers within the band gap. With this type of numerical modeling, there are two basic approaches: an attempt to model behaviors and understand specific phenomena with a model that may or may not correspond to a specific mineral (Bøtter-Jensen *et al.*, 1995; McKeever *et al.*, 1997a, 1997b), and developing a model that corresponds to the trap and recombination structure of a specific mineral (Bailey, 2001). The current work, while based upon models of quartz, generally follows the first approach and does not attempt to model all the characteristics of any certain mineral.

The model used for this study consists of 4 traps (i, i=L, 1-3) and one recombination center (4). Real minerals have more than one recombination center, but the purpose of this study is to determine the effects of low temperature traps without the added complexity of multiple recombination centers. The electron traps consist of: (L) a low temperature, optically active trap with a TL peak near –50°C, (1) a trap with a TL peak around 100°C that is not optically active to simulate moderately shallow traps that act as competitors for charge, (2) the main dosimetric trap (at least under terrestrial conditions) that is optically active and has a TL peak near 300°C, and (3) a deep, thermally disconnected trap. A band diagram of this model is given in Figure 4.8, and the parameters for the traps and recombination center are given in Table 4.1 (the various parameters will be discussed below). The parameters of the traps and recombination center have largely been based upon Bøtter-Jensen *et al.* (1995) and McKeever *et al.* (1997a), but the energy depth (E) and frequency factors (s) have been adjusted so that the TL peaks are in the desired position.

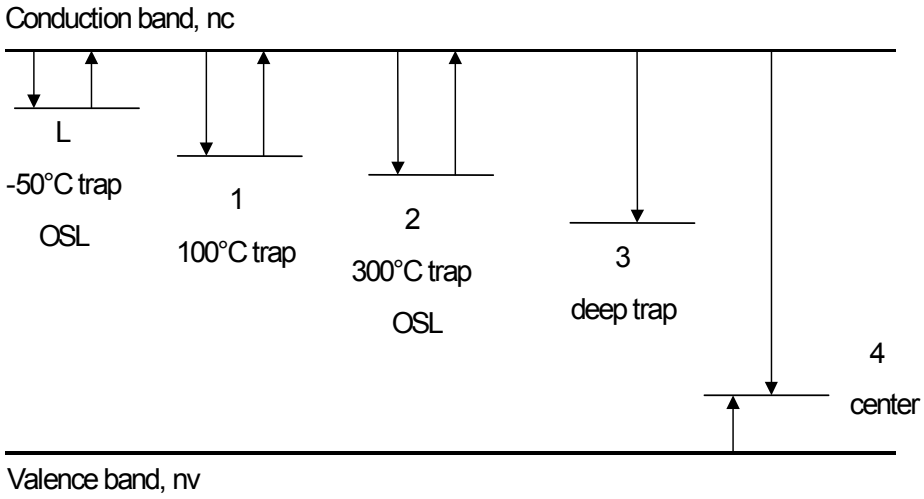

Figure 4.8 Band diagram representing the traps and recombination center for numerical modeling of low temperature traps and the OSL process. See Table 4.1 for the parameters used.

Level	N(cm^{-3})	E(eV)	s(s^{-1})	A ($cm^3 s^{-1}$)	Am ($cm^3 s^{-1}$)
L*	10^{11}	0.6	$5x10^{12}$	10^{-9}	-
1	10^{11}	0.9	$5x10^{12}$	10^{-9}	-
2*	10^{11}	1.7	10^{14}	10^{-10}	-
3	10^{11}	-	-	10^{-10}	-
4	$1.1x10^{12}$	-	-	$4x10^{-10}$	$2x10^{-9}$

* optically active

Other parameters:

f=$1*10^{8}$ cm^{-3}/s (irradiation rate~1Gy/s)

f2=$1*10^{-2}$ s^{-1} (optical excitation rate)

β=+/ - 5 °/s (heating rate)

Table 4.1 Parameters for the 4 traps and one recombination center used in the numerical simulations of low temperature traps and the OSL process. See text for the equations used.

The numerical modeling operates by solving a set of simultaneous, non-linear differential rate equations that describe the flow of charge in the system during all aspects of the luminescence process (i.e., irradiation, relaxation, heating, and optical stimulation). The equations assume that electron transport is via the conduction band, and that the crystal is a closed system (i.e., electrons are not lost to other processes). In general, the rate equations used for modeling the luminescence process with i traps and j recombination centers are:

$$\frac{dn_c}{dt} = f + \sum_i n_i f_i + \sum_i n_i s_i \exp(\frac{-E_i}{k_b T}) - n_c \sum_i (N_i - n_i) A_i - n_c \sum_i m_j A m_j \qquad (4.1)$$

for the conduction band

$$\frac{dn_i}{dt} = -n_i f_i - n_i s_i \exp(\frac{E_i}{k_B T}) + n_c (N_i - n_i) A_i \qquad (4.2)$$

for the i traps

$$\frac{dm_j}{dt} = n_v (M_j - m_j) A_j - n_c m_j A m_j \qquad (4.3)$$

for the j recombination centers, and

$$\frac{dn_v}{dt} = f - n_v \sum_j (M_j - m_j) A_j \qquad (4.4)$$

for the valence band.

$$T = T_0 + \beta * t \qquad (4.5)$$

for the temperature of the crystal. In these equations f is the radiation ionization rate (pair production rate, cm^{-3}/s), n_i is the concentration of electrons in the ith trap (cm^{-3}), f_i is the optical excitation rate for the ith trap (s^{-1}), s_i is the frequency factor for the ith trap (s^{-1}), E_i is the trap depth of the ith trap (eV), k_B is Boltzmann's constant, T is the

temperature (K), n_c is the concentration of free electrons, n_v is the concentration of free holes, N_i is the concentration of defects (available traps) for the ith trap (cm^{-3}), m_j is the concentration of holes in the jth recombination center (cm^{-3}), M_j is the concentration of defects (available hole traps) for the jth recombination center (cm^{-3}), A_i is the electron trapping probability of the ith trap (cm^3/s), A_j is the hole trapping probability of the jth recombination center (cm^3/s), and Am_j is the electron-hole recombination probability at the jth recombination center (cm^3/s), t is time (s), and β is the heating rate (K/s) (McKeever *et al.*, 1997a). Also note that the recombination centers are thermally stable (i.e., do not have E and s values).

For the model used in the current work, the specific equations can be written out, keeping in mind that traps L and 1 (the only optically active traps) have the same optical excitation rate f_2 and that only one recombination center (4) is used:

$$\frac{dn_c}{dt} = f + n_L f_2 + n_2 f_2 + n_L s_L \exp(\frac{-E_L}{k_B T}) + n_1 s_1 \exp(\frac{-E_1}{k_B T}) + n_2 s_2 \exp(\frac{-E_2}{k_B T}) + n_3 s_3 \exp(\frac{-E_3}{k_B T})$$

$$- n_c(N_L - n_L) - n_c(N_1 - n_1) - n_c(N_2 - n_2) - n_c(N_3 - n_3) - n_c m_4 A m_4 \quad (4.6)$$

$$\frac{dn_L}{dt} = -n_L f_2 - n_L s_L \exp(\frac{E_L}{k_B T}) + n_c(N_L - n_L) A_L \quad (4.7)$$

$$\frac{dn_1}{dt} = -n_1 s_1 \exp(\frac{E_1}{k_B T}) + n_c(N_1 - n_1) A_1 \quad (4.8)$$

$$\frac{dn_2}{dt} = -n_2 f_2 - n_2 s_2 \exp(\frac{E_2}{k_B T}) + n_c(N_2 - n_2) A_2 \quad (4.9)$$

$$\frac{dn_3}{dt} = -n_3 s_3 \exp(\frac{E_3}{k_B T}) + n_c(N_3 - n_3) A_3 \quad (4.10)$$

$$\frac{dm_4}{dt} = n_v(M_4 - m_4) A_j - n_c m_4 A m_4 \quad (4.11)$$

$$\frac{dn_v}{dt} = f - n_v(M_4 - m_4)A_4 \ . \tag{4.12}$$

$$T = T_0 + \beta t \tag{4.13}$$

The above equations can be further simplified by making the quasiequilibrium assumption. Mathematically, this assumption is:

$$\left|\frac{dn_c}{dt}\right| \langle\langle \left|\frac{dn}{dt}\right|, \left|\frac{dm}{dt}\right| \ . \tag{4.14}$$

Physically, this means that the electron population of the conduction band changes very little compared with the changes in the trap population (Chen and McKeever, 1997). Taken together with the assumption that the conduction band is initially empty, we can assume that electrons never accumulate in the conduction band during the luminescence process and:

$$\frac{dn_c}{dt} \cong 0 \tag{4.15}$$

Combining the assumptions embodied by equation 4.13 with the rate equations 4.5-4.11, we can write:

$$n_c = \frac{f + n_L s_L \exp(\frac{-E_L}{k_B T}) + n_1 s_1 \exp(\frac{-E_1}{k_B T}) + n_2 s_2 \exp(\frac{-E_2}{k_B T}) + n_L f_2 + n_2 f_2}{(N_L - n_L)A_L + (N_1 - n_1)A_1 + (N_2 - n_2)A_2 + (N_3 - n_3)A_3 + m_4 A m_4} \tag{4.16}$$

$$n_v = \frac{f}{(M_4 - m_4)A_4} \tag{4.17}$$

$$\frac{dn_L}{dt} = -n_L f_2 - n_L s_L \exp(\frac{E_L}{k_B T}) + n_c(N_L - n_L)A_L \tag{4.18}$$

$$\frac{dn_1}{dt} = -n_1 s_1 \exp(\frac{E_1}{k_B T}) + n_c(N_1 - n_1)A_1 \tag{4.19}$$

$$\frac{dn_2}{dt} = -n_2 f_2 - n_2 s_2 \exp(\frac{E_2}{k_B T}) + n_c (N_2 - n_2) A_2 \tag{4.20}$$

$$\frac{dn_3}{dt} = -n_3 s_3 \exp(\frac{E_3}{k_B T}) + n_c (N_3 - n_3) A_3 \tag{4.21}$$

$$\frac{dm_4}{dt} = n_v (M_4 - m_4) A_j - n_c m_4 A m_4 \tag{4.22}$$

$$T = T_0 + \beta t \tag{4.23}$$

where equations 4.18-4.23 are the same as equations 4.7-4.11, 4.13.

Since there is only one recombination center, the luminescence (radioluminescence, TL, or OSL depending upon the stimulation method) signal is given by:

$$I = -n_c m_4 A m_4 \ . \tag{4.24}$$

It is important to note that this expression for the luminescence intensity does not contain any explicit dependence on temperature. In other words, thermal quenching of the luminescence center is not considered at this time in the model. Thermal quenching considerations have not been considered because the first goal is to focus on the influence of low temperature traps and finding a thermal quenching function that satisfies both the low temperature quenching results and higher temperature (like those used in normal terrestrial dating) quenching results is not straightforward.

Equations 4.16-4.23 can be solved for any of the operations involved in the luminescence process by changing the values of certain parameters: (a) for irradiation, f_2=0, β=0; (b) for relaxation (after irradiation or stimulation), f=0, f_2=0, β=0; (c) for heating, cooling, or TL, f=0, f_2=0, β=±5; (d) for bleaching or OSL, f=0, β=0. In addition, the dose rate can be easily varied by setting the optical excitation rate f_2 as:

$$f_2 = 1x10^{-2} s^{-1} * DoseRate \tag{4.25}$$

where DoseRate=1 corresponds to a dose rate of 1 Dose Unit/s[2]. Dose rates typical of both natural and laboratory environments can then be simulated.

The numerical modeling was carried out by solving equations 4.16-4.23 using *Mathematica* (Wolfram Research, Inc.) and self-written code. The value of the quasiequilibrium assumption becomes apparent at this point as differential equations do not have to be solved for the valence and conduction band, but rather equations 4.16 and 4.17 can be evaluated at each necessary point. Charge neutrality of the model was also checked throughout the operations by verifying that

$$n_c + n_L + n_1 + n_2 + n_3 - n_v - m_4 \approx 0. \tag{4.26}$$

The software was then used to determine the basic luminescence characteristics of the model (Section 4.4.2), simulate the SAR procedure (including dose recovery and D_e estimation) at normal terrestrial temperatures (Section 4.4.3), and simulate the SAR procedure at martian temperatures while varying the irradiation and stimulation temperatures during the dose recovery or estimation process (Section 4.4.4). The last part of Section 4.4 discusses these results and gives suggestions for further experiments.

4.4.2 Basic Luminescence Characteristics of the Model

Before discussing the basic luminescence characteristics of the model, simulation of the geologic history of the crystal needs to be described. Initially, all populations (n_v, n_c, n_L, n_1, n_2, n_3, and m_4) were set to zero to correspond to crystallization or formation of the crystal. A dose of approximately 200 Dose Units was then given at a dose rate of

[2] The value of f_2 was taken from McKeever *et al.* (1997a). This value is supposed to correspond to 1 Gy/s, but no physical reasoning is given. Therefore, "Dose Units" is used in place of Gy. This makes no difference in the qualitative results of the model.

$6.342x10^{-11}$ Dose Units/s (approximately 2 mDose Units/yr) at 25°C, corresponding to 100,000 years of irradiation at the natural dose rate. Bleaching for 10,000 seconds at 25°C was then performed to simulate geological bleaching in nature. After simulating the "geologic dose and bleaching," the "sample" was subjected to a 20 Dose Units irradiation at the natural dose rate (corresponding to 10,00 years of natural irradiation) and 6000 seconds of bleaching at 25°C for 3 cycles. This simulation of the geologic history of the crystal was performed before every calculation and "experiment" presented in this section.

The TL curve predicted by the model was first examined. In fact, TL was used in development of the model in order that parameters (mainly E and s for the various traps) could be adjusted to produce TL peaks in the desired positions. Since the position of the low temperature peaks is important, the previously described geologic history was carried out at –100 °C. A radiation dose of 5 Dose Units at a dose rate of 0.1 Dose Units/s was then given, and the TL was calculated while heating from –100°C to 500°C at a heating rate of 5 °C/s. The results of this calculation are shown in Figure 4.9 which shows the entire TL curve (Figure 4.9 (a)) and the range from –100 °C to 0°C in detail (Figure 4.9 (b)). The curve shows peaks at approximately –50°C, 100°C, and 300°C, and these peak positions led to the labels used in Figure 4.8. It is important to note the relative intensity of the TL peaks, in particular that the 100°C TL peak is much more intense than the other peaks, as this detail will become important in later discussions.

The sensitivity changes produced by the model from repeated cycles of irradiation, preheating, and OSL measurement were also studied. After simulating the geologic history at 25 °C, a preheat at 100°C for 10 s was administered and the samples

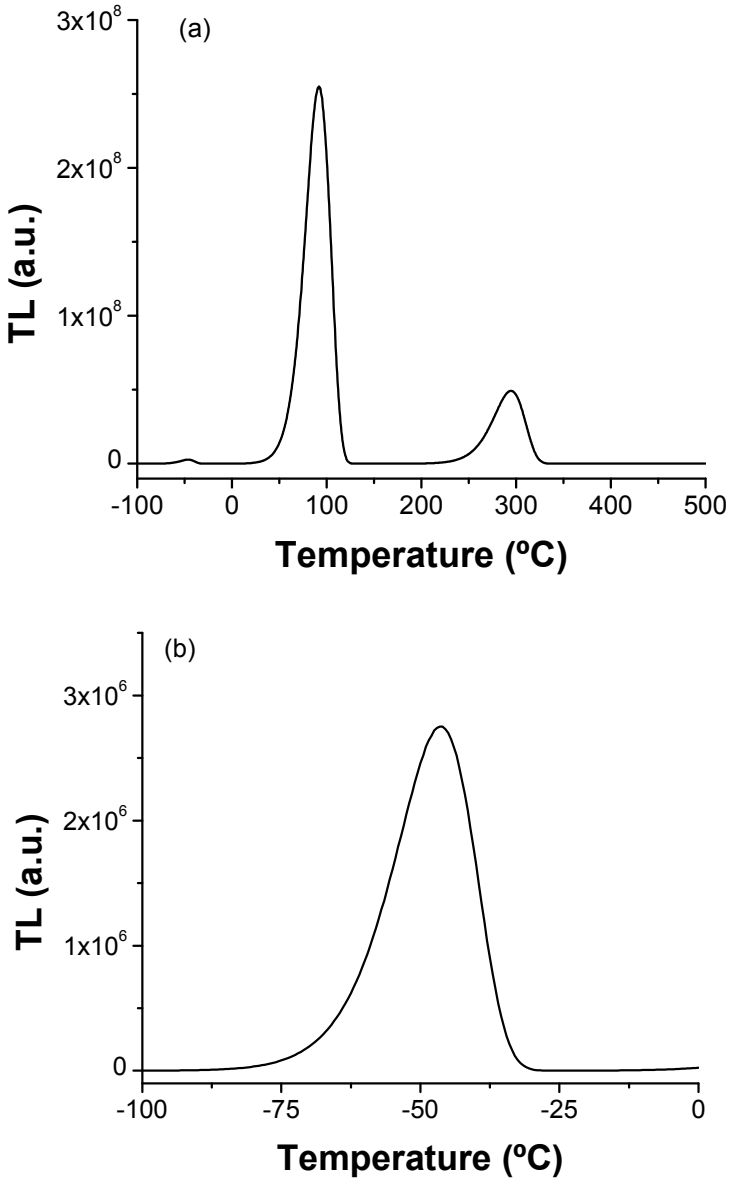

Figure 4.9 TL from the model of Figure 4.8. The geologic history was simulated at –100°C, and a 5 Dose Units dose at a laboratory dose rate was then given. The TL was calculated while heating from –100°C to 0°C at a heating rate of 5 °C/s. Graph (a) shows the entire TL curve, while (b) shows the curve only from –100°C to 0°C.

were bleached for 600 s at 125°C to ensure that the optically active traps were empty. The amount of sensitivity change was then found by performing 10 cycles consisting of: (1) 20 Dose Units irradiation at a dose rate of 0.1 Dose Units/s and 25°C, (2) a preheat at 100 °C for 10 s, and (3) OSL for 600 s at 125°C. The resulting OSL signals decreased by 3% over the 10 cycles for the 1 s signal (the sum of the intensity from the first second minus the average of the last 5 s of stimulation) and 10 % for the full integral (sum of the intensity over the 600 s stimulation minus the average of the last 5 s of stimulation multiplied by 600). This amount of sensitivity change is certainly less than that displayed by either feldpsars (Section 2.2.3) or quartz (Murray and Wintle, 2000). However, the mechanisms generally believed to be the cause of sensitivity change, strong competition during irradiation and stimulation for feldspars (Duller, 1997) and mobility of holes during heating in quartz (Murray and Wintle, 2000), are not included in this model. Therefore, the lack of displayed sensitivity changes in this model is not surprising.

The next step in characterization of the model was to construct an OSL dose response curve. Again, after simulating the geologic history at 25°C, a preheat at 100°C for 10 s and a bleach for 600 s at 125°C were administered. A dose response curve was then constructed for doses from 0.1 to 26214.2 Dose Units using a regenerative-dose procedure without a sensitivity-correction, irradiations with a dose rate of 0.1 Dose Units/s at 25°C, a preheat at 100°C for 10 s, and OSL measurements for 600 s at 125°C. The results for the 1 s integral and the full integral are shown in Figure 4.10 (a) and (b) respectively. Both graphs show linearity up to at least 200 Dose Units, and using the 1 s integral extends the linearity range up to 1000 Units. While both graphs begin to show sub-linear behavior for doses larger than 1000 Dose Units, neither method shows

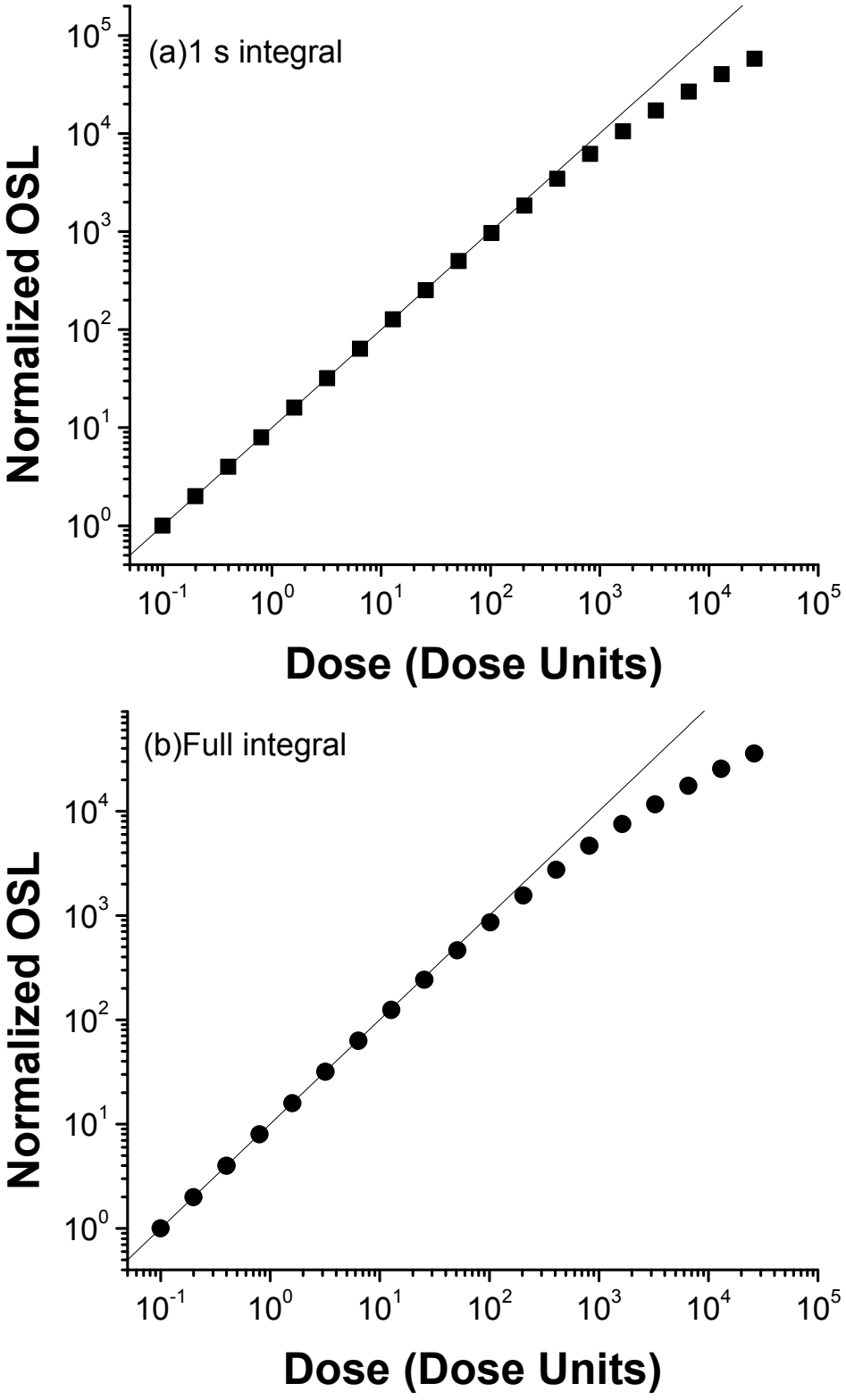

Figure 4.10 OSL dose response curves (normalized to the first dose) for the model of Figure 4.8. Graph (a) is for the 1 s integral and graph (b) is for the full integral.

complete saturation at 26214.2 Dose Units (the largest radiation dose given). Natural materials certainly saturate at doses much lower than this, but for the purposes of this model such a situation is not important.

Several simulations were run to compare the behavior of the model and sediments when irradiations and/or OSL measurements are performed at low temperature. The first such simulation calculated the RL signal during continuous irradiation at a dose rate of 0.1 Dose Units/s as the model was cooled from 25°C to –100°C. The results, along with the previous results from albite and the Mars mixtures, are shown in Figure 4.11. As expected, the RL of the model does not reproduce the RL of the studied samples since the model does not contain any explicit thermal dependence of the luminescence signal (thermal quenching). Instead, a roughly 30 % decrease in RL is seen in the model as the temperature is lowered due to the low temperature trap becoming a competitor for the electrons at these temperatures. A model that adequately describes the entire luminescence process may eventually be necessary, but an accurate description of the luminescence efficiency is not necessary to study the effects of low temperature traps on the dose recovery process.

The experiment of Figure 4.5 was then simulated by irradiating at 25°C and calculating the OSL signal when stimulating at different temperatures. The results for the model and the previously studied minerals are show in Figure 4.12. The model shows an initial substantial decrease in OSL with decreasing temperature as the lower temperature traps capture more charge during stimulation. As the stimulation temperature is lowered even further, the OSL signal changes little. This type of behavior is not typical of albite due to the enhanced luminescence efficiency of albite with decreasing temperature, but

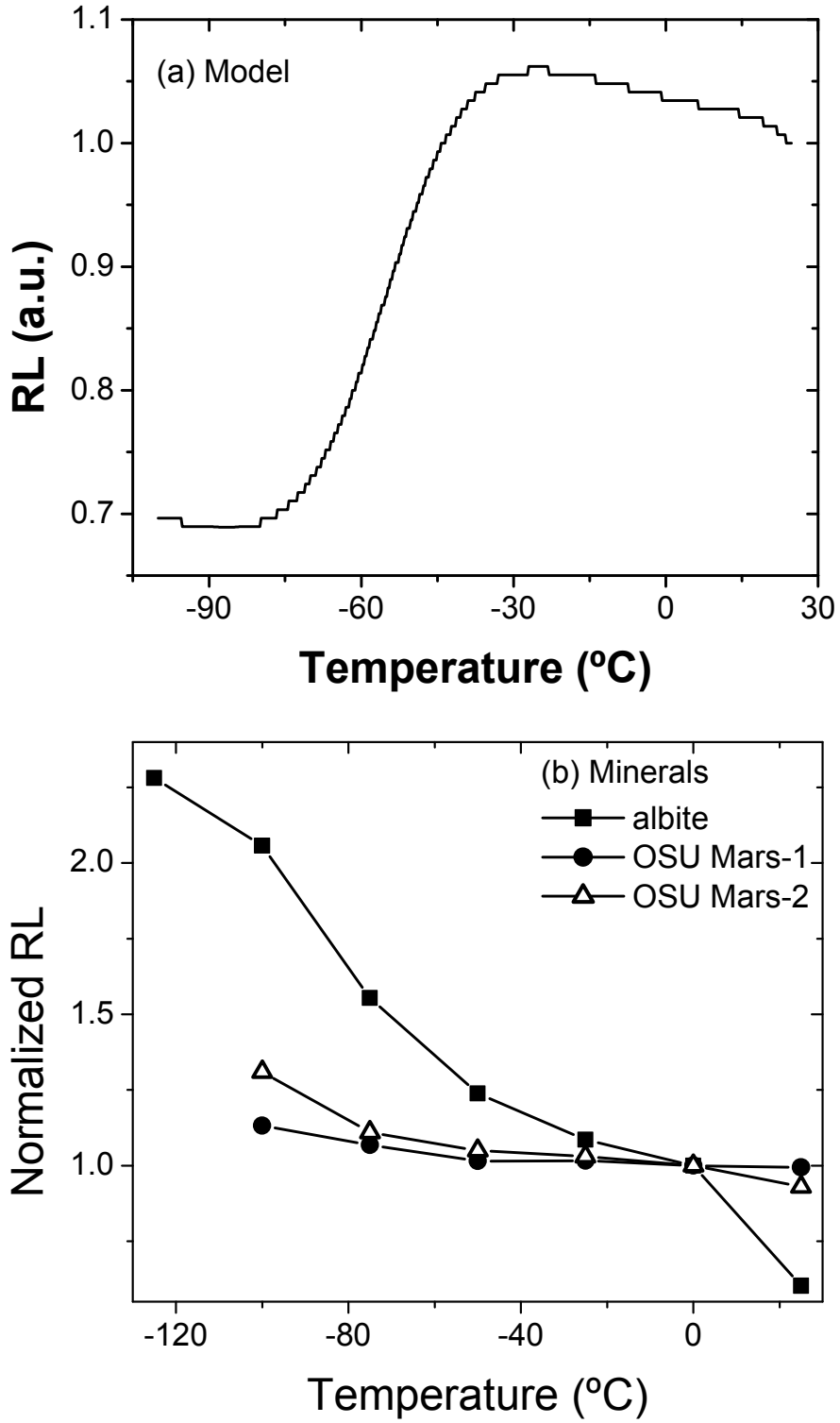

Figure 4.11 RL results for the model of (a) Figure 4.8 and (b) albite, OSU Mars-1, and OSU Mars-2.

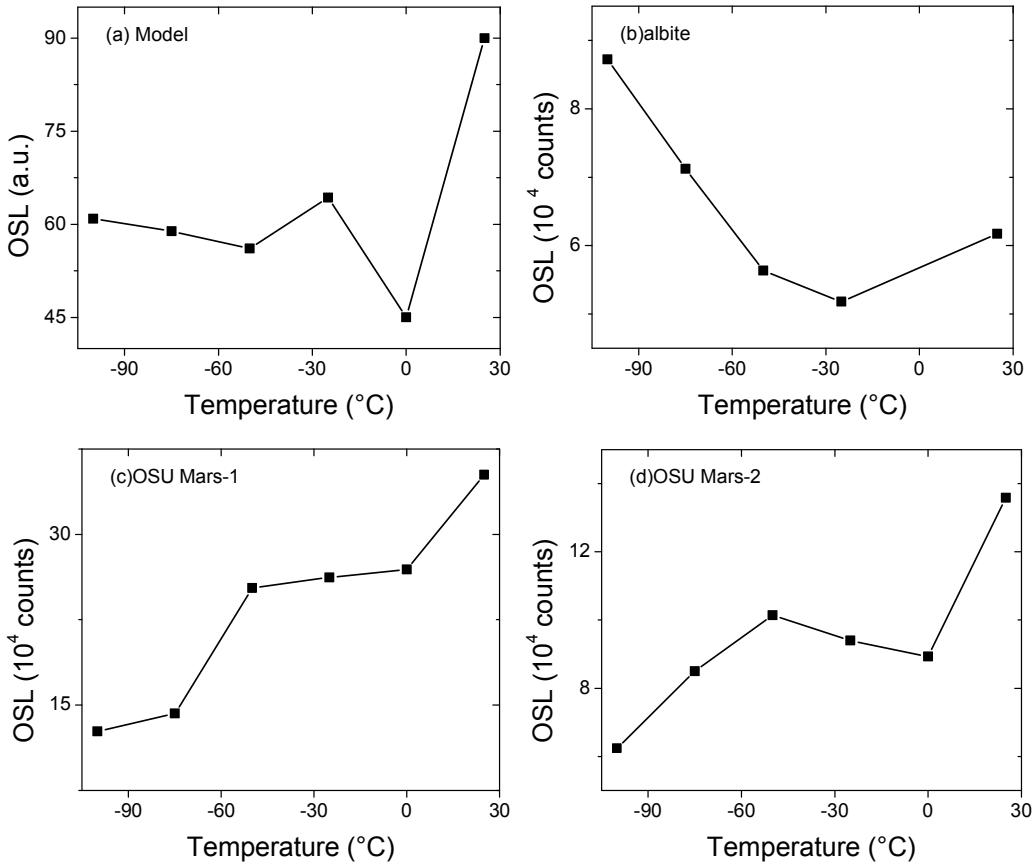

Figure 4.12 OSL from (a) the model for Figure 4.8 and (b) albite, (c) OSU Mars-1, and (d) OSU Mars-2 that have been irradiated at 25°C and stimulated at various temperatures as described in the text.

the behavior does mimic the results from the Mars mixtures where luminescence efficiency was not seen to be strongly temperature dependent. The model may therefore be suitable for some types of minerals.

The experiment of Figure 4.6 was also simulated by irradiating at various temperatures between 25°C and –100°C and calculating the OSL signals while stimulating at 25°C. The results for the model and the previously studied minerals are show in Figure 4.13. The results from the model can only be compared with the results from OSU Mars-1 and OSU Mars-2, and those two minerals show slightly different trends (neither sample showed large changes in OSL intensity). OSU Mars-1 contained a greater abundance of low-temperature optically active trapping states and therefore showed a decrease in OSL as the irradiation temperature was lowered and these trapping states begin capturing charge. Both the model and OSU Mars-2, however, show an increase in OSL with decreasing irradiation temperature. This increase is probably caused by competing traps (trap 1 in the model) that capture charge at lower irradiation temperatures and the charge is then thermally transferred to higher temperature traps prior to OSL measurement. Again, the model appears to be suitable for some minerals but not all of the minerals studied.

As a final check of the model, the experiment of Figure 4.7 was simulated by both irradiating and stimulating at various temperatures from 25°C to –100°C. The results from both the model and studied minerals are shown in Figure 4.14. Again, the model results do not show the same trend as the results from albite but are similar to the results form the Mars mixtures. As in Figure 4.11, this is probably due to the results from albite being dominated by the increase in luminescence efficiency with decreasing temperature

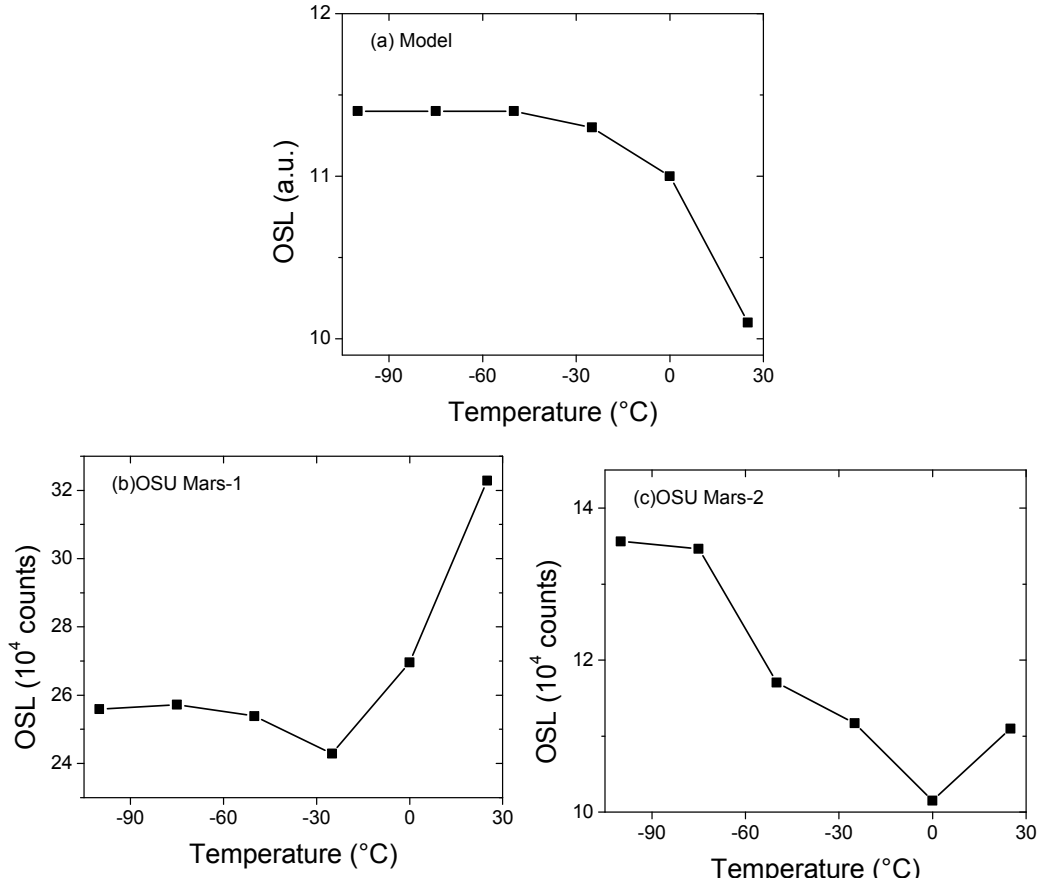

Figure 4.13 OSL from (a) the model for Figure 4.8 and (b) OSU Mars-1, and (c) OSU Mars-2 that have been irradiated at various temperatures and stimulated at 25°C as described in the text.

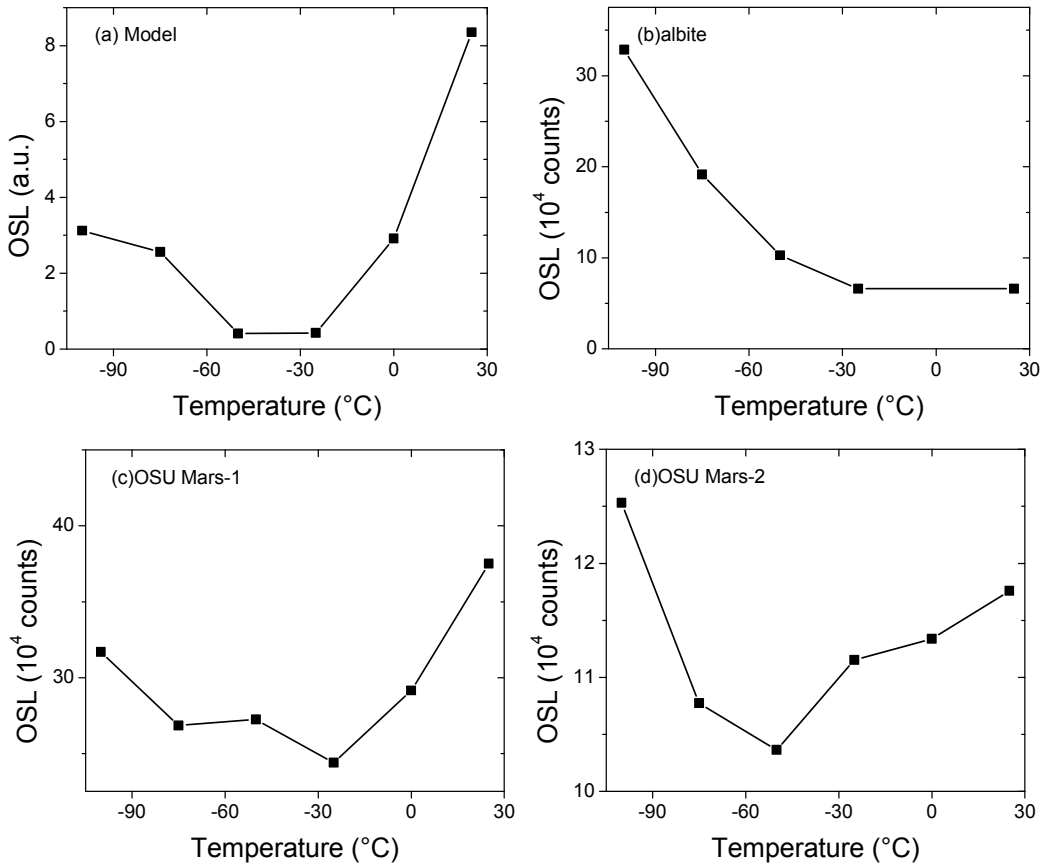

Figure 4.14 OSL from (a) the model for Figure 4.8 and (b) albite, (c) OSU Mars-1, and (d) OSU Mars-2 that have been irradiated at and stimulated at various temperatures as described in the text.

while the Mars mixtures and the model are dominated by the competition of low temperature traps during irradiation and stimulation.

In summary, the model qualitatively reproduces some of the effects seen in real materials that have been irradiated and/or stimulated at low temperatures. The model has optically active traps with TL peaks in the approximate positions seen in the minerals tested, although the intensities of these peaks are not necessarily similar. In addition, the model can produce OSL similar to that produced by the Mars mixtures for OSL stimulation at various temperatures, irradiation at various temperatures, and both irradiation and OSL stimulation at various temperatures. However, apart from the TL results, the model does not seem to be a good surrogate for albite. While a more sophisticated model (including the temperature dependence of the luminescence efficiency or recombination center) could more accurately portray this mineral, that may not be necessary at this time as albite is not expected in large abundances on the martian surface.

4.4.3 Dose Recovery and Dose Estimation at Terrestrial Temperatures

Before testing the effects of low temperature traps on dose recovery and dose estimation techniques when a known or natural dose is given at a low temperature, the model was first tested to verify that both a known dose and natural dose could be recovered when administered at 25^{o}C. To test this, a 10 Dose Units known dose, at the lab dose rate of 0.1 Dose Units/s, or a 10 Dose Units natural dose, at a natural dose rate of 2 mDose Units/yr, was given after simulating the geological history of the sample. Then, the SAR procedure was used to either recover the known dose or estimate the natural dose (terminology used to be consistent with experimental techniques). The parameters

of the SAR procedure were: a preheat at 200°C for 10 s after both the regeneration dose and the test dose, OSL measurement at 125°C for 600 s, a 2.5 Dose Units test dose delivered at 0.1 Dose Units/s and 25°C, and regeneration doses of 8, 10, 12, and 8 (repeat point) Dose Units delivered at 0.1 Dose Units/s and 25°C. The results of both experiments are summarized below.

The results of attempting to recover a known dose delivered at 0.1 Dose Units/s and 25°C are shown in Figure 4.15. The dose recovery ratios for both the full and 1 s integrals are 1.004, indicating that a known dose can be satisfactorily recovered under these conditions. While not surprising, this is a crucial step in further validating the model.

While recovering a dose given at the laboratory dose rate is certainly necessary, successfully estimating a natural dose delivered at a much lower dose rate is more desirable in a model attempting to simulate natural materials. The results of estimating such a natural dose are shown in Figure 4.16. The dose recovery ratios of 1.02 (for both integrals) show that the model can accurately recover a dose delivered at the natural dose rate. This result is encouraging for future studies involving natural irradiations at a lower temperature.

4.4.4 Dose Recovery and Dose Estimation at Martian Temperatures

A series of simulations was undertaken to investigate what laboratory irradiation temperatures and OSL stimulation temperatures are optimal for recovering or estimating a dose delivered at –100°C. For these simulations, the geologic history was simulated at a temperature of –100°C as well. As before, both natural doses (delivered at a dose rate of 2 mDose Units/yr) and laboratory doses (delivered at 0.1 Dose Units/s) of 10 Dose

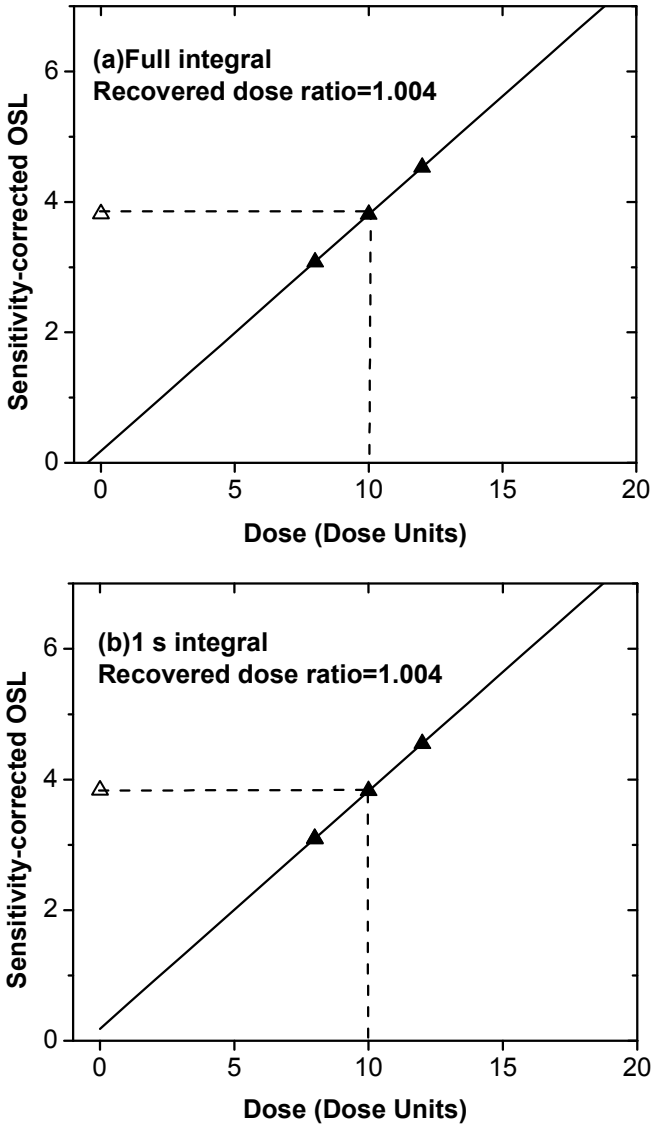

Figure 4.15 Results of the dose recovery simulation for a known dose delivered at 0.1 Dose Units/s and 25°C. The open triangle is the known dose, and the solid triangle represents the regeneration doses. In addition to the graphical representation, the dose recovery ratio (given dose/recovered dose) is also given when using both (a) the full OSL integral and (b) the first 1 s OSL integral (appropriate background signal subtracted in both cases).

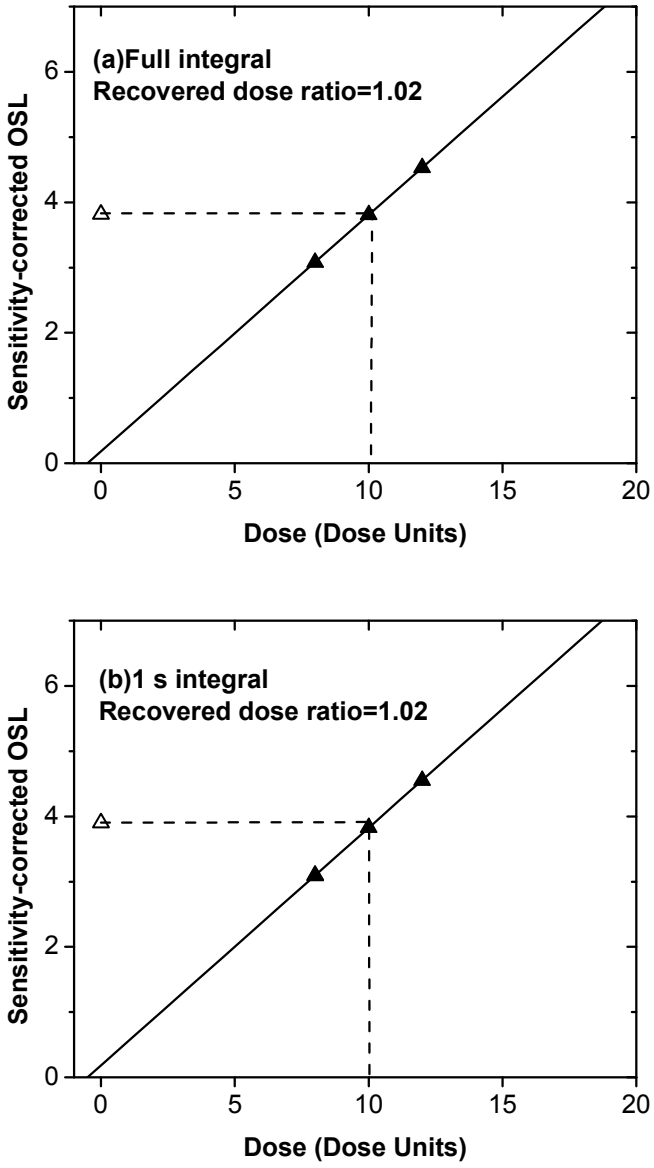

Figure 4.16 Results of the dose estimation simulation for a natural dose delivered at 2 mDose Units/yr and 25°C. The open triangle is the natural dose, and the solid triangle represents the regeneration doses. In addition to the graphical representation, the dose recovery ratio (given dose/recovered dose) is also given when using both (a) the full OSL integral and (b) the first 1 s OSL integral (appropriate background signal subtracted in both cases).

Units were given, and the SAR procedure was used to recover these doses. However, in these simulations, the parameters of the SAR procedure were varied in order to determine how low temperature traps affect the dose recovery process. The tested parameters of the SAR procedure were: (a) laboratory irradiation and stimulation at –100°C, (b) laboratory irradiation at –100°C and stimulation at 25°C, and (c) laboratory irradiation and stimulation at 25°C. No preheats were used in these simulations as preheating is difficult to perform with the low temperature OSL system.

The results of the dose recovery experiment, where a known dose of 10 Dose Units is given at the laboratory dose rate, are given in Figure 4.17. For the case where all irradiations and stimulations are at –100°C (Figure 4.17 (a)), the dose recovery error was very small. However, the other cases produced erroneous results. When the irradiations were given at –100°C and the OSL was measured at –25°C, the OSL from the 10 Dose Units known dose was considerably larger than any of the regeneration dose or test dose signals resulting in an extraordinarily large recovered dose. Such a large OSL signal was produced by the influence of the 100°C trap. This trap is not populated (at least not fully populated) during irradiations at 25 °C, but it effectively traps charge during irradiations at –100°C. Due to the large concentration of trapping centers, the trap has a large population after the geologic history simulation and this charge is not liberated during the simulation of natural bleaching. Then, during heating to 25°C, electrons are released from this trap and many are retrapped in the 300°C trap thus increasing the OSL signal. In addition, charge is thermally liberated from this trap during the OSL measurement at 25°C further increasing the luminescence signal. Most of the charge in the 100°C is liberated during the initial heating and OSL measurement, so the subsequent OSL signals

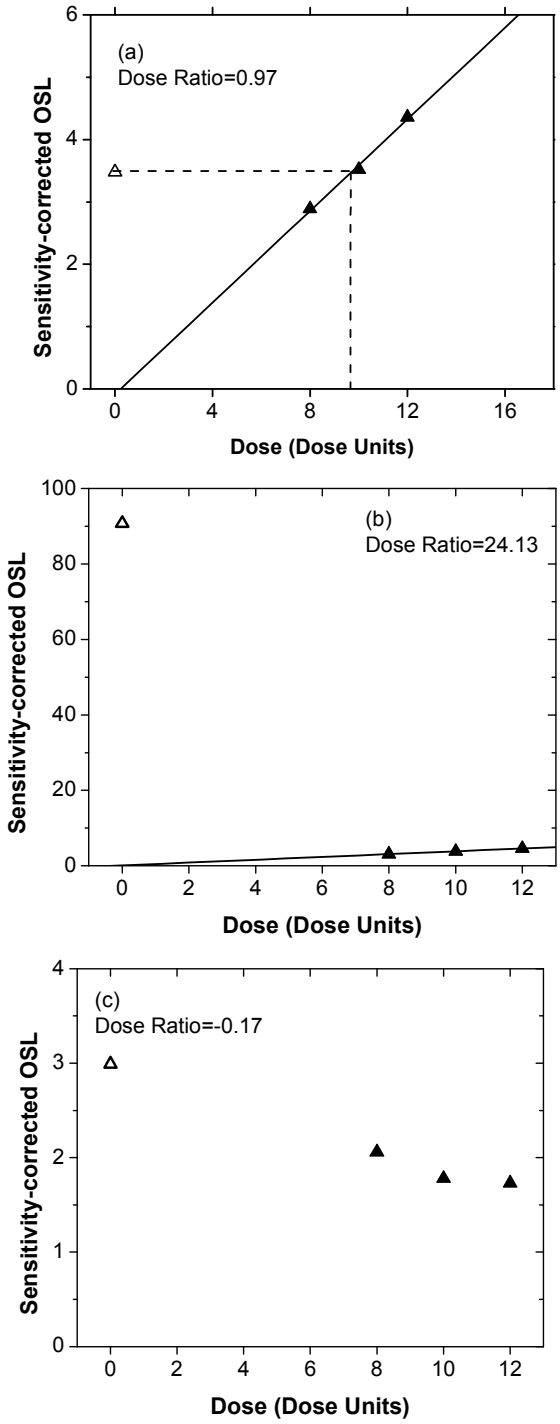

Figure 4.17 Results of the dose recovery simulations for a known dose delivered at 0.1 Dose Units/s and -100°C. The open triangle is the known dose, and the solid triangles represent the regeneration doses in each case. In addition to the graphical representation, the dose recovery ratio (given dose/recovered dose) is also given when using the first 1 s OSL integral. The three cases are: (a) laboratory irradiation and stimulation at –100°C, (b) laboratory irradiation at –100°C and stimulation at 25°C, and (c) laboratory irradiation and stimulation at 25°C.

from test doses and regeneration doses are smaller as they derive mainly from charge trapped in the 300°C trap.

Although the results from performing the irradiations (after delivering the known dose) and stimulation at 25°C appear different, the large errors (the recovered dose ratio is actually negative) are a result of the measurement temperature and the influence of the 100°C trap. The OSL signal from the known dose is comparable to the previous simulation (i.e., it is larger than expected), but the OSL signals from the test doses and regeneration doses are at least of the same magnitude. In addition, the sensitivity-corrected signals actually decrease with increasing dose (Figure 4.17(c)). The large initial OSL signal is again the result of the 100°C trap being populated and not emptied during the geologic history simulation as discussed previously. However, the subsequent test dose and regeneration dose OSL are larger than in the previous simulation because the irradiations are performed at 25°C at which temperature the 100°C does not effectively compete for charge. This results in a larger population for the 300°C trap (as compared to the previous simulation), larger OSL signals, and smaller sensitivity-corrected-values. The decrease in sensitivity-corrected OSL signals with increasing dose again has to do with the irradiation temperature. In the previous simulation, the 100°C trap is populated with each irradiation, charge is transferred with each heating, and thermally liberated charge contributes to each luminescence signal. During this simulation, the 100°C trap is not repopulated during irradiations at 25°C but instead a small amount of charge remaining in the 100°C trap is transferred during each heating. However, the amount of charge transferred (and also the amount contributing directly to luminescence) is smaller with each measurement cycle resulting in decreasing sensitivity-

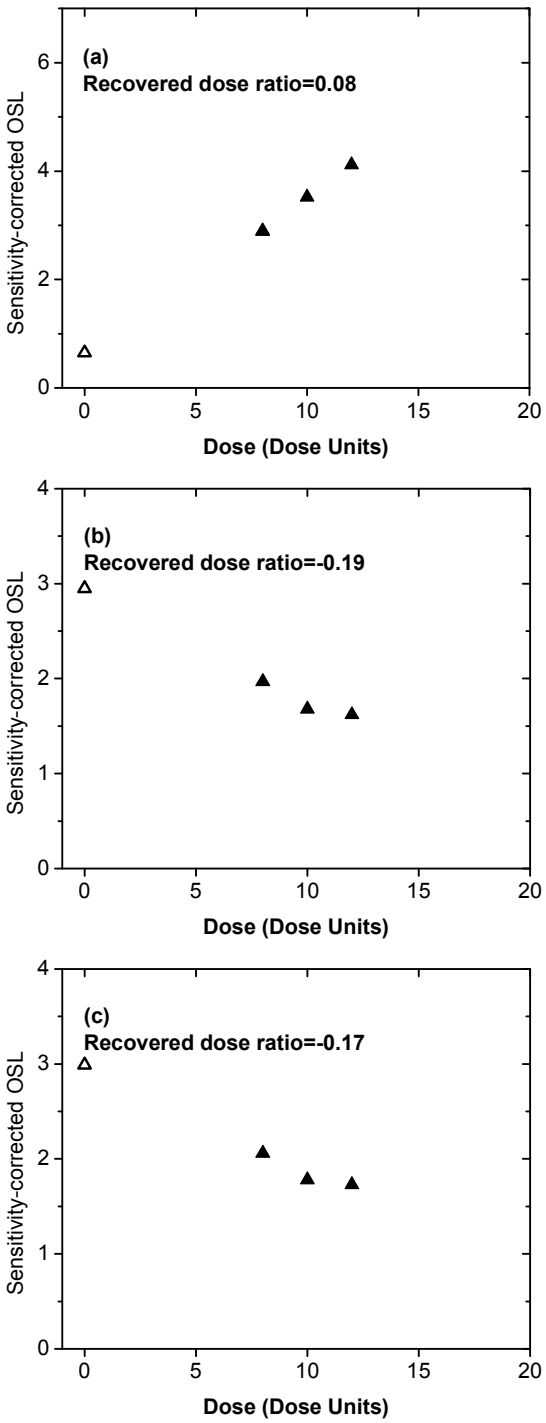

Figure 4.18 Results of the dose estimation simulations for a natural dose delivered at 2 mDose Units/yr and -100°C. The open triangle is the known dose, and the solid triangles represent the regeneration doses in each case. In addition to the graphical representation, the dose recovery ratio (given dose/recovered dose) is also given when using the first 1 s OSL integral. The three cases are: (a) laboratory irradiation and stimulation at –100°C, (b) laboratory irradiation at –100°C and stimulation at 25°C, and (c) laboratory irradiation and stimulation at 25°C.

corrected signals. Although a temperature for irradiation and measurement could probably be found where the increased trapping efficiency of the 300°C trap balances the effects of the 100°C trap, this approach is not advisable as that temperature would be heavily dependent on the particular trap structure of the material.

Even though the dose recovery simulations above were largely unsuccessful, similar simulations where the known dose was replaced by a 10 Dose Units natural dose (delivered at a dose rate of 2 mDose Units/yr) were carried out since they could be instructive. The results of these three simulations are shown in Figure 4.18. As expected, none of the methods were able to accurately estimate the natural dose. For the simulation where all the irradiations and stimulations were at –100°C (Figure 4.18(a)), the OSL signal (both the natural OSL signal and the sensitivity-corrected OSL signal) from the natural dose was an order of magnitude smaller than the OSL signals from the regenerations doses. This is due to the fact that the –50°C trap is not effectively populated during natural irradiation at –100°C and a low dose rate and therefore does not contribute to the natural OSL signal, but the -50°C trap does trap a significant amount of charge during the regeneration and test dose irradiations at –100°C and a higher dose rate resulting in larger OSL signals. The results from the two remaining dose estimation simulations, performing the laboratory irradiations at –100°C and the stimulations at 25°C (Figure 4.18(b)) and performing both the laboratory irradiations and stimulations at 25°C (Figure 4.18(c)), show similar results to the corresponding dose recovery simulations. The data show a smaller sensitivity-corrected OSL from the natural dose (as compared to the dose recovery simulations) due to the –50°C trap not being populated during natural irradiations and therefore not thermally transferring its charge during the

first heating. The sensitivity-corrected OSL signals from the regeneration doses again decrease with increasing dose due to the effects of the 100°C trap as previously discussed. So, none of the tested parameters are able to accurately estimate a natural dose delivered at –100°C for this model.

This section has shown that finding appropriate parameters for the model of Figure 4.8 when using the SAR procedure to recover a known or natural dose is difficult. However, it should be noted that most difficulties arise from the effects of the 100°C trap which is not optically active and traps a large concentration of electrons. While optically inactive traps are present in the tested materials, there do not appear to be traps with concentrations as large as the 100°C trap of the present model. This model and set of parameters may be valid for certain materials, but the next section will explore altering the parameters of the model to simulate a slightly different trap structure.

4.5 Further Numerical Simulations

The influence of the 100°C trap in the previous model seemed to dominate the behavior of the system during dose recovery and dose estimation simulations. While there certainly are optically inactive shallow traps in most minerals, the traps usually do not have a concentration as large as in the previous model. Therefore, the parameters of the model were changed to incorporate a smaller 100°C trap with a smaller electron capture probability (the electron capture probability for the low temperature trap was also lowered to make it equal to the main dosimetric trap), and other parameters had to be adjusted accordingly to preserve charge neutrality as shown by Table 4.2 (i.e., the concentrations of 3 and 4). The rate equations, however, have not changed and are the same as Equations 4.16-4.23.

Level	N (cm^{-3})	E (ev)	s (s^{-1})	A ($cm^3 s^{-1}$)	Am ($cm^3 s^{-1}$)
L*	10^{11}	0.6	$5x10^{12}$	**10^{-10}**	-
1	**10^{9}**	0.9	$5x10^{12}$	**10^{-10}**	-
2*	10^{11}	1.7	10^{14}	10^{-10}	-
3	**$5x10^{11}$**	-		10^{-10}	-
4	**$5x10^{12}$**	-		$4x10^{-10}$	$2x10^{-9}$

* optically active

Other parameters:

$f=1x10^{8}$ cm^{-3}/s (irradiation rate~1 Gy/s)

$f2=1x10^{-2}$ s^{-1} (optical excitation rate)

$\beta = \pm 5$ °C/s (heating rate)

Table 4.2 Parameters for the 4 traps and one recombination center used in the numerical simulations of low temperature traps and the OSL process in Section 4.5. The parameters in bold are those that have been changed from the model of Section 4.4. See text for the equations used.

4.5.1 Basic Luminescence Characteristics

The luminescence characteristics of the modified model were first simulated, including the geological history. Then, those measurements that had already been made with the low temperature OSL system were simulated (Section 4.3). These characteristics are compared to both the original model as well as the results from the previously studied minerals.

The TL of the modified model was first simulated after the geological history (simulated at –100°C) and a 5 Dose Units dose (delivered at 0.1 Dose Units/s). The TL from the modified model is shown along with the TL from the original model in Figure 4.19. The three traps have approximately the same peak temperatures, but the size of the 100°C trap has been drastically reduced, and this has resulted in a proportionally larger –50°C trap due to reduced competition from the 100°C trap.

The dose response curves for the modified model differ slightly from those of the original model (Figure 4.20). First, the modified model does not show sublinear (saturating) behavior until a larger dose. Also, the modified model shows some small supralinearity (around a couple of hundred Dose Units), although no attempt was made to mathematically analyze this phenomenon.

The RL signal was again simulated while the model was cooled from 25°C to -100°C. Since temperature dependence of the recombination center was not included in the modified model, the RL signal was not expected to mimic the thermal quenching noted with the various minerals. However, the RL from the modified model does not show a significant decrease at lower temperatures that the RL from the original model showed (Figure 4.21) because the –50°C trap does not capture as much charge. Still,

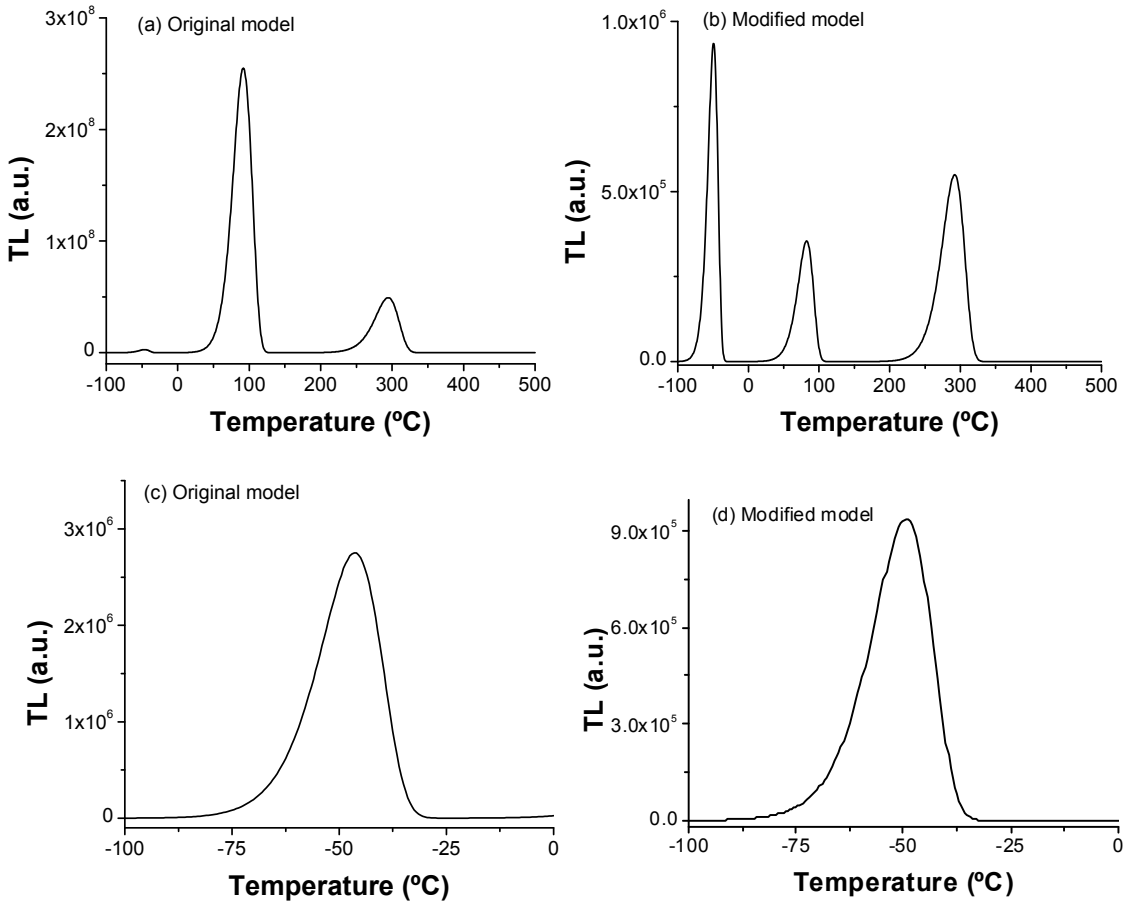

Figure 4.19 TL from the original ((a) and (c)) and modified ((b) and (d)) models. The geologic history was simulated at –100°C, and a 5 Dose Units dose at a laboratory dose rate was then given. The TL was calculated while heating from –100°C to 0°C at a heating rate of 5 °C/s. Graphs (a) and (b) show the entire TL curve, while (c) and (d) show the curve only from –100°C to 0°C.

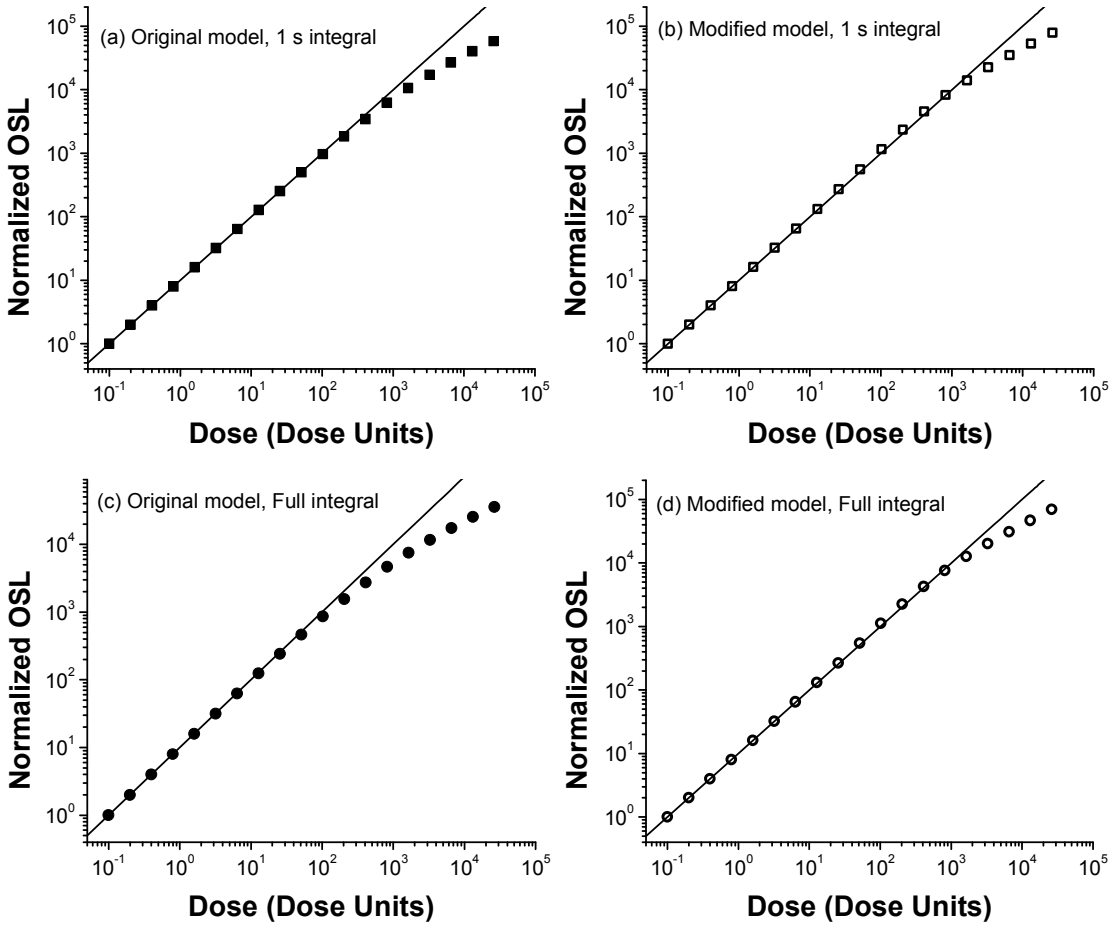

Figure 4.20 OSL dose response curves (normalized to the first dose) for the original ((a) and (c)) and modified models ((b) and (d)). Graphs (a) and (b) are for the 1 s integral and graphs (c) and (d) are for the full integral.

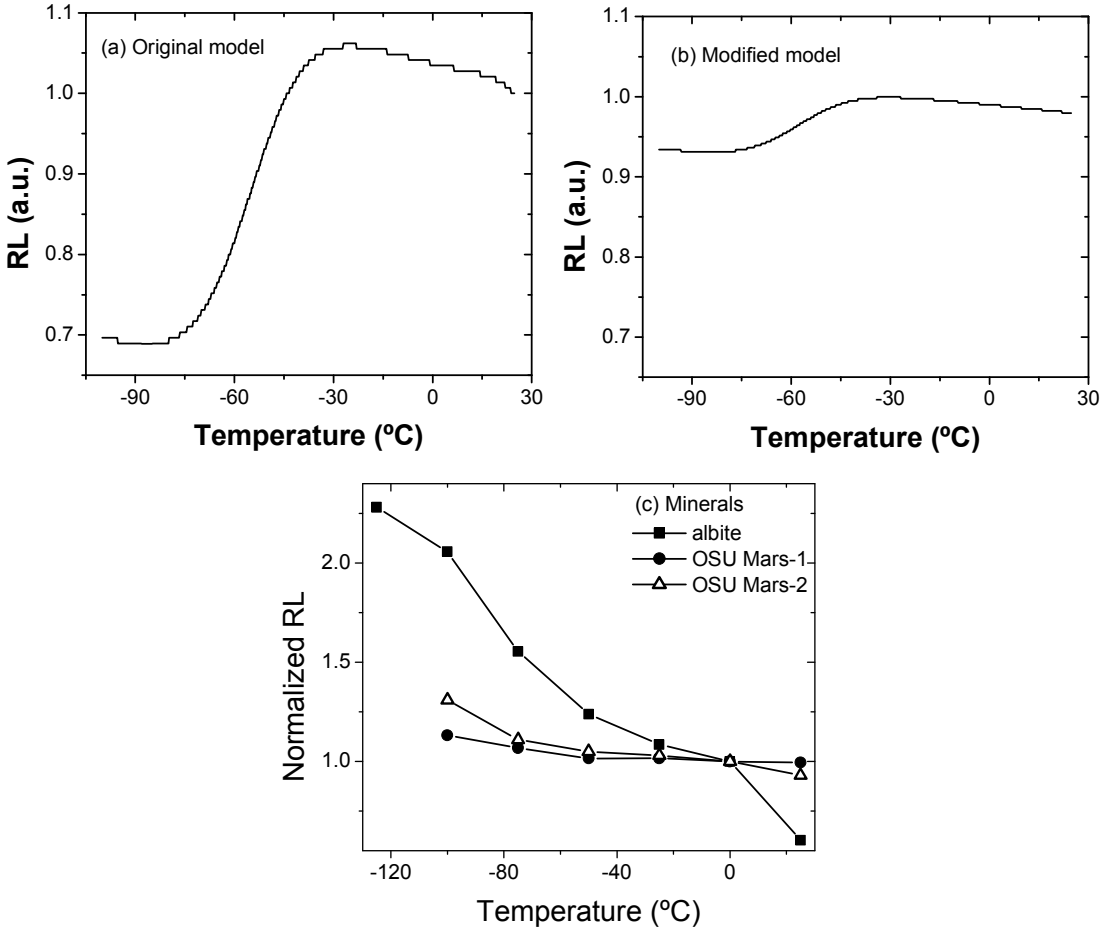

Figure 4.21 RL results for the model of (a) original model, (b) modified model, and (c) albite, OSU Mars-1, and OSU Mars-2.

neither model accounts for the increase in RL in minerals, and a thermal dependence of the recombination center would have to be included to account for this effect.

Several simulations were performed to compare the behavior of the modified model (and the original model) to previous measurements of minerals that had been irradiated and optically stimulated at various temperatures. The first simulation involved irradiating at 25°C and optically stimulating at various temperatures, and the results are shown in Figure 4.22. The OSL from the modified model (Figure 4.22 (b)) showed little change as the measurement temperature was lowered indicating that the 100°C and -50°C traps are not effective competitors (with the recombination center) for charge during stimulation. This trend does not match either albite which displayed an increased OSL with decreasing measurement temperature due to increased luminescence efficiency or the martian simulants which showed decreasing OSL with decreasing measurement temperature due to competition from low temperature traps.

The results from irradiations performed at various temperatures while OSL measurement was at 25°C are shown in Figure 4.23. The results from the modified model were largely the same as for the original model in that an increased OSL with decreasing irradiation temperature was seen. Again, this effect is probably due to charge being thermally transferred from the low temperature trap to the higher temperature trap. The effect roughly corresponds to the measurements made on OSU Mars-2.

The final comparison of the model to measurements from minerals was to simulate varying the irradiation and OSL measurement temperature together. The results for both models and the various minerals are shown in Figure 4.24. The modified model showed virtually no change in OSL intensity from 25°C to –50°C (as opposed to the

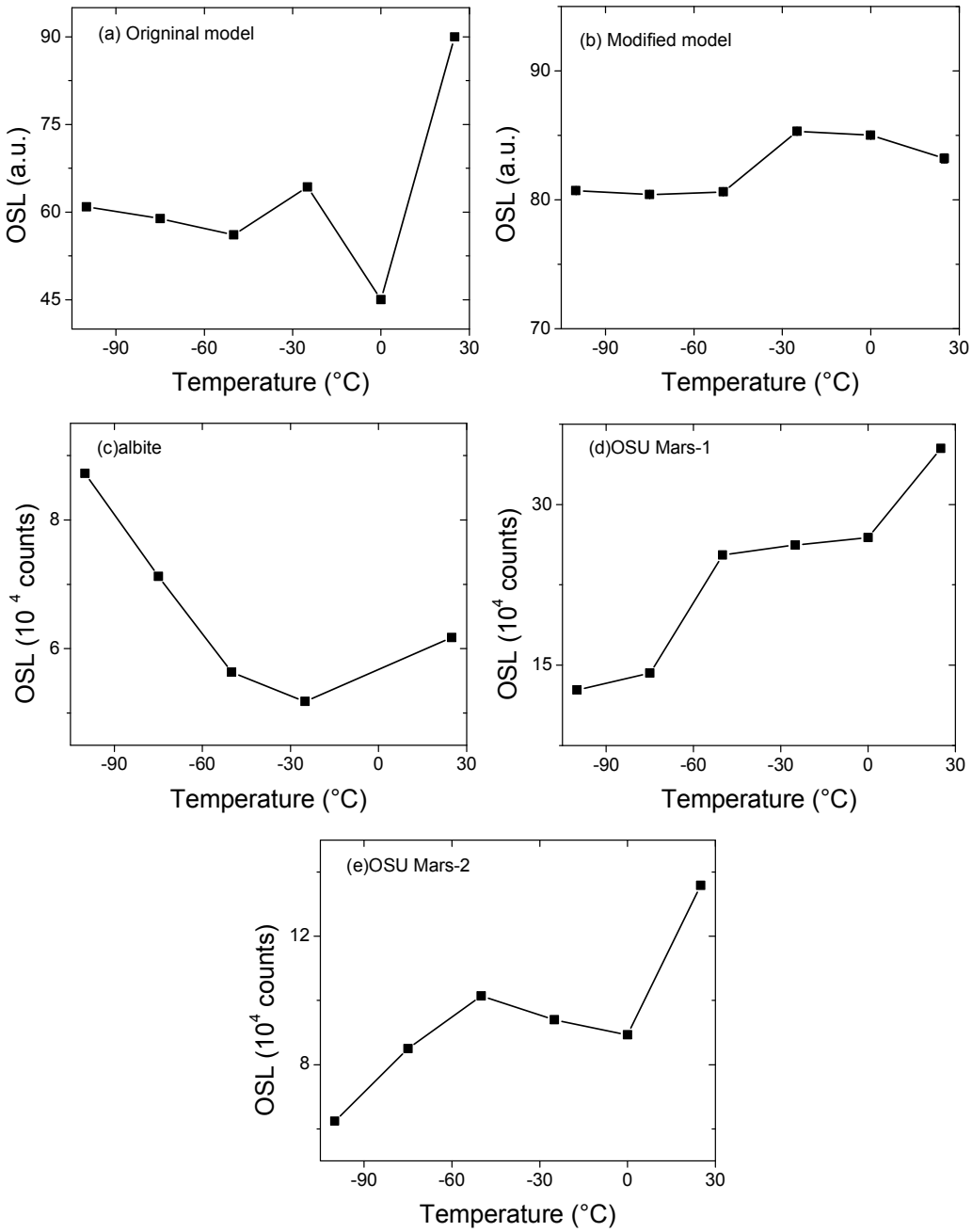

Figure 4.22 OSL from (a) the original model, (b) the modified model, (c) albite, (d) OSU Mars-1, and (e) OSU Mars-2 that have been irradiated at 25°C and stimulated at various temperatures as described in the text.

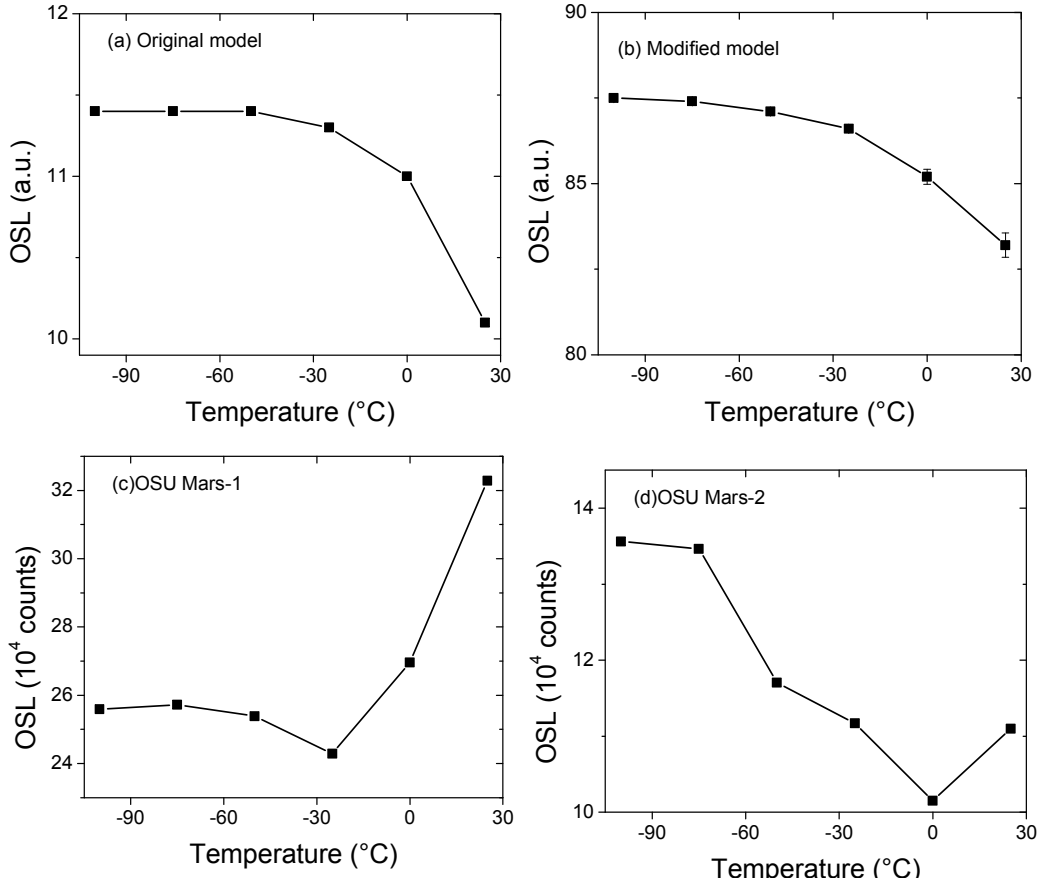

Figure 4.23 OSL from (a) the original model, (b) the modified model, and (c) OSU Mars-1, and (d) OSU Mars-2 that have been irradiated at various temperatures and stimulated at 25°C as described in the text.

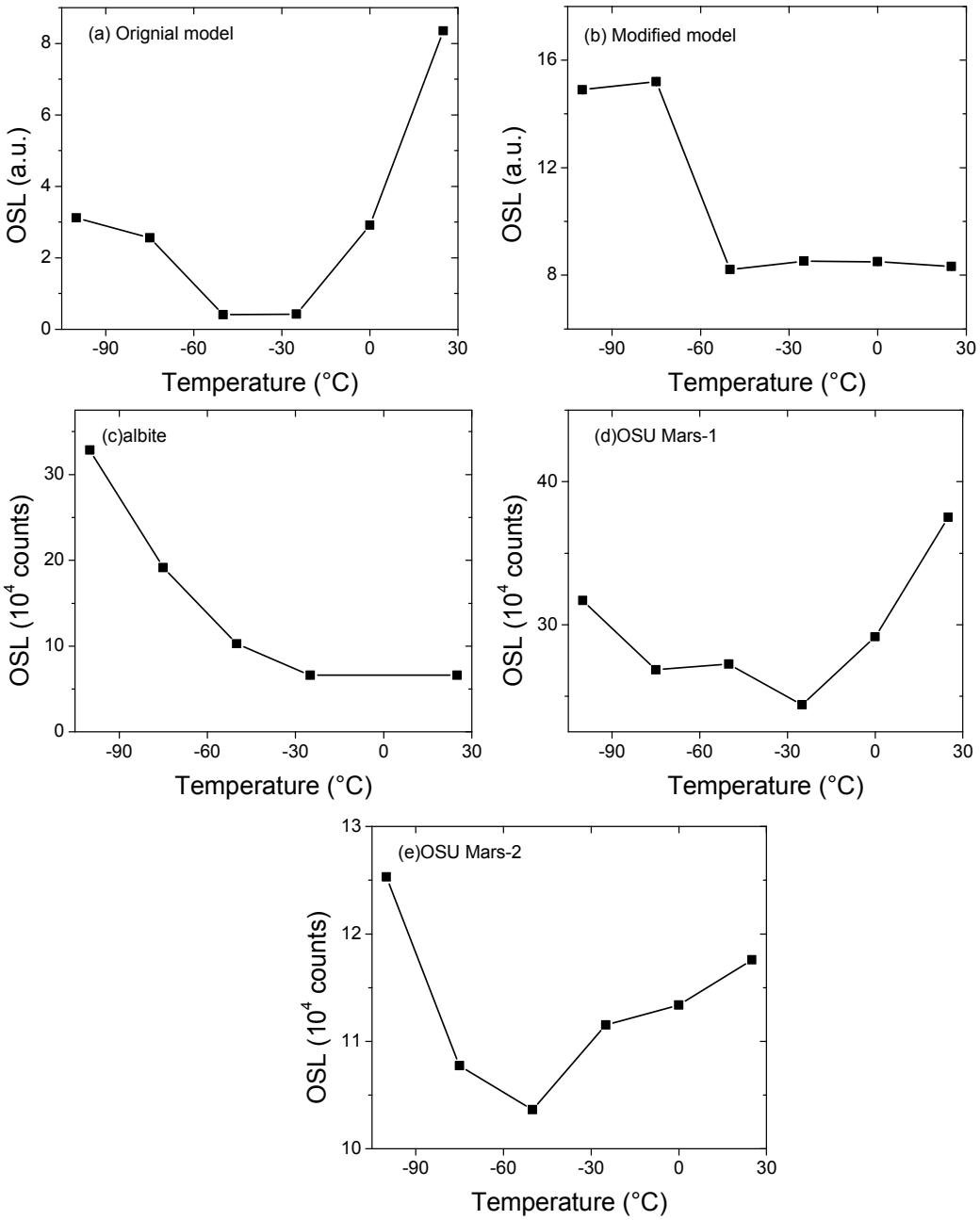

Figure 4.24 OSL from (a) the original model, (b) the modified model, and (c) albite, (d) OSU Mars-1, and (e) OSU Mars-2 that have been irradiated at and stimulated at various temperatures as described in the text.

original model which showed a significant decrease over this temperature range), again indicating that the influence of the 100°C trap has been greatly reduced. However, between -50°C and -75°C, the OSL intensity sharply increased due to the population and subsequent optical stimulation of the -50°C trap. This trend more or less matches the results from albite (although the cause in that case was largely an increased luminescence efficiency) and OSU Mars-2.

In summary, the modified model does not seem to match all of the characteristics of the studied minerals. In some respects, the modified model does mimic the results from minerals (TL, dependence on irradiation temperature, dependence on irradiation and OSL measurement temperature combined), while in other respects the modified model does not reflect the results from minerals (RL, dependence on OSL measurement temperature). The original and modified models may then represent two extremes of minerals found in nature: one extreme (the original model) where optically inactive shallow traps have a large concentration and heavily influence the luminescence process, and the other extreme (the modified model) where optically inactive shallow traps have a smaller concentration and the competition effects among the various traps govern the luminescence process.

4.5.2 Dose Recovery and Dose Estimation at Terrestrial Temperatures

Even though the original model was able to accurately recover known doses (delivered at a laboratory dose rate of 0.1 Dose Units/s) and estimate natural doses (delivered at a natural dose rate of 2 mDose Units/yr) as evidenced by Figures 4.15 and 4.16, simulations were conducted to ensure that the modified model retained this ability. The results of the dose recovery simulation are given in Figure 4.25, and the results of the

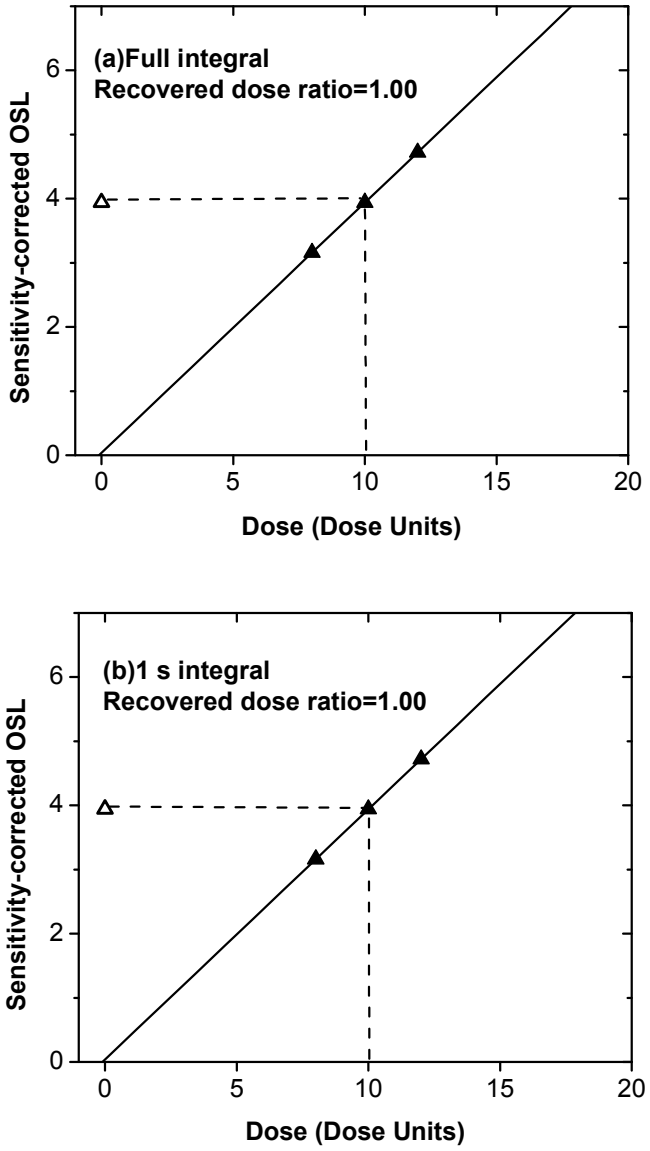

Figure 4.25 Results of the dose recovery simulation with the modified model for a known dose delivered at 0.1 Dose Units/s and 25°C. The open triangle is the known dose, and the solid triangles represent the regeneration doses. In addition to the graphical representation, the dose recovery ratio (given dose/recovered dose) is also given when using both the (a) full OSL integral and the first (b) 1 s OSL integral (appropriate background signal subtracted in both cases).

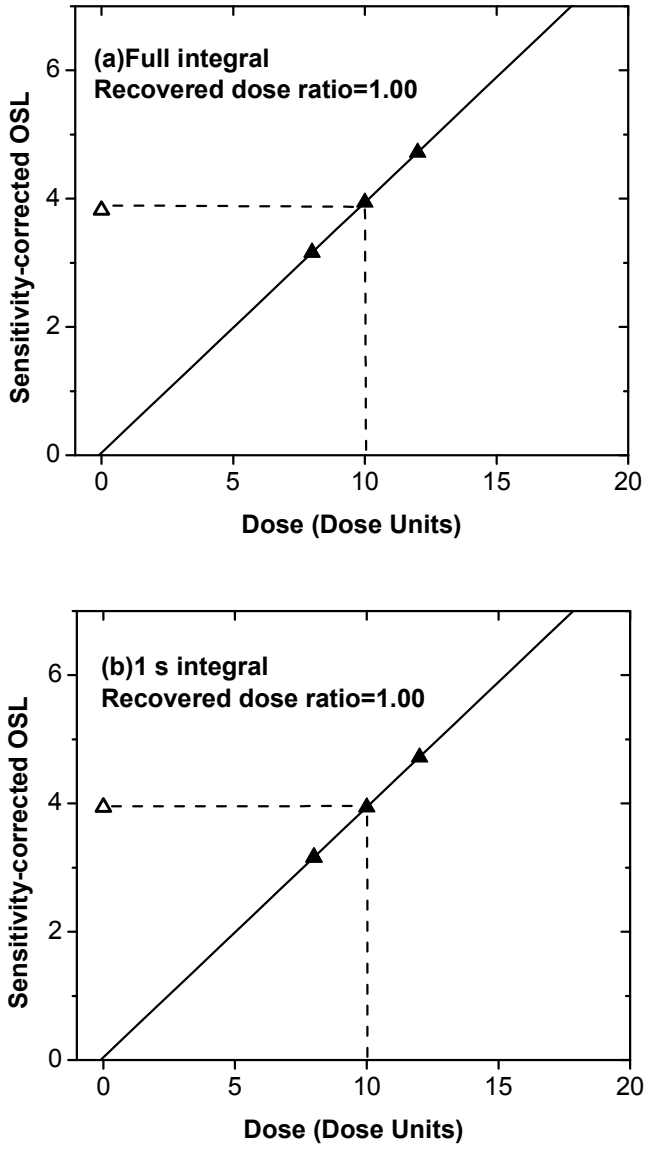

Figure 4.26 Results of the dose estimation simulation with the modified model for a natural dose delivered at 2 mDose Units/yr and 25°C. The open triangle is the natural dose, and the solid triangles represent the regeneration doses. In addition to the graphical representation, the dose recovery ratio (given dose/recovered dose) is also given when using both the (a) full OSL integral and the first (b) 1 s OSL integral (appropriate background signal subtracted in both cases).

D_e estimation simulation are given in Figure 4.26. Both the known dose and the natural dose could be recovered.

4.5.3 Dose Recovery and Dose Estimation at Martian Temperatures

A significant difference was seen between the original and modified models when dose recovery and dose estimation procedures were simulated at martian temperatures (i.e., the known doses and natural doses are delivered at -100°C). For the original model, known doses could only accurately be recovered when both the calibration irradiations and OSL measurements were performed at –100°C as thermal transfer from the 100°C trap resulted in large signals from the known dose (Figure 4.17). For the modified model, however, there is no significant thermal transfer of charge from the 100°C trap and the known dose can be reasonably recovered by either performing all calibration irradiations and OSL measurements at –100°C (Figure 4.27(a)), performing the calibration irradiations at –100°C and OSL measurements at 25°C (Figure 4.27(b)), or performing both the calibration irradiations and OSL measurements at 25°C (Figure 4.27(c)). While these results indicate a greater flexibility in the choice of procedural parameters, the model must be tested further by attempting to recover natural doses delivered at -100°C.

The simulation results for estimating a natural dose delivered at -100°C with the modified model are shown in Figure 4.28. If both the calibration irradiations and OSL measurements are performed at -100°C (Figure 4.28 (a)), there is a drastic underestimation of the natural dose (dose ratio = 0.55). This is to be expected since the -50°C trap is not effectively populated during natural irradiation (the lifetime of the trap is small compared to the irradiation time) and therefore does not contribute to the natural OSL signal. The –50°C trap is populated during laboratory irradiations at -100°C which

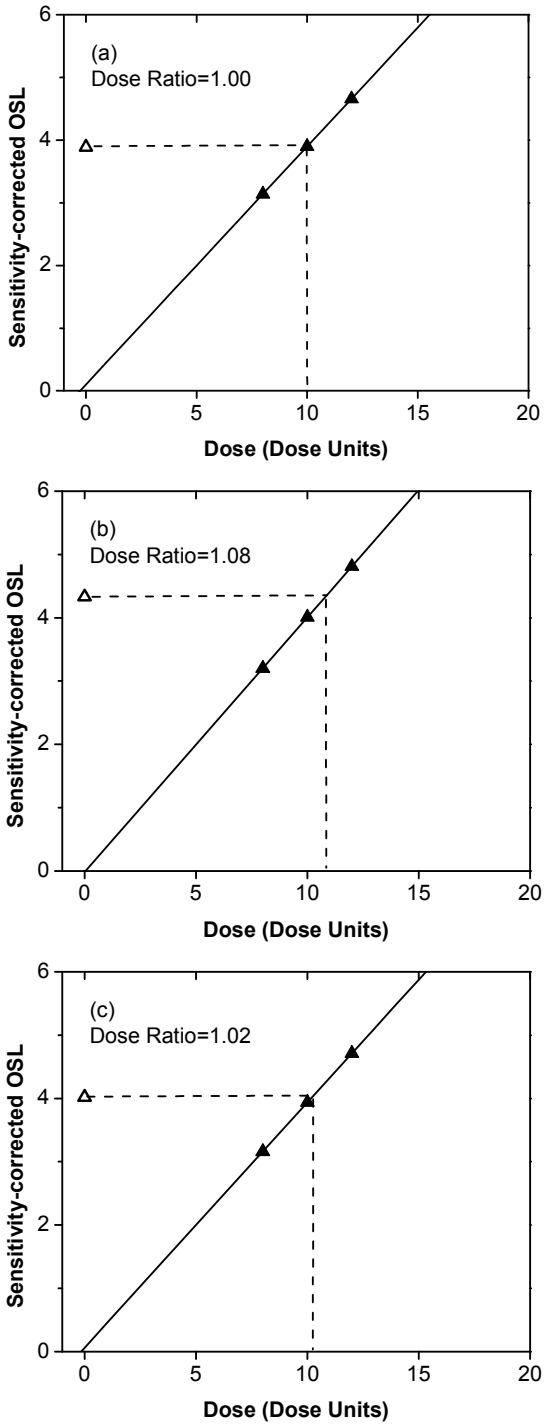

Figure 4.27 Results of the dose recovery simulations with the modified model for a known dose delivered at 0.1 Dose Units/s and -100°C. The open triangle is the known dose, and the solid triangles represent the regeneration doses in each case. In addition to the graphical representation, the dose recovery ratio (given dose/recovered dose) is also given when using the first 1 s OSL integral. The three cases are: (a) laboratory irradiation and stimulation at –100°C, (b) laboratory irradiation at –100°C and stimulation at 25°C, and (c) laboratory irradiation and stimulation at 25°C.

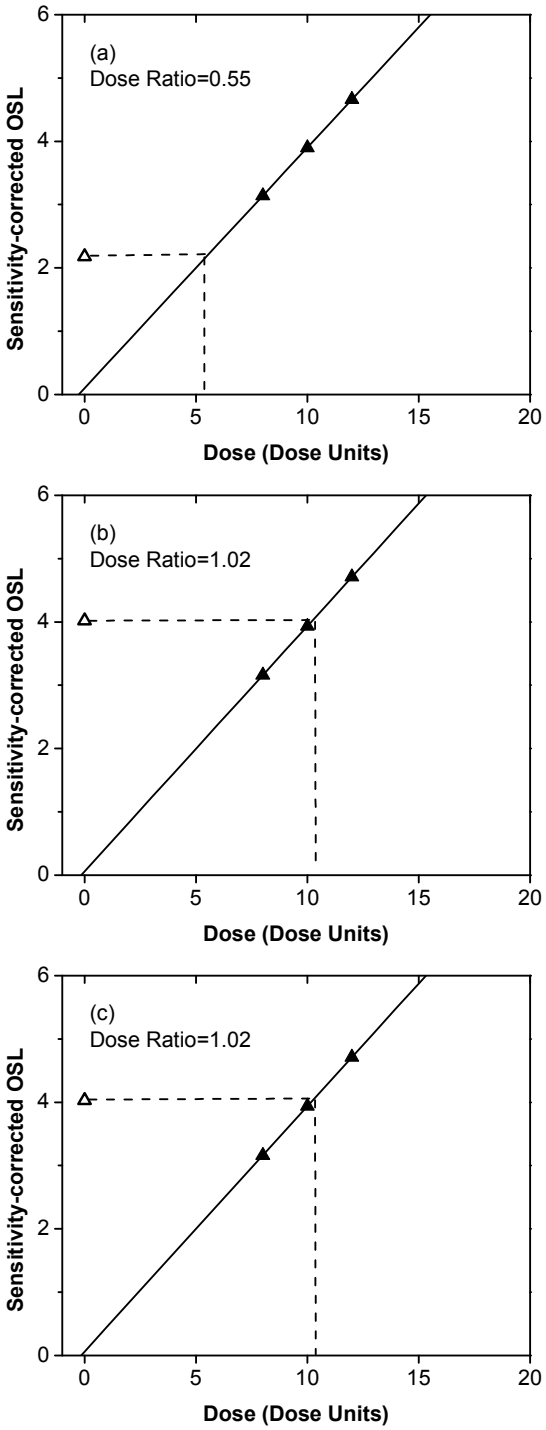

Figure 4.28 Results of the dose estimation simulations with the modified model for a natural dose delivered at 2 mDose Units/yr and -100°C. The open triangle is the known dose, and the solid triangles represent the regeneration doses in each case. In addition to the graphical representation, the dose recovery ratio (given dose/recovered dose) is also given when using the first 1 s OSL integral. The three cases are: (a) laboratory irradiation and stimulation at –100°C, (b) laboratory irradiation at –100°C and stimulation at 25°C, and (c) laboratory irradiation and stimulation at 25°C.

results in proportionally larger OSL signals and an underestimation of the natural dose. However, graphs (b) and (c) of Figure 4.28 show that that natural dose can be accurately estimated by measuring OSL at 25°C and irradiating for calibration at either -100°C or 25°C (dose ratios of 1.02 in either case). These results are to be contrasted with those of the original model (Figure 4.18) where the influence of the 100°C trap caused a decrease in OSL with increasing calibration dose. The simulations with the modified model then imply that natural doses can be estimated from materials that have optically active low temperature traps and low concentrations of optically inactive shallow traps.

Before presenting the results of dose recovery experiments using the previously described low temperature system, it is helpful to review the results of the modeling work. For the original model where the 100°C trap had a large concentration, a dose delivered at the laboratory dose rate of 0.1 Dose Units/s could only be recovered when all calibration irradiations and OSL measurements were performed at -100°C; thermal transfer of charge from the 100°C trap to the main dosimetric trap made dose recovery impossible for any procedure that used elevated temperatures for either irradiation or OSL measurement. The original model was not able to accurately estimate a natural dose delivered at -100°C with any of the procedures used.

The results from the modified model, where the 100°C trap had a much lower concentration, were very different. A laboratory dose could be recovered by performing all procedures at -100°C or by measuring OSL at 25°C and performing calibration irradiations at either -100°C or 25°C. A natural dose could not be recovered when OSL measurements were performed at -100°C, but the natural dose could be recovered when OSL was measured at 25°C and calibration irradiations were performed at either -100°C

or 25°C. These results imply that the OSL stimulation temperature should be higher than the peak temperature of any optically active low temperature traps so that those traps do not influence the OSL from either the natural or laboratory doses.

4.6 Dose Recovery for Irradiation at Low Temperatures

Using the modeling results as a guide for potential procedures, dose recovery experiments were undertaken using the previously described low temperature OSL system (Section 4.2). Samples of OSU Mars-1 and OSU Mars-2 were given 5 Gy doses, and the SAR procedure was used for the dose recovery process. Regeneration doses of 4, 5, and 6 Gy along with a test dose of 1.25 Gy were used, but no preheats (or cutheats) were used due to practical constraints imposed by the cryostat of the low temperature OSL system. Several different combinations of irradiation and OSL measurement temperature were used, including an experiment conducted completely at 25°C that was treated as a "control" experiment as low temperature traps were not involved in the luminescence process. The details of the procedural parameters along with the dose recovery ratios are given in Table 4.3. In two experiments (5 and 6), the known dose was delivered in stages at three different temperatures to simulate the diurnal variation of the temperature on Mars.

Although not every conceivable combination of irradiation and optical stimulation temperatures have been tested, the data of Table 4.3 indicate that the stimulation temperature must be equal to or greater than the maximum temperature that the sample experienced during irradiation. In the two cases where the OSL stimulation temperature was lower than the maximum temperature during irradiation (experiment numbers 4 and 5), there was a significant underestimation off the known dose presumably due to charge

Experiment number	Known Dose Temp. (^{o}C)	Regeneration Dose Temp. (^{o}C)	OSL stimulation Temp. (^{o}C)	Dose ratio (recovered/ administered) OSU-Mars-1	Dose ratio (recovered/ administered) OSU-Mars-2
1	25	25	25	1.01±0.25	1.02±0.14
2	-100	-100	-100	1.07±0.77	0.98±0.11
3	-100	25	25	1.01±0.04	0.94±0.32
4	25	-100	-100	0.33±0.64	0.26±0.01
5	1.7 Gy at –100 1.7 Gy at –50 1.7 Gy at 25	-100	-100	0.60±0.09	0.39±0.15
6	1.7 Gy at –100 1.7 Gy at –50 1.7 Gy at 25	25	25	0.95±0.52	1.04±0.28

Table 4.3 Procedural parameters for the dose recovery experiments conducted in the low temperature OSL system. The temperatures of the known dose irradiation, the regeneration (and test) dose irradiations, and the OSL measurement are given along with the dose recovered ratio for OSU Mars-1 and OSU Mars-2. Note that in experiments 5 and 6 the known dose was delivered in stages at three different temperatures to simulate the diurnal temperature variation on Mars.

being retrapped in low temperature traps during optical stimulation. Furthermore, considering the results of the modeling work, the OSL stimulation temperature needs to be higher than the peak TL temperature of any unstable optically active low temperature traps so that these traps do not influence the OSL from either the natural or laboratory doses. These results place limitations on both potential procedures for OSL dating on Mars and the instrument design for the robotic module to carry out the experiments.

4.7 Concluding Remarks for Chapter 4

This chapter has been largely concerned with addressing some of the issues presented by the low ambient temperatures of Mars. It is well understood that the luminescence process can be thermally dependent in numerous ways including low temperature traps normally not accessible under terrestrial conditions, geological stability of the electron traps, thermal assistance in the stimulation process, and thermal dependence of the recombination process (Section 4.1). Some of these properties were studied for albite, OSU Mars-1, and OSU Mars-2 using a low temperature OSL system (Section 4.2) in Section 4.3. It was found that optically active traps are present in these materials (Figure 4.4), the recombination process is thermally dependent to different degrees in these materials (Figure 4.3), and the OSL process is dependent upon both the irradiation and OSL measurement temperatures (Figures 4.5-4.7). These results were used to develop some general models of the luminescence process when low temperature traps are present.

Two slightly different models of the luminescence process were explored in Sections 4.4 and 4.5. Both models consisted of an optically active main dosimetric trap (peak temperature of 300°C), a 100°C optically inactive trap, an optically active -50°C

(low temperature) trap, and a thermally stable recombination center. The two models differed mainly in the concentration of the 100°C trap: the original model incorporated a high concentration while the modified model had a reduced concentration. With the notable exception of the luminescence efficiency or thermal dependence of the recombination process, the two models can account for the observed behavior of the minerals (Figures 4.11-4.14 and 4.21-4.24). The two models differed in their ability to recover laboratory and natural doses. Due to the influence of the 100°C trap, the original model was not able to accurately recover laboratory or natural doses. The modified model, however, did not show the same trends and it was found that either a laboratory or natural dose could be recovered if the OSL measurement temperature was higher than the maximum temperature during irradiation and the peak TL temperature of any optically active low temperature traps involved in the luminescence process. The findings were used to guide further experiments that attempted to recover known doses delivered at low temperatures.

Finally, the low temperature OSL system was used to recover known doses delivered in a variety of ways while varying the irradiation and OSL measurement temperatures during the dose recovery process. It was found that known doses delivered at room temperature (25°C), -100°C, and stepwise at three different temperatures (see Table 4.3) could be accurately recovered from OSU Mars-1 and OSU Mars-2 as long as the OSL measurement temperature was equal to or greater than the maximum temperature during delivery of the known dose (there appeared to be little dependence on irradiation temperature). Taking into account these results along with the results of the modeling work, it is recommended that procedures be adopted (and an instrument be

designed to carry out these procedures) that utilize OSL measurement temperatures higher than ambient temperatures experienced in nature to reduce the influence of any unstable low temperature traps in the luminescence process. These experiments did not investigate the effects of preheating the samples and no preheating temperatures or procedures can be suggested based upon the current findings.

CHAPTER FIVE

FUTURE DIRECTIONS

This dissertation has addressed some of the scientific challenges that must be overcome in order to apply OSL dating techniques to in-situ martian studies. Some of the other issues were mentioned and briefly discussed in Chapter 1 (Section 1.3). In addition to the basic radiation dosimetry research of this endeavor, a miniaturized OSL dating module must be constructed and tested under terrestrial conditions before use on Mars. Building such a module presents a series of technical and engineering challenges of its own (see Appendix B). In this chapter, some of those remaining scientific issues will be discussed and suggestions made for future research in order to fully develop the necessary techniques and expertise for in-situ OSL dating of martian soils.

5.1 Martian Simulants and Dose Estimation Procedures

Chapters 2 and 3 were largely concerned with development of a polymineral OSL dating procedure and testing the effectiveness of that procedure with various martian simulants and meteorites. While the proposed procedure (Tables 2.5 and 3.1) appears promising and the studied simulants do have the requisite properties for OSL dating, further research is needed.

Exploration of Mars by remote spacecraft (orbiters) and landers/rovers is an ongoing process that will continue to identify new minerals present in the martian regolith. For instance, recent data from the OMEGA visible and infrared imaging

spectrometer aboard the European Space Agency's (ESA) Mars Express mission has identified olivine, nontronite, kieserite, and sand dunes of gypsum (Bibring *et al.*, 2005; Langevin *et al.*, 2005). As these and other new data become available, the identified minerals and sedimentary deposits need to have their luminescence properties characterized.

In addition to characterizing other minerals and new martian simulants, it would be valuable to test the proposed polymineral procedure with terrestrial polymineral sedimentary samples that have independent age controls. Thus, the procedure should be tested with sediments from many different environments including a "good" OSL dating environment on Earth (e.g., a sand dune), an area that has minerals characteristic of a martian environment (e.g., a Hawaiian volcano), and an environment with similar temperature conditions as Mars (e.g., aeolian sediment trapped in polar ice). By using the proposed procedure to date materials from these areas with independent age controls a more complete evaluation of the procedure can be made.

5.2 Temperature Considerations

Chapter 4 describes experiments and simulations designed to investigate the effect of a lower ambient temperature on the luminescence process of martian simulants. The information gained from these experiments and simulations is valuable and will certainly guide future experiments and instrument design. However, the experiments conducted thus far have only used blue stimulation, and any OSL experiments conducted on Mars will likely use infrared stimulation as well. The low temperature OSL system needs to be modified to include IR stimulation, and the behavior of martian simulants when stimulated by infrared at low temperatures should be characterized. In addition, the

necessary preheating conditions for a radiation dose delivered at low temperatures need to be determined.

5.3 Anomalous Fading

The phenomenon of anomalous fading in feldspathic materials was discussed in Section 1.1.2. When certain feldspars are given a radiation dose, the luminescence intensity (whether measured by TL or OSL) is diminished if measured after a period of storage (as compared to immediate readout) even though the calculated thermal lifetime of the traps may be on the order of 10^5 years. The phenomenon was first discovered by Wintle (1973) while conducting TL dating of a recent lava flow, and has subsequently been identified in many feldspars from various environments. As most luminescent materials on Mars are expected to be of feldspathic composition, finding methods of dealing with anomalous fading for in-situ dating studies if of paramount importance.

Two approaches exist to dealing with anomalous fading: correcting the D_e for any anomalous fading that has occurred and finding a luminescence signal (TL or OSL) that does not fade. Many accurate dates have been reported when using feldspars by measuring the fading rate of the material and then using this rate to correct the D_e of the sample (Lamothe *et al.*, 2001; Auclair *et al.*, 2003; Huntley and Lamothe, 2001; Lamothe and Auclair, 2000). Although this approach is apparently successful, it can only be applied to a D_e in the linear portion of the growth curve and measuring the fading rate takes a considerable amount of time (up to a year). Therefore, correcting for anomalous fading by measurement of the fading rate would probably not be useful for in-situ OSL dating studies on Mars.

Isolating a luminescence signal that does not fade, or at least one that fades

significantly less than the signals commonly used, is more promising for the current project. The luminescence studies in this dissertation, as well as other luminescence studies of martian simulants by other members of the OSU lab, have used a UV detection window centered on 340 nm, and other luminescence dating studies have included the use of a blue detection window for feldspars (although this window can obviously not be used with blue stimulation). Both of these signals show significant fading for many types of feldspathic materials (Huntley and Lamothe, 2001). Non-fading or slowly-fading luminescence signals in the far-red detection window (590-750 nm) has been used to produce accurate dates for feldspars using TL (Vicosekas, 2000) and infrared-stimulated OSL (Lai *et al.*, 2002; Lai *et al.*, 2003; Fattahi and Stokes, 2003). Normally, using the far-red detection window presents problems due to the quantum efficiency of photomultiplier tubes, but the proposed use of photodiodes for luminescence detection on Mars (see Appendix B) largely eliminates this concern. Therefore, the luminescence properties, particularly the characterization of anomalous fading, of the far-red emission of feldspars and martian simulants should be further investigated.

Isolating a component of the OSL decay signal (whether infrared or blue stimulated) that does not fade may also be possible. In the initial studies that applied POSL to feldspars using a green laser, Sanderson and Clark (1994) found that neither the fast or slow components showed significant fading. While later studies that used IR stimulation did not find stable components (Clark *et al.,* 1997; Clark and Bailiff, 1998), recent work at the Risø National Laboratory (Denby *et al.*, 2005; Tsukamoto *et al.*, 2005) has been able to isolate stable components of the POSL signal from feldspars when using IR stimulation. Further research aimed at using POSL with feldspars, potentially in

combination with a far-red detection window, in order to isolate a non fading luminescence signal is needed.

5.4 Bleaching Characteristics

One of the primary assumptions of OSL dating is that the OSL signal can be zeroed or reset by exposure to sunlight during transport. Under terrestrial conditions, only minutes of sunlight exposure are typically necessary to sufficiently bleach most sediments (Aitken, 1998). However, due to the nature of the atmosphere, the solar spectrum at the surface of Mars is different than on Earth. Table 5.1 gives the UV irradiance for both Earth and Mars and shows that Mars has a much higher irradiance for shorter wavelengths. The enhanced UV irradiance at shorter wavelengths could promote electrons to the conduction band of the materials and hence give rise to a luminescence signal instead of bleaching the sediments. Further calculations from the OSU luminescence dosimetry lab using the libRadtran software package show that the presence of dust in the martian atmosphere reduces the irradiance at longer wavelengths at the surface, and the total irradiance at the martian surface is 40% to 45 % that on a clear Earth day (Deo *et al.*, 2005). Clearly, the solar spectrum on Mars and its effect on the bleaching of sediments warrants further studies.

The OSU luminescence dosimetry lab now has a solar simulator and appropriate filters to mimic the solar spectrum of the martian atmosphere. Experiments are being conducted by Dr. Regina Kalchgruber to determine if sediments can be bleached by the martian solar spectrum, and, if so, how much time is required for complete bleaching. The potential of the enhanced UV irradiance to induce an OSL signal is also being directly tested by subjecting bleached aliquots to the martian solar spectrum. The

Wavelength (nm)	Spectral UV irradiance ($\mu W/cm^2/nm$)	
	Earth*	Mars**
206	$<10^{-4}$	0.08
250		0.02
326	50	1.2
400	100	2.5

* http://www.bmayer.de/index.html?global.html&1 ; 08-07-2003
** www-mars.lmd.jussieu.fr/granada2003/abstract/catling.pdf ; 08-07-2003

Table 5.1 Spectral UV irradiance for Earth and Mars.

outcome of these tests will be of utmost importance to the feasibility of OSL dating on the surface of Mars.

5.5 Annual Dose Rate

Several estimates of the natural radiation dose rate on Mars have been made. Radioactive elements within the soil are expected to contribute approximately 0.4 mGy/yr (Milekowsky *et al.*, 2000). These estimates are based on study of martian meteorites and may not reflect the abundance of radioactive minerals at all points in the martian regolith. Better estimates of the abundance of radioactive minerals may be possible using information from elemental maps produced by spectrometers such as the one aboard the Odyssey mission (Saunders *et al.*, 2004).

The annual radiation dose rate on Mars is dominated by the contributions from GCR and SPE, and modeling of these contributions suggests that the surface dose rate due to GCR and SPE is approximately 54 mGy/yr. At a depth of 2m, the GCR and SPE will still contribute about 27 mGy/yr (Wilson *et al.*, 1995; McKeever *et al.*, 2003). Of course, these estimates are global averages. The models need to be refined so that the annual dose rate could be estimated for any point on the surface (or below the surface) on Mars, and the varying composition of the regolith, ice/frost cover, and magnetic anomalies (Verigin *et al.*, 2001) needs to be considered for these calculations.

Rather than modeling and calculating the annual radiation dose rate on Mars, the possibility of directly measuring the radiation dose rate for an in-situ experiment should be explored. Al_2O_3:C luminescence dosimeters have been successfully used in terrestrial studies to measure the annual dose rate delivered to a sedimentary deposit (Burbidge and Duller, 2003; Kalchgruber *et al.*, 2003; Kalchgruber and Wagner, (In Press)). Similar

procedures could be used on Mars to directly measure the radiation dose rate in-situ, although the technical challenges of depositing and retrieving the Al_2O_3:C dosimeters may be daunting. In addition, some modeling would still be necessary to account for fluctuations in the GCR and SPE contributions.

In modeling the dose rate and designing the miniaturized OSL instrument, it has been assumed that the low LET particles that make up 95 % of the absorbed dose from GCR and SPE contributions (Benton and Benton, 2001) also give rise to the OSL signal. That is, it is assumed that high LET particles (LET greater than 10 kev/μm) are less efficient at filling the electron traps in luminescent materials. In order to quantify this assumption, it is necessary to measure the OSL response of natural sediments and martian simulants to heavy charged particle irradiations as has been done in development of Al_2O_3:C for space dosimetry (Gaza *et al.*, 2004; Yukihara *et al.*, 2004). This is necessary for comparison with the OSL generated from a single, low LET source (X-ray) for calibration purposes.

5.6 Sample Sorting

Although chemical separation of specific minerals will probably not be possible on an in-situ martian instrument, some physical sorting off the sample will be necessary. In luminescence dating, magnetic particles are generally removed from a sample during the sample preparation process. Magnetic or metallic particles do not produce either OSL or TL and may block luminescence produced by other grains. As martian soils are expected to contain a large percentage of magnetic particles (Madsen *et al.*, 2005), it is important to remove a large proportion of these particles to enhance the luminescence signal. Experiments need to be undertaken to determine what percentage of magnetic

particles are acceptable in a sample for OSL study and thereby define how effective magnetic particle removal needs to be.

The grain size of the sample also needs to be controlled. In terrestrial applications, either coarse grains (e.g., 90-125 μm) or fine grains (e.g., 4-11 μm) are generally chosen depending upon what is most readily available from the sample. Both the annual radiation dose rate and the calibration source dose rate must be adjusted appropriately for the grain size chosen as the alpha contribution to the annual dose rate is important for fine grains but not important for coarse grains (Aitken, 1985, 1998). Therefore, a grain size range must be chosen for the in-situ OSL experiments to be conducted on Mars so that the dose rate from the irradiation source can be calibrated correctly and the annual radiation dose rate can be calculated effectively.

5.7 Discussion

During the development of the techniques and instrumentation necessary for in-situ OSL dating studies on Mars, many more issues and challenges will arise. The research teams (both the luminescence specialists and the instrumentation engineers) will need to be able to realize these challenges and address them quickly. For instance, during the course of designing the instrument, is has been realized that static electricity in the martian atmosphere may pose a serious problem to instrument design (See Appendix B) as well as the luminescence process. As a result, a project is currently underway to determine if static electricity can induce an OSL or TL signal in natural minerals. This ability to adapt to urgent needs and concerns while addressing some of the more fundamental issues outlined above will be essential for the successful completion of this project.

CHAPTER SIX

SUMMARY AND DISCUSSION

6.1 Summary

Developing the techniques and equipment to perform in-situ OSL dating experiments on the surface of Mars or with a terrestrial field instrument is an enormous project that will require much work and experimentation. This dissertation has attempted to address a small part of that project, namely to develop polymineral procedures that can date feldspathic materials and to study the effects of low ambient temperatures. Although more research is need in these areas (see Sections 6.1 and 6.2), significant progress has been made.

Chapter 2 describs a study of the basic luminescence characteristics of various feldspar separates. It was found that the SAR procedure (Table 1.1) could be adapted for coarse-grain feldspars, but the traditional cutheat should be replaced by a preheat equal in temperature and duration to the preheat used after the regeneration dose. In addition, it was found that using the infrared-stimulated OSL signal from a post-IR blue stimulation sequence both reduced the amount of sensitivity change and extended the potential age range for feldspars. Experiments conducted on quartz separates found that the cutheat could be replaced by a preheat in the SAR procedure. These experiments led to the final set of experiments described in the chapter that explored the luminescence properties of several mixtures of quartz and feldspars. It was found that the modified SAR procedure

of Tables 2.5 and 3.1 (replacing the cutheat with a preheat, using a post-IR blue-stimulation sequence) could correct for sensitivity changes in the mixtures, recover known doses using both feldspar-dominated and quartz-dominated signals, and accurately estimate quartz D_es for up to 50% "feldspar contamination."

Chapter 3 describes tests of the proposed SAR procedure (Tables 2.5 and 3.1) on several martian simulants (JSC Mars-1, OSU Mars-1, OSU, Mars-2) and martian meteorites (ALH 77005,74, Shergotty, Zagami, EET 79001,170). A series of experiments confirmed that the procedure could correct for sensitivity changes, produce the desired dose response curves, and recover known doses from both the linear and non-linear portions of the dose response curves. Based upon the results from Chapters 2 and 3, it is suggested that the SAR procedure of Tables 2.5 and 3.1 be adopted for polymineral samples.

Chapter 4 addresses some of the issues presented by the low ambient temperature of Mars. In order to study these issues, the low temperature TL/OSL system of Figure 4.2 was developed (with the assistance of Dr. Eduardo Yukihara). Experiments using this system showed that albite, OSU Mars-1, and OSU Mars-2 do have optically-active low temperature traps. In addition, the OSL intensity for these minerals are affected by the irradiation temperature as well as the OSL stimulation temperature. Dose recovery experiments indicated that the OSL stimulation temperature needs to be at least equal to the highest temperature during irradiation, but accompanying numerical simulations of a "natural dose" indicate that the OSL stimulation temperature needs to be significantly higher than highest temperature experienced during natural irradiation. This finding is important for engineering considerations as the ability to maintain and elevated sample

1. Regeneration radiation dose (D_i)
2. Preheat at $T_P{}^oC^{\#}$ for 10 s
3. Measure IRSL @ $T_R^{\#,*}$ (IR_i)
4. Measure OSL @ $T_O^{\#,*}$ (R_i)
5. Fixed test radiation dose (TD_i)
6. Preheat at $T_P{}^oC^{\#}$ for 10 s
7. Measure IRSL @ $T_R^{\#,*}$ (IT_i)
8. Measure OSL at @ $T_O^{\#,*}$ (T_i)
9. Repeat steps 1-8 for a range of regeneration doses including a repeat point and a 0 Gy Dose.
10. Find sensitivity-corrected IRSL ($IL_i=IR_i/IT_i$)
11. Find sensitivity-corrected OSL ($L_i=R_i/T_i$)

#T_P, T_R, and T_O to be determined from experiment
*T_R and T_O need to be higher than highest natural irradiation temperature

Table 6.1 Suggested polymineral dose estimation procedure.

temperature will be required. These findings have led to Table 7.1, the final suggested polymineral procedure.

6.2 Discussion

This dissertation has focused on developing the experimental techniques that are necessary for performing in-situ OSL dating on Mars, but the implications or interpretation of these dates have not been discussed. While the science involved in developing these techniques may be interesting in its own right, the project is futile unless we keep in mind the impact of the dates produced by the OSL technique.

The first thing to consider about the potential OSL dates from Mars is that they will be the first such dates from the planet. On Earth, OSL dating is typically used to develop the chronology of a particular site or geographic region. However, on Mars, the OSL dates will be used to create a geologic chronology for the entire planet. Due to this situation, the "acceptable errors" for martian OSL dates may be much larger than typical errors associated with OSL dating on Earth. For example, on Earth, OSL dating may be trying to link a particular flood deposit to a historically known flood and therefore a relatively small error is desired. On Mars, though, the fact that a flood deposit could be dated by OSL techniques would be a breakthrough regardless of the associated error as martian flood deposits are expected to be much older than ages accessible to OSL dating.

The errors associated with OSL dates from Mars will certainly be much larger than the errors from similar dates on Earth. As discussed throughout this dissertation, martian OSL dating will be carried out on polymineralic samples, and the error associated with equivalent dose estimation procedures for polymineral samples is larger than for procedures with mineral separates. Yet, most of the increase in errors will result from

uncertainties in the radiation dose rate. It is assumed that the majority of the natural radiation dose rate on Mars comes from GCR and SPE, and calculations that derive an annual dose rate from these sources are subject to large errors themselves. In addition, the radiation dose rate (from GCR and SPE) must be calculated at the burial depth of the sample by determining how the GCR and SPE dose rate attenuates with depth in the regolith, and this attenuation with depth has large associated errors as it is calculated based on assumptions about the martian regolith. The depth of the sample (from the surface) also adds uncertainty as the calculations assume one burial depth (i.e., the sample has been buried at the same depth since exposure to light). A varying depth from the surface during burial would result in large errors in the radiation dose rate, although calculations indicate that an error in the burial depth of 2 m would lead to ~ 50 % errors in the radiation dose rate (Figure 1.15). Considering these sources of error, OSL dates from Mars could easily have associated errors of 50 %.

Regardless of the errors, the geologic and climatic implications of OSL dates from different martian contexts needs to be considered. As already mentioned, if martian flood deposits produce OSL ages it would imply that water has been active on the martian surface in the "recent" past (last 1 million years). In this situation, the date from one sample could change notions about the climatic and hydrological cycle of Mars. Generally, though, multiple samples from the same location will be required to produce a geological chronology.

An OSL date from a martian aeolian deposit would only tell us when that sample was deposited (i.e., when a sufficiently strong wind storm occurred). We know that Mars is a windy planet, so this information alone would not be particularly enlightening.

However, if samples could be taken from several stratigraphic layers of an aeolian deposit, we could find out how often (say, every thousand or every ten thousand years) strong wind storms occur on Mars. Similarly, OSL dates from different layers of a flood deposit could tell us how often water has been active on the surface of Mars. Taken together, this information could tell us about the climatic stability of Mars and the potential hazards for manned exploration of Mars.

References

Aiken, M. J., 1985. Thermoluminescence Dating. Academic Press, London.

Aitken, M. J., 1998. An Introduction to Optical Dating. Oxford University Press, Oxford.

Akselrod, M. S., McKeever, S. W. S., 1999. A radiation dosimetry system using pulsed optically stimulated luminescence. Radiation Protection Dosimetry 81, 167-176.

Akselrod, M. S., Agersnap Larsen, N., McKeever, S. W. S., 2000. A procedure for the distinction between static and dynamic radiation exposures of personal radiation badges using pulsed optically stimulated luminescence. Radiation Measurements 32, 215-225.

Albee, A. L., 2003. The unearthly landscapes of Mars. Scientific American 13 (3), 34-44.

Allen, C. C., Jager, K. M., Morris, R. V., Lindsrom, D. J., Lockwood, J. P., 1998. JSCMars-1: a martian soil simulant. Space 98, Proceedings of the Conference American society of Civil Engineers, 469-476.

Auclair, M., Lamothe, M., Huot, S., 2003. Measurement of anomalous fading for feldspar IRSL using SAR. Radiation Measurements 37, 487-492.

Bailey, R. M., 2001. Towards a general kinetic model for optically and thermally stimulated luminescence in quartz. Radiation Measurements 33, 17-45.

Bailiff, I. K., 1997. Retrospective dosimetry with ceramics. Radiation Measurements 27, 923-941.

Bailiff, I. K., Stepanenko, V. F., Göksu, H. Y., Jungner, H., Balmukhanov, S. B., Balmukhanov, T. S., Khamidova, L. G., Kisilev, V. I., Kolyado, I. B., Kolizshenkov, T. V., Shoikhet, Y. N., Tsyb, A. F., 2004. The application of retrospective luminescence dosimetry in areas affected by fallout from the Semipalatinsk Nuclear Test Site: an evaluation of potential. Health Physics 87, 625-641.

Bandfield, J. L., 2002. Global mineral distributions on Mars. Journal of Geophysical Research 107, 2001JE001510.

Bandfield, J. L., Hamilton, V. E., Christensen, P. R., 2000. A global view of martian surface compositions from MGS-TES. Science 287, 1626-1630.

Banerjee, D., 2001. Supralinearity and sensitivity changes in optically stimulated luminescence of annealed quartz. Radiation Measurements 33, 47-57.

Banerjee, D, Blair, M., D. W. G. Sears, and S. W. S. McKeever, 2002. Dating of Martian Meteorites: Characterization of Luminescence from a Martian Soil Simulant and Martian Meteorites. LPSC XXXIII, Houston, TX, 2002.

Banerjee, D., Murray, A. S., Bøtter-Jensen, L., Lang, A., 2001. Equivalent dose estimation using a single aliquot of polymineral fine grains. Radiation Measurements 33, 73-94.

Banerjee, D., Blair, M., Lepper, K., and McKeever, S. W. S., 2002. Optically stimulated luminescence signals of polymineral fine grains in the JSC Mars-1 soil simulant sample. Radiation Protection Dosimetry 101, 321-326.

Banerjee, D., Bøtter-Jensen, L., Murray, A. S., 1999. Retrospective dosimetry: preliminary use of the single-aliquot regeneration (SAR) protocol for the measurement of quartz dose in young house bricks. Radiation Protection Dosimetry 84, 421-426.

Banerjee, D., Bøtter-Jensen, L., Murray, A. S., 2000. Retrospective dosimetry: estimation of the dose to quartz using the single-aliquot regenerative-dose protocol. Applied Radiation Isotopes 52, 831-844.

Barnett, S. M., Bailiff, I. K., 1997. The temperature dependence of luminescence in some feldspars (80-300 K). Journal of Physics D: Applied Physics 30, 683-689.

Benton, E.R., Benton, E.V., 2001. Space radiation dosimetry in low-Earth orbit. Nuclear Instruments and Methods B 184, 255–294.

Bibring, J. P., Langevin, Y., Gendrin, A., Gondet, B., Poulet, F., Berthe, M., Soufflot, A., Arvidson, R., Mangold, N., Mustard, J., Drossart, P., and the OMEGA team, 2005. Mars surface diversity as revealed by the OMEGA/Mars Express observations. Science 307, 1576-1581.

Blackwell, B., 1995. Electron spin resonance dating. In: Dating Methods for Quaternary Deposits, Rutter, N.W. and Catto, N. R., eds., Geological Association of Canada, St. John's, Newfoundland.

Bøtter-Jensen, L., Agersnap Larsen, N., Mejdahl, V., Poolton, N. R. J., Morris, M F., McKeever, S. W. S., 1995. Luminescence sensitivity changes in quartz as a result of annealing. Radiation Measurements 24, 535-541.

Bøtter-Jensen, L., Bulur, E., Duller, G. A. T., Murray, A. S., 2000. Advances in luminescence instrument systems. Radiation Measurements 32, 523-528.

Bøtter-Jensen, L., Ditlefsen. C., Mejdahl, V., 1991. Combined OSL (infrared) and TL studies of feldspars. Nuclear Tracks Radiation Measurements18, 257-263.

Bøtter-Jensen, L., McKeever, S. W. S., Wintle, A, G., 2003. Optically stimulated luminescence dosimetry. Elsevier, Amsterdam.

Bridges, N. T., Herkenhoff, K. E., 2002. Topography and geologic characteristics of aeolian grooves in the south polar layered deposits of Mars. Icarus 156, 387-398.

Bulur, E., 1996. An alternative technique for optically stimulated luminescence (OSL) experiment. Radiation Measurements 26, 701-709.

Bulur, E., 2000. A simple transformation for converting CW-OSL curves to LM-OSL curves. Radiation Measurements 32, 141-145.

Burbidge, C. I., Duller, G. A. T., 2003. Combined gamma and beta dosimetry, using Al_2O_3:C, for in situ measurements on a sequence of archaeological deposits. Radiation Measurements 37, 285-291.

Chen, R. McKeever, S. W. S., 1997. Theory of Thermoluminescence and Related Phenomena. World Scientific, Singapore.

Christenssen, P. R., et al., 1992. Thermal Emission Spectrometer experiment: Mars Oberver mission. Journal of Geophysical Research 97, 7719-7734.

Christensen, P. R. et al., 2001. Mars Global Surveyor Thermal Emission Spectrometer experimenter: investigation description and surface science results. Journal of Geophysical Research 106, 823-871.

Clark, R. J., Bailiff, I. K., 1998. Fast time-resolved emission spectroscopy in some feldspars. Radiation Measurements 29, 553-560.

Clark, M. L., Rendell, H. M., Sanchez-Munoz, L, Garcia-Guinea, J., 1997. A comparison of luminescence spectra and structural composition of perthitic feldspars. Radiation Measurements 27, 137-144.

Clifford S. M., Crisp, D., Fisher, D. A., Herkenhoff, K. E., Smrekar, S. E., Thomas, P. C., Wynn-Williams, D. D., Zurek, R. W., Barnes, J. R., Bills, B. G., Blake, E. W., Calvin, W. M., Cameron, J. M., Carr., M. H., Christensen, P. R., Clark, B. C., Clow, G. D., Cutts, J. A., Dahl-Jensen, D., Durham, W. B., Fanale, F. P., Farmer, J. D., Forget, F., Gotto-Azuma, K., Grard, R., Haberle, R. M., Harrison, W., Harvey, R., Howard, A. D., Ingersoll, A. P., James, P. B., Kargel, J. S., Kieffer, H. H., Larsen, J., Lepper, K., Malin, M. C., McCleese, D. J., Murray, B., Nye, J.

F., Paige, D. A., Platt, S. R., Plaut, J. J., Reeh, N., Rice, J. W., Smith, D. E., Stoker, C. R., Tanaka, K. L., Mosley-Thompson, E., Thorsteinsson, T., Wood, S. E., Zent, A., Zuber, Zwally, H. J., 2000. The state and future of Mars polar science and exploration. Icarus 144, 210-242.

Denby, P. M., Bøtter-Jensen, L., Murray, A. S., 2005. Application of pulsed OSL to the separation of the luminescence components from a mixed quartz/feldspar sample. LED 2005, Cologne, Germany, 2005.

Deo, S., Kalchgruber, K., Mayer, B., 2005. Radiative transfer calculations for atmosphere of Mars in the 200-900 nm range. LPSC XXXVI, Houston, TX, 2005.

Doran, P. T., Clifford, S. M., Forman, S. L., Nyquist, L., Papanastassiou, D. A., Stewart, B. W., Sturchio, N. C., Swindle, T. D., Cerling, T., Kargel, J., McDonald, G., Nishiizumi, K., Poreda, R., Rice, J. W., Tanaka, K., 2004. Mars chronology: assessing techniques for quantifying surficial processes. Earth-Science Reviews 67, 313-337.

Duller, G. A. T., 1991. Equivalent dose determination using single aliquots. Nuclear Tracks Radiation Measurements 18, 371-378.

Duller, G. A. T., 1992. The use of a single aliquot method for intercalibration between radioactive sources. Ancient TL 10, 8-11.

Duller, G. A.T., 1995. Infrared bleaching of the thermoluminescence of four feldspars. Journal of Physics D: Applied Physics 28, 1244-1258.

Duller, G. A. T., 1997. Behavioral studies of stimulated luminescence from feldspars. Radiation Measurements 27, 663-694.

Duller, G. A. T., Bøtter-Jensen, L., 1993. Luminescence from potassium feldspars stimulated by infrared and green light. Radiation Protection Dosimetry 47, 683-688.

Edgett, K. S., Malin, M. C., 2000. Rock stratigraphy in Gale crater, Mars. Lunar and Planetary Science Conference XXII, Abstract No. 1005.

Fattahi, M., Stokes, S., 2003. Red luminescence from potassium feldspar for dating applications: a study of some properties relevant for dating. Radiation Measurements 37, 647-660.

Gaza, R., Yukihara, E. G., McKeever, S. W. S., 2004. The response of ooptically and thermally stimulated luminescence from Al_2O_3 to high-energy heavy charged particles. Radiation Measurements 38, 417-420.

Galbraith, R. F., Roberts, R. G., Laslett, G. M., Yoshida, H., Olley, J. M., 1999. Optical dating of single and multiple grains of quartz from Jinmium Rock Shelter, northern Australia: part 1, experimental design and statistical models. Archaeometry 41, 339-364.

Gilbert, E. S., Land, C. E., Simon, S. L., 2002. Health effects from fallout. Health Physics 82, 726-735.

Greeley, R., 1992. Saltation impact as a means for raising dust on Mars. Planetary and Space Science 50, 151-155.

Greeley, R., Lancaster, N., Lee, S., Thomas, P., 1992. Martian aeolian processes, sediments, and features. In: Kieffer, H. H., Jakosky, B. M., Snyder, C. W., Mathews, M. S. (Eds.), Mars, University of Arizona Press, Tucson, pp.1-33.

Grün, R., 1997. Electron spin resonance dating. In: Chronometric Dating in Archaeology, Taylor, R. E. and Aitken, M. J., eds. Plenum Press, New York.

Haskell, E. H., 1993. Accident dosimetry using environmental materials: the role of thermoluminescence. Radiation Measurements 21, 87-93.

Howard, A. D., 2000. The role of eolian processes in forming surface features of the martian polar layerd deposits. Icarus 144, 267-288.

Huntley, D. J., Godfrey-Smith, D. I., Thewalt, M. L. W., 1985. Optical dating of sediments. Nature 313, 105-107.

Huntley, D. J., Lamothe, M., 2001. Ubiquity of anomalous fading in K-feldspars and the measurement and correction for it in optical dating. Canadian Journal of Earth Sciences 38, 1093-1106.

Huot, S., Lamothe, M., 2003. Variability of infrared stimulated luminescence properties from fractured feldspar grains. Radiation Measurements 37, 499-503.

Hütt, G., Jaek, I., Tchonka, J., 1988. Optical dating: K-feldspars optical response stimulation spectra. Quaternary Science Reviews 7, 381-385.

Kalchgruber, R., Blair, M. W., McKeever, S. W. S., In Press. Dose recovery with plagioclase and pyroxene samples as surrogates for martian surface sediments. Radiation Measurements.

Kalchgruber, R., Fuchs, M., Murray, A. S., Wagner, G. A., 2003. Evaluating dose-rate distributions in natural sediments using α-Al_2O_3:C grains. Radiation Measurements 37, 293-297.

Kalchgruber, R. Wagner, G. A., In Press. Separate assessment of natural beta and gamma dose-rates with TL from α-Al_2O_3:C single-crystal chips. Radiation Measurements.

Kieffer, H. H., Jakosky, B. M., Snyder C. W., 1992. The planet Mars: from antiquity to present. In: Kieffer, H. H., Jakosky, B. M., Snyder, C. W., Mathews, M. S. (Eds.), Mars, University of Arizona Press, Tucson, pp.1-33.

Koutnik, M. R., Byrne, S., Murray, B. C., Tiogo, A. D., Crawford, Z. A., 2005. Eolian controlled modification of the martian south polar layered deposits. Icarus 174, 490-501.

Kristianpoller, N., Chen, R., Israeli, M., 1974. Dose dependence of thermoluminescence peaks. Journal of Physics D: Applied Physics 7, 1063-1072.

Kuzmin, R. O., Greeley, R., Rafkin, S. C. R., Haberle, R., 2001. Wind-related modification of some small impact crater on Mars. Icarus 153, 61-70.

Lai, Z., Arnold, L., Stokes, S., Bailey, R., Fattahi, M., 2002. Detection of far-red IRSL from loess. Ancient TL 20, 41-46.

Lai, Z., Stokes, S., Bailey, R., Fattahi, M., Arnold, L., 2003. Infrared stimulated red luminescence from Chinese loess: basic observations. Quaternary Science Reviews 22, 961-966.

Lamothe, M., Auclair, M., 2000. The *fadia* method: a new approach in luminescence dating using the analysis of single feldspar grains. Radiation Measurements 32, 433-438.

Lamothe, M., Duller, G. A. T., Huot, S., Wintle, A. G., 2001. Measuring a laboratory radiation dose in feldspar using SAR. 1st North American Luminescence Dating Workshop, Tulsa, OK.

Langevin, Y., Poulet, F., Bibring, J. P., Gondet, B., 2005. Sulfates in the north polar region of Mars detected by OMEGA/Mars Express. Science 307, 1584-1586.

Lepper, K., 2001. Development of an objective dose distribution analysis method for OSL dating and pilot studies for planetary applications. Unpublished Doctor of Philosophy thesis, Oklahoma State University.

Lepper, K., McKeever, S.W.S., 2000. Characterization of fundamental luminescence properties of the Mars soil simulant JSC Mars-1 and their relevance to absolute dating of martian sediments. Icarus 144, 295-301.

Madsen, M. B., Arneson, H. M., Bertelsen, P., Bell III, J. F., Binau, C. S., Gellert, R., Goetz, W., Gunnlaugsson, H. P.,. Herkenhoff, K. E., Hviid, S. F., Johnson, J. R.,

Kinch, K. M., Klingelhöfer, G., Knudsen, J. M., Leer, K., Madsen, D. E., McCartney, E., Merrison, J., Ming, D. W., Morris, R. V., Olsen, M., Proton, J.B., Rodionov, D., Sims, M., Squyres, S. W., Wdowiak, T., Yen, A. S., and the Athena Science Team, 2005. An update on results from the magnetic properties experiments on the Mars exploration rovers, Spirit and Opportunity. LPSC XXXVI, Houston, TX, 2005.

Malin, M. C., Edgett, K., S., 2000. Evidence for recent groundwater seepage and runoff on Mars. Science 288(5475), 2330-2336.

Malin, M. C., Edgett, K. S., Carr, M H., Danielson, G. E., Davies, M. E., Hartman, W. K., Ingersoll, A. P., James, P. B., Masursky, H., McEwen, A. S., Soderblom, L. A., Thomas, P., Veverka, J., Caplinger, M. A., Ravine, M. A., Soulanille, T. A., Warren, J. L., Aeolis Yardangs, NASA's Planetary Photojournal (http://photojournal.jpl.nasa.gov/), Catalog number MOC2-443, August 5, 2003.

Malin, M. C., Edgett, K. S., Carr, M H., Danielson, G. E., Davies, M. E., Hartman, W. K., Ingersoll, A. P., James, P. B., Masursky, H., McEwen, A. S., Soderblom, L. A., Thomas, P., Veverka, J., Caplinger, M. A., Ravine, M. A., Soulanille, T. A., Warren, J. L., Dark Valley in Newton Crater, NASA's Planetary Photojournal (http://photojournal.jpl.nasa.gov/), Catalog number MOC2-418, July 11, 2003.

Malin, M. C., Edgett, K. S., Carr, M H., Danielson, G. E., Davies, M. E., Hartman, W. K., Ingersoll, A. P., James, P. B., Masursky, H., McEwen, A. S., Soderblom, L. A., Thomas, P., Veverka, J., Caplinger, M. A., Ravine, M. A., Soulanille, T. A., Warren, J. L., Dunes in Noachis, NASA's Planetary Photojournal (http://photojournal.jpl.nasa.gov/), Catalog number MOC2-998, February 10, 2005.

Malin, M. C., Edgett, K. S., Carr, M H., Danielson, G. E., Davies, M. E., Hartman, W. K., Ingersoll, A. P., James, P. B., Masursky, H., McEwen, A. S., Soderblom, L. A., Thomas, P., Veverka, J., Caplinger, M. A., Ravine, M. A., Soulanille, T. A., Warren, J. L., Dunes of the North, NASA's Planetary Photojournal (http://photojournal.jpl.nasa.gov/), Catalog number MOC2-1046, March 30, 2005.

Malin, M. C., Edgett, K. S., Carr, M H., Danielson, G. E., Davies, M. E., Hartman, W. K., Ingersoll, A. P., James, P. B., Masursky, H., McEwen, A. S., Soderblom, L. A., Thomas, P., Veverka, J., Caplinger, M. A., Ravine, M. A., Soulanille, T. A., Warren, J. L., Gullies and Sand, NASA's Planetary Photojournal (http://photojournal.jpl.nasa.gov/), Catalog number MOC2-941, December 15, 2004.

Malin, M. C., Edgett, K. S., Carr, M H., Danielson, G. E., Davies, M. E., Hartman, W. K., Ingersoll, A. P., James, P. B., Masursky, H., McEwen, A. S., Soderblom, L. A., Thomas, P., Veverka, J., Caplinger, M. A., Ravine, M. A., Soulanille, T. A.,

Warren, J. L., Intercrater Dunes, NASA's Planetary Photojournal (http://photojournal.jpl.nasa.gov/), Catalog number MOC2-984, January 27, 2005.

Malin, M. C., Edgett, K. S., Carr, M H., Danielson, G. E., Davies, M. E., Hartman, W. K., Ingersoll, A. P., James, P. B., Masursky, H., McEwen, A. S., Soderblom, L. A., Thomas, P., Veverka, J., Caplinger, M. A., Ravine, M. A., Soulanille, T. A., Warren, J. L., Mars Shoreline Tests: A Banded Mesa in Acidalia Planita, NASA's Planetary Photojournal (http://photojournal.jpl.nasa.gov/), Catalog number MOC2-183, October 1, 1999.

Malin, M. C., Edgett, K. S., Carr, M H., Danielson, G. E., Davies, M. E., Hartman, W. K., Ingersoll, A. P., James, P. B., Masursky, H., McEwen, A. S., Soderblom, L. A., Thomas, P., Veverka, J., Caplinger, M. A., Ravine, M. A., Soulanille, T. A., Warren, J. L., Zephyria Outflow Features, NASA's Planetary Photojournal (http://photojournal.jpl.nasa.gov/), Catalog number MOC2-866, October 1, 2004.

Markey, B. G., McKeever, S. W. S., Akselrod, M. S., Bøtter-Jensen, L., Agersnap Larsen, N., Colyott, L. E., 1997. The temperature dependence of optically stimulated luminescence from α-Al_2O_3. Radiation Protection Dosimetry 65, 185-189.

McKeever, S. W. S., 1985. Thermoluminescence of solids. Cambridge University Press, Cambridge.

McKeever, S. W. S., Agersnap Larsen, N., Bøtter-Jensen, L., Mejdahl, V., 1997a. OSL sensitivity changes during single aliquot procedures: computer simulations. Radiation Measurements 27, 75-82.

McKeever, S. W. S., Akselrod, M. S., Markey, B. G., 1996. Pulsed optically stimulated luminescence dosimetry using Al_2O_3:C. Radiation Protection Dosimetry 65, 267-272.

McKeever S. W. S., Banerjee, D., Blair, M., Clifford S. M., Clowdsley, M. S., Kim, S. S., Lamothe, M., Lepper, K., Leuschen, M., McKeever, K. J., Prather, M., Rowland, A., Reust, D., Sears, D. W. G., Wilson, J. W., 2003. Concepts and approaches to in situ luminescence dating of martian sediments. Radiation Measurements 37, 527-534.

McKeever, S. W. S., Bøtter-Jensen, L.,Agersnap Larsen, N., Duller, G. A. T., 1997b. Temperature dependence of OSL decay curves: Experimental and theoretical aspects. Radiation Measurements 27, 161-170.

McKeever, S. W. S., Chen, R., 1997. Luminescence models. Radiation Measurements 27, 625-661.

Mejdahl, V., Bøtter-Jensen, L., 1994. Luminescence dating of archaeological materials using a new technique based on single aliquot measurements. Quaternary Geochronology (QSR) 13, 551-554.

Milekowsky, C., Cucinotta, F.A., Wilson, J.W., Gladman, B., Horneck, G., Lindgren, L., Melosh, J., Rickman, H., Valtonen, M., Zheng, J.Q., 2000. Natural transfer of viable microbes in space 1. From Mars to Earth and Earth to Mars. Icarus 145, 391–427.

Murray, A. S., Mejdahl, V., 1999. Comparison of regenerative-dose single-aliquot and multiple-aliquot (SARA) protocols using heated quartz from archaeological sites. Quaternary Geochronology (QSR) 18, 223-229.

Murray, A. S., Roberts, R. G., 1998. Measurement of the equivalent dose in quartz using a regenerative-dose single-aliquot protocol. Radiation Measurements 29, 503-515.

Murray, A. S., Wintle, A. G., 1998. Factors controlling the shape of the OSL decay curve in quartz. Radiation Measurements 29, 65-79.

Murray, A. S., Wintle, A. G., 2000. Luminescence dating of quartz using an improved single-aliquot regenerative-dose protocol. Radiation Measurements 32, 57-73.

Olley, J. M., Caitcheon, G., Murray, A. S., 1998. The distribution of apparent dose as determined by optically stimulated luminescence in small aliquots of fluvial quartz: implications for dating young sediments. Quaternary Science Reviews 17, 1033-1040.

Parker, T. J., Saunders, R. S., Schneeberger, D. M., 1989. Transitional morphology in West Deuteronilus Mensae, Mars-Implications for modification of the lowland upland boundary. Icarus 82, 111-145.

Parker, T. J., Gorsline, D. S., Saunders, R. S., Pieri, D. C., Schneeberger, D. M., 1993. Coastal geomorphology of the Martian northern plains. Journal of Geophysical Research 98, 11061-11078.

Pelkey, S. M., Jakosky, B. M., Christensen, P. R., 2003. Surficial properties in Melas Chasma, Mars, from Mars Odyssey THEMIS data. Icarus 165, 68-89.

Pelkey, S. M., Jakosky, B. M., Christensen, P. R., 2004. Surficial properties in Gale Crater, Mars, from Mars Odyssey THEMIS data. Icarus 167, 244-270.

Poolton, N. R. J., Bøtter-Jensen, L., Johnsen, O., 1995a. Influence on donor electron energies of the chemical composition of K, Na, and Ca aluminosilicates. Journal of Physics: Condensed Matter 7, 4751-4762.

Poolton, N. R. J., Bøtter-Jensen, L., Johnsen, O., 1995b. Thermo-optical properties of optically stimulated luminescence in feldspars. Radiation Measurements 24, 531-534.

Poolton, N. R. J., Wallinga, J., Murray, A. S., Bulur, E., Bøtter-Jensen, L., 2002a. Electrons in feldspars I: on the wavefunctions of electrons trapped at simple lattice defects. Physical Chemistry Minerals 29, 210-216.

Poolton, N. R. J., Ozanyan, K. B., Wallinga, J., Murray, A. S., Bøtter-Jensen, L., 2002b. Electrons in feldspars II: a consideration of the influence of conduction band-tail states on luminescence processes. Physical chemistry Minerals 29, 217-225.

Prescott, J. R., Hutton, J T., 1988. Cosmic ray and gamma ray dosimetry for TL and ESR. Nuclear Tracks and Radiation Measurements 14, 223-227.

Preusser, F., 2003. IRSL dating of K-rich feldspars using the SAR protocol: comparison with independent age control. Ancient TL, 21, 17-23.

Richardson, C. A., 1994. Effects of bleaching on the sensitivity to dose of the infra-red stimulated luminescence of potassium-rich feldspars from Ynyslas, Wales. Radiation Measurements 23, 587-591.

Roberts, H. M., Wintle, A. G., 2003. Luminescence sensitivity changes in of polymineral fine-grains during IRSL and [post-IR] OSL measurements. Radiation Measurements 37, 661-671.

Rodriguez, J. A. P., Sasaki, S., Kuzmin, R. O., Dohm, J. M., Tanka, K. L., Miyamoto, H., Kurita, K., Komatsu, G., Fairen, A. G., Ferris, J. C., 2005. Outflow channel sources, reactivation, and chaos formation, Xanthe Terra, Mars. Icarus, *In Press*.

Sanderson, D. C. W., Clark, R. J., 1994. Pulsed photostimulated luminescence of alkali feldspars. Radiation Measurements 23, 633-639.

Saunders, R. S., Arvidson, R. E., Badwhar, G. D., Boynton, W. V., Christensen, P. R., Cucinotta, F. A., Feldman, W. C., Gibbs, R. G., Kloss Jr., C., Landano, M. R., Mase, R. A., McSmith, G. W., Meyer, M. A., Mitrofanov, I. G., Pace, G. D., Plaut, J. J., Sidney, W. P., Spencer, D. A., Thompson, T. W., Zeitlin, C. J., 2004. 2001 Mars Odyssey mission summary. Space Science Reviews 110, 1-36.

Simon, S. L., Baverstock, K. F., Lindholm, C., 2003. A summary of evidence on radiation exposures received near to the Semipalatinsk nuclear weapons test site in Kazakhstan. Health Physics 84, 718-725.

Simon, S. L., Bouville, A., 2002. Radiation dose to local populations near nuclear test sites worldwide. Health Physics 82, 706-725.

Spooner, N. A., 1993. The validity of optical dating based on feldspar. Unpublished Doctor of Philosophy thesis, University of Oxford.

Spooner, N. A., 1994. On the optical dating signal from quartz. Radiation Measurements 23, 593-600.

Takada, J., Hoshi, M., Rozenson, R., Endo, S., Yamamoto, M., Nagatomo, T., Imanaka, T., Gusev, B. I., Tchaijunosova, N. J., 1997. Environmental radiation dose in Semipalatinsk area near Nuclear Test Site. Health Physics 73, 524-527.

Templer, R. H., 1985. The removal of anomalous fading in zircon. Nuclear Tracks and Radiation Measurements 10, 531-537.

Templer, R. H., 1986. The localized transition model of anomalous fading. Radiation Protection Dosimetry 17, 493-497.

Tsukamoto, S., Denby, P. M., Murray, A. S., Bøtter-Jensen, L., 2005. Time-resolved pulsed luminescence from feldspars: new insights into fading. LED 2005, Cologne, Germany, 2005.

Verigin, M. I., Kotova, G. A., Remizov, A. P., Szego, K., Tatrallyay, M., Slavin, J., Rosenbauer, H., Livi, S., Riedler, W., Schwingenschuh, K, Zhang, T. L., 2001. Evidence of the influence off equatorial martian crustal magnetization on the position of the planetary magnetotail boundary by Phobos 2 data. Advanced Space Research 28, 885-889.

Vicosekas, R., 1985. Tunneling radiative recombination in labbradorite: its association with anomalous fading of thermoluminescence. Nuclear Tracks and Radiation Measurements 10, 521-529.

Vicosekas, R., 1993. Tunneling radiative recombination in K-feldspar sanidine. Nuclear Tracks and Radiation Measurements 21,175-178.

Vicosekas, R., 2000. Monitoring anomalous fading of TL of feldspars by using far-red emission as a gauge. Radiation Measurements 32, 499-504.

Vicosekas, R., Spooner, N. A., Zink, A., Blanc, P., 1994. Tunnel afterglow, fading, and infrared emission in thermoluminescence of feldspars. Radiation Measurements 23, 377-385.

Vicosekas, R., Zink, A., 1999. Use of the far red TL emission band of alkali feldpsars for dosimetry and dating. Quaternary Geochronology 18, 271-278.

Wallinga, J., Murray, A. S., Wintle, A. G., 2000a. The single-aliquot regenerative-dose (SAR) protocol applied to coarse-grain feldspar. Radiation Measurements 32, 529-533.

Wallinga, J., Murray, A. S., Duller, G. A. T., 2000b. Underestimation of equivalent dose in single-aliquot optical dating of feldspars caused by preheating. Radiation Measurements 32, 691-695.

Wallinga, J., Murray, A. S., Boetter-Jensen, L.. 2002. Measurement of the dose in quartz in the presence of feldspar contamination. Radiation Protection Dosimetry 101, 367-370.

Wilson, J.W., Badavi, F., Cucinotta, F., 1995. HZETRN: description of a free space ion and nucleon transport and shieldingcomputer program, NASA TP-3495.

Wintle, A. G., 1973. Anamolous Fading of Thermoluminescence in Mineral Samples. Nature 245, 143-144.

Wintle, A. G., 1975. Thermal quenching of thermoluminescence in quartz. Journal of the Roay Astronomy Society 41, 107-113.

Wintle, A, G., 1977. Detailed study of a thermoluminescent mineral exhibiting anomalous fading. Journal of Luminscence 15, 385-393.

White, W. B., Matsumura, M., Linnehan, D. G., Furukawa, T., Chandrasekhar, B. K., 1986. Absorption and luminescence of Fe^{3+} in single-crystal orthoclase. American Mineralogist 71, 1415-1419.

Wolfram research, Inc., 1999. Mathematica, Edition 4.0. Wolfram Research, Inc, Champaign, IL.

Yukihara, E.G., Gaza, R., McKeever, S. W. S., Soares, C. G., 2004. Optically stimulated luminescence and thermoluminescence efficiencies for high-energy heavy charged particle irradiation in Al_2O_3:C. Radiation Measurements 38, 59-70.

Yukihara, E. G., Whitley, V. H., Blair, M. W., Banerjee, D., McKeever, S. W. S., 2002. Optically stimulated luminescence of feldspar samples using linearly modulated blue light stimulation. LED 2002, Reno, NV, 2002.

Zimbelman, J. R., 2003. Decameter-scale ripple-like features in Nirgal Vallis as revealed in THEMIS and Moc imaging data. Sixth International conference on Mars, Abstract No. 3028.

Zink, A., Vicosekas, R., Bos, A., J., J., 1995. Comparison of ‘blue’ and ‘infrared’ emission bands in thermoluminescence of alkali feldpars. Radiation Measurements 24, 513-518.

Zurek, R. W., 1992. Introduction to the Mars atmospehere. In: Kieffer, H. H., Jakosky, B. M., Snyder, C. W., Mathews, M. S. (Eds.), Mars, University of Arizona Press, Tucson, pp.1-33.

APPENDIX A

RETROSPECTIVE DOSIMETRY USING BRICKS FROM THE SEMIPALATINSK REGION OF KAZAKHSTAN

The Optically and Thermally Stimulated Phenomena Lab at OSU participated in a National Cancer Institute (NCI) study to determine the absorbed radiation doses deposited in bricks near the Semipalatinsk Nuclear Test Site. The radiation doses stem from several nuclear device tests including both atmospheric and surface tests, the principal ones occurring in 1949 (Bailiff *et al.*, 2004) but continuing through the mid 1950s (Simon *et al.*, 2003). The area has been the focus of studies on the deleterious health effects of radiation exposure and on radiation dose reconstruction (Gilbert *et al.*, 2002; Simon and Bouville, 2002; Simon *et al.*, 2003). The latter has involved the use of luminescence retrospective dosimetry (Takada *et al.*, 1997; Bailiff *et al.*, 2004). OSU's participation in the NCI study involved measuring OSL to determine absorbed radiation doses from various bricks collected in the Semipalatinsk region as part of an intercomparison between laboratories and an epidemiology study.

Researchers at NCI collected the bricks from the affected areas and shipped them to OSU. OSU then provided depth-versus-dose profiles for two of the bricks, absorbed dose measurements for slices just beneath the surface of the bricks, and absorbed dose measurements for 3 bricks that were part of an international

intercomparison. Although analysis of the depth-versus-dose profiles attempted to determine the natural dose due to internal radiation, OSU did not attempt independent estimates of the natural background dose as has been done by other researchers (Banerjee *et al.*, 2000).

A.1 Introduction to Retrospective Dosimetry

Retrospective dosimetry attempts to reconstruct the radiation dose that a population has been exposed to as a result of nuclear accidents or testing. Radiation dosimeters and measurement devices are usually not in place or available at the time or in the location of these tests and accidents, so retrospective methods must be used to determine the radiation dose delivered to the area. Luminescence retrospective dosimetry is a specialization of luminescence dating and uses many of the same techniques.

In retrospective dosimetry, luminescence dating techniques are used to measure the total absorbed radiation dose (D_E) from natural (e.g., quartz extracted from bricks) or man-made (e.g., porcelain from fixtures) materials near the area of the nuclear test or accident. The total absorbed dose that is measured consists of two components: the natural or background dose ($D_{BG)}$ due to radiation from the material or environment, and the event or accident dose (D_A) from nuclear testing or accidents. The background dose can be estimated by using materials of known age, measuring the natural radioactivity of the sample, and then calculating the background dose of the sample. The accident dose can then simply be found by

$$D_A = D_E - D_{BG} \ . \tag{A.1}$$

Early applications of luminescence retrospective dosimetry used TL methods and required a multiple-aliquot approach (Haskell, 1993; Bailiff, 1997). The advent of the

SAR procedure made an OSL single-aliquot approach to retrospective dosimetry both practical and accurate (Banerjee *et al.*, 1999; Banerjee *et al.*, 2000). Since a very small amount of material is required for the SAR procedure, depth-versus-dose profiles can be measured in bricks or other materials from the area. The depth-versus-dose profiles allow the researcher to determine if the material has been exposed to a significant accident dose (Bailiff, 2004) and how the accident dose attenuates in the material. The SAR procedure of Table 1.1 with a 220°C preheat and a 170°C cutheat was used for the retrospective dosimetry measurements made by OSU.

A.2 Sample Preparation

Ten bricks from the Semipalatinsk area were delivered to OSU for the initial study. Before absorbed doses could be measured from the bricks, cores were drilled from the bricks and cut into 10 mm sections. The intercomparison samples arrived as cores and were sliced into 10 mm slices. This section describes how the samples were cored, sliced, and processed to obtain pure quartz samples.

A.2.1 Coring and Drilling

Each of the 10 bricks that were approximately 7 cm x 13 cm x 36 cm. The first step was to remove a core from the center of each brick. The cores were removed using a Core Bore M-3 drilling rig and a Milwaukee Dymo-drill, fitted with a 1½" (3.8 cm) inside-diameter core drilling bit. The drilling apparatus was mounted on a custom-made base (constructed at OSU) that allowed for continuous water flow to both aid cutting and prevent heating of the cores (necessary to prevent thermal depletion of the luminescence signals, Figure A.1). All coring was done under low level lighting, and care was taken to

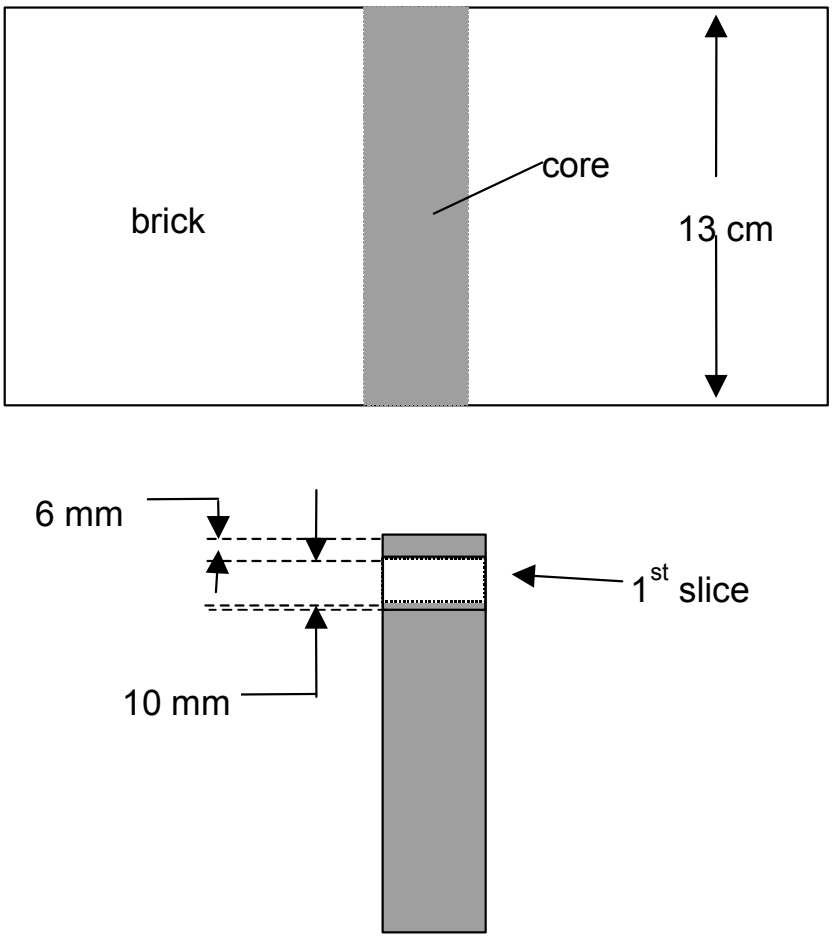

Figure A.1 Representation of the coring and slicing of the bricks from Semipalatinsk.

ensure that the edges of the core were at least 5 mm from the outer side of the brick so that no part of the core had been previously exposed to light.

Each core was approximately 13 cm in length. The brick cores were sliced using a Buehler Isomet™ 1000 low speed saw. The saw uses a 6" (15.2 cm) diamond-tipped blade, low operating speeds, and a fluid lubrication system that serves to reduce heating and deformation of the sample. The first 6 mm of each core was removed and discarded in case the luminescence signals from the surface material had been partially bleached. One 10 mm slice was then removed from each core (Figure A.1). Later, based upon the initial OSL results from these samples, two bricks were chosen for full depth-dose profiling along the whole length of the core. Nine additional 10 mm slices were removed from these two bricks.

The intercomparison samples had been previously sliced from larger bricks that had been uniformly irradiated. One slice of each brick was sent to seven different laboratories. The received slices were approximately 5 mm x 6.5 cm x 13 cm. As before, the outer 6 mm of each slice was removed and one 10 mm slice was then removed from each slice with the Buehler Isomet™ 1000 low speed saw.

A.2.2 Sample Processing

Each brick slice (from both the Semipalatinsk samples and the intercomparison samples) was chemically processed in order to obtain 63-150 μm quartz grains. The brick samples were first gently crushed using a non-agate mortar and pestle. The resulting grains were then wet-sieved to isolate the 63-150 μm fraction. These polymineral grains were then chemically treated to isolate quartz grains.

Chemical processing was carried out inside a fume hood with proper ventilation. To remove carbonates, the samples were first repeatedly washed with 12 % HCl until no further reaction occurred. A 50-minute etch in hydrofluoric acid (48 %) was then performed to remove feldspathic materials and the outer rind of the quartz grains. After the HF etch, the samples were again washed with HCl. Finally, the samples were washed three times with deionized water and placed in an oven at 50°C for 24 hours to dry.

Initial experiments revealed that 5 of the 10 bricks yielded quartz with very low luminescence levels, even after a 10 Gy laboratory irradiation had been applied. These samples may have been affected by physical contaminants that were blocking the luminescence, and therefore they were subjected to an additional HCl wash followed by a 5-minute hydrogen peroxide (30%) treatment. This treatment successfully increased the luminescence output, although it was still relatively low when compared with the other bricks.

A.3 Measurements and Results

The absorbed dose measurements were carried out using the previously described SAR procedure using a 220°C preheat, 170°C cutheat, and blue stimulation (470) nm. One of the previously described Risoe DA-15 automated TL/OSL readers, with a $^{90}Sr/^{90}Y$ source delivering 120 mGy/s, was used for all of the OSL measurements.

A.3.1 Measurements

Initial measurements were made on two aliquots from the first slice of each of the 10 brick cores. The results yielded an approximation of the samples' D_e and the sensitivity. These estimates aided the subsequent choice of regeneration doses to be given during the SAR method, and yielded relative estimates of each brick's OSL response to

irradiation (i.e., sensitivity). From these initial investigations, it was evident that 5 bricks (N1, N4, N5, N7, and N9) had large OSL signals, 3 bricks (N3, N6, N10) had weak OSL signals, and 2 bricks (N2, N8) yielded almost no OSL signal.

Further absorbed dose measurements were conducted on those 5 bricks that gave large OSL signals. The SAR procedure was used to measure the equivalent dose for an additional 20 aliquots, for a total of 22 aliquots. An average and standard deviation of the mean was calculated for each sample. Based upon these results, two bricks (N1 and N4) were further selected for measuring depth-versus-dose profiles.

After the two depth-versus-dose profiles were completed, the 5 bricks that yielded low OSL signals were again examined. Since these samples had been chemically treated in the same manner as the other samples, it was determined that the low sensitivities were a result of either incomplete firing and sensitization of the quartz grains during manufacture of the brick or that, as alluded to above, contaminants blocked the luminescence. In an attempt to remove possible contaminants, the 5 samples were treated with hydrogen peroxide as previously indicated. This treatment was successful in increasing the OSL signals, but the signals were still relatively weak (compared to the other samples). As a result, these samples yielded a large scatter in the subsequent equivalent dose estimations.

A.3.2 Results

For the each of the studied brick slices, several quantities were calculated based upon the OSL measurements and D_e estimations. The numerical average of the equivalent doses from all of the aliquots (for each sample) was termed the "Average D_e." The weighted mean of these doses, taking into account the individual uncertainties σ_{De}

associated with each measurement, is termed the "Weighted Average." Where possible, the D_e data were used to construct histograms or dose distributions for each sample. The median of the σ_{De} values was used as an objective bin width for each histogram as suggested by Lepper (2001). The "Weighted Standard Deviation" is the standard deviation of the histogram. The histograms also give the mode and median of the distribution.

The absorbed doses from the first slice (6-16 mm) of eight of the bricks are reported in Table A.1. The Table gives the average D_e, the weighted average D_e, the weighted standard deviation (except where noted), the number of aliquots measured, and differentiates between "high sensitivity" and "low sensitivity" samples. The histograms for the high sensitivity samples are shown in Figure A.2, and the histograms for the low sensitivity samples are shown in Figure A.3. The significance and interpretation of the histograms are discussed later.

Depth-versus-dose profiles were measured for two bricks, designated N1 and N4. Each of the absorbed dose measurements derives from a 10 mm slice of the brick core. The depth-versus-dose profiles are shown if Figures A.4 (brick N1) and A.7 (brick N4), and the corresponding histograms are shown in Figures A.5 and A.6 (brick N1) and A.8 and A.9. Note that brick N1 showed a clear attenuation of dose with depth and could be fit by an (exponential + linear) function, but brick N4 did not show a clear dose attenuation with depth and could not be fit with the above function. The absorbed doses for the profiles, along with the average D_e, the weighted average D_e, the weighted standard deviation, and the number of aliquots measured, are given in Tables A.2 (brick N1) and A.3 (brick N4).

Brick	Ave D_e (Gy)	Weighted Ave. D_e (Gy)	Weighted St. Dev. (Gy)	*N*
N5*	0.193	0.199	0.113	22
N7*	0.111	0.119	0.063	22
N9*	0.253	0.273	0.115	22
N2#	0.260	0.292	0.190	19
N3#	0.086	0.090	0.234	18
N6#	0.132	0.159	0.134	22
N8#	0.063	0.082	0.116	19
N10#$	0.192	N.A.	0.111	7

* High sensitivity samples
# Low sensitivity samples
$ No dose distribution. Standard deviation is from errors of individual measurements.

Table A.1 Absorbed doses from the first slice (6-16 mm) of eight bricks. The table lists the average D_e, the weighted average D_e, the weighted standard deviation, and the number of aliquots measured. High and low sensitivity samples are also differentiated.

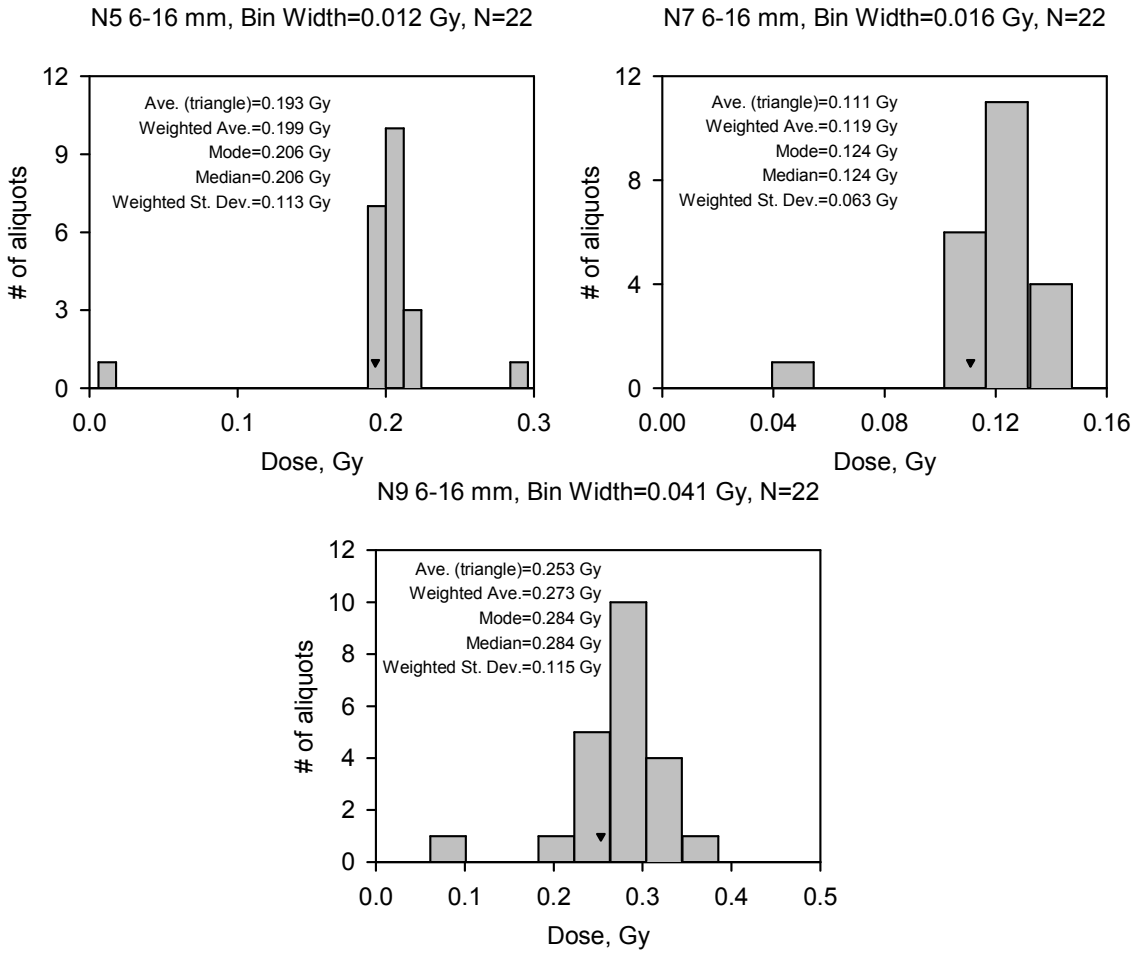

Figure A.2 Histograms for high sensitivity samples. The histograms give the numerical average (triangle), the weighted average (considering the σ_{De}), the mode and median of the distribution, and the weighted standard deviation of the histogram.

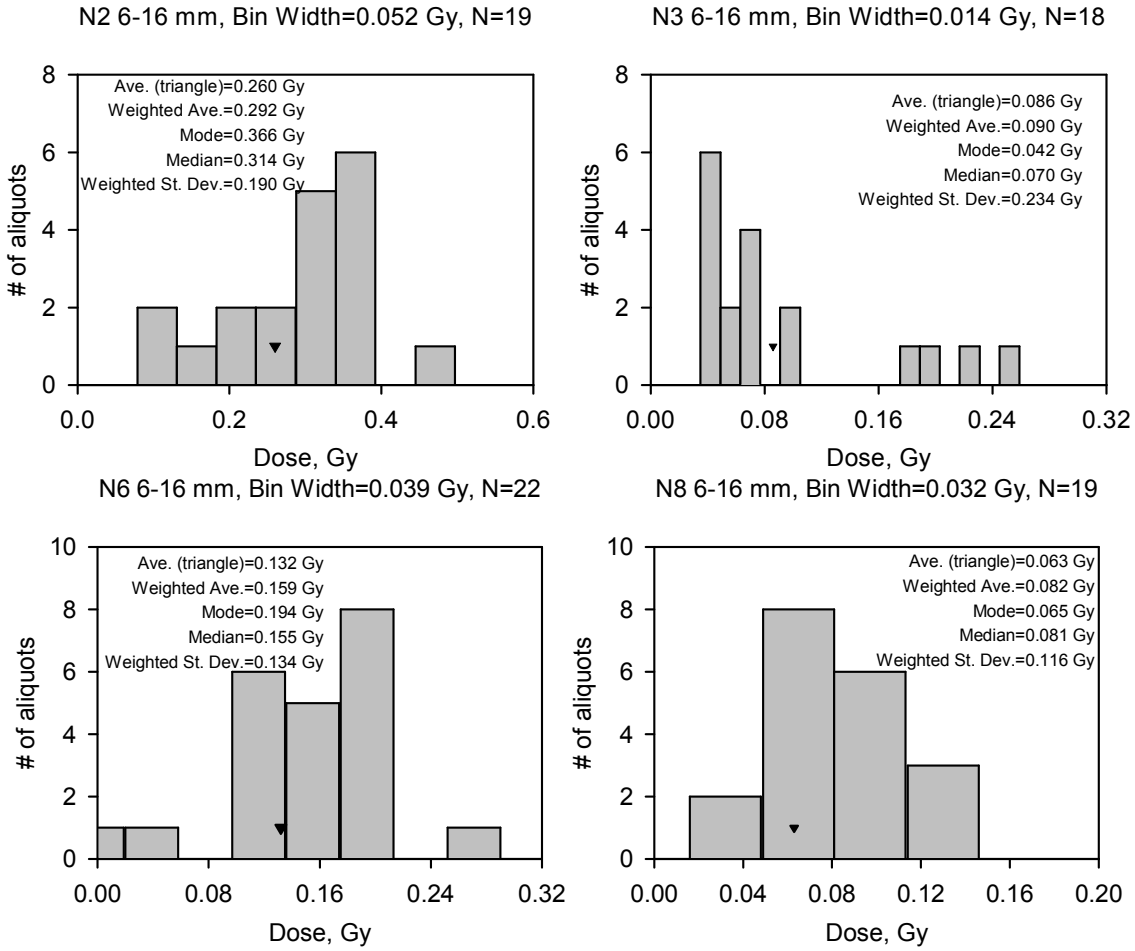

Figure A.3 Histograms for low sensitivity samples. The histograms give the numerical average (triangle), the weighted average (considering the σ_{De}), the mode and median of the distribution, and the weighted standard deviation of the histogram.

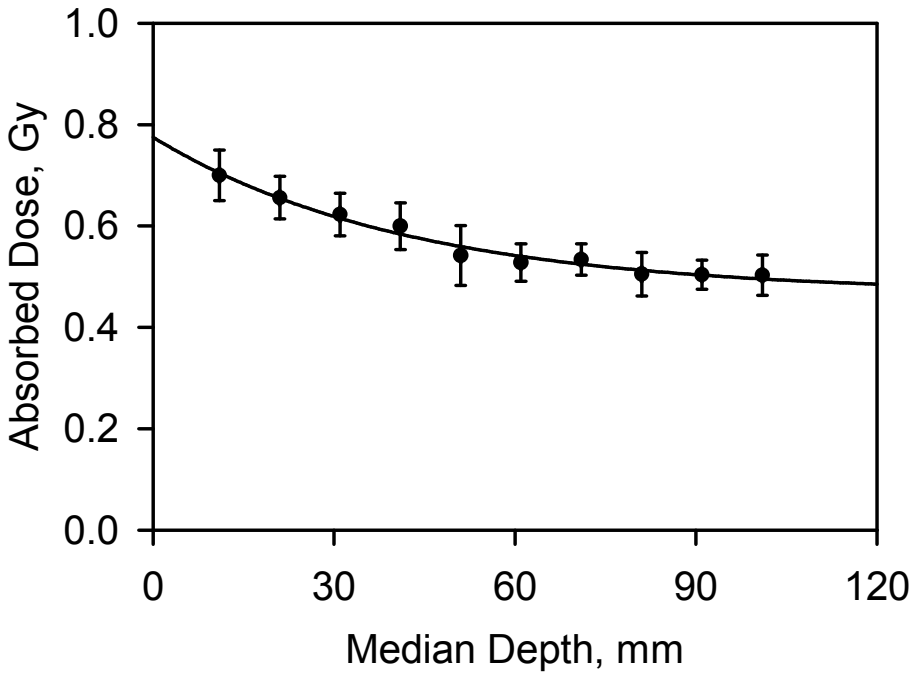

Figure A.4 Absorbed doses (natural doses not subtracted) as a function of median depth for brick N1. The relationship has been fitted using the sum of a constant (*i.e.*, natural dose) and a decaying exponential.

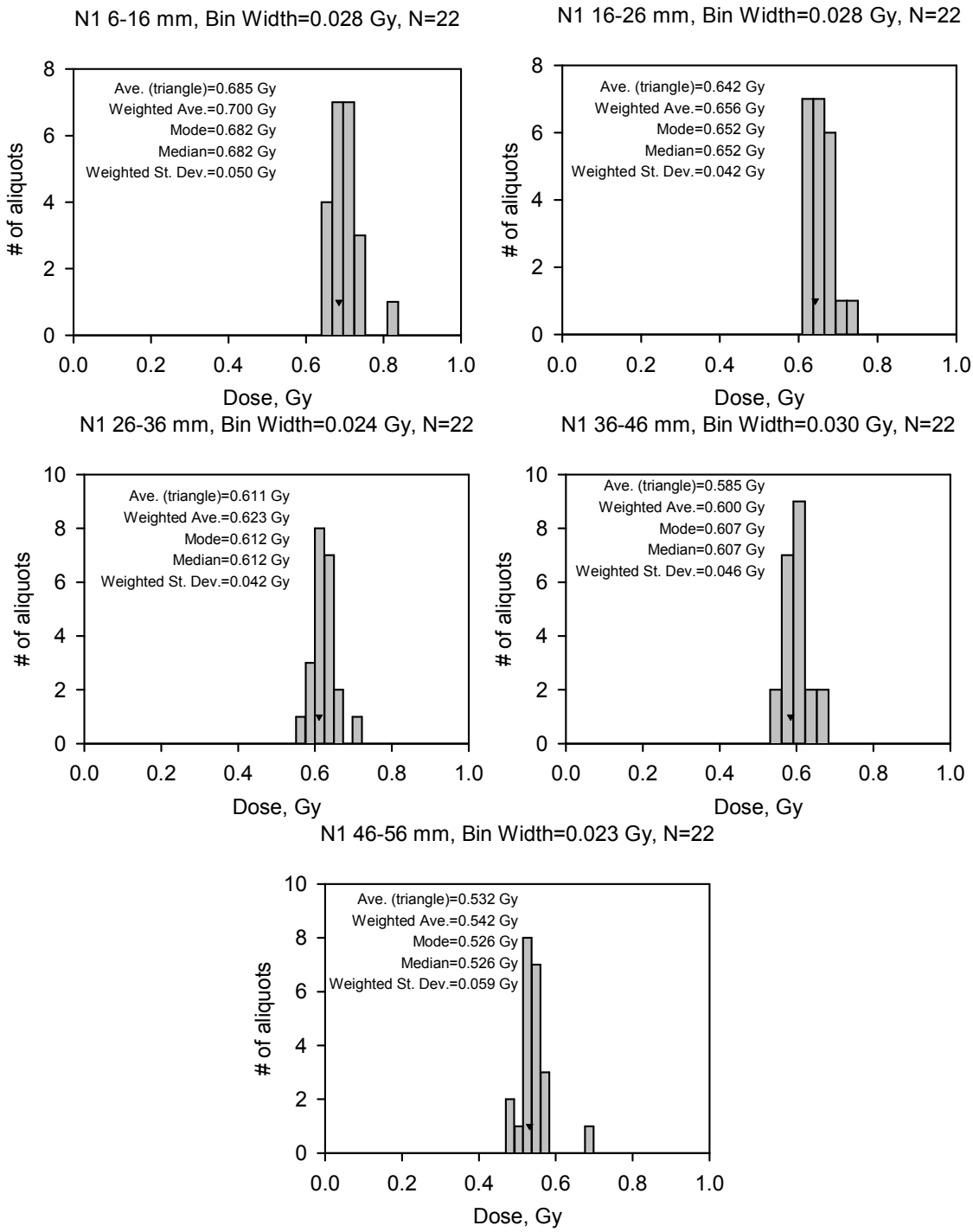

Figure A.5 Histograms for brick N1 (up to 50 mm median depth). The histograms give the numerical average (triangle), the weighted average (considering the σ_{De}), the mode and median of the distribution, and the weighted standard deviation of the histogram.

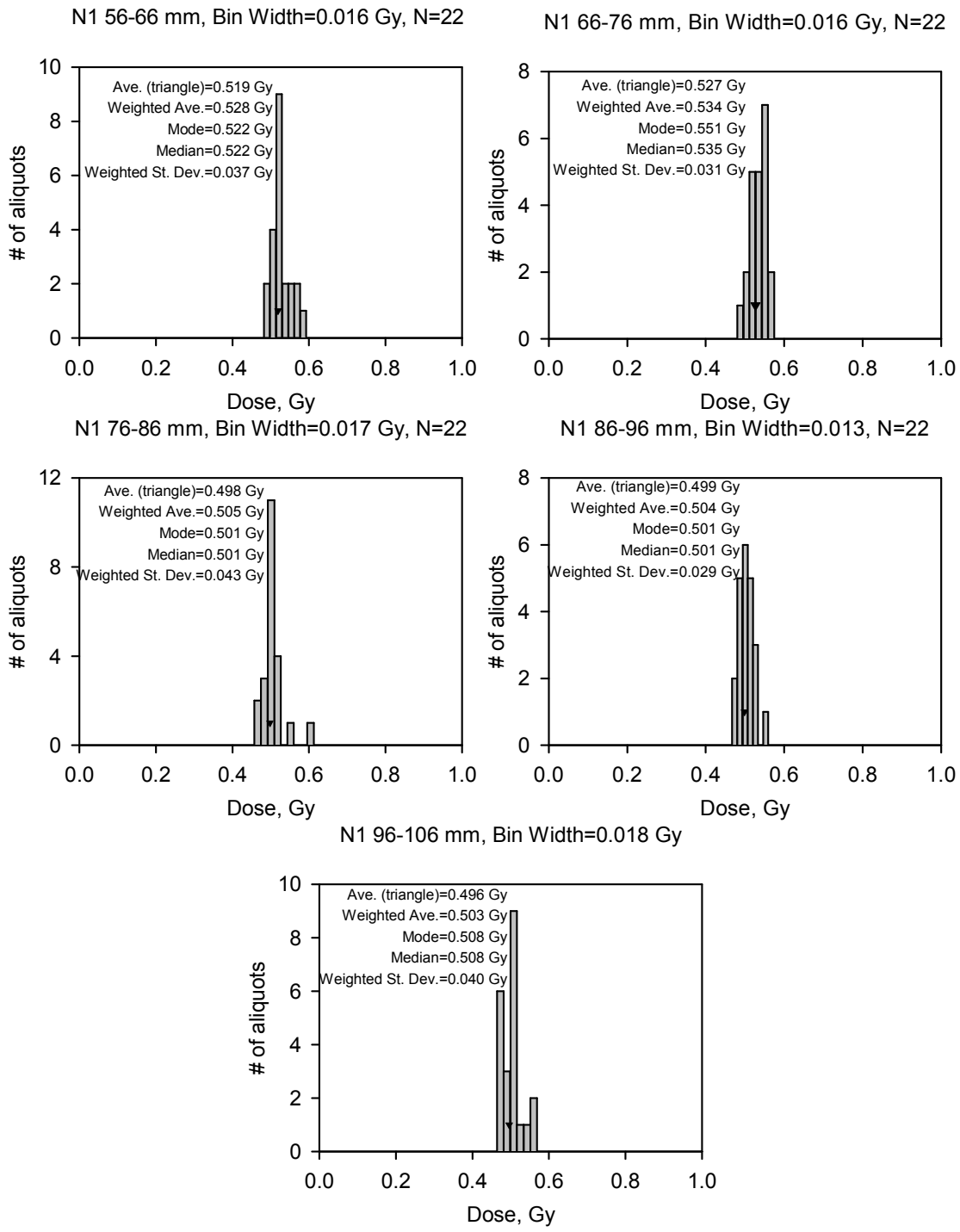

Figure A.6 Histograms for brick N1 (greater than 50 mm median depth). The histograms give the numerical average (triangle), the weighted average (considering the σ_{De}), the mode and median of the distribution, and the weighted standard deviation of the histogram.

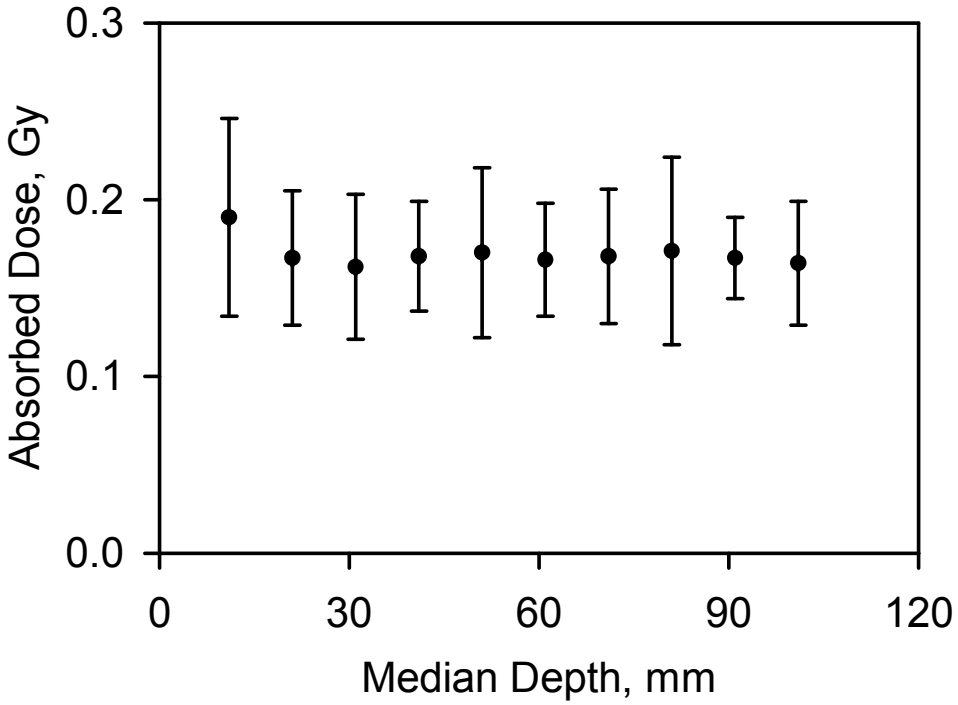

Figure A.7 Absorbed doses (natural doses not subtracted) as a function of median depth for brick N4.

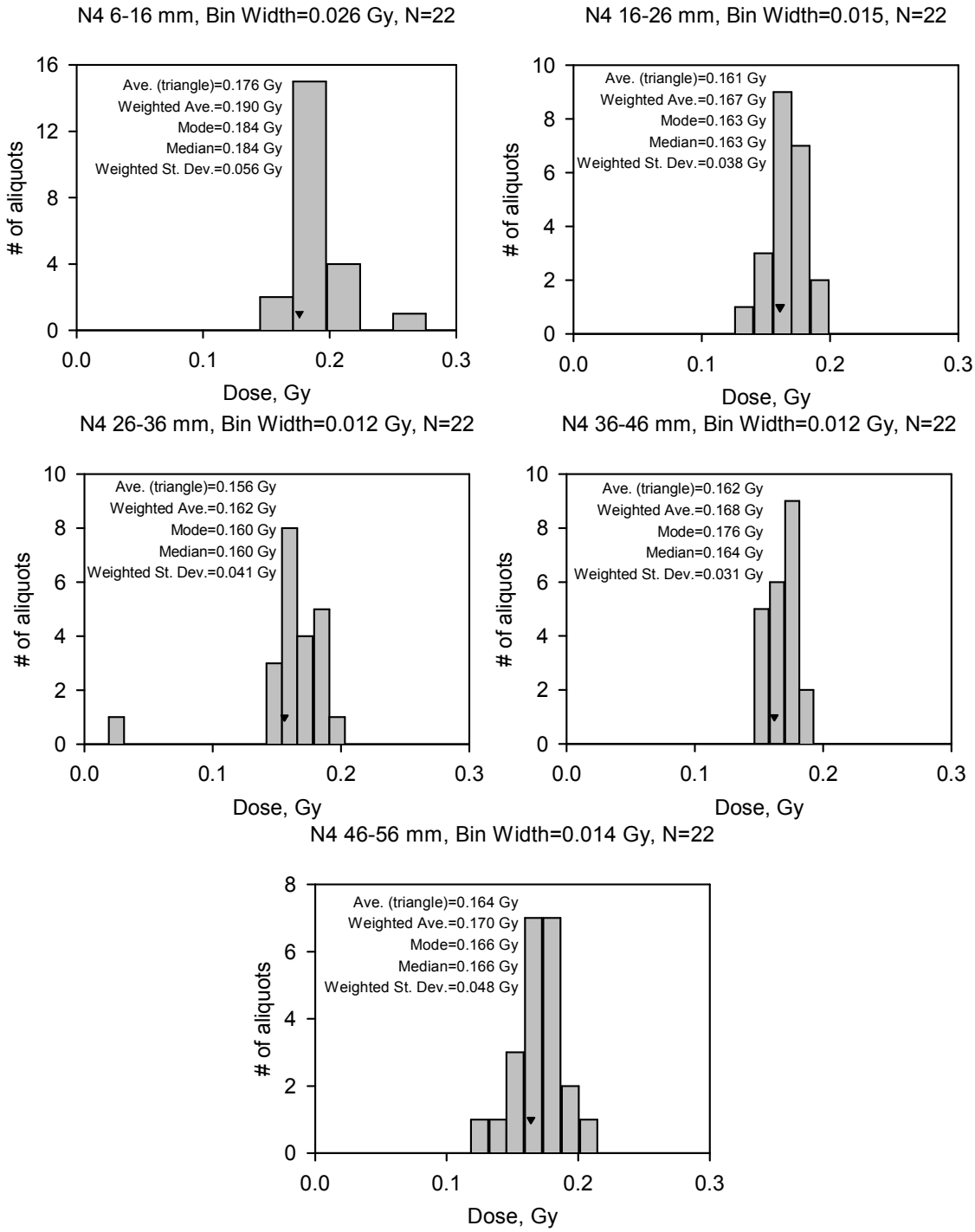

Figure A.8 Histograms for brick N4 (up to 50 mm median depth). The histograms give the numerical average (triangle), the weighted average (considering the σ_{De}), the mode and median of the distribution, and the weighted standard deviation of the histogram.

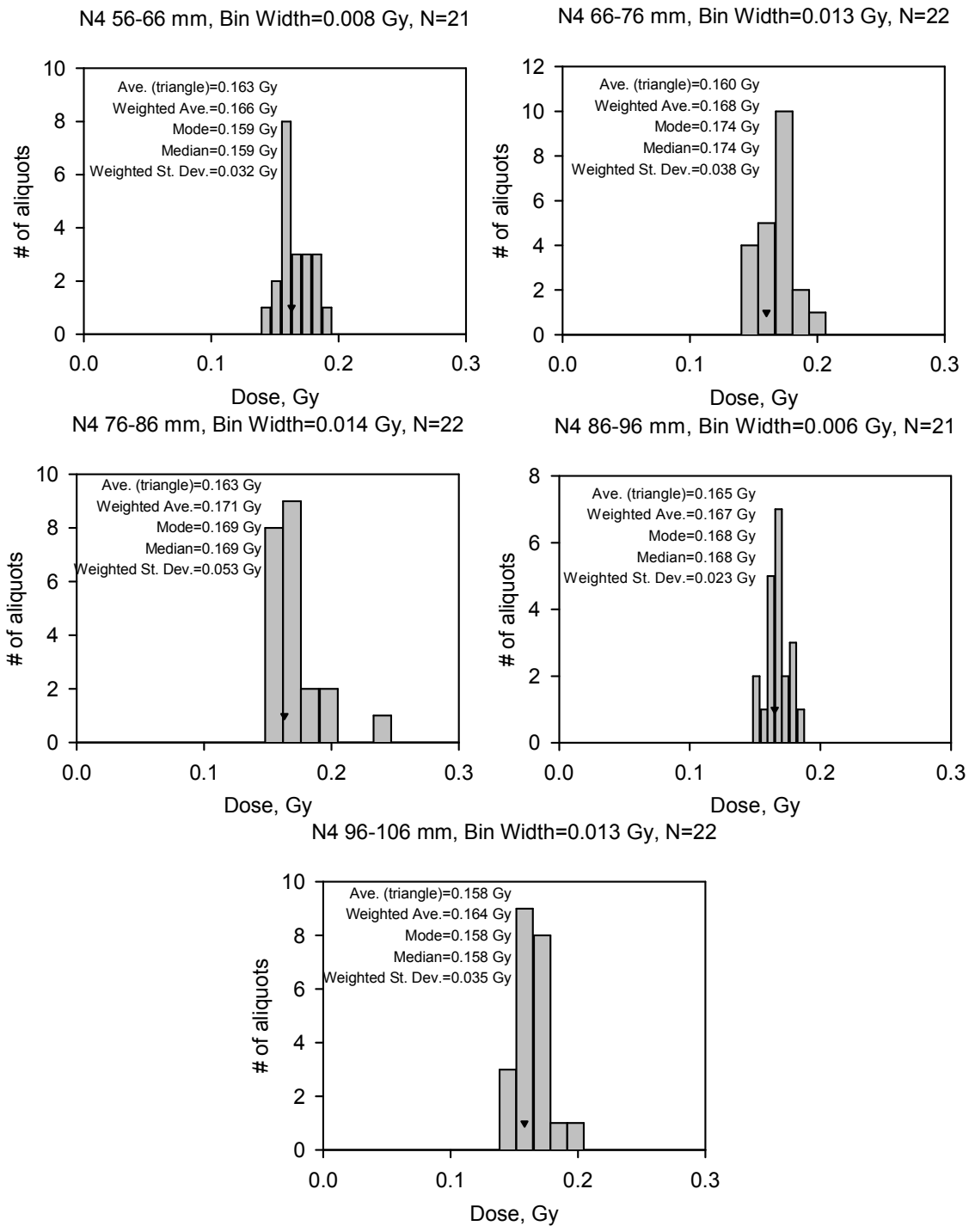

Figure A.9 Histograms for brick N4 (greater than 50 mm median depth). The histograms give the numerical average (triangle), the weighted average (considering the σ_{De}), the mode and median of the distribution, and the weighted standard deviation of the histogram.

Depth (mm)	Ave D_e (Gy)	Weighted Ave. D_e (Gy)	Weighted St. Dev. (Gy)	*N*
6-16	0.685	0.700	0.050	22
16-26	0.642	0.656	0.042	22
26-36	0.611	0.623	0.042	22
36-46	0.585	0.600	0.046	22
46-56	0.532	0.542	0.059	22
56-66	0.519	0.528	0.037	22
66-76	0.527	0.534	0.031	22
76-86	0.498	0.505	0.043	22
86-96	0.499	0.504	0.029	22
96-106	0.496	0.503	0.040	22

Table A.2 Absorbed doses from the depth-versus-dose profile of brick N1. The table lists the average D_e, the weighted average D_e, the weighted standard deviation, and the number of aliquots measured.

Depth (mm)	Ave D_e (Gy)	Weighted Ave. D_e (Gy)	Weighted St. Dev. (Gy)	*N*
6-16	0.176	0.190	0.056	22
16-26	0.161	0.163	0.038	22
26-36	0.156	0.162	0.041	22
36-46	0.162	0.168	0.031	22
46-56	0.164	0.170	0.048	22
56-66	0.163	0.166	0.032	21
66-76	0.160	0.168	0.038	22
76-86	0.163	0.171	0.053	22
86-96	0.165	0.167	0.023	21
96-106	0.158	0.164	0.035	22

Table A.3 Absorbed doses from the depth-versus-dose profile of brick N4. The table lists the average D_e, the weighted average D_e, the weighted standard deviation, and the number of aliquots measured.

Brick	Ave D_e (Gy)	Weighted Ave. D_e (Gy)	Weighted St. Dev. (Gy)	*N*
SP183R[$]	0.166		0.074	10
SP17-2R[$]	0.377		0.050	6
SP96093R	0.425	0.435	0.120	22

[$] No dose distribution. Standard deviation is from errors of individual measurements.

Table A.4 Absorbed doses from the first slice (6-16 mm) of the intercomparison samples. The table lists the average D_e, the weighted average D_e, the weighted standard deviation, and the number of aliquots measured.

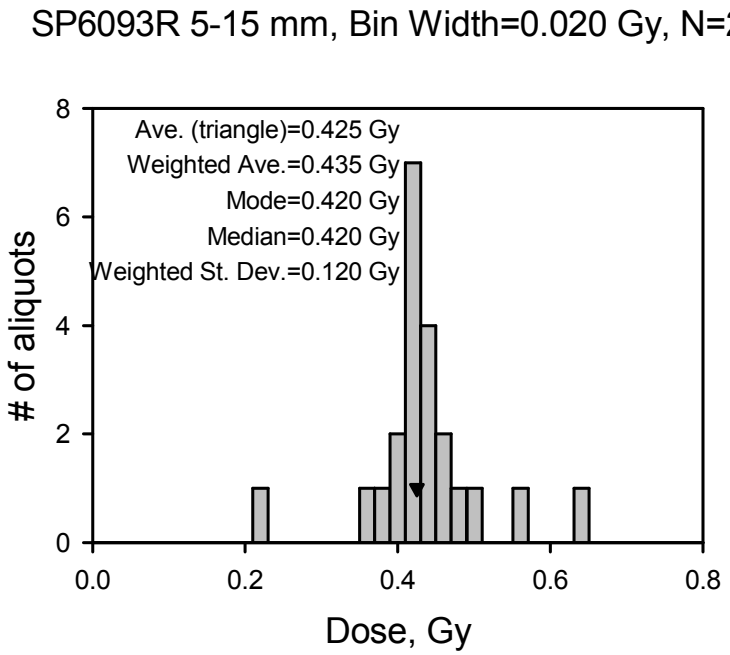

Figure A.10 Histogram for intercomparison sample. The histogram gives the numerical average (triangle), the weighted average (considering the σ_{De}), the mode and median of the distribution, and the weighted standard deviation of the histogram.

For the three intercomparison samples, only the first slice (6-16 mm) of each was analyzed. The measured absorbed dose, again along with the average D_e, the weighted average D_e, the weighted standard deviation, and the number of aliquots measured, are reported in Table A.4. Since there was generally less material available for the intercomparison samples, a sufficient number of aliquots to construct a meaningful histogram could only be measured for one sample (SP96093R). This histogram is shown in Figure A.10.

A.4 Discussion

The histograms or absorbed dose distributions created as part of this study were used as a tool to evaluate which measurements were reliable. Other (luminescence dating) studies have used analysis of dose distributions to distinguish well-bleached from poorly bleached samples or to statistically determine the "correct" D_e (Lepper, 2001; Galbraith *et al.*, 1999; Olley *et al.*, 1998). Sophisticated interpretation and analysis of the dose distributions were not attempted for these retrospective dosimetry measurements because a sufficient number of aliquots were not measured to warrant detailed statistical analysis. Instead, a "tight" distribution was taken to represent a reliable absorbed dose measurement as the numerical average D_e was generally consistent with the weighted average D_e, the mode, and the median while these statistics generally were not consistent for "broad" distributions. The dose distributions then helped the researchers differentiate "high sensitivity" and "low sensitivity" samples as well as choose those brick cores that would be most suitable for dose-versus-depth profiling.

The measurements for the depth-dose profile in brick N1 (Figure A.4) indicate an exponential attenuation of the dose from the front surface, down to a constant background

level. The background level can be interpreted as the natural absorbed dose for this brick (from radioisotopes within the brick) and the excess doses above this level at the various depths are assumed to be the accident doses. Figure A.4 represents the absorbed doses without subtracting the natural background dose. It is apparent that the brick has a high natural dose. If we take the constant value D_0 from the fitting of the following expression to the data,

$$D = D_0 + D' * exp(-b * x), \tag{A.2}$$

to be the natural dose in this brick, the natural dose D_0 is found to be 0.466 ± 0.17 Gy. In this expression, D' is the surface dose, b is the attenuation constant, and x is the depth below the surface. Figure A.11 shows the results with this background level subtracted.

The related data for brick N4 (Figure A.7) are equivocal. Although there may be an enhanced signal near the surface, the error bars for this sample preclude an analysis based on (A.2), and there is no clear depth-dose profile from the sample. Taking the mean of last few data as the background, and subtracting this from the data of Figure A.7 yields A.12.

A.5 Conclusions

OSL using the SAR technique is an informative method for determining absorbed doses in heated quartz from bricks. The dose distribution histograms are of particular use since they graphically display the uncertainty associated with the dose determination and add a degree of confidence to the evaluated data in ways not possible with conventional OSL or TL methods. The use of depth-versus-dose profiles to determine the natural or background dose of a sample, and subsequently the accident dose, could be a viable alternative to calculating the background dose (using a measured radiation dose rate and the known age off the sample). However, a direct comparison of the results from dose-

versus-depth profiling and traditional methods is needed before this method can become routine.

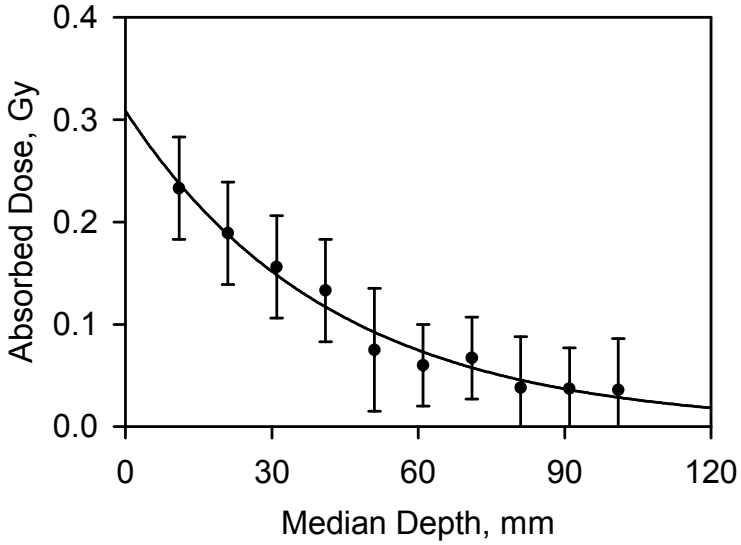

Figure A.11 Depth-versus-dose profile for brick N1 with a background level of D_0 = 0.466 Gy subtracted. The relationship has been fitted using a decaying exponential.

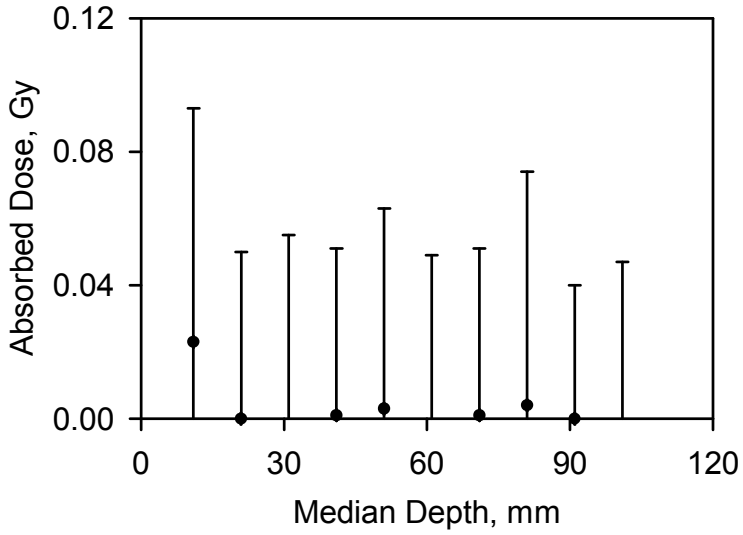

Figure A.12 Depth-versus-dose profile for brick N4 with a background level subtracted.

APPENDIX B

PROGRESS TOWARDS DEVELOPING A MINIATURIZED OSL SYSTEM FOR IN-SITU MARTIAN STUDIES

The experiments described in this dissertation along with the accompanying discussions have addressed the scientific challenges to developing OSL dating for Mars. Of equal importance is the design and fabrication of a small volume, small mass, and low power OSL instrument that will be able to perform the necessary functions for OSL dating on the surface of Mars. This instrument is currently being designed and built by Nomadics Inc. of Stillwater, OK. The engineers at Nomadics are actively working with the luminescence dating researchers at OSU to define the required functions of the OSL system and identify appropriate components. This appendix gives an overview of the system design, the major challenges to developing the OSL instrument, and the current progress.

B.1 Identifying Components of OSL Module

Before any specific design plans were created for the OSL module, Nomadics and OSU worked together to identify the components (subsystems) of the OSL module. This work resulted in the system block diagram of Figure B.1. As discussed in Chapter 7, grain size selection and magnetic particle removal will be necessary for successful OSL dating, and these processes are included in the diagram. In addition, a mechanism to dispense or create the aliquots along with an aliquot transport system are required. Of

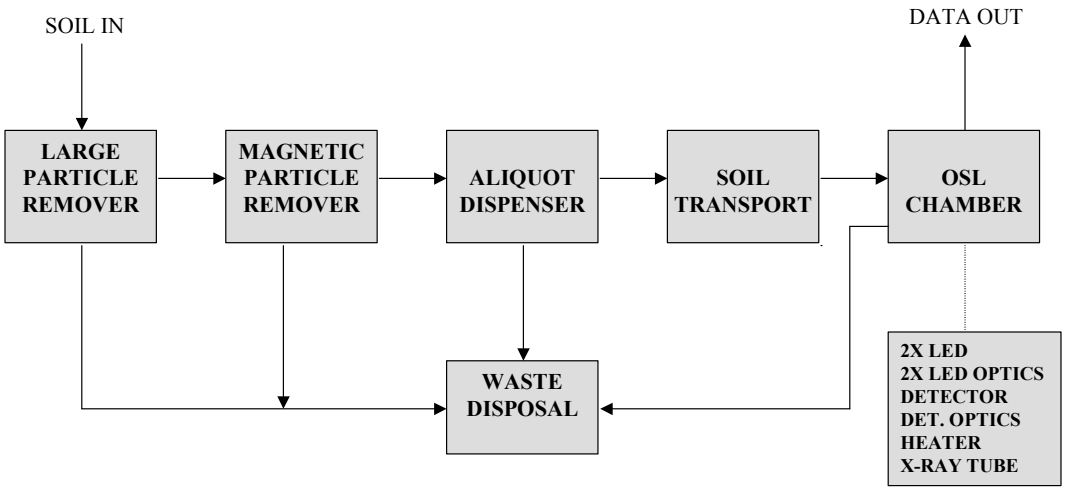

Figure B.1 System block diagram for the OSL module as developed by Nomadics and OSU.

course, a critical component of the module will be the OSL chamber itself, and some of the components of the OSL chamber were also identified at this time. It was decided that design and fabrication of prototypes for the aliquot transport system and OSL chamber would be addressed first.

B.2 Aliquot Transport System

After several suggested designs, a linear sample transport system has been adopted. One of the major concerns in designing this system was handling samples of fine dust that may be subject to static electricity. To circumvent this problem, the samples will be "trapped" between two layers of adhesive tape. Both layers of tape will need to be able to withstand temperatures from –40°C to approximately 210°C while remaining flexible, and the tape should not fluoresce in the spectral regions of interest. Kapton (polyamide) has been targeted for the bottom layer of tape that is in contact with the heater, and FEP Teflon has been chosen for the covering layer on the optically stimulated side of the samples. The thermal properties of the materials have not been tested yet, but neither tape appears to fluoresce in the UV detection window that is currently being used when stimulated by wavelengths of interest. Dose response curves have been measured for both Kapton and FEP to ensure that they do not produce an OSL signal. The dose response for Kapton is shown in Figure B.2, and no significant radiation-induced OSL signal can be detected up to 1000 Gy. The initial sample of FEP tape that was tested was coated with a silicone adhesive, and Figure B.3 (a) shows that this tape has a significant radiation-induced OSL signal. However, when a sample of FEP tape without any adhesive was tested (Figure B.3(b), no significant radiation-

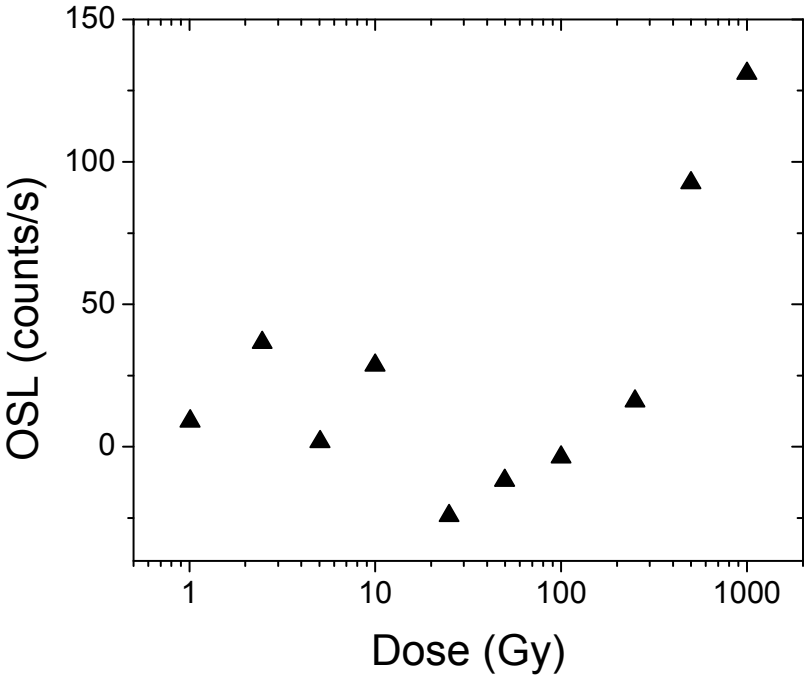

Figure B.2 Dose response for Kapton tape. The tape was preheated at 200°C for 10 s after each radiation dose, and blue-stimulated OSL was measured for 100 s at room temperature. The OSL signal is the integrated counts for the first 1 s minus the average of the last 5 s of stimulation.

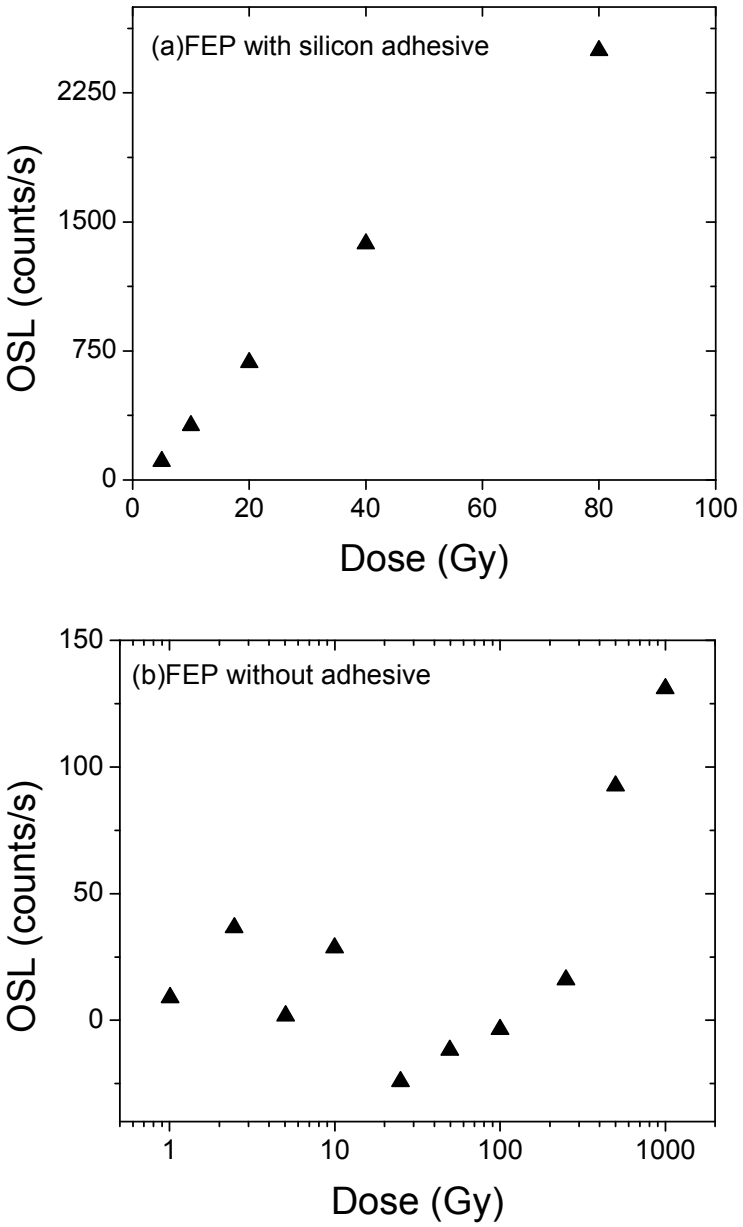

Figure B.3 Dose response for FEP tape (a)with silicone adhesive and (b) without adhesive. The tape was preheated at 200°C for 10 s after each radiation dose, and blue-stimulated OSL was measured for 100 s at room temperature. The OSL signal is the integrated counts for the first 1 s minus the average of the last 5 s of stimulation.

induced OSL signal can be detected up to 1000 Gy. Further research is required to find a suitable adhesive for the FEP tape.

The aliquot transport system will be similar to a "reel-to-reel" tape player. The Kapton tape (bottom layer) will be continuous and wound around two spools. As the aliquots are placed on the tape (the aliquot dispensing mechanism is yet to be determined), a strip of FEP (or potentially some other material if a suitable adhesive can not be found for FEP) will cover the aliquot. The FEP will not be a on a continuous roll so that the transport system can move in either direction (i.e., a previously measured sample can be measured again). The indexing system has not been fully designed. The most likely candidate is a series of holes along the side of the tape.

B.3 OSL Chamber

The OSL chamber aboard the module for dating must be able to perform all the necessary functions of a desktop OSL system but needs to be compact and lightweight. The necessary functions include heating (for preheating, elevated OSL measurement temperature, and possible elevated temperature irradiation), irradiation, stimulation by blue and infrared light, and light detection. A drawing and photo of the OSL chamber (supplied by Nomadics) is shown in Figure B.4, and details about the components of this chamber are given below.

Stimulation Sources

The OSL chamber will contain both blue and infrared LED arrays for optical stimulation. Innovations in Optics LumiBright LEDs have been chosen for the blue diodes, and a Roithner Lasertechnik LED870-66-60 epoxy lens type InfraRed illuminator will be the infrared stimulation source. Constant current drivers have been built for both

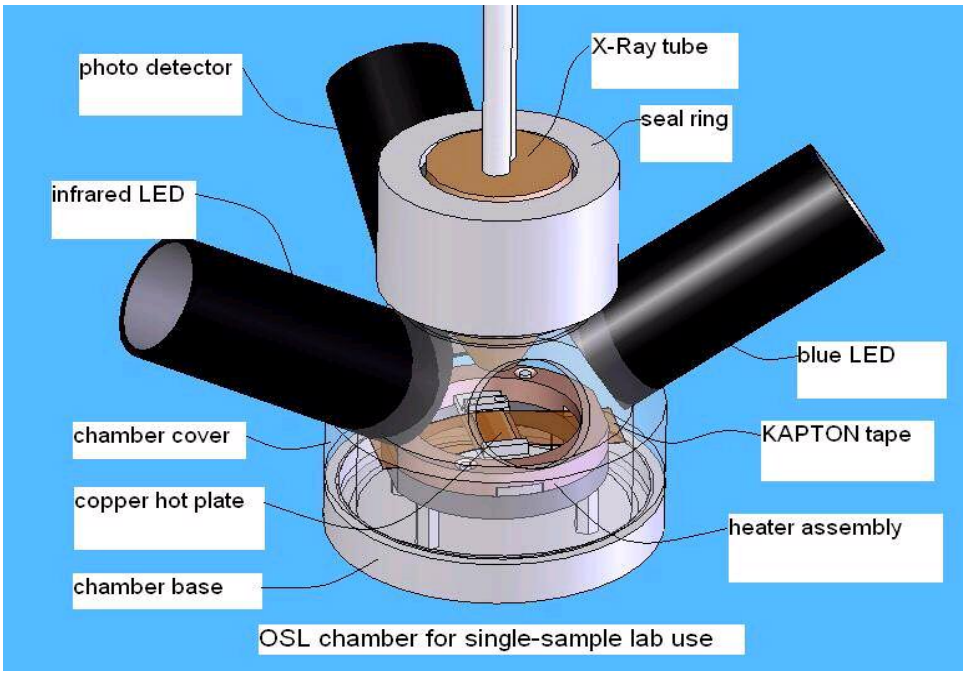

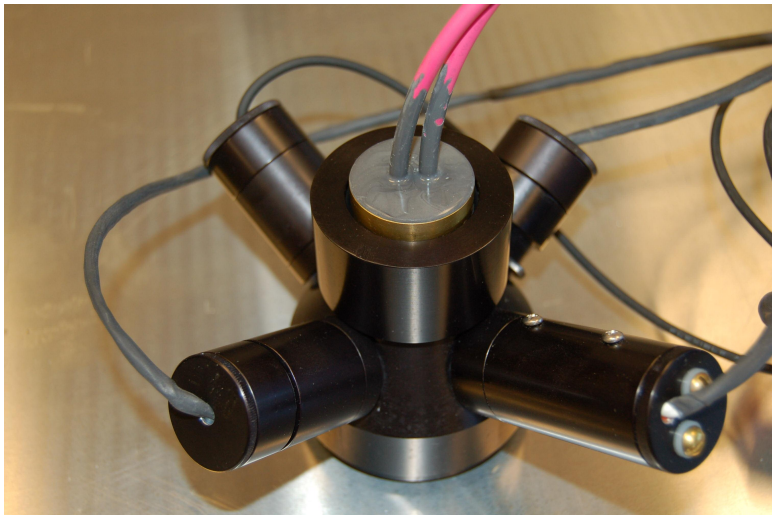

Figure B.4 Drawing and photo of OSL chamber (supplied by Nomadics). The drawing has a view through a spare port in the (here transparent) aluminum OSL chamber top cover.

of these diode arrays and the arrays are functioning. The low temperatures of Mars will affect the efficiency of these diodes, but temperature will not be compensated for in the circuitry of the diodes. Rather, the temeperature will be reported in the data returned to Earth, and temperature compensation will be done as part of the data analysis on Earth.

Light Collection

Light collection in most OSL systems is accomplished via a photomultiplier tube (PMT) that is sensitive in the blue and UV region. However, PMTs generally require a lot of power and are sensitive to vibration and shock (which a Mars module would certainly experience). Therefore, a Hamamatsu S2386 silicon photodiode has been chosen for light detection, and a low noise, high gain transimpedance amplifier has been built for the photodiode. Initial experiments indicate that the photodiode should be able to detect signals as low as 1.8 pW (roughly the smallest signal detectable by commonly used PMTs).

Unfortunately, the chosen photodiode is not as sensitive to UV light as the type of PMTs used in terrestrial OSL dating. To offset this disadvantage, the photodiode is more sensitive to red light than most PMTs. Therefore, a second photodiode has been added to the OSL chamber design to be placed in the spare port (the port through which the chamber is viewed in Figure B.4). One of the photodiodes will have filters appropriate for detecting a UV signal while the other photodiode will filters appropriate for detecting a red signal, and thus simultaneous monitoring of two detection windows will be possible.

Irradiation Source

Radioactive isotopes are typically used for calibration irradiations in terrestrial based OSL dating studies, but these isotopes have distinct disadvantages for a module to be sent to Mars. The radioactive elements pose a health risk to any workers that must construct or work with the instrument in preparation for space flight, and the sources would require heavy shielding (probably lead) to protect both the OSL instrumentation as well as other instrumentation on the space flight. Therefore, a Moxtek "Bullet" miniature X-ray system (4W, 40 kVp) has been chosen for the calibration radiation source (the same X-ray system used in the low temperature OSL system of Chapter 4). The X-ray system is equivalent to a 1 Ci radioactive source and requires little shielding (McKeever *et al.*, 2003).

B.4 Future Directions

More designing and fabrication of the miniaturized OSL instrument is required. A basic design of the sample transport system has been devised, but this system still needs to be constructed. In addition, systems to sort the material by size and magnetic susceptibility as well as to dispense aliquots of the proper size need to be designed and built. The engineers at Nomadics will be primarily responsible for these tasks, but the luminescence dating experts at OSU will assist in this process.

APPENDIX C

ELECTRON PARAMAGNETIC RESONANCE MEASUREMENTS

The focus of this dissertation has been development of OSL dating techniques for in-situ application on Mars. The overall project, however is to develop a combined electron paramagnetic resonance (EPR) and OSL dating instrument to be used on Mars through the Planetary Instrument Definition and Development Program (PIDDP) with NASA (JPL Contract No. 1265427 under NASA RTOP No. 344-36-55-19). Towards this project, I conducted EPR studies at the Jet Propulsion Laboratory (JPL) during three summers in the Graduate Student Researcher's Program (GSRP, grant # NGT5-50420). The EPR research focused on measuring EPR signals from many of the same mixtures used in OSL studies to determine if EPR geological age dating could be used on the same martian materials as OSL dating. This chapter then describes the theory behind EPR measurement and EPR dating and presents the EPR measurements conducted at JPL.

C.1 Theoretical and Experimental Background

EPR is a dosimetric technique that measures the radiation dose absorbed by certain materials. Ionizing radiation ejects negatively charged ions from the valence band leaving behind positively charged holes. While most of these electrons and holes recombine in a short time, some can be trapped at defect sites (electron in traps and holes in recombination centers) within the crystal structure (Grün, 1997; Figure 1.1 (a) and

(b))). The electron traps can be depopulated by either thermal or optical excitation, forming the basis for TL and OSL dating (Aitken, 1985, 1998). EPR, on the other hand, measures the trapped charge population, which is proportional to the absorbed radiation dose, without depopulating the traps.

EPR exploits the fact that unpaired trapped electrons have a small current and magnetic field. When free electrons encounter an external magnetic field, H, their energy level splits into two energy levels, E_+ and E_- (Zeeman splitting). By adding energy of magnitude ΔE, an electron can be promoted from the lower to the upper level:

$$\Delta E = E_+ - E_- = g * \mu_B * H$$

$$= h * \upsilon \qquad \text{(C.1)}$$

where g = Lande's factor, μ_B is the Bohr magneton, H = external field strength, h = Planck's constant, and υ =the frequency of the energy. The same energy is given off when electrons relax back to the lower state (Blackwell, 1995).

The electron population in the two levels can be described by a Boltzman distribution:

$$I = \frac{N_-}{N_+} = e^{\frac{\Delta E}{k_b * T}} = e^{\frac{h*\upsilon}{k_b * T}} = e^{0.048*\frac{\upsilon^*}{T}} \qquad \text{(C.2)}$$

where I is the EPR signal intensity, T is the temperature in K, and v^* is the frequency. The absorbed microwave radiation is thus directly proportional to the concentration of paramagnetic centers (Blackwell, 1995).

The EPR experiments described in this chapter were carried out at JPL on a Bruker 300E EPR spectrometer in the lab of Dr. Sam Kim. The spectrometer measures the EPR signal by placing the sample in a microwave field of constant intensity while the magnetic field is slowly varied by an electromagnet. When resonance is reached, the

sample absorbs microwave energy which is directly proportional to the number of paramagnetic centers in the sample. The spectrometer records the intensity of the EPR signal, I, as the first derivative.

Paramagnetic centers formed in materials by naturally occurring radiation certainly give rise to an EPR signal that can be measured in the lab, but the materials must also be calibrated using known radiation doses so that the natural radiation dose (and eventually the age) of the sample can be determined. To do this, the outer layers of a sample are removed and the sample is separated in to about 10 aliquots. These aliquots are then given known gamma doses (including 0 Gy) to construct a dose response curve. The paleodose, D_e, can then be extrapolated from this curve with random errors from 2 to 7 % and a systematic error (from gamma source calibration) from 2 to 5% (Grün, 1997). The D_e is assumed to be the dose accumulated since the material formed, although the EPR signal can be reset by exposure to light or heat in certain cases.

Once the D_e is known, the age of the sample can be determined by measuring the natural dose rate as is done in luminescence dating. Often, the outer layers of a material are removed to eliminate the effect of alpha and beta particles (50 μm for alpha particles, 2 mm for beta particles). The U, Th, and K concentrations are measured by either delayed neutron counting neutron activation analysis or gamma ray, TL, or OSL dosimetry at the site (Blackwell, 1995), and the cosmic ray dose is calculated based upon the geographic location, altitude, and thickness of overlying sediments (Grün, 1997).

With the equivalent dose (in Gy) and the natural dose rate (in Gy/yr), the age of the sample can then de determined by:

$$\text{Age(Years)} = \frac{\text{D}_\text{E}\,\text{(Gy)}}{\text{Dose Rate(Gy/yr)}} \ . \qquad \text{(C.3)}$$

C.2 EPR Measurements of Martian Simulants

Although many of the same issues previously discussed as challenges to developing OSL dating on Mars apply to developing EPR dating for Mars, this section focuses on basic measurements of the EPR signal from martian simulants and minerals likely to be found on Mars. The EPR measurements roughly follow the order of OSL studies in that feldspar separates were first studied, followed by mixtures of quartz and feldspars, then the martian soil simulants OSU Mars-1 and OSU Mars-2. As the minerals or mineral mixtures were previously discussed their composition is not discussed here.

C.2.1 Feldspar samples

EPR measurements were first made on three feldspar separates: oligoclase, microcline, and anorthoclase. The samples were irradiated by a Co^{60} source at JPL delivering 1.46 Gy/min. Examples of EPR spectra from these three feldspars are shown in Figure C.1. The goal of the experiment was to determine dose response curves for each of the minerals. Since measuring the EPR spectrum of a mineral does not remove the charge from the traps (i.e., the EPR signal is not erased by measurement), an additive dose procedure was used. The EPR signal of each sample was first measured before any radiation dose was given. A radiation dose was then given to the samples and the EPR signal was measured. A further radiation dose was given, and the subsequent EPR signal represented the signal from the total radiation dose given. This process was repeated until the maximum dose was reached.

As these minerals are generally not used in EPR dating, much of the available experimental time was used to find a radiation-induced signal. For anorthoclase, as can be seen in Figure C.1 (a), no radiation-induced signal could be detected. If a radiation-

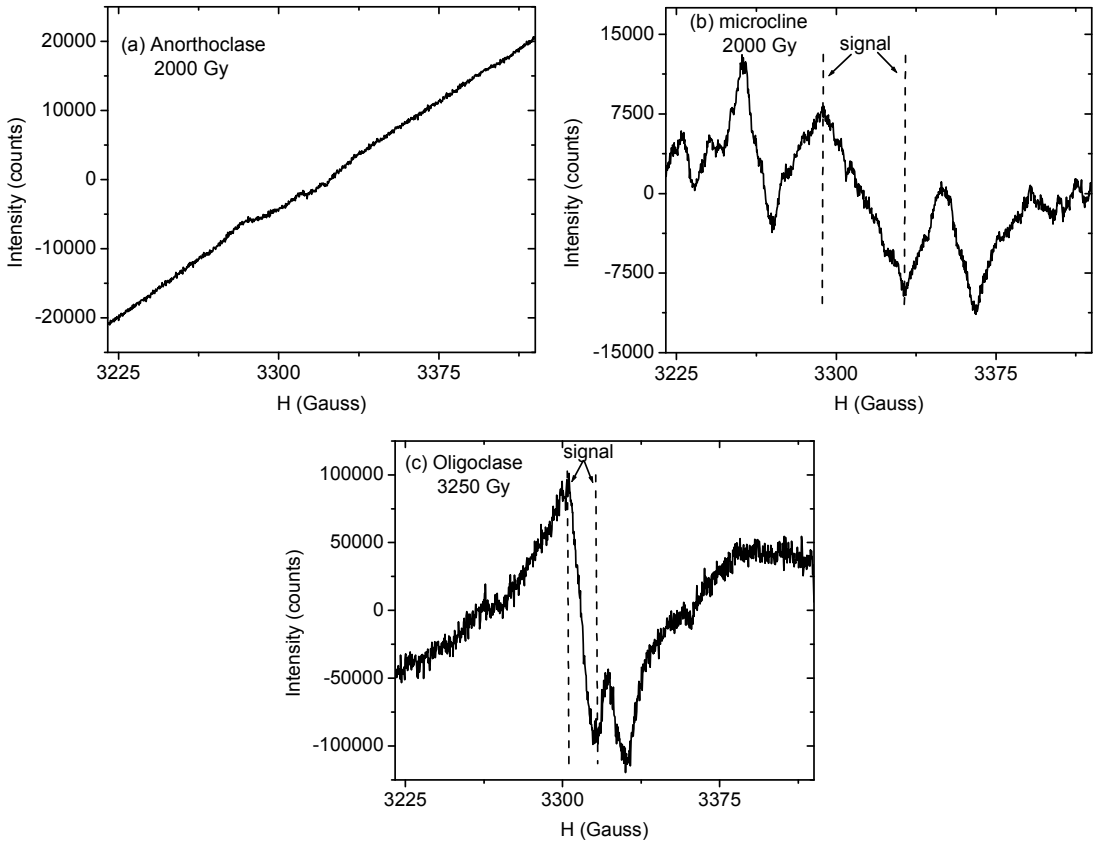

Figure C.1 Examples of EPR spectra from feldspar minerals. Each graph gives the mineral name and the radiation dose given to produce the spectra. The signal was defined as the total area under the curves, but no background was subtracted.

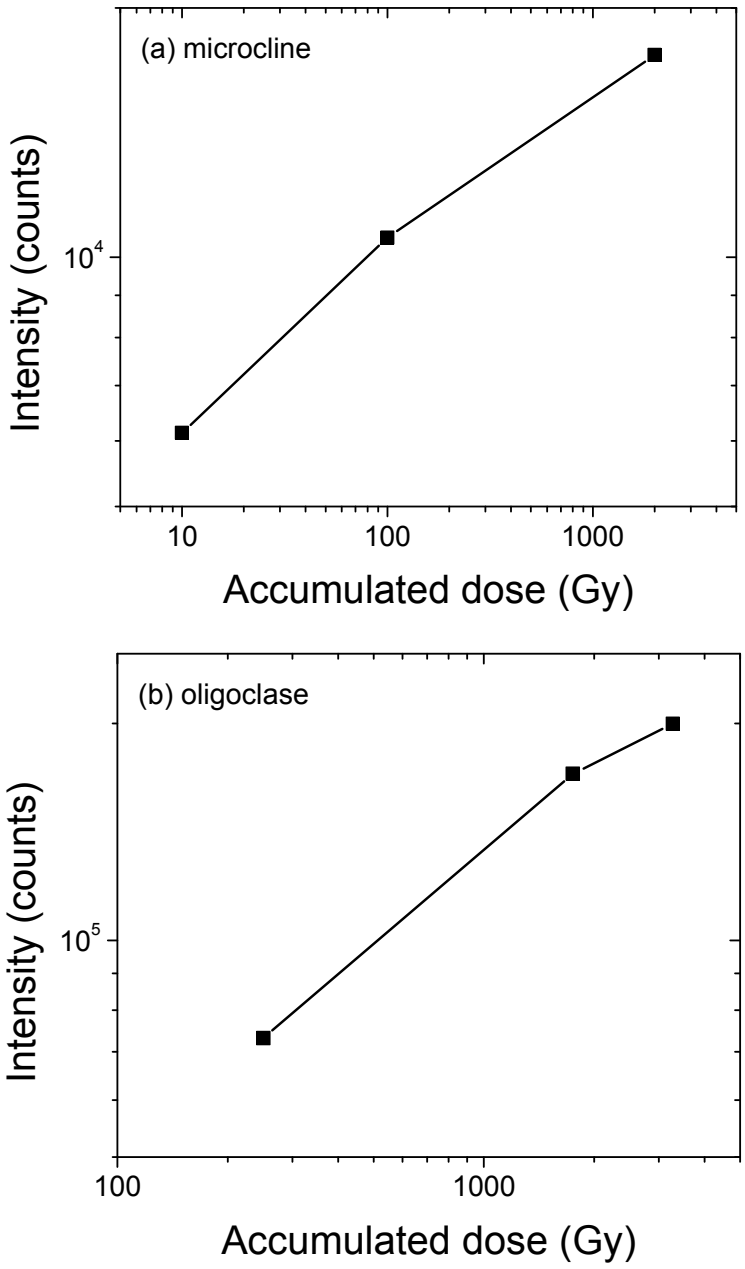

Figure C.2 EPR dose response curves for feldspar minerals.

induced signal is present in anorthoclase, it is apparently masked by the presence of a ferromagnetic material (most likely iron). For microcline and oligoclase a radiation-induced signal could be measured, but the EPR signals for these samples apparently have low sensitivity to radiation. The dose response curves that were measured for microcline and oligoclase are shown in Figure C.2. Due to the lack of data points, no linear or supralinear regions of the dose response curves can be determined. However, the curves due appear to be in saturation by doses of 2000 Gy.

C.2.2 Quartz and Feldspar Mixtures

The quartz (sample 495A) and feldspar (albite) mixtures that were created for experiments in Chapter 2 (Section 2.4) were also used for EPR measurements. The three mixtures are: Mixture #1- 75 % quartz and 25 % feldspar, Mixture #2- 50 % quartz and 50 % feldspar, and Mixture #3- 25 % quartz and 75% feldspar. The samples were again irradiated by a Co^{60} source at JPL delivering 1.27 Gy/min. Examples of EPR spectra from all three mixtures are shown Figure C.3. Based upon these spectra, three different radiation-induced signals were identified: signal #1- from 3294.267 Gauss to 3306.389 Gauss, signal #2- from 3311.667 Gauss to 3314.404 Gauss, and signal #3- from 3315.186 Gauss to 3322.615 Gauss. As these minerals had not previously been studies in detail, a determination could not be made as to which mineral produces which signal.

Dose response curves for the three mixtures were constructed using an additive dose method as previously described. For each spectrum, the intensity of each of the above defined signals was determined by summing the intensity of the designated regions. However, signals could only be detected for doses larger than 3600 Gy, and the dose response curves therefore have only 3 points. These dose response curves are

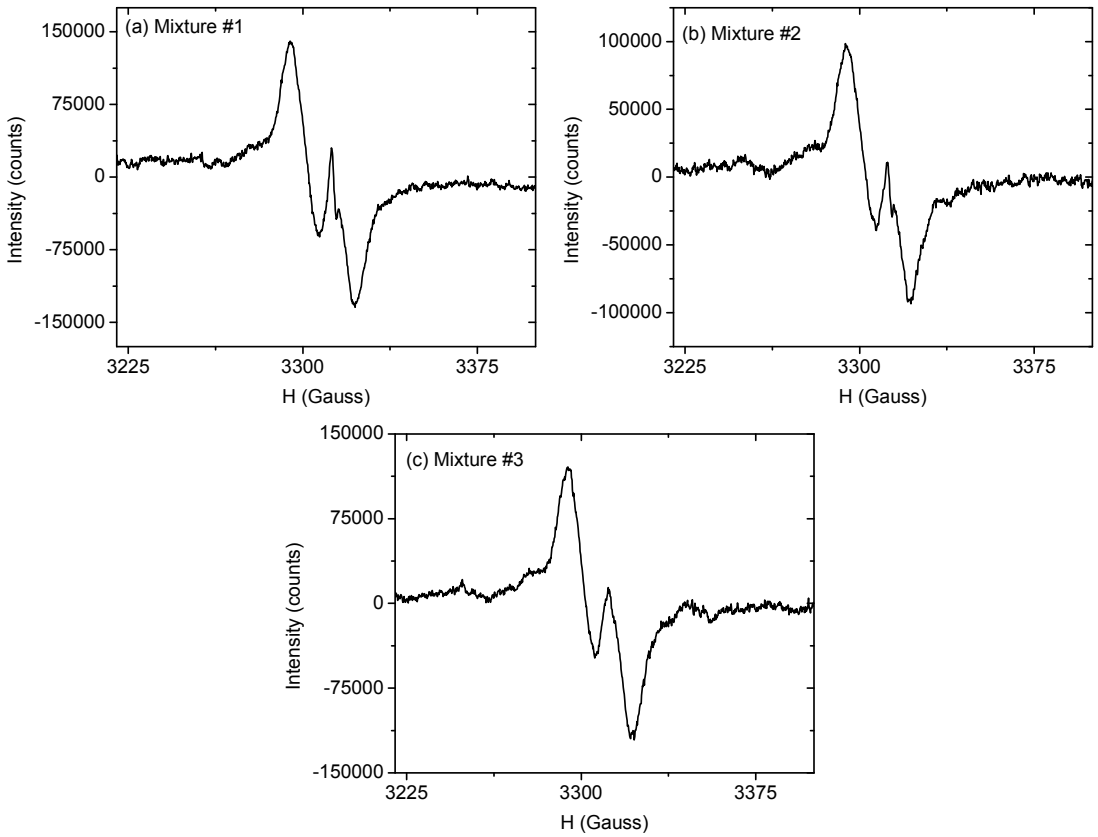

Figure C.3 Examples of EPR spectra from quartz and feldspar mixtures. All spectra were measured after a 7000 Gy radiation dose. Each graph gives the mixture number.

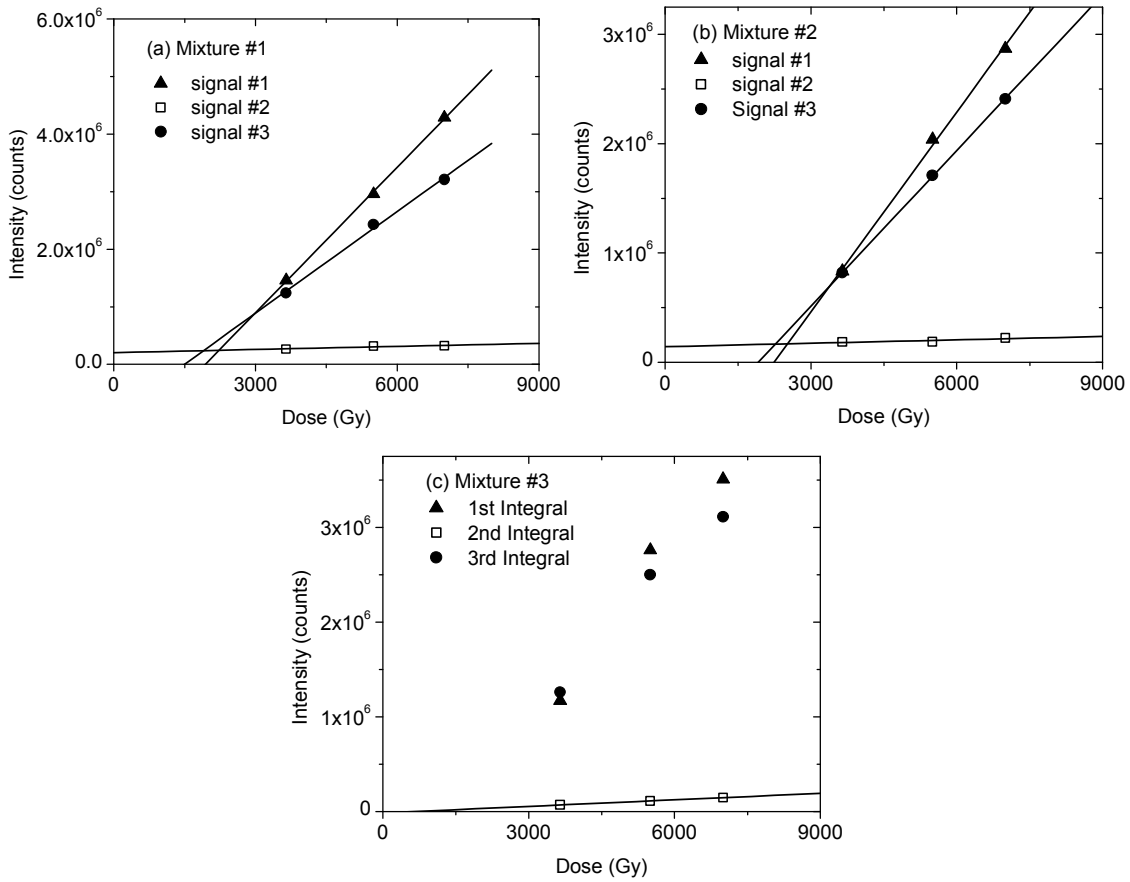

Figure C.4 Dose response curves for quartz and feldspar mixtures. Each graph shows results from a different mixture, and all three signals from each mixture are plotted on the same graph. The straight lines represent linear fits of the data (note that they do not pass through zero). For Mixture #3, signals #1 and #3 could not be fit linearly.

shown in Figure C.4. Signal #2 proved to be a very weak signal that increased moderately in intensity for the given doses. Signals #1 and #3, however, both increased substantially over the given dose range and should be detectable at much lower doses with increased expertise in EPR measurement (i.e., optimized measurement conditions). Most of the dose response curves could be fit with a linear function that does not pass through the origin, implying that the saturation dose for these signals is very large. For Mixture #3, however, signals #1 and #3 could not be fit with a linear function. The reason these signals could be fit with a linear function for Mixtures #1 and #2 but not for Mixture #3 is not clear. Due to the scarcity of data points, no supralinearity could be detected.

C.2.3 Martian Soil Simulants

The martian soil simulants OSU Mars-1 and OSU Mars-2 (see chapter 1 and Chapter 3) were also studied using EPR techniques. For these materials, samples were irradiated at OSU with doses ranging from 0 Gy to 3000 Gy, and the EPR signals were measured at JPL. For these measurements, the weight of each sample was measured, and mass-normalized EPR signals were produced for each simulant and radiation dose. Unfortunately, no radiation-induced EPR signal could be detected for the measurement conditions used.

C.2.4 Concluding Remarks

The EPR measurements described here were preliminary measurements to determine if the same martian simulants used for OSL research give rise to EPR signals. It has been shown that certain feldspar separates and mixtures of quartz and feldspar do have EPR signals that increase monotonically with dose. However, more

characterization of the EPR signals from martian simulants is required including research with other simulants, optimization of the measurements parameters (e.g., measurement temperature, preheating), and characterization of the EPR signals (e.g., calculation of the g-values, susceptibility to optical stimulation).

VITA

Michael Wayne Blair

Candidate for the Degree of

Doctor of Philosophy

Dissertation: DEVELOPMENT OF OPTICALLY STIMULATED LUMINESCENCE TECHNIQUES FOR APPLICATION TO TERRESTRIAL AND MARTIAN STUDIES

Major Field: Physics

Biographical:

Personal Data: Born in Hamliton, OH, October 20, 1976; married on September 11, 2004.

Education: Received a Bachelor of Science degree in Physics and Anthropology from Western Kentucky University in December 1999, graduated with honors – Summa cum Laude. Senior Honors Thesis title: Archaeoastronomy at the Shiloh Mound Group. Completed the requirements for the Doctor of Philosophy degree with a major in Physics at the Oklahoma State University in December 2005.

Experience: Undergraduate physics tutor and lab assistant at Western Kentucky University, 1999. Archaeology field technician for Algonquin Consultants in Cincinnati, OH, 2000. Physics teaching assistant at Oklahoma State University, 2000-2001. Graduate research assistant in physics at Oklahoma State University, 2001-2005.

Professional Memberships: Sigma Pi Sigma physics honor society, Lambda Alpha anthropology honor society, Phi Kappa Phi national honor society, Golden Key national honor society, Western Kentucky University Alumni Association.

Name: Michael Wayne Blair Date of Degree: December, 2005

Institution: Oklahoma State University Location: Stillwater, Oklahoma

Title of Study: DEVELOPMENT OF OPTICALLY STIMULATED LUMINESCENCE DATING TECHNIQUES FOR APPLICATION TO TERRESTRIAL AND MARTIAN STUDIES

Pages in Study: 291 Candidate for the Degree of Doctor of Philosophy

Major Field: Physics

Scope and Method of Study: Geological processes including aeolian and fluvial activity have shaped the surface of Mars. The temporal timescale on which these events have taken is place is important for understanding the geological history of Mars including time periods in which life may have developed on the planet. However, methods do not currently exist that can be used in-situ on Mars to constrain the recent (younger than 1 million years) geological timescale. It has been suggested that optically stimulated luminescence (OSL) dating, which measures the radiation dose and dose rate minerals are exposed to over time and hence the burial time, can be developed as an in-situ tool for delineating the timing of these recent events. This study attempts to develop some of the necessary techniques for measuring the radiation dose in martian minerals by studying martian soil simulants and meteorites.

Findings and Conclusions: Most of the luminescent materials that will be encountered on Mars are different from those typically used for OSL dating on Earth. However, the techniques used for absorbed radiation dose determination in terrestrial OSL dating studies can be adapted to martian simulants and meteorites with a few minor but important changes. These changes have to do with the heat treatment of the samples prior to OSL readout as well as the temperature of irradiation and OSL measurement due to the ambient temperature of Mars. While many scientific challenges must still be overcome for this project, this study provides a basis for further study of martian simulants.

ADVISER'S APPROVAL: Dr.Stephen W. S. McKeever_____